FLANGE STABILITY BRACING BEHAVIOR IN METAL BUILDING FRAME SYSTEMS

A Thesis
Presented to
The Academic Faculty

by

Akhil Sharma

In Partial Fulfillment
of the Requirements for the Degree
Master of Science in the
School of Civil and Environmental Engineering

Georgia Institute of Technology
May 2011

FLANGE STABILITY BRACING BEHAVIOR IN METAL BUILDING FRAME SYSTEMS

Approved by:

Dr. Donald W. White, Advisor
School of Civil and Environmental Engineering
Georgia Institute of Technology

Dr. Roberto T. Leon
School of Civil and Environmental Engineering
Georgia Institute of Technology

Dr. Kenneth M. Will
School of Civil and Environmental Engineering
Georgia Institute of Technology

Date Approved: November 12, 2010

To my parents, Amrit Lal Sharma and Renu Sharma
for their overwhelming support, patience and love

ACKNOWLEDGEMENTS

I would like to express my deepest gratitude to all those who gave me the opportunity to complete this thesis. Special thanks are due to my advisor Professor Donald W. White whose help, stimulating suggestions and encouragement helped me in all the time of research for and writing of this thesis. I am deeply indebted to my committee members, Professor Roberto T. Leon and Professor Kenneth M. Will for all their help and support.

The sponsorship from Metal Building Manufacturers Association (MBMA) for this research is greatly appreciated. Also, I would like to thank Mr. Duane Becker, Chief Industries for the suggestions and help that he provided for me.

I want to thank all my friends for all their help, support, interest and valuable hints.
I am obliged to Dr. Yoon Duk Kim for all her assistance and advice on this study.

Special thanks are due to my parents for their support and encouragement that made this possible.

TABLE OF CONTENTS

LIST OF TABLES

LIST OF FIGURES

SUMMARY

The objective of this research is to evaluate the stiffness and strength demands on flange braces in metal building systems. This objective is accomplished by a targeted study of the effects of various attributes of metal building systems not fully addressed in existing bracing design procedures. Special emphasis is placed on attributes such as unequal brace spacing and stiffness, end brace point flexibility, nonprismatic member geometry, special requirements at knee joints and the specific configuration of combined girt/purlin, flange diagonal, diaphragm and X bracing systems used in metal building construction.

A sub-objective of the research is the demonstration of how virtual test simulation via full nonlinear finite element analysis may be applied to solve a structural engineering research problem that would be difficult to address by any other means. When conducted properly, virtual test simulation can serve as a valuable companion to experimental testing since attributes such as residual stresses and critical geometric imperfections can be controlled precisely and with relative ease in virtual test simulation.

Both highly simplified and more complex but relatively rigorous procedures are considered, with the ultimate goal being improved economy and safety of flange stability bracing in metal buildings.

CHAPTER 1

INTRODUCTION

1.1 Problem Statement

Stability bracing is defined as any bracing system where all the primary forces are zero. The only calculated forces in the stability bracing members and components are due to unavoidable geometric imperfections in the structure being braced and the second-order (stability) effects caused by member internal forces acting through the amplified imperfections in the structure. Generally, a stability brace must satisfy two key design requirements (Winter 1958; Yura 1995):

1. It must have sufficient strength to withstand the forces delivered by the member or members being braced; and
2. It must have sufficient stiffness to limit the brace point displacements, and thus limit the second-order amplification of these displacements and the corresponding brace forces.

If a brace does not satisfy both of these requirements, the bracing system and/or the member being braced may fail prematurely. Reduced bracing stiffness allows greater out-of-plane deformations of the physical imperfect structure, which in turn can result in larger forces in the bracing system. If the bracing stiffness is too small, the required bracing forces can be excessive.

The most recent codified requirements for stability bracing of columns, beams and beam-columns can be found in Appendix 6 of the 2005 and 2010 AISC Specifications. These provisions provide simplified design equations for several important but basic bracing situations, namely “relative” and “nodal” lateral bracing of columns and beams, and “nodal” and “continuous” torsional bracing of beams. Unfortunately, the stability bracing systems in metal building construction as well as other general structures often

do not match well with these basic cases. Therefore, practical stability bracing design typically involves significant interpretation and extrapolation of the basic rules. The interpretation and extrapolation of these rules is often likely to result in conservative designs; however, the true conservatism or lack of conservatism of the various ad hoc extrapolations is largely unknown.

The above situation is certainly the case for the flange bracing systems in metal building frames. In many metal building structures, the flange bracing systems for the primary frames are composed of:

- Outset purlins and girts, connected to the outside flange of the primary members, combined with different types of roof and wall diaphragms,
- X-bracing using light structural members, rods or cables, positioned either close to the outside flange or at the middle of the web depths, and
- Flange diagonal braces on one or both sides of the primary members, framing between the girts and purlins and a connection point on or near the inside flange of the frame members.

A simplified illustration of these arrangements, minus roof and wall diaphragms, is shown with two parallel main frames in Fig. 1.1. Different roof and wall systems provide a wide range of diaphragm stiffnesses. In addition, rod, cable or light-weight structural members employed as X-bracing in planes parallel to the building envelope can have various sizes and overall configurations. Furthermore, flange diagonal braces are commonly located only at selected locations where the inside flange needs to be restrained out-of-plane to satisfy member lateral torsional buckling design requirements.

There are various attributes of metal building frame systems that strictly place their flange stability bracing design outside the specific scope of AISC Appendix 6:

1. The primary frame members are generally nonprismatic. The AISC Appendix 6 rules address only prismatic members.

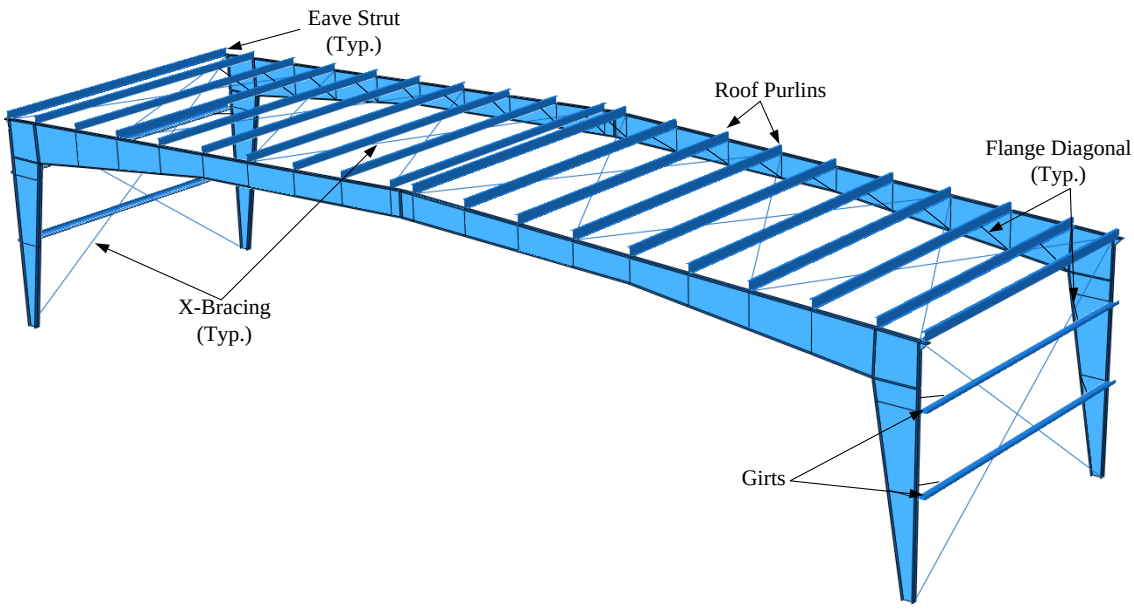

Fig. 1.1. Two representative clear-span metal building frames shown with outset girts and purlins and X-bracing parallel to the building envelope.

2. The primary frame members transmit both axial load and moment, that is, they perform as beam-columns. A new Appendix 6 Section 6.4 has been added to the 2010 AISC stability bracing provisions to address beam-columns. These provisions specify a simple ad hoc addition of the strength and stiffness requirements for relative and nodal lateral bracing. Although, these rules are believed to be conservative, there has been little to no background research to understand their accuracy, correctness, or implications. For cases involving torsional bracing for flexure combined with relative or nodal bracing for axial force, the provisions state that "the required strength and stiffness shall be combined or distributed in a manner that is consistent with the resistance provided by the element(s) of the actual bracing details." The author suggests that this clause is a prime example of what has been coined by Professor John Breen

as provisions having a high "fog index" (Breen 2008). The proper interpretation of how this provision should be applied is beyond the reach of most if not all stability bracing experts.

3. The axial load and moment in the primary members generally vary along the member lengths. The Appendix 6 rules are based on the assumption of constant axial load along the member lengths.
4. Although purlins are usually provided at constant spacing along most of the roof girder length, their spacing typically is not constant near the ridge or the eaves. Interestingly, these are the locations where the bracing demands can be the largest, since the internal moments and flexural stresses are often the largest there. Furthermore, often the girts are not placed at a constant spacing along the columns. Typically, one girt is placed at a height that passes above any doors, windows, etc. in the exterior wall, one or more girts may be placed at a lower height, and additional girts may be placed between the top of the doors, etc. and the top of the columns as needed. In addition, diagonal braces to the inside flanges of the primary frame members are typically placed only where the inside flange needs additional restraint. This results in a variable spacing of the inside flange brace points along the member lengths. The AISC Appendix 6 nodal bracing provisions (lateral and torsional) are based on the assumption of equal brace spacing.
5. The AISC nodal bracing provisions are based on the assumption of equal brace stiffnesses. Unfortunately, with the exception of cases with one or two intermediate nodal braces, equal stiffness nodal lateral bracing practically never

exists in building and bridge structures. This is because it is rare that discrete nodal braces are all of equal size or length, tied back essentially to a structural system massive enough such that it is effectively rigid. As illustrated in Fig. 1.2, once the flexibility of the "back-bone" structural system to which the nodal lateral braces are attached is taken into account, the bracing stiffness provided at each of the nodal braces has to vary along the length of a member being braced. For instance, the stiffness provided at the middle brace in Fig. 1.2 is different than that provided at the other two intermediate brace points since the flexible wall or diaphragm that the nodal braces are tied to provides less resistance to a unit displacement at the middle brace than at the other locations.

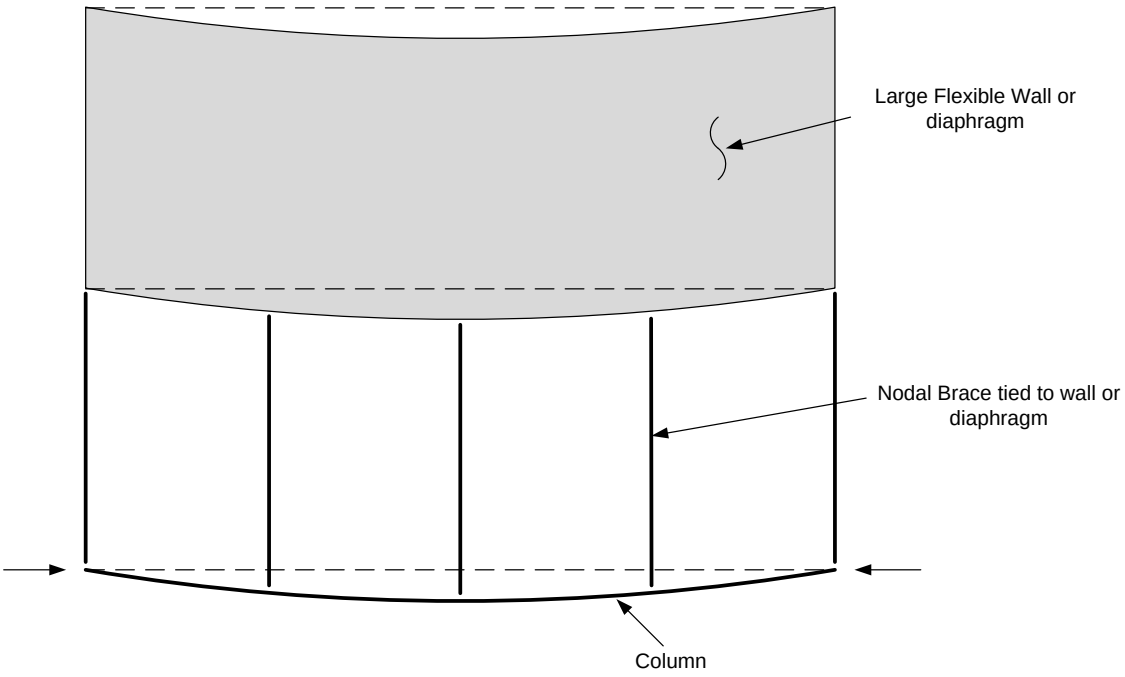

Fig. 1.2. Example nodal bracing tied to a large flexible wall or diaphragm such that the stiffnesses are different at each of the nodal braces.

The bracing system shown in Fig. 1.2 is actually the combination of a nodal and a relative bracing system connected in series. The struts tying the column

back to the wall or diaphragm are discrete nodal braces. However, these braces are then supported by the wall or diaphragm. The deformations illustrated in the figure are predominantly shear deformation of the wall or diaphragm system. As discussed in detail subsequently in Chapter 2 of this report, a relative bracing system is one in which the relative buckling displacements between adjacent brace points are restrained by shear stiffness. That is, relative bracing is effectively "shear panel" bracing, The total deflection at any one of the discrete brace points along the column in Fig. 1.2 is the sum of the deflection from the deformation of the struts (the nodal bracing) and the wall or diaphragm system (the relative or shear panel bracing). Hence, the total stiffness provided at any of the brace points is the stiffness provided by these systems acting in series. The combination of the stiffnesses in series is not a simple scalar one though, since the diaphragm or wall flexibility affects the lateral bracing stiffness at all of the brace points.

If the deformations in the wall or diaphragm system of Fig. 1.2 were dominated by flexure rather than shearing, then this bracing system would be a combined "nodal" and "lean-on" bracing system. As discussed in more detail in Chapter 2, the lean-on bracing idealization commonly involves one or more other flexural members, possibly also loaded in axial compression, connected to a more critical flexural member (column or beam). The less critical members help resist the flexural (column) or lateral-torsional (beam) buckling displacements of the critical member. That is, the more critical flexural member "leans on" the less

critical flexural member(s). Any flexibility of the ties between the members is typically neglected in lean-on bracing systems.

In general, if the wall or diaphragm system in Fig. 1.2 has significant flexibility in both shear *and* flexure, then the column and its bracing system fall even further outside of the specific idealizations commonly employed for bracing design. The common relative, nodal and lean-on bracing idealizations are explained in detail in Chapter 2 of this report.

In addition to the above considerations, which cause the effective lateral bracing stiffness at the brace points to vary along the length of a member, it is useful to consider the behavior of typical torsional bracing systems. For instance, when flange diagonal braces in metal building frames are considered as torsional braces, it is important to note that even if the same girts or purlins and the same flange diagonal cross-sections are used throughout the frame, the bracing stiffness provided to the inside flange changes due to changes in the depth of the members. In addition, it is common to have:

- A larger purlin overlap;
- A different angle of inclination of a diagonal brace;
- A switch from one-sided to two-sided diagonal bracing;
- A larger size purlin; or
- An additional larger bracing purlin

at specific locations where the engineer estimates that the bracing requirements are larger. This of course means that the discrete bracing stiffnesses are larger at these locations.

Lastly, if one considers the lateral bracing from the purlins and girts acting with the diaphragm bracing from the roof and wall systems, as well as with the X-bracing parallel to the roof or walls, the lateral bracing stiffness provided at the girts and purlins is larger at the panel points of the X-bracing and smaller at the locations between these points. The panel points of the X-bracing can be referred to as "hard" or "stiff" brace points whereas the other girt or purlin locations can be considered as "soft" or "flexible" brace points.

6. Although a knee joint is commonly considered as the end of a column as well as the end of a roof girder, the bracing at the joint may not be sufficient to make these points act as if they are rigidly braced. The AISC Appendix 6 provisions are based on the idealization that the bracing at the ends of the members is rigid compared to the intermediate bracing along the member lengths. Strictly speaking, the AISC Appendix 6 provisions do not provide any guidelines for the design of bracing at the end of a member (unless there is no bracing within the span, or relative bracing is employed within the span, in which case the relative bracing rules apply).
7. At the inside corner of the knee joints of a frame, such as the one shown in Fig. 1.1, the bracing system restrains several different deformations of both the column and the roof girder. For example, if the engineer designs a torsional brace at the end of the roof girder, this brace also provides minor-axis flexural restraint at the top of the column. Similarly, torsional restraint at the top of the column corresponds to weak-axis flexural restraint of the roof girder. As a result, depending on the specific configuration of the structure and its components,

either of the above torsional braces may end up seeing greater demands from potentially unintended weak-axis flexural restraint of the other member. Even if one considers the brace at the inside of the knee as an ordinary lateral brace, the brace functions to resist the out-of-plane movement of both of the members as well as the panel zone at the inside of the knee. Roof pitch complicates the situation further, since the roof girder is then connected to the column at other than a 90^o angle.

In addition to the above scenario, if the roof girder is more critical than the column with respect to say lateral-torsional buckling, the warping and weak-axis bending stiffness at the top of the column (in conjunction with the out-of-plane support from the eave strut, purlins, longitudinal lateral bracing, and wall diaphragm bracing can assist the torsional brace at the end of the roof girder in restraining any twisting at the end of the roof girder. Conversely, if the column is more critical with respect to lateral-torsional buckling, the warping and out-of-plane flexural stiffness of the roof girder, acting in conjunction with the eave strut, girts, longitudinal lateral bracing and roof diaphragm bracing, can assist in restraining the twist at the top of the column.

Furthermore, there are other stiffness interactions at the knee. For instance, the torsional stiffness of one of the members, enhanced by its torsional bracing system, can provide weak-axis bending and warping restraint at the end of the other member.

8. In contrast to the above behavior, the Appendix 6 rules address the basic stability bracing of only a single member, or several parallel members that are tied

together. The member ends are assumed to be free to rotate and free to warp in the stability bracing equation developments. More lightly loaded unbraced lengths of a given main frame may assist a more critically loaded unbraced length via the continuity of the members across the brace points. Of course, for an ideal infinitely elastic system, continuity effects can also impose larger demands on some bracing components. This is the case for example due to "prying" or "lever" action, where one part of a member is tending to provide restraint to say a critical unbraced length. These continuity effects are accounted for to a certain extent in the nodal lateral, nodal torsional and continuous torsional bracing equations of the AISC Appendix 6. However, the continuity effects in many structures can be much more complex than those associated with the basic Appendix 6 bracing rules (e.g., see (Plaut 1993) and (Stanway et al. 1992a & b)).

Member continuity effects can be particularly beneficial in cases such as members with shorter spacing between braces, wider flanges, and/or cases in which the member strength limit state involves significant inelastic action. In these types of situations, the bracing stiffness demands can be reduced due to member inelastic stiffness reduction while the members may still provide substantial resistance to brace point movement (Tran 2009).

In addition, end lateral bending and/or warping restraint generally tends to increase the member buckling resistance, and hence, it tends to reduce the force and stiffness demands placed on the bracing (Tran 2009).

9. The AISC Appendix 6 rules address only the maximum force demand for all of the braces in a nodal bracing system composed of equally-spaced braces of equal stiffness. However, particularly when one considers a typical roof girder with:
   - A large number of purlin and/or flange diagonal braces,
   - A significant gradient in the axial forces and/or moments along its length, and
   - The braces near the knee, for example, being a large distance along the member from those at the ridge,

   it is intuitively clear that the brace forces at the maximum axial force and/or moment locations should be much larger than those at other remote brace points where the member internal forces are smaller. In fact, one would expect that the stiffness requirements may vary substantially along the member lengths as well.
10. Restraint of the primary frame members generally can come from a combination of various types of bracing. It is well known from prior research, e.g., Yura and Phillips, (1992), Tran (2009), and Yura and Helwig (2009), that for beam bracing, a combination of both lateral and torsional restraint is much more effective than either of these types of bracing alone. In fact, adding just a very small amount of incidental lateral restraint at a torsional brace can reduce the demands on the torsional brace dramatically while not inducing any significant demands on the incidental lateral bracing (Tran 2009). The AISC Appendix 6 does not recognize any benefits of combined torsional and lateral bracing.

    Yura et al. (1992) have developed equations accounting for the influence of combined continuous lateral and torsional bracing on the elastic buckling resistance of steel I-section members, as well as recommendations for the use of

these models to represent equally-spaced, equal-stiffness, combined, nodal lateral and nodal torsional bracing. However, the author is not aware of any research on combined relative (shear panel) bracing and torsional bracing. This combination is believed to be more representative of the bracing configurations in many metal building systems.

The lateral bracing of the primary frame members by the girts and purlins can come from a variety of stiffness contributions including:

- Shear stiffness of the X-bracing truss system;
- Shear stiffness of the roof and wall diaphragms;
- Strong- and weak-axis bending and twisting of the girts and purlins in conjunction with the diaphragm deformations; as well as
- Transfer of girt and purlin axial forces from the bracing of a critical main frame to other more lightly loaded frames that the critical frame is effectively leaning on.

AISC Appendix 6 does not address lean-on bracing, and even if it did, it would be difficult in general to count on any one of the main frames being more lightly loaded than another under all the strength loading conditions. Nevertheless, this incidental contribution to the stability bracing of a critical frame can indeed occur, and potentially it can have a significant effect.

In metal building frame members with reversed curvature bending along their length, part of the member may be braced by relative bracing, e.g., from wall or roof diaphragms at the outside flange, and part of the member may be braced by torsional bracing, e.g., from flange diagonals to the inside flange. It is well known

that lateral bracing of the compression flange tends to work more effectively than torsional bracing, and that combined lateral and torsional bracing (or lateral bracing of both flanges) works best. In the above cases, it is likely that the outside flange is restrained by the relative bracing at the torsional braces, thus improving the torsional bracing efficiency at those points.

Although it is believed that many of the above ten attributes often result in conservative bracing designs, the sources of the potential inherent conservatism of the ad hoc application of the Appendix 6 stability bracing equations is largely unknown in many practical situations.

Nodal stability bracing systems in steel structures have traditionally been designed for strength by assuming a maximum strength demand of 2 % of the member axial force, P_r, the flange axial force, M_r / h_o, or in case of torsional bracing, the member moment M_r. However, it is well established that stability bracing systems cannot in general be designed for just force alone (Winter 1958; Yura 1993, 1995 and 2001; Nethercot and Lawson 1992; Ziemian 2010; AISC 2010). Although for some structures, light incidental framing may easily provide enough strength and stiffness to brace the structure, one cannot expect small purlins and flange diagonal braces (for example) to be sufficient to adequately restrain the main frames when the span lengths, member depths, and/or flange sizes exceed a certain threshold. Even if the strength of the bracing system is sufficient, by satisfying say the traditional 2 % brace force design rule, a system that does not provide sufficient stiffness will experience excessive brace point displacements potentially resulting in an unsafe situation. The stiffness demand rather than the strength demand on the bracing often controls the bracing design, particularly for span lengths

greater than 60 ft (Duane Becker, personal communication). At the present time (2010), the actual demands on the stability bracing in representative "real" metal building frames are largely unknown.

This research is a continuation of related work conducted by Tran (2009). Specific accomplishments achieved by Tran include:

- Confirmation of various refined 3D FEA tools and procedures for predicting the elastic buckling loads for various beam benchmark problems developed in the seminal research by Yura (1993 and 2001) and vice versa. The cases considered include beam members with both full and partial lateral as well as nodal torsional bracing.
- Use of these 3D FEA tools to generate virtual test simulation load-deflection solutions for a large number of the benchmark problems provided in the seminal research by Yura (1993 and 2001). To the knowledge of the author, these are the first published load-deflection studies providing refined estimates of the brace forces due to geometric imperfections and stability effects for these benchmark problems. Yura and Phillips (1992) and Yura et al. (1992) have previously conducted a number of related experimental tests.
- Assessment of reduced bracing stiffness demands sufficient to develop column "fully braced" strengths (i.e., the strengths based on $K = 1$, or $KL_b = L_b$), due to inelastic stiffness reduction in the members being braced. The magnitude of the reduction in the stiffness demands due to these effects depends, of course, on the extent of yielding achieved in the members at the strength limit.

- Assessment of torsional bracing stiffness demands for various fundamental benchmarks originally developed by Yura (1993 and 2001), including the influence of member inelastic actions. Tran found that the AISC torsional bracing stiffness requirements were in some cases significantly conservative relative to the true requirements, but that the more refined torsional bracing stiffness requirements from which the AISC equations were developed generally provided accurate characterizations of the torsional bracing stiffness requirements for full bracing considering these benchmarks.
- Assessment of reduced bracing demands due to continuity effects in members having multiple intermediate nodal lateral brace points. Tran found good behavior using bracing stiffnesses in the order of one-half the most refined AISC Appendix 6 limits in various column and beam benchmarks of this type. In addition, he found that some reduction in the required stiffnesses was possible for cases with a single intermediate lateral brace, but the potential reductions in these cases were not as large.
- Assessment of reduced torsional bracing stiffness requirements due to light (possibly incidental) lateral bracing. Nodal lateral bracing stiffness values smaller than 10% of the most refined AISC Appendix 6 requirements were found to significantly reduce the stiffness and strength demands on the torsional braces. However, the studies were not sufficiently comprehensive to allow for the development of design rules.

- Validation of various column and beam plastic zone analysis virtual test simulation models against other prediction models as well as the results from physical tests.
- Demonstration of important differences between the physical response of geometrically-imperfect partially-inelastic members and common elastic analytical models of the members. Figure 1.3 shows a typical result from Tran (2009) using several different models for the weak-axis flexural-buckling resistance of a W14x90 column (F_y = 50 ksi) supported by four intermediate equal-stiffness discrete (nodal) braces spaced at a constant distance of L_b = 15 ft (L_b / r_y = 48.6). This plot shows the increase in the column strength with increases in the elastic brace stiffness. The brace stiffness β, normalized by L_b / P_e, is plotted on the horizontal axis, where $P_e = \pi^2 EI / L_b^2$ is the fully-braced elastic buckling resistance of the column. The column strength P_{max}, normalized by the fully-braced column elastic buckling resistance P_e, is plotted on the vertical axis. Several important observations can be made from this plot:
  1. Three different calculations predict essentially the same strength of the member for different values of brace stiffness:
     a. The AISC Direct Analysis Method (DM), where the member is modeled using a pseudo-elastic analysis with a reduced inelastic stiffness $0.8\tau_b EI_y$ and an out-of-straightness and out-of-alignment producing the largest potential destabilizing effect, and the maximum resistance is determined as the limit where the AISC beam-column interaction equation with $\phi_c P_n = 0.9P_y$ and $\phi_b M_n = 0.9M_{py}$ is first breached by the internal member forces.

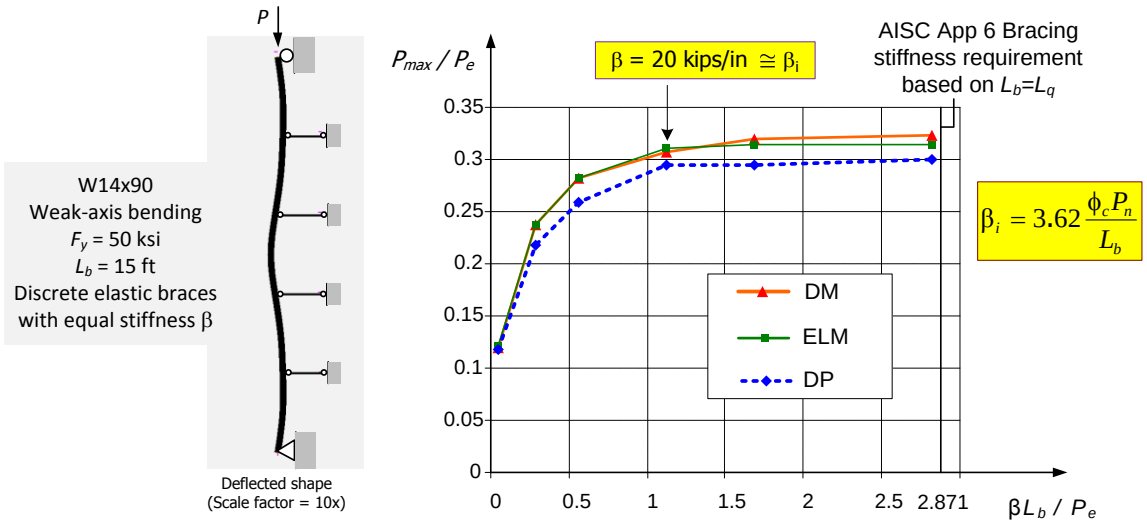

Fig. 1.3. Knuckle curves developed by Tran (2009) for the weak-axis flexural buckling of a W14x90 member restrained by discrete flexible braces.

b. The AISC Effective Length Method (ELM), but implemented using an "exact" inelastic buckling analysis of the column and its bracing system using a member flexural rigidity of $0.877\phi_c\tau_a EI$, where τ_a is the column inelastic stiffness reduction factor based directly on the AISC column strength curve.

c. A plastic zone or distributed plasticity (DP) virtual test simulation analysis in which nominal residual stresses are included in a full nonlinear FEA analysis of the geometrically imperfect column (with the same imperfections as in case (a) above), thus capturing the spread of plasticity through the cross-sections and along the member lengths.

2. The maximum strength is significantly smaller than the elastic buckling resistance, due to the effects of yielding.

3. The column deformations localize within the member's critical unbraced length at the strength limit.

4. The member reaches its maximum possible strength $\phi_c P_{n(K=1)}$ using $K = 1$, i.e., the strength associated with rigid bracing, for all practical purposes, at values of the bracing stiffness only slightly larger than the "ideal" bracing stiffness, taken as $\beta_i = 3.62\ \phi_c P_{n(K=1)}$. The AISC Appendix 6 provisions generally require a brace stiffness much larger than this limit. This is largely because they are based on developments from elastic stability analysis rather than considering the inelastic stability behavior of the system.
5. The member maximum strength generally decreases very gradually as the brace stiffness is reduced from large values approaching rigid bracing down to a particular limit, at or slightly less than $\beta = \beta_i$ in this example. At this limit, the strength then becomes sensitive to further reductions in the brace stiffness.

Various authors have observed the above type of behavior in different types of stability bracing problems, and the curves shown in Fig. 1.3 are often referred to as "knuckle" curves, the name originally coined by Horne and Grayson (1983). These curves highlight the changes in the system strength with changes in the brace or general restraint stiffness. The types of curves shown in Fig. 1.3, along with curves indicating the brace forces at the strength limit as a function of the brace stiffness, provide arguably the most direct assessment of general stability bracing effectiveness. As such, this research focuses much of its attention on the development of knuckle curves for complex bracing configurations in metal building frames.

Knuckle curves are often used to determine the restraint stiffness necessary to achieve a certain percentage of the rigidly-braced strength of the member or structural system, i.e., the strength attained if all the brace points are constrained to have zero lateral dis-

placement. Stanway et al. (1992b) suggest that a bracing stiffness sufficient to develop 90 % of the rigidly-braced structural resistance is a reasonable criterion for bracing design. However, the jury is still out on the most appropriate definition of the "knuckle value."

In many situations, the system strength behavior is insensitive to changes in the bracing stiffness. For such cases, the braces can be designed for a lower stiffness demand without affecting the strength of the system. The knuckle curves identify when the changes in the brace stiffness start to have a substantial impact on the system strength.

1.2 Research Objectives and Goals

The main objective of this research is to evaluate the strength and stiffness demands on the flange bracing for a range of representative metal building members and frames. These demands are investigated using refined full-nonlinear shell finite element analysis capabilities implemented in the ABAQUS 6.9 (Simulia 2009) software system. The associated analysis models are sufficient to fully capture all of the limit states associated with the stability bracing strength and stiffness requirements as well as the member strength behavior, given the input of proper boundary conditions, initial residual stresses and initial geometric imperfections. As such, they are referred to here as virtual test simulation models. Whereas Tran (2009) focused predominantly on the bracing demands for various isolated column and beam members, this research focuses predominantly on the evaluation of the flange bracing behavior for entire framing systems. Furthermore, whereas Tran (2009) considered both simplified elastic analysis models as well as refined inelastic virtual test simulations, this research focuses predominantly on the use of refined virtual test simulation capabilities, referred to by Tran as plastic zone shell finite element procedures, for the development of benchmark solutions.

Appendix 1 of the 2010 AISC Specification provides new detailed guidelines for the use of refined inelastic analysis to assess the design strength of steel structures. The

development of the virtual test simulation models in this research is largely based on this guidance, and involves the application of the plastic zone shell finite element models employed by Tran (2009) as well as by Kim (2010). When conducted properly, virtual test simulation can serve as a valuable companion to experimental testing since attributes such as residual stresses and critical geometric imperfections can be controlled precisely and with relative ease in a virtual test simulation.

The ultimate objectives of this research are to provide:

1. A much clearer understanding of the actual demands on flange braces in metal building systems, and
2. Recommendations for improved accuracy, safety, economy and simplicity in the design of metal building flange bracing systems.

In this research, special emphasis is placed on the unique attributes of the flange bracing design in metal building frames discussed in the previous section. In summary, these attributes include:

1. Tapered webs and other non-prismatic geometries;
2. Combined axial load and bending moment;
3. Variation in axial force and bending moment along the member lengths;
4. Unequal brace spacing;
5. Unequal brace stiffnesses;
6. Member end conditions in which effective rigid restraint of the lateral displacements and twist rotations may not exist;
7. Complex interactions between the separate members and between the members and the various bracing components at knee joints;
8. Member continuity and end lateral bending and/or warping restraint effects, particularly in cases involving larger numbers of intermediate braces ;

9. Differences in brace strength and stiffness demands at different brace points along the length of members containing multiple braces; and
10. Beneficial interactions between (or combined effects of) various types of bracing.

A sub-objective of this research is the investigation and demonstration of how virtual test simulation can be applied to solve a structural engineering research problem that would be difficult to address by any other means. Appendix 1 of the AISC Specification allows the use of virtual test simulation to design a structure if the analysis takes into account initial geometric imperfections and the spread of yielding including the effects of initial residual stresses.

The specific goals of this research are as follows:

- Investigate the influence of a range of geometric conditions on the bracing requirements for metal building members and framing systems, with emphasis on gaining a better understanding of the system response.
- Investigate the effect of using significantly different bracing stiffnesses than estimated by Appendix 6 type calculations for typical metal building frames.
- Assess the influence of unequal brace spacing on brace force requirements.
- Investigate the influence of combined lateral and torsional bracing in typical metal building structural systems.
- Investigate the effect of unequal torsional brace stiffness on system behavior and brace force requirements.
- Investigate the brace strength and brace stiffness requirements at locations away from critical regions.
- Assess the influence of the stiffness contributions from typical roof and wall diaphragms toward the enhancement of overall system stability.

As noted at the beginning of this chapter, stability bracing strictly is not subjected to any forces other than those coming from the member forces acting through amplified

member geometric imperfections. This is the definition of stability bracing adopted in Appendix 6 of the AISC Specification. However, also strictly speaking, there are no physical structural components that completely fit this definition. For example, diagonal braces from girts or purlins to the inside flange of a metal building frame are subjected to axial forces coming from snow, wind and other applied loadings on the roof system. The girts and purlins are of course deformed in bending by these same loads. In addition, wall or roof X-bracing systems, possibly supplemented with the shear resistance from wall or roof structural panels, provide a primary function of transferring wind or seismic longitudinal forces to the building foundation. However, as discussed in Chapter 2, the wall and roof panels also serve to develop girt and/or purlin locations as brace points on the outside flanges. With the exception of brief discussions of combined primary (applied load) and secondary (stability bracing) effects in Chapter 2, this research focuses only on the determination of stability bracing forces and stiffness requirements.

1.3 Organization

This study is organized into nine chapters. Chapter 2 gives an overview of some of the key literature on stability bracing and reviews key background information. Chapter 3 discusses the detailed implementation of the virtual test simulation capabilities employed in this research. Chapters 4 through 8 then introduce specific case study problems, present virtual test simulation results for these problems, and evaluate the design implications of the findings from these tests. Chapter 4 addresses a roof girder example, Chapter 5 presents a sidewall column example, and Chapters 6 to 8 study several representative metal building frames. Finally, Chapter 9 summarizes the findings of this research and provides recommendations for further work.

CHAPTER 2

BACKGROUND

This chapter presents essential background information on bracing requirements for columns and beams and discusses key results from previous research on column and beam bracing. Section 2.1 first gives a broad overview of different types of bracing and summarizes key associated modeling idealizations. Sections 2.2 and 2.3 then focus on important fundamentals for the two types of column bracing addressed in the AISC Specification Appendix 6, relative and nodal column bracing. These discussions are important to the consideration of flange bracing in metal building systems first because metal building members are generally subjected to axial loads and must be braced sufficiently to develop the member axial resistances. Furthermore, the lateral bracing of beams is commonly handled as an extrapolation from column stability bracing solutions, by treating the beam compression flange as an equivalent column. Section 2.4 concludes the discussion of column bracing by highlighting the key differences between column relative and nodal bracing.

Section 2.5 addresses additional fundamental beam bracing requirements, with emphasis on beam torsional bracing. This is followed by Section 2.6, which summarizes the specific 2010 AISC Appendix 6 bracing rules including substantial refinements provided in the Appendix 6 commentary. Many engineers struggle with including the various commentary refinements to the bracing rules. Therefore, the reader may find these summaries to be a useful guide for applying the AISC commentary refinements. The chapter closes by detailing one example application of the AISC Appendix 6 requirements to various non-Appendix 6 considerations in a representative clear span

metal building frame in Section 2.7, and by outlining one potential simplification of the AISC bracing rules in Section 2.8. Both the application of the AISC bracing requirements as well as these simplified rules are scrutinized in the subsequent chapters.

2.1 Bracing Types

Stability braces are used to increase the buckling strength of structural members and framing systems. An adequate bracing system requires sufficient brace stiffness in addition to sufficient brace strength. The purpose of the strength requirement is to provide essential stabilizing forces. The purpose of the stiffness requirement is to limit the displacement of the braced member or structure at the brace points, and thus limit the second-order amplification of the internal brace and member forces and the potential reduction in the member strength due to brace point movement.

Substantial prior research has been conducted to investigate bracing design requirements for elastic and inelastic members. Much of this research has culminated in the work by Yura (1993, 1995, 2001). The bracing requirements for beams and columns discussed in Appendix 6 of the AISC 2005 and 2010 Specifications are largely due to these advances. Discussions of the basic types of bracing can be found in Yura (1993 and 1995), Yura and Helwig (1999), Galambos (1998), Griffis and White (2011), Trahair and Nethercot (1982) and Ziemian (2010). The following explanations are intended to highlight the key characteristics of these bracing types.

Bracing systems are commonly categorized into four types: relative, nodal, continuous and lean-on. Figure 2.1 shows simple illustrations of these four categories for columns. In the view of the author, *relative bracing* should be named more clearly as *shear panel bracing*. This type of bracing is provided by tying the member being braced

to a diaphragm panel, or to the panel points of an X-bracing system, at selected brace locations. In the underlying relative bracing model, the member being braced is represented generally as a set of pin-connected struts forming a bar chain. The bar chain is connected to the bracing panels at each of the brace points, and the stiffness of the bracing system is the shear stiffness of the bracing panels. The bracing resistance is provided by the resistance of the shear panels to the *relative* lateral movement of the brace points.

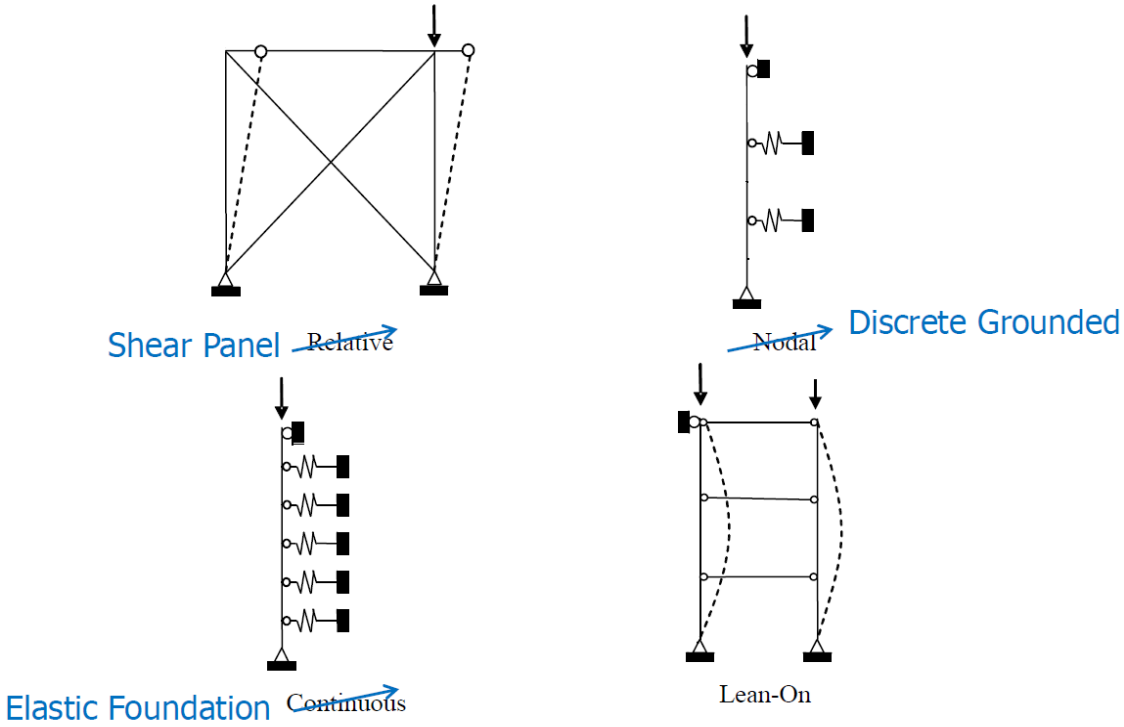

Fig. 2.1. Types of column bracing.

Nodal bracing can be named alternately as *discrete grounded bracing*. That is, nodal bracing models usually assume that equal stiffness discrete grounded springs are attached at equal spacing to a *continuous* elastic or inelastic column that is being braced. The column is modeled using either its elastic or inelastic flexural rigidity, EI or τEI. The brace springs are assumed to be grounded to a massive fixed (immovable) object. As

noted in Chapter 1, it is difficult generally to achieve equal-stiffness lateral bracing for systems that have more than two intermediate nodal braces. However, beam torsional bracing systems do match with the equal-stiffness assumption, when the torsional bracing is provided by the same size girt or purlin and the same flange diagonals at each of the brace points, and the member depth is the same at each of the brace points. Various approximate solutions of the general nodal bracing model are discussed subsequently in Section 2.1.1.

Nodal bracing effectively becomes *continuous bracing* in the limit that the number of braces approaches infinity. However, similar to the situation noted above for nodal bracing systems, it is often difficult to match the continuous bracing model to conditions in the field except for some types of torsional bracing. Timoshenko and Gere (1963) summarize the solution for the elastic buckling of a column braced continuously by an elastic foundation. They indicate that this solution also may be applied to discrete elastic bracing with good accuracy as long as there are at least three lateral supports per half-length of the buckled bar (or basically two lateral braces inside each half-length of the buckling waves and one lateral brace at the inflection points between the half-lengths). Timoshenko and Gere cite the problem of the buckling of railway rails under thermal loading as one application of this solution. They also summarize the solution for elastic buckling of a bar on an elastic foundation subjected to distributed axial loads. They show that this solution may be used to estimate the lateral buckling load of a prismatic top chord of a through truss braced by equal-stiffness, equally-spaced verticals and diagonals. They cite several references where this approach has been extended to evaluate chords of variable cross-section with varying rigidities of the elastic supports along the length.

Yura et al. (1992) have developed closed-form equations for the elastic lateral-torsional buckling of I-section beam members with:

- Torsionally simply-supported (fork) end conditions, but otherwise rigidly restrained against twist and lateral displacement at their ends, and
- Continuous lateral, continuous torsional, or combined continuous lateral and torsional bracing along the beam length.

They use these solutions to solve for the elastic buckling load of members with multiple intermediate equally-spaced equal-stiffness discrete braces by mapping the discrete braces to the equivalent continuous bracing model using the tributary length between the braces. For beams with a single intermediate brace, they show with one exception that the equivalent continuous brace stiffness can be estimated by dividing the lateral or torsional brace stiffness of the single brace by 75 % of the total beam length. The exception is for a single torsional brace and top-flange loading, where they divide the single brace stiffness by the total length.

Many types of bracing often considered as nodal or continuous are actually a better fit to the *lean-on bracing* model. One example of lean-on bracing, shown in Fig. 2.1, is the case of two equal size columns tied together at selected heights by horizontal struts. If one of these columns is subjected to larger axial load than the other, it cannot generally buckle laterally at its critical load without bending the other member. Compatibility of the lateral displacements is maintained between the two columns by the horizontal struts. Therefore, the column with the larger axial load *leans* against the other column, and the critical load of the system is not achieved until the combined loads on the two columns reach an overall system lateral buckling load level. This buckling load may be

approximated as the sum of the two column buckling loads calculated separately. Lean-on bracing occurs effectively whenever one member is tied to another member or component that flexes along with the member in its buckling mode. The flexural stiffness of the less critical member or component provides additional buckling strength to the system. As noted in Section 1.1, lean-on bracing idealizations typically do not consider any member shear flexibility.

The AISC Specification Appendix 6 specifically addresses basic relative, nodal and continuous bracing requirements for columns and beams. It does not explicitly address lean-on bracing. However, lean-on bracing effects can be captured via a proper second-order load-deflection analysis to determine the member and component force requirements, as well as via an eigenvalue buckling analysis to determine the system buckling load.

The Appendix 6 provisions address various relative and nodal bracing requirements. Therefore, a number of details of the relative and nodal bracing idealizations are discussed in more detail below for several basic column cases. Beam bracing requirements are discussed after that.

In general, the following statements can be made about the different types of bracing encountered in practice:

- Some bracing elements predominantly prevent only relative movement between adjacent brace points (effectively they act as shear springs, i.e., they act as relative bracing).
- Some bracing elements resist predominantly the absolute lateral deflection or twisting at a brace point relative to ideal fixed (grounded) locations (effectively,

they act as axial or torsional springs, i.e., they act as lateral or torsional nodal bracing).

- Some bracing elements tie one member to other members so that the group of members cannot fail laterally without buckling together (effectively, they act as lean-on bracing).
- In many situations, bracing systems can possess certain attributes of all three of the above types of bracing.

2.2 Fundamental Column Relative Bracing Requirements

2.2.1 Column Relative Bracing Analysis Models

The analysis model required by the AISC (2010) Chapter C Direct Analysis Method of design (referred to subsequently as the DM) can be used to determine an accurate estimate of the demands on column relative (shear panel) braces (Griffis and White 2011). Section A6.1 of the AISC Specification states, "A second-order analysis that includes an initial out-of-straightness of the member to obtain brace strength and stiffness [including out-of-alignment of the brace points] is permitted in lieu of the requirements of this appendix." The DM analysis model satisfies these requirements.

The general application of the DM to stability bracing design entails:

1. A base reduction of all the elastic stiffnesses by the factor 0.8, as well as
2. An initial out-of-alignment within the unbraced lengths of $\Delta_o = 0.002L$, and
3. An initial out-of-straightness within the unbraced lengths of $\delta_o = 0.001L$

where L is the unbraced length. The 0.8 stiffness reduction accounts for the combined consideration of:

1. The softening that occurs in any structure due to the onset and spread of yielding as the strength limit is approached, as well as
2. The uncertainty in estimating the structure stiffness at the strength limit.

The out-of-alignment of $\Delta_o = 0.002L$ and the out-of-straightness of $\delta_o = 0.001L$ are the base maximum geometric imperfection tolerances specified for columns in the AISC (2010) Code of Standard Practice.

It should be recognized that the analysis model specified by the DM is intended as a simple but coarse approximation of a rigorous virtual test simulation analysis. The more rigorous virtual test simulation models have been commonly referred to in the literature as "refined inelastic," "plastic zone," "spread of plasticity," and "advanced" analysis models. One can say that the analysis model of the DM is simply a "poor person's plastic zone analysis." With the increasing robustness and capabilities of analysis tools readily available to the design engineer, it is expected that the more rigorous tools will see greater usage. This is particularly true with respect to limit states such as column torsional-flexural buckling and/or beam lateral-torsional buckling, where ordinary frame analysis methods typically do not provide an accurate characterization of even the elastic stiffness of the structure (e.g., consider the use of only the member torsional rigidity of only GJ in ordinary frame analysis models, completely neglecting the contributions from warping rigidity EC_w). Refined inelastic analysis procedures give the engineer the ability to make a rigorous assessment of the bracing requirements pertaining to torsional-flexural and lateral-torsional buckling limit states.

Appendix 1 of the 2010 AISC Specification addresses the application of these more rigorous analysis models for design. Basically, the geometric imperfection modeling

requirements of Appendix 1 are the same as those for a DM analysis, but given that the effect of yielding on the structural response is represented precisely, the elastic stiffnesses are reduced only by a factor of 0.9. In addition, the yield strengths are factored by 0.9 in the Appendix 1 rules for distributed plasticity analysis, similar to the factoring of the column, beam and beam-column resistances in the DM. These 0.9 factors are intended to account for uncertainty in stiffness and strength under ultimate strength conditions, and are equivalent to the use of $\phi = 0.9$ in steel member design.

For the assessment of column flexural buckling related limit states such as discussed in the following sections, the DM provides a sufficient characterization of the response. The next section focuses on the application of the DM to relative column bracing problems.

2.2.2 Explicit Second-Order Analysis Solution for Relative Bracing

Figure 2.2 shows the basic column and shear panel idealization for determining the demands on column relative bracing per the 2010 AISC Specification. As noted previously, pins are inserted at each of the brace points in this analysis model, and the idealized imperfect (misaligned) column is stabilized by a bracing system panel idealized as a shear spring with a nominal elastic stiffness β, or with a reduced elastic stiffness $\overline{\beta} = 0.8\beta$ in the DM analysis model. Since the generalized column is pinned at all the brace points, the consideration of column out-of-straightness in the model is not necessary. By placing the pins at the brace points, the buckling of the column between the brace points, and the lateral sidesway buckling of the column and its bracing system (associated with lateral displacement of the brace points), are completely decoupled. The second-order

analysis solution for this problem via the DM analysis model can be expressed with relative ease using the equation (Griffis and White 2011):

$$\overline{V}_{br} = \Sigma P \left(\frac{1}{1 - \frac{\alpha \Sigma P / L}{\overline{\beta}}} \right) \frac{\Delta_o}{L} \tag{2-1}$$

where

$\overline{V}_{br}$ = Required bracing shear force for a given total column axial load ΣP in the column or columns being braced. The over-bar is included on this variable and all other variables that are influenced by the 0.8 stiffness reduction of the DM.

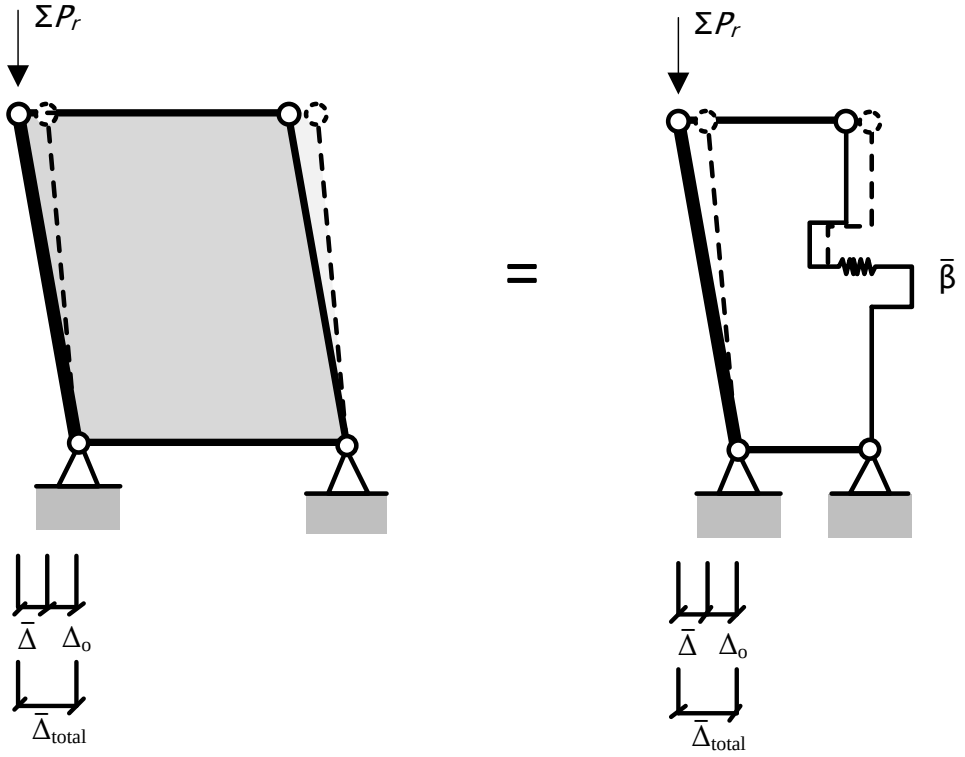

Fig. 2.2. Basic column and shear panel analysis model for determining the demands on column relative bracing.

ΣP = Generalized axial force applied to the column or columns being braced. The relative bracing model applies to any set of columns that are rigidly connected to the shear panel (i.e., a panel of a truss, a shear diaphragm panel, etc.) at the brace points. In this general case, ΣP is the summation of all the axial loads in the columns stabilized by the bracing system.

α = Factor to convert the loading to the ultimate strength load level, taken equal to 1.6 for ASD and 1.0 for LRFD. For a general second-order analysis, one must factor up the ASD loads by multiplying by $\alpha = 1.6$, perform the analysis of the structure, and then factor down the corresponding internal forces by dividing by $\alpha = 1.6$. However, in the final algebraic form of Eq. (2-1), the multiplication and division by $\alpha = 1.6$ on the first term cancels out, leaving the only occurrence of α inside of the second-order amplifier shown in brackets in the equation.

L = Unbraced length between the brace points.

$\overline{\beta}$ = Reduced elastic stiffness of the shear panel, taken equal to 0.8 of the nominal shear stiffness for the DM analysis solution.

Δ_o = Initial out-of-alignment (i.e., out-of-plumbness) of the unbraced length under consideration.

In the limit that $\Sigma P = \Sigma P_r$, where ΣP_r is the total required axial load supported by the generalized column and stabilized by the bracing system, one obtains the required bracing shear force. This force must be developed by the bracing system shear panel.

Equation (2-1) is an exact solution for the idealized theoretical model shown in Fig. 2.2. It should be noted that this equation can be written succinctly as the P-Δ shear force in the loaded configuration

$$\overline{V}_{br} = \Sigma P \frac{\overline{\Delta}_{total}}{L} \tag{2-2}$$

where

$$\overline{\Delta}_{total} = \left(\frac{1}{1 - \frac{\alpha \Sigma P / L}{\overline{\beta}}} \right) \Delta_o \tag{2-3}$$

is the total second-order shear displacement of the panel in the ultimate strength loading condition. The brace point movement relative to the initial zero-load imperfect geometry is ($\overline{\Delta}_{total} - \Delta_o$), which produces a force in the shear panel of $\overline{V}_{br} = \overline{\beta}\left(\overline{\Delta}_{total} - \Delta_o\right)$.

Griffis and White (2011) generalize the above equation to also include the influence of non-zero primary (applied lateral) forces in the bracing system. However, such bracing systems are "general" bracing systems rather than stability bracing systems. The focus in this research is on stability bracing. In the general case, Δ_o in Eq. (2-3) may be replaced by ($\Delta_o + \overline{\Delta}_1$), where $\overline{\Delta}_1$ is the first-order relative "sidesway" deflection between the ends of the unbraced length due to the applied loads on the structure, calculated at the ultimate load level on the ideal geometrically perfect structure using the reduced elastic stiffness. In other words, the bracing deformation is obtained by summing the initial imperfection and the additional first-order deflection due to the applied loads on the reduced stiffness model, but then also amplifying both of these displacements to account for the second-order (stability) effects. The bracing force is then generally equal to the bracing stiffness

multiplied by this second-order displacement. It should be emphasized that one cannot just add the stability bracing forces (obtained by the stability bracing equations) to the first-order forces calculated in the bracing system. The first-order forces in the bracing system, due to the applied loads on the structure, also have to be amplified to account for the second-order effects.

Interestingly, for columns with multiple intermediate relative braces, such as the example shown in Fig. 2.3, the above Eq. (2-1) is still an exact solution for each of the individual shear panels and unbraced lengths, assuming that the idealization is still one in which pins are inserted in the column model at each of the brace points so that there is no continuity of the idealized column(s) through the brace points. It can be shown that each of these unbraced lengths and their corresponding shear-panels act independently of one another. That is, they each behave as self-contained, self-equilibrating assemblies. As such, the free-body diagrams of each of the individual unbraced lengths and their corresponding shear springs do not include any lateral force transfer from one unbraced length to the next. The lateral force transfer between adjacent segments must be zero at any of the pins, since if a single cut is made at any pin and a free-body diagram is drawn for the full structure above or below this point, the lateral (shear) force at the cut must be zero for total horizontal equilibrium. Therefore:

1. The stability of each segment is independent of the other unbraced lengths.
2. The only attributes causing demands on the shear spring at any given level are:
    a. The total axial load transferred in the column(s) through that level, and
    b. The out-of-alignment of the column(s) within that level.

3. The shape of the imperfection pattern, e.g., whether it is a zig-zag or a uniform out-of-plumbness, does not influence the bracing behavior.

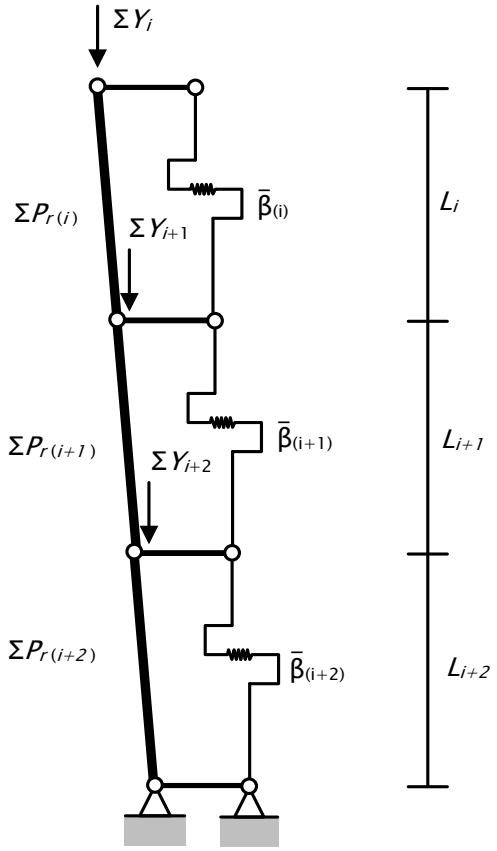

Fig. 2.3. Relative bracing model for a column with multiple relative braces along its length.

It should be noted that the above relative bracing model does not include any overall overturning flexibility. Therefore, any build-up of overturning moment due to, for example, out-of-plumbness of the stories above a given level under consideration, does not have any impact on the response. The overturning in each story is equilibrated by a force in the shear spring at that story. The shear panels are assumed effectively to have rigid boundary elements and the overall rigid body rotation of the edges of the panels perpendicular to the member being braced are assumed to be prevented, as shown in Fig. 2.4.

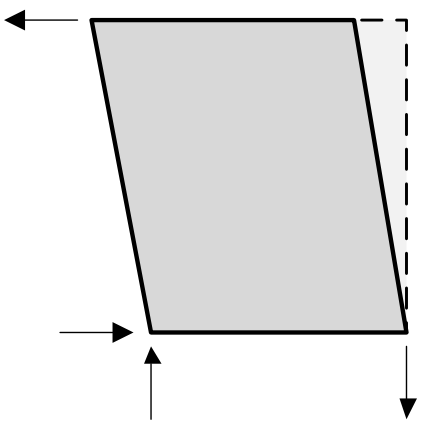

Fig. 2.4. Shear panel kinematics and free-body diagram.

One can build a simple second-order matrix analysis model to demonstrate the above attributes. The column segments and the horizontal struts in Fig. 2.3 can be modeled using truss elements. The individual shear springs can be modeled using Euler-Bernoulli beam elements with their nodes fully restrained against rotation at each of the braced positions. The rigidity of these beam elements, EI_i, is set such that the transverse shear beam stiffness term, $12EI_i/L^3$, is equal to the desired value of $\overline{\beta}_i$.

It is interesting to note that if the system in Fig. 2.3 is restrained by an additional (possibly much stiffer) relative bracing system between its top and bottom, the additional system can be represented by another shear spring between the bottom and top of the model parallel to the other three shear springs that are tied together in series (see Fig. 2.5). For a general load case, the additional shear spring enhances the buckling response of the overall system shown in the figure. However, in the limit that:

- ΣY_{i+1} and ΣY_{i+2} are zero such that the internal axial force is constant along the three unbraced lengths, $\Sigma P_{r(i)} = \Sigma P_{r(i+1)} = \Sigma P_{r(i+2)} = \Sigma Y_i$,
- All of the shear panel lengths L_i, L_{i+1} and L_{i+2} are the same, and

- All of the shear panel stiffnesses are the same, i.e., $\overline{\beta}_{(i)} = \overline{\beta}_{(i+1)} = \overline{\beta}_{(i+2)}$

all of the intermediate shear panels are equally critical, and thus the system buckling load is the same, equal to the buckling load of the system in Fig. 2.3, regardless of the stiffness of the additional shear spring. Also, it is interesting to note that, given the above attributes, the system buckling load is independent of the number of unbraced lengths. That is, the overall length of the system could be extended to include any number of the lengths L_i without changing the buckling resistance of the system.

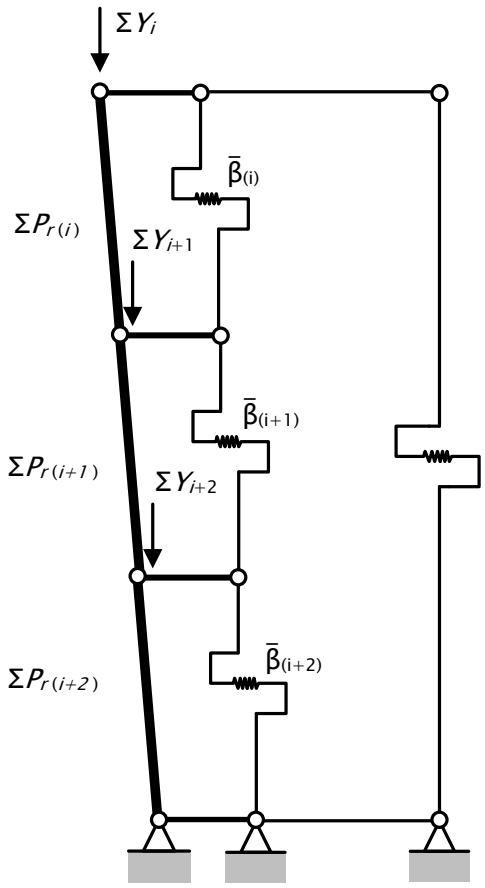

Fig. 2.5. Basic column and shear panel analysis model for a column with two relative bracing systems in parallel.

The model in Fig. 2.5 is akin to the relative bracing of a column by X bracing at "hard" brace points combined with "soft" bracing by tying the column to wall or roof

shear panels via the girts or purlins at other intermediate brace locations. The additional bracing placed in parallel with the other braces reduces the overall lateral displacement in the imperfect structural system, but it does not affect the overall buckling load of the column and its bracing system in the limit that all the intermediate panels are equally critical. The buckling behavior of the idealized system involves multiple buckling modes that all have the same eigenvalue buckling load. Interestingly, this is close to the physical response for a group of adjacent shear panels or unbraced lengths in many (but not all) practical situations.

If the ratio $\Sigma P_{r(i)} / L_i \overline{\beta}_{(i)}$, varies among the different unbraced lengths in Fig. 2.5, then the buckling load is increased by the additional shear spring. One should note that this is yet another situation where a basic bracing model of the AISC Specification Appendix 6 provides a conservative prediction of the more detailed structural system behavior.

Since the relative bracing system behavior is often such that the bracing panels are almost equally critical, at least for a few adjacent panels, it is useful to focus on the model of an individual panel as shown in Fig. 2.2 for assessment of the essential relative bracing responses. Thus, the following discussions focus solely on the relative bracing model for an individual unbraced length, as shown in Fig. 2.2.

One should note that the provision of the X-bracing system parallel to the wall or roof panels is often essential to provide a sufficient load path for transfer of any longitudinal forces on the structure to the foundations, i.e., assuming that the wall or roof panels are not sufficient to transfer these forces on their own. Also, the X bracing is often essential to restrict the overall longitudinal deflections in the structure to tolerable limits. However, with respect to the typical stability bracing behavior and the development of the girt or

purlin locations as brace points, the response is dominated by the wall and roof diaphragm panels.

2.2.3 Ideal versus Required Relative Bracing Stiffnesses

The ideal bracing stiffness (β_i) is defined as the stiffness at which lateral buckling would occur for a bracing system supporting a perfectly plumb column subjected to an axial load $\alpha\Sigma P_r$, where ΣP_r is the required total axial load (ASD or LRFD) and α is the factor to convert these loads to the ultimate strength load level (1.6 for ASD and 1.0 for LRFD). If the provided stiffness ($\overline{\beta}_{act}$) is equal to the ideal bracing stiffness, the second-order amplification of the bracing panel shear displacement and shear force becomes unbounded as the required total axial load level ΣP_r is approached.

Note that the variable $\overline{\beta}_{act}$ has been substituted here for $\overline{\beta}$. This is simply to emphasize that this is the "actual" or "provided" stiffness. It is important also to note that in the previous discussions, the subscripts (i), (i+1), etc. denote a given shear panel, unbraced length or story level. However, the subscript i, without parentheses, generally denotes the *ideal* bracing stiffness.

Therefore, one can observe from Eqs. (2-1) or (2-3) that

$$\beta_i = \frac{\alpha\Sigma P_r}{L} \tag{2-4}$$

for the basic relative bracing model. It is important to note that the ideal bracing stiffness is given by Eq. (2-4) also for the column with intermediate brace points in Fig. 2.3, and that this equation typically gives an accurate to conservative estimate of the ideal bracing stiffness for the column in Fig. 2.5.

Unfortunately, the above ideal bracing stiffness is not adequate for any relative bracing system having unavoidable geometric imperfections. Figure 2.6 shows the variation of the shear panel bracing force versus the normalized column axial load level, obtained from Eq. (2-1), for three different bracing stiffness values, $\bar{\beta}_{act} = \beta_i, 2\beta_i$, and $3\beta_i$. One can observe that $\bar{\beta}_{act} = \beta_i$, is actually not ideal at all; the bracing system will fail before the required column strength is developed if the system has a stiffness only equal to this value. Generally, as the provided relative bracing stiffness increases, the overall second-order amplification of the responses, and specifically the second-order shear panel displacement and internal shear force become smaller. This can be observed directly from Eq. (2-1).

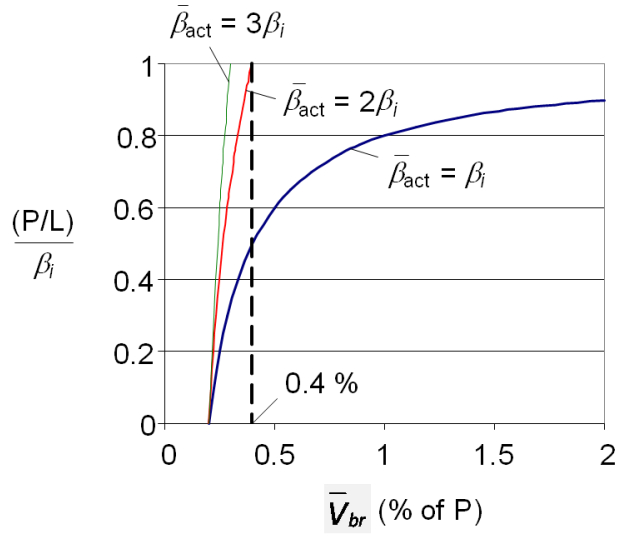

Fig. 2.6. Shear panel bracing force versus the axial load level for three different brace stiffnesses.

AISC Appendix 6 effectively recommends that the provided brace stiffness should be at least $2.0/\phi = 2.0/0.75 = 2.67$ times the ideal brace stiffness for design by LRFD and $2.0\Omega/\alpha = 2.5$ times the ideal brace stiffness for design by ASD. However, the Specification implicitly allows the use of smaller brace stiffness values when the strength

and stiffness demands are based on an explicit second-order analysis. For $\Delta_o = 0.002L$, and when the reduced elastic stiffness is $\overline{\beta}_{act} = 1.25\beta_i$ (or when $\beta_{act} = \overline{\beta}_{act}/0.8 = 1.56\beta_i$), a shear panel bracing force of $0.01P_r$ and a second-order amplification of 5.0 are obtained in the reduced stiffness model of Eqs. (2-1) through (2-3), That is, if one is willing to design the shear panel bracing for 1 % of the column axial force, the DM shows that the idealized relative bracing model gives acceptable structural performance if the shear panel stiffness is only $1.56\beta_i$. This is only 58 % of the AISC Appendix 6 LRFD relative bracing stiffness requirement or 62 % of the Appendix 6 ASD relative bracing stiffness requirement. However, the resulting second-order amplification factor of 5.0 means that the idealized bracing system response will be very sensitive to minor changes in the bracing stiffness or in the column axial load at the corresponding strength limit.

2.2.4 Clarification of Important Attributes of the AISC Column Relative Bracing Equations

The 2010 AISC column relative bracing equations have several attributes that can be potentially confusing or misleading. The following discussions are intended to clarify the key concepts:

1. The bracing strength demand is a *transverse shear* force normal to the axis of the member or members being braced, developed in the shear panel (or panels) resisting the relative moment of any two adjacent brace points. To emphasize this important fact, the term V_{br} is used for the strength requirement in this work.
2. For relative (shear panel) bracing of multiple columns, the column axial load in the relative bracing equations should be the summation of all the column axial loads stabilized by the shear panel. To emphasize this important fact, this report

uses ΣP_r to represent the total column axial loads for the columns being stabilized.

3. When considering bracing of multiple columns, the net destabilizing effect is equal to the total ΣP_r acting through a weighted average Δ_o of all the columns. The AISC Specification allows the engineer to relax the out-of-alignment tolerance to values less than $0.002L$ when it can be justified that the actual weighted average out-of-alignment is smaller than this base value. However, for routine design, it is commonly assumed that all the columns are out-of-plumb (or mis-aligned) by $0.002L$ in the same direction for calculating the brace strength demands. This is one additional source of conservatism in the ordinary application of the AISC Appendix 6 bracing equations.

   It should be noted that the above comments are based on the assumption of zero slip or other connection deformations required to engage the relative bracing system. Situations where deformations may be required to engage the bracing may be addressed by adding the expected "slip" displacement to the above $0.002L$ imperfection. As discussed in the 2010 AISC commentary, bracing strength requirements generally may be assumed to vary in proportion to the assumed initial imperfection. This assumption is exact for the relative bracing model, but in addition, it is a reasonable approximation for nodal lateral and torsional bracing.

4. The relative bracing stiffness and strength requirements are *per tier* or *per panel shear* requirements. *They do not correspond to the total force that must be transferred from a given brace point.* In the simple case of a column with a single mid-span brace point, the total lateral force transferred from the column to the

bracing system is equal to two times the shear force taken by each of the bracing panels.

2.2.5 Influence of Column Continuity through the Brace Points

The astute reader will note that columns are often continuous through the individual brace points, rather than being perfectly pin-connected at these locations. Furthermore, at the column ends, there is often some rotational restraint (incidental or by design) provided by the building foundation or by other framing. Tran (2009) analyzes the influence of column flexural continuity through the brace points for a number of practical example problems. The justification for the AISC model of using perfect pins at the brace points for calculation of the relative bracing demands is the fact that, in many situations, the brace stiffness dominates and the additional help from the flexural continuity of the member, or the rotational end restraint provided to the member, is somewhat small. In addition, the pin idealization allows for a very simple analysis of the relative bracing behavior. However, the member continuity and end restraint effects can provide a significant benefit in some cases.

It should be noted that the Direct Analysis Method (the DM) analysis model itself says nothing about placing pins at the various brace points for the analysis of stability bracing response. The insertion of pins at the brace points is a separate idealization that simplifies the assessment of the stability bracing behavior. In fact, if one is conducting an explicit second-order analysis of a number of members and their relative bracing system, it is often simpler from a modeling perspective to include the continuity of the columns through the brace points rather than to insert pins at all of the braces. The continuity of the columns, any end rotational restraint, and any additional parallel relative bracing

systems such as the one shown in Fig. 2.5, all result in coupling of the various unbraced lengths. This leads generally to the need to consider: (1) the shape of the out-of-alignment imperfections, (2) the out-of-straightness of the columns between the brace points, and (3) greater complexity in the assessment of the stability bracing response.

2.3 Fundamental Column Nodal (Discrete Grounded) Bracing Requirements

2.3.1 Column Nodal Bracing Models

Nodal bracing problems also can be analyzed using the analysis requirements specified by the Direct Analysis Method. However, as outlined in Section 2.1, the braces are modeled as "discrete grounded springs" and the continuity of the column through the brace points is explicitly considered in the AISC nodal bracing models. The "discrete grounded" nature of the bracing springs and the continuity of the column through the brace point locations cause some fundamental differences in both the structural behavior and the analysis requirements. Regarding the structural behavior, the column continuity can lead to substantial coupling between the responses of the different unbraced lengths. With respect to the analysis requirements, the following differences exist for nodally braced members, compared to the prior idealization of members braced by shear panels:

1. The flexural rigidity of the column ($\tau_b EI$) needs to be considered,
2. The proper pattern must be selected for the initial geometric imperfections (the proper pattern, according AISC (2010) Chapter C, Section C2.2a, is the one that maximizes the destabilizing effects).

Otherwise, the requirements are effectively the same as in the relative bracing model.

To satisfy the above requirements, the nominal maximum out-of-alignment in any unbraced length is still $0.002L_b$, where L_b is the unbraced length. However, the direction

of the initial out-of-alignment of each unbraced length must be selected in general to produce the maximum destabilizing effect. For very stiff bracing approximately equal to or exceeding the full-bracing stiffness (defined below), a zig-zag pattern tends to be the most critical (although the local out-of-alignment of a single brace produces essentially the same maximum force at that brace). For very soft bracing approaching zero stiffness, the direction of the initial out-of-alignment should be affine to the direction of the movement in each panel associated with the buckling of the member having zero intermediate bracing.

It is important to note in general that rigid end brace points, if and when they are assumed, should not necessarily be specified with zero initial imperfections. These points should be moved laterally to accommodate the orientations of the out-of-alignment in each of the unbraced lengths in order to maximize the potential overall destabilizing effects.

In addition, as noted in the discussion of relative bracing, a general virtual test simulation method (a plastic zone analysis, spread of plasticity analysis, etc.) can be employed in lieu of analyzing the structure by the DM. For purposes of design using a plastic zone analysis, the 2010 AISC Appendix 1 requires a factor of 0.9 on the strength and stiffness terms ($0.9F_y$ and $0.9E$). Additionally, it requires that the proper initial geometric imperfection be applied to the structure. This imperfection is typically the same as the one that would be selected for the DM analysis model. As stated previously in Section 2.2.1, the analysis model of the DM is simply just a "poor person's plastic zone analysis."

2.3.2 Ideal Nodal Bracing Stiffness

The definition of the *ideal stiffness* for nodal bracing is essentially the same at that given in Section 2.2.3 for relative bracing: The ideal stiffness (β_i) is the stiffness (of the bracing system) corresponding to incipient buckling (of the structure and its bracing system) at the required column axial load level of αP_r. This stiffness is calculated generally by solving the eigenvalue buckling problem for the nodal bracing model of a perfectly plumb column. There appears to be some confusion between the terms *ideal bracing stiffness* and *full bracing stiffness* in the literature. Therefore, the definition of *full nodal bracing stiffness* is addressed below.

2.3.3 Full Nodal Bracing Stiffness

Winter (1958) defined full nodal bracing stiffness as "equivalent in effectiveness to immovable lateral support." Yura (1996) later relaxed this requirement and defined full nodal bracing stiffness as the stiffness sufficient to develop the column resistance based on $K = 1.0$ for the longest unbraced segment. Given either of these definitions, there are several types of full bracing stiffness one can consider:

1. The full bracing stiffness corresponding to the underlying elastic eigenvalue buckling model, that is, the stiffness necessary to develop the elastic buckling load of the ideal perfectly straight, perfectly aligned (plumb) member.
2. The full bracing stiffness associated with an inelastic column buckling model, where the column stiffness is modified by a stiffness reduction factor τ that varies as a function of the column axial load level, but the member is still idealized as perfectly straight.

3. The required bracing stiffness necessary to develop the design resistance $\phi_c P_n$ in LRFD or P_n/Ω in ASD for the physical member having unavoidable initial imperfections.

The first two of the above values can be said to be the *ideal* elastic and inelastic *full bracing* stiffnesses, denoted below by β_{iF}. The third is the practical, or required, full bracing stiffness necessary for design.

2.3.4 Partial Nodal Bracing Stiffness

In many situations in practice, the applied load level may be substantially smaller than the design capacity based on $K = 1$. In these situations it may be desirable to determine a reduced stiffness requirement necessary for the bracing to be able to just support the column only up to the required applied load level.

Consider the perfectly-straight elastic column with a single intermediate brace at its mid-height shown in Fig. 2.7. When the stiffness of the brace is very small or zero, the column buckles in a symmetric mode. As the brace stiffness is increased, the buckling load increases but the column still fails in a symmetric mode involving displacement at the brace point. In this case, the column is said to be *partially braced*. However, when the brace stiffness is large enough, the perfectly straight column will buckle into the anti-symmetric *S*-shape with zero displacement at the brace point as shown in Fig. 2.7(b). In this case, the column is said to be *fully braced*.

For the physical column containing initial geometric imperfections, the *full bracing stiffness* generally must be larger than the *ideal full bracing stiffness*. Winter's (1958) bar-chain model (discussed subsequently in Section 2.3.5.1) is often used to quantify this behavior. From Winter's model, one can observe that, if the additional lateral brace point

displacement due to the application of the column axial load is to be limited to $\Delta = \Delta_o$, then β must be greater than or equal to $2\beta_i$ (see Section 2.3.5.1).

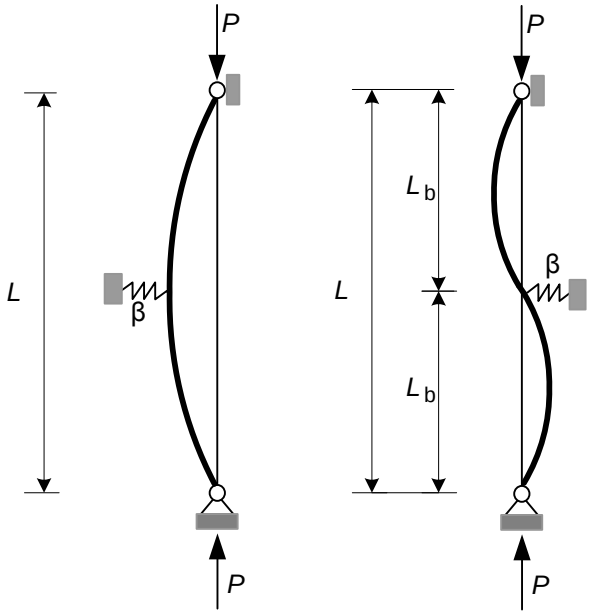

Fig. 2.7. Columns with a single intermediate brace: (a) partially-braced column and (b) fully-braced column.

In cases involving partial bracing, the bracing stiffness is not sufficient to develop the member buckling strength associated with $K = 1$ (using the modified definition of full bracing recommended by Yura (1996)). For columns such as the one shown in Fig. 2.7, in which the boundary conditions are such that the buckling effective length factor is never less than one (i.e., $KL_b = L_b$), the eigenvalue buckling strength is a constant maximum value and the eigenvalue buckling displacement is zero at the brace point(s) for brace stiffnesses larger than this limit. For stiffnesses smaller than this value, the eigenvalue buckling strength is reduced and the eigenvalue buckling displacement at the brace point(s) is non-zero. Again, generally in column bracing design, the brace stiffness

must be larger than the ideal full bracing stiffness if the physical (imperfect) column needs to support loads up to its strength $\phi_c P_n$ or P_n/Ω_c corresponding to $K = 1$.

For columns in which the boundary conditions are such that K can be less than 1.0, the member eigenvalue buckling strength continues to increase if the brace stiffness is increased above the *ideal full bracing stiffness* value, using Yura's (1996) definition of full bracing. These cases include columns with unequal brace spacing, where the longer unbraced lengths are rotationally restrained by the shorter ones if the brace stiffness is sufficiently large, columns where the end conditions provide rotational restraint, and general non-prismatic columns, where the different unbraced lengths are not equally critical and thus the weaker lengths are rotationally restrained by the stronger ones.

The AISC Appendix 6 nodal bracing equations are targeted only at developing the column full bracing strength (for $K = 1$), with the exception of the use of the L_q nodal bracing rule (discussed below in Section 2.3.5), which is a simple approximation of partial bracing behavior.

Figure 2.8 shows the influence of the bracing system stiffness on the normalized strength of columns having different numbers of equally-spaced equal stiffness nodal braces, as well as columns supported by relative (shear panel) braces. The vertical axis of the plot is the column buckling load expressed as a fraction of the fully-braced elastic or inelastic buckling strength, and the horizontal axis is the bracing stiffness expressed as a fraction of the value necessary to achieve the fully-braced strength. The elastic and inelastic buckling strengths are the strengths explained in the list items 1 and 2 in Section 2.3.3. Generally, the fully-braced buckling strength is the column load corresponding to

buckling of the member in a single half sine-wave between the brace points. The following observations may be drawn from this plot:

1. For relative bracing, the gain in the member strength with increases in the shear panel stiffness from zero is linear all the way up to the fully-braced condition. At the full bracing limit, buckling of the member occurs between the idealized pins at the brace points and no further strength gain is achievable.
2. For elastic buckling of nodally-braced columns, the overall shape of the strength gain curve with increases in the bracing stiffness is increasingly convex for the cases with larger values of *n*, where *n* is the number of intermediate nodal braces.

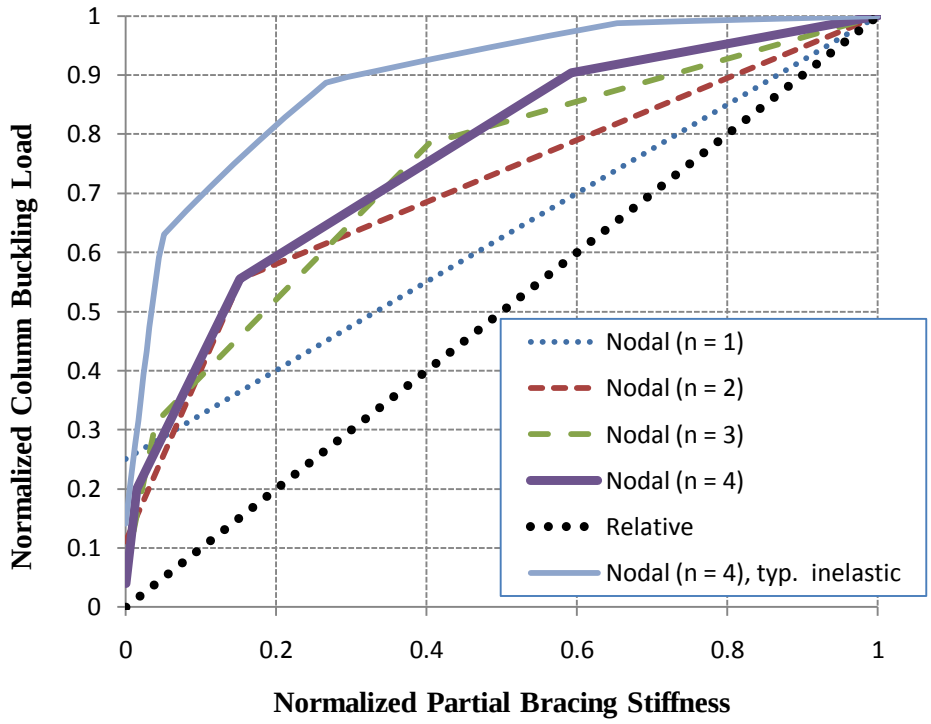

Fig. 2.8. Interaction between member strength and bracing stiffness.

3. For inelastic buckling of nodally-braced columns, the column inelastic stiffness reduction generally tends to make the curves even more convex. That is, as the

column becomes more and more yielded, the elastic brace stiffnesses become more and more effective at restraining the column against any overall buckling involving brace point movement. The example $n = 4$ inelastic curve shown in Fig. 2.8 shows that the column buckling strength is reduced to only about 95 % of the fully-braced column buckling strength when the bracing stiffness is reduced by 50 %. The specific curve in the figure is taken from the example shown previously in Fig. 1.3, and for which the detailed calculations are provided by Tran (2009).

The solutions in Fig. 2.8 indicate that the system response is relatively insensitive to changes in nodal bracing stiffness in the vicinity of the stiffness values required for full bracing strength. However, it is worthwhile to note that if the buckling capacity for the unbraced column, but with an inelastic stiffness reduction factor τ associated with the desired load level for the braced column with a number of intermediate braces $n \geq 1$,

$$P_E = \frac{\pi^2 E_T I}{L^2} \tag{2-5a}$$

is taken as a base reference strength, the ratio of the buckling load at full bracing to the reference strength is as shown in the second column of Table 2.1. In addition, the ratio of the stiffness required to achieve full bracing to the constant P_E / L, where $L = (n + 1) L_b$ is the full length of the column, is shown in the third column of the table. The fourth column of the table shows the required bracing stiffness for full bracing normalized by the critical load P_{cr} for the different numbers of intermediate nodal braces, where

$$P_{cr} = \frac{\pi^2 E_T I}{L_b^2} \tag{2-5b}$$

Table 2.1. Buckling load at full bracing and ideal bracing stiffness as a function of number of intermediate braces

N	P_{cr} / P_E	$\beta_{iF} / (P_E / L)$	$\beta_{iF} L / P_{cr}$
1	4	16	4
2	9	81	9
3	16	218	13.6
4	25	454	18.2

One can observe that, as long as the column is long enough and the buckling loads are small enough such that *elastic* flexural buckling governs, the bracing stiffness required to fully brace the column for elastic buckling and a given L_b increases dramatically with increasing n, but at a decreasing rate for larger n. However, if one considers the fact that most columns with a large number of intermediate braces will fail within the inelastic buckling range, the bracing stiffness needed to develop a member buckling capacity of say $0.98P_{cr}$ is much smaller than the β_{iF} for the inelastic buckling problem. This is due to the column inelastic stiffness reduction and is illustrated by the top curve in Fig. 2.8.

The AISC nodal bracing rules are generally $2.0/\phi = 2.0/0.75 = 2.67$ for LRFD and $2\Omega/\alpha = 2.5$ for ASD larger than a corresponding estimated ideal nodal bracing stiffness. Tran (2009) presents various virtual test simulation solutions to investigate the implications of using β values smaller than these limits. These solutions indicate that for large n, particularly for typical inelastic cases, the loss of strength with a reduction in the bracing stiffness is relatively small such that the member often may be considered essentially as still fully braced down to brace stiffness values as low as $1.3\beta_{iF}$. His solutions with $n = 1$ indicate good performance with about $1.9\beta_{iF}$, i.e., a larger fraction of the ideal bracing stiffness is needed to obtain full bracing response when n is small.

It is important to note that for beam-columns, the practice of relaxing the bracing stiffness requirements based on partial bracing response effectively reduces the column axial design resistance, $\phi_c P_n$ or P_n/Ω_c, toward the applied axial load, P_u or P_a. Therefore, theoretically there may be zero bracing capacity left to brace against bending moments applied to the member. Due to this potential problem, Section 6.4 of the 2010 AISC Specification disallows the use of L_q for beam-columns.

2.3.5 Nodal Bracing Second-Order Analysis Solutions

Nodal bracing second-order analysis solutions are somewhat more complex than the column relative bracing solution discussed in Section 2.2.1. This complexity is caused largely by the member continuity effects through the brace point locations. Stated alternately, the second-order flexure of the column under increasing axial loads generally induces additional brace point forces. These column bending effects can be substantial in some cases with unequal brace spacing and/or stiffness (Stanway et al. 1992a and b), and they are not captured in any of the present design standards including the 2010 AISC Appendix 6. Yura (1996) addresses the calculation of the eigenvalue buckling resistance of nodally-braced columns with unequal unbraced lengths, but does not address the corresponding nodal bracing force requirements.

The second-order analysis model for a given column with intermediate nodal braces is reasonably straightforward. However, obtaining closed form expressions for the results from general second-order nodal bracing solutions is difficult, even for the cases of equally-spaced, equal-stiffness bracing of prismatic columns.

Possibly of greater importance, as noted in Section 1.1, equal-stiffness nodal bracing rarely if ever exists for cases with more than two intermediate nodal braces. Nevertheless,

the nodal bracing developments still provide a useful base for understanding and interpreting other more general bracing requirements.

Several approximate nodal bracing solutions for columns with equally-spaced, equal-stiffness braces are discussed below. The first two approaches are focused on estimating fully-braced column strengths and the corresponding bracing demands. This is followed by three estimates pertaining to partial bracing.

2.3.5.1 Winter's Full Bracing Model

Winter (1958) introduced a simple method to calculate the stiffness and strength requirements for column nodal bracing to work effectively as fixed immovable supports. He recommended a rigid link model with fictitious hinges at the brace points, i.e., a bar chain (see Fig. 2.9a), for this calculation. This simplification is based on the fact that a perfectly straight column that:

- Buckles in a fully-braced mode

and has

- Equally spaced, equal stiffness braces and
- No end rotational restraints

will have inflection points and zero moment at each of its brace points when it reaches its strength limit.

For the case of a column with a single nodal brace at its mid-span, the brace force-deformation equations and the moment equilibrium equations for the free-body diagram shown below (Fig. 2.9b) may be combined to write

$$(\beta\Delta)\, L / 2 = P_e\, (\Delta+\Delta_o) \qquad (2\text{-}6a)$$

or after some algebraic simplification,

$$\beta = \beta_i \left(1 + \frac{\Delta_o}{\Delta} \right) \tag{2-6b}$$

where

β = the actual brace stiffness

Δ_o = the initial imperfection amplitude

Δ = the lateral displacement of the column at the brace point, relative to the initial imperfect geometry, due to the application of the axial loading,

β_i = the ideal brace stiffness, that is, the brace stiffness corresponding to incipient buckling of the bracing system at the applied load P_e

= $\frac{2P_e}{L}$ for the column with a single mid-span nodal brace.

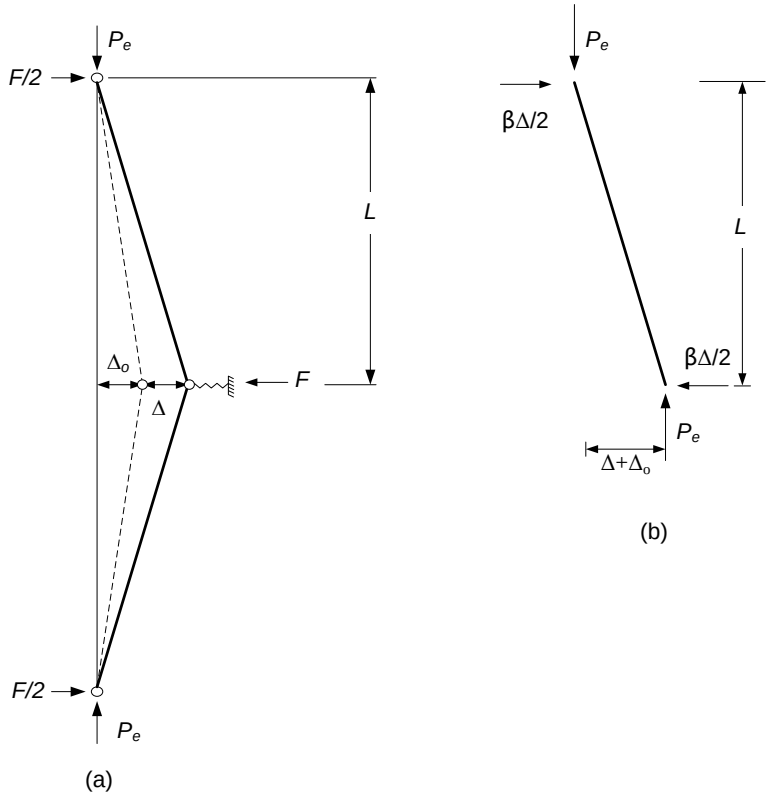

Fig. 2.9 Winter's (1958) model, (a) bar-chain model with a single intermediate nodal brace, (b) free body diagram.

It should be emphasized that Eq. (2-6b) can be used in two different ways:

1. For a specified limit on the ratio of the additional deflection of the brace point under load to the initial geometric imperfection, Δ/Δ_o, this equation gives the fundamental bracing stiffness required for the idealized model to achieve equilibrium at the member buckling load level P_e.
2. Alternately, for a given provided bracing stiffness, β, this equation can be solved for the ratio of Δ/Δ_o that will occur in the idealized "pinned out" nodal bracing model at the member buckling load P_e.

Winter (1958) showed that Eq. (2-6b) also applies for columns with multiple intermediate braces, as long as the initial geometric imperfections are the most critical pattern, i.e., the one affine to the lowest eigenvalue buckling load of the bar-chain model. In addition, he showed that the ideal bracing stiffness of the bar-chain model with equal-stiffness equally-spaced nodal braces is $\beta_i = \frac{3P_e}{L}$ for a column with two intermediate nodal braces, $\frac{3.41P_e}{L}$ for a column with three intermediate nodal braces and $\frac{3.63P_e}{L}$ for a column with four intermediate nodal braces. These solutions match exactly with the analytical solutions obtained for a simply-supported continuous elastic prismatic column braced by the corresponding number of equal-stiffness equally-spaced nodal braces. **(**It should be noted that L here is the unbraced length between the brace points, whereas in the previous sections, it was the total column length.)

It should be emphasized that Winter assumed $P = P_e$ to justify his idealization of placing an internal hinge in the column at the brace point. Generally, Winter's model

tends to be conservative for $P < P_e$. This is due to the fact that the continuous column provides some resistance to brace point movement for $P < P_e$.

The brace strength requirement for the column in Fig. 2.9 may be obtained simply by multiplying both sides of Eq. (2-6b) by the brace point displacement Δ, i.e.,

$$P_{br} = \beta\Delta = \beta_i(\Delta + \Delta_o) = \beta_i \frac{\Delta_o}{1 - \frac{\beta_i}{\beta}} \tag{2-6c}$$

Furthermore, it is important to note that this equation applies also for cases with multiple intermediate braces, as long as the pattern for the initial geometric imperfections has the same shape as the critical buckling mode for the column and its bracing system.

It is interesting to determine what the corresponding additional brace point displacement Δ and the corresponding required bracing stiffness β are from Eqs. (2-6b) and (2-6c) if $\Delta_o = 0.002L$ and if P_{br} is limited to $0.02P_e$ for different numbers of intermediate nodal braces n. If one sets P_{br} to $0.02P_e$ and Δ_o to $0.002L$, uses the variable c_1 to denote the coefficient in the expressions for β_i, and uses the variable c_2 to denote the ratio Δ/Δ_o, then Eq. (2-6c) may be written as

$$0.02P_e = \frac{c_1 P_e}{L}(0.002L + 0.002Lc_2) = 0.002c_1P_e(1 + c_2) \tag{2-6d}$$

Upon solving for c_2, one obtains

$$c_2 = \frac{10}{c_1} - 1 \tag{2-6e}$$

If this expression is then substituted into Eq. (2-6b), and if the bracing system stiffness necessary to satisfy the above limit on the bracing force is expressed as c_3P_e/L, Eq. (2-6b) may be written as

$$c_3 \frac{P_e}{L} = c_1 \frac{P_e}{L}\left(1 + \frac{1}{c_2}\right) \tag{2-6f}$$

or

$$c_3 = c_1\left(1 + \frac{1}{c_2}\right) \tag{2-6g}$$

The solution to these equations for n = 1 through 4, and for $n = \infty$, is summarized below in Table 2.2. The last column of the table shows that, for $\Delta_o = 0.002L$, the ratio of the brace stiffness required to limit the brace strength requirement to 2 % of the column axial force ranges from $1.25\beta_i$ for one intermediate brace to $1.67\beta_i$ for $n = \infty$. In addition, the fourth column shows that the amplification of the initial imperfections (AF) reduces rapidly from 5.0 for n = 1 toward 2.50 as n becomes large.

Table 2.2. Bracing coefficients summarizing the behavior and stiffness requirements according to Winter's model for columns with different numbers of equally-spaced equal-stiffness nodal braces, initial out-of-alignment of $\Delta_o = 0.002L$, and the required brace strength limited to 2 % of the column force.

n	$c_1 = \frac{\beta_i}{(P_e/L)}$	$c_2 = \frac{\Delta}{\Delta_o}$	$AF = 1 + c_2$	$c_3 = \frac{\beta}{(P_e/L)}$	$\frac{\beta}{\beta_i}$
1	2	4	5.0	2.50	1.25
2	3	2.33	3.33	4.29	1.43
3	3.41	1.93	2.93	5.18	1.52
4	3.63	1.75	2.75	5.70	1.57
∞	4	1.50	2.50	6.67	1.67

Table 2.3 shows another result based on Winter's model. Suppose that it is desired to limit the amplification of the initial geometric imperfections to AF = 4.0, and thus c_2 =

$\Delta/\Delta_o = 3.0$, for any number of intermediate nodal braces. $AF = 4.0$ may be considered as a maximum "safe" limit on the second-order amplification, since beyond this value of the amplification, the structural response becomes very sensitive to minor changes in load or stiffness. In this case, from Eq. (2-6b), the required brace stiffness β must be greater than or equal to $1.33\beta_i$ for any value of n. The brace forces at the strength limit are then obtained from Eq. (2-6c). One can see from the last column of this table that, in this case, the brace forces vary from 1.6 % of the column force for a single intermediate brace to 3.2 % of the column force as the number of intermediate braces becomes large.

Table 2.3. Bracing coefficients summarizing the behavior and stiffness requirements according to Winter's model for columns with different numbers of equally-spaced equal-stiffness nodal braces, initial out-of-alignment of $\Delta_o = 0.002L$, and a second-order amplification of $AF = 4.0$ ($\Delta/\Delta_o = 3.0$) at the strength limit ($\beta/\beta_i = 1.33$).

n	$c_1 = \frac{\beta_i}{(P_e / L)}$	$c_3 = \frac{\beta}{(P_e / L)}$	$\frac{P_{br}}{P_e}$ (%)
1	2	2.66	1.6
2	3	3.99	2.4
3	3.41	4.54	2.7
4	3.63	4.83	2.9
∞	4	5.32	3.2

It should be noted that all of these solutions are based on the specific idealization posed by Winter. Relatively rigorous solutions can be obtained for any given geometry and brace properties using plastic zone analysis. For example, based on a commonly used mapping of the above solutions to design calculations, Tran (2009) substitutes $\phi_c P_n$ = 1000 kips for P_e to estimate the weak-axis bracing requirements for a W14x90 nodally-

braced column with F_y = 50 ksi, L = 15 ft (L/r_y = 48.6), and n = 4. The knuckle curve corresponding to his distributed plasticity analysis solution is shown previously in Fig. 1.3. His distributed plasticity analysis solution using $1.33\beta_i$ = 26.7 kips/inch indicates a column maximum resistance of P_{max} = 940 kips and a brace force of approximately 2.0 % of P_{max} at the strength limit.

Tran also shows plastic zone solutions for weak-axis buckling of different W14x90 columns (F_y = 50 ksi) with a single intermediate nodal brace and a complete range of unbraced lengths. He finds that for L/r = 20 and 30, $\beta = 1.3\beta_i$ is sufficient for the column to develop 98 % of its capacity obtained using rigid lateral bracing. Furthermore, for L/r = 20, the brace force at the maximum column strength limit is 1.4 % of the column load P_{max}, whereas for L/r = 30, the brace force at the maximum column strength limit is 2.5 % of P_{max}.

It should be noted that both of these solutions as well as the previous solution with four intermediate braces involve substantial inelastic action prior to the column reaching its maximum strength. For columns with a single intermediate brace and $L/r \geq 80$, Tran found that $\beta = 1.9\beta_i$ consistently developed 98 % of the rigidly-braced column capacity. These columns also show distributed yielding at their maximum strength, but the response is increasingly dominated by elastic stability effects as L/r is increased. In these cases, P_{br}/P_{max} ranged from 2.6 % for L/r = 80 to 4.9 % for L/r = 140 at the maximum strength limit. However, the geometric imperfections that produce these maximum brace forces result in a larger column strength (P_{max}) than the load P_{max}* obtained with geometric imperfections that produce the maximum column destabilizing effect and thus

the minimum axial capacity of the column. In the analyses that maximize the brace force, the brace force at the column load $P_{max}^* < P_{max}$ ranges from 1.1 to 1.7 % of P_{max}.

The main point to be drawn from the above discussions is that Winter's equations provide only a gross approximation of the responses from rigorous distributed plasticity analysis solutions.

2.3.5.2 Plaut's Approximations

Plaut (1993) found that Winter's model does not always give a conservative estimate of the brace stiffness requirements. He showed that the assumed hinges at the brace points fail to account for the influence of internal bending moments (i.e., continuity effects) at these points in an actual imperfect *elastic* column. As a result, Plaut (1993) modified Winter's solution for the column with a single brace at its mid-height and recommended that the brace stiffness should be related to the brace point deflection for this case by the equation

$$\beta = \frac{2P_e}{L_b}\left(1+1.5\frac{\Delta_o}{\Delta}\right) = \beta_i\left(1+1.5\frac{\Delta_o}{\Delta}\right) \qquad (2\text{-}7)$$

rather than Eq. (2-6b). It should be noted that also the required brace strength is increased as a result of this modification. The AISC Appendix 6 nodal bracing strength requirements in fact are increased from 0.8 % to 1.0 % in part as a result of Plaut's developments.

If $\beta/\beta_i = 1.3$ is substituted into Eq. (2-7), this equation gives a resulting $\Delta/\Delta_o = 5.0$. In addition, the corresponding brace force at the strength limit is obtained as $\beta\Delta = 0.026P_e$. That is, the brace force is estimated to be 2.6 % of the column load at the strength limit. This solution gives a better upper-bound of the brace strength requirements from Tran's

(2009) plastic zone analyses for weak-axis buckling of W14x90 columns with $L/r = 20$ and 30. With $\beta/\beta_i = 1.9$, Eq. (2-7) gives $\Delta/\Delta_o = 1.67$ and the corresponding brace force is 1.3 % of the column axial load at the strength limit. This estimate of the brace force is significantly better than the one obtained using Winter's model with $\beta/\beta_i = 1.9$ ($P_{br} = 0.0084P_e$). However it is a little low compared to the bracing force requirements determined by Tran for weak-axis buckling of his W14x90 columns with L/r larger than 100.

Plaut also discusses the general requirements for a single brace at any location along a column. However, the effects of continuity, the second-order elastic bending response of the column, and the "prying" action on the intermediate brace associated with the restraint of the longer unbraced length defy description by a simple equation such as Eq. (2-7) in this more general case. Stanway et al. (1992a & b) obtain similar findings to those of Plaut (1995). One interesting fundamental attribute for a column with a single arbitrarily located intermediate brace is that the eigenvalue buckling mode always exhibits non-zero brace point displacement, unless of course the intermediate brace is ideally rigid or is located at the member mid-length.

2.3.5.3 AISC L_q Approach for Partial Bracing

If the stiffness of the nodal braces is less than the required nodal full-bracing stiffness, the column and its bracing system generally are unable to develop an axial load equal to the value associated with $K = 1$ (using the definition of full bracing given by Yura (1996)). However, as explained previously, substantial (albeit smaller) axial loads may still be developed (see Fig. 2.8).

The AISC Specification allows the use of the length L_q instead of L_b in its equations for the nodal bracing stiffness requirements, where L_q is defined as the effective unbraced

length KL ($> L_b$) at which the available column strength is equal to the required column strength. The specific AISC column nodal bracing equations are listed subsequently in Section 2.6.1.2.

Figure 2.10 compares the approximate solution for the partially-braced column buckling strength using the L_q approach to the exact solution for columns with one and two intermediate nodal braces. One can observe that the L_q approximation works best for columns with a small number of intermediate brace points and for brace stiffnesses close to the full bracing stiffness, i.e., the stiffness at which there is no additional strength gain with further increases in the stiffness. However, as the brace stiffness approaches zero, the solution for the column strength by the L_q approach approaches zero. Therefore, for small values of partial brace stiffness, the L_q approach can be quite conservative.

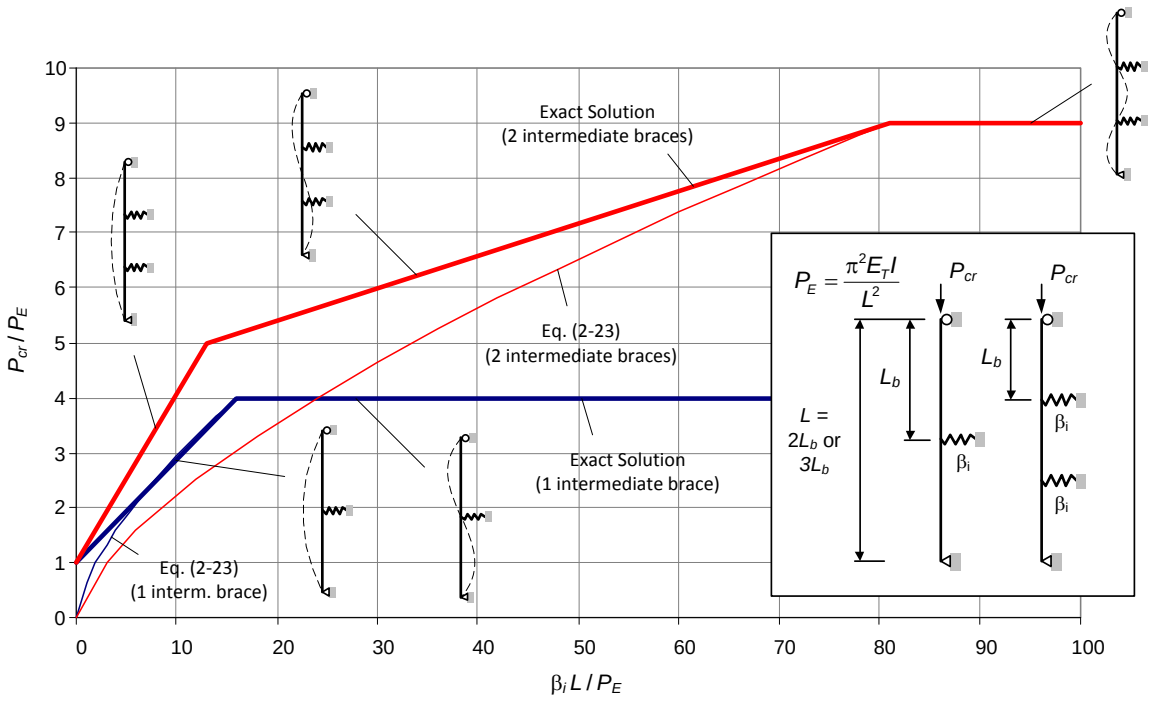

Fig. 2.10. Comparison of approximate column buckling resistance for partial bracing by the AISC L_q approach.

Per the intent of AISC Appendix 6, either of the solutions in Fig. 2.10 would be multiplied by a factor of $2/\phi = 2.67$ for LRFD and $2/\Omega = 2.5$ for ASD to obtain the required bracing stiffness. The AISC strength requirement is taken as 1 % of the axial load applied to the column. For a column with a single intermediate brace, this required strength is derived by multiplying Plaut's Eq. (2-7) for a fully-braced column by an assumed $\Delta = \Delta_o = 0.002L_b$. Winter's Eq. (2-6b) gives a corresponding strength requirement of 0.8% of the applied axial load. In both of these solutions, the applied axial load $P_r = \phi_c P_n$ (LRFD) or P_n/Ω_c (ASD) = P_e is implicitly assumed (with P_e calculated using the corresponding elastic or inelastic column rigidity τEI).

2.3.5.4 Lutz and Fisher's Approximations for Partial Bracing

Lutz and Fisher (1985) have recommended several approximations for partial bracing derived from fundamental analytical solutions. For columns with a single intermediate brace, they use the following equation, which is for all practical purposes an exact expression for the ideal bracing stiffness (i.e., the dark solid sloped line in Fig. 2.10) multiplied by a factor of 2.0:

$$\beta_{reqd} = 5.33\frac{(P^* - P_{E\tau})}{L_b} \qquad (2\text{-}8a)$$

where

$P_{E\tau} = \pi^2 \tau EI/L^2$ = the elastic or inelastic buckling load for the column with zero intermediate bracing, with the inelastic stiffness reduction factor calculated based on the axial force to be developed by the column.

L_b = length between braces, assumed equal for all the unbraced lengths

L = total column length

P^* = axial load to be developed by the column

τ = column inelastic stiffness reduction factor

In the context of the 2005 and 2010 AISC Specifications, the axial load P^* may be taken as P_u / ϕ_c for LRFD (with $\phi_c = 0.9$) and as $\Omega_c P_a$ for ASD (with $\Omega_c = 1.67$), and the inelastic stiffness reduction factor may be calculated as

$$\tau = 0.877\ \tau_a = -0.877(2.724\ (P^*/P_y) \ln (P^*/P_y) \quad \text{for } P^*/P_y > 0.39 \qquad (2\text{-}8b)$$

$$\tau = 0.877 \quad \text{for } P^*/P_y \leq 0.39 \qquad (2\text{-}8c)$$

For columns with two intermediate braces, Lutz and Fisher (1985) recommend

$$\beta_{reqd} = 6P^* L_b / L_e^2 \qquad (2\text{-}9a)$$

where L_e is the effective length of the buckled column, which may be calculated by writing $P^* = \pi^2 \tau EI / L_e^2$ and solving for L_e:

$$L_e = \pi\sqrt{\tau EI / P^*} \qquad (2\text{-}9b)$$

This equation is an accurate to conservative curve fit to the exact partial bracing solution shown by the lighter solid line in Fig. 2.10, multiplied again by a factor of 2.0.

For three or more intermediate braces, Lutz and Fisher propose an equation that amounts to a transition between:

1. The ideal continuous-bracing stiffness equation for small P^*, multiplied by the brace spacing L_b and
2. The ideal discrete full bracing stiffness for P^* approaching the fully-braced column strength,

with the result again multiplied by the factor 2.0. The resulting equation for the required stiffness is

$$\beta_{reqd} = \left[5 + 3\left(\frac{L_b}{L_e} \right)^4 \right] \frac{P^* L_b}{L_e^{\,2}} \tag{2-9c}$$

which may be written as

$$\beta_{reqd} = \left[5 + 3\left(\frac{P^*}{P_{e\tau}} \right)^2 \right] \frac{P^*}{P_{e\tau}} \frac{P^*}{L_b} \tag{2-9d}$$

with

$$P_{e\tau} = \frac{\pi^2 \tau EI}{L_b^2} \tag{2-9e}$$

It is important to note that the partially braced column generally provides some resistance to the brace point displacements via its elastic or inelastic flexural rigidity τEI. This stiffness contribution is reduced due to second-order P-δ effects in the column, but not to the extent that the member behaves as if it has pins at all of its brace points. The above equations from Lutz and Fisher capture this continuity effect. For a column with $n > 2$, one can see clearly from Eq. (2-9d) that the bracing stiffness demand varies directly with the ratio of the column applied axial load to the idealized inelastic or elastic buckling resistance of the individual unbraced lengths, $P_{e\tau}$, determined using $K = 1$.

Bishop et al. (2010) show that the above equations provide an accurate characterization of the results from plastic zone analysis (virtual simulation) studies of nodally braced columns. Equations (2-6) are based on the idealization that the column has pins at each of the intermediate brace points. This is an accurate characterization at the full bracing limit, but does not recognize the substantial resistance to brace point movement that the column flexural rigidity can provide when the applied axial load is less than the theoretical load corresponding to fully-braced buckling.

Lutz and Fisher (1985) approximate the required brace forces as $\beta_{act}\Delta$, where β_{act} is the actual provided brace stiffness. Furthermore, they solve Winter's Eq. (2-6b) for Δ to estimate the brace point deflection as

$$\Delta = \frac{\beta_i}{\beta_{act} - \beta_i}\Delta_o \tag{2-10}$$

This provides a simple calculation of the brace strength requirements. However, Eq. (2-10) is based on Winter's idealization of the column with pins inserted at each of the brace points. Therefore, Eq. (2-10) is only an estimate.

2.3.5.5 Yura's Solution for Partially-Braced Column Buckling Strengths

Yura (1996) used Winter's idealization to determine critical loads for column partial nodal bracing. He demonstrated his approach using a bar-chain model with three intermediate braces. He showed astutely that Winter's idealization can be configured to accurately predict the column buckling load for different brace stiffnesses (varying from partial bracing to full bracing stiffness). However, Yura (1996) only addresses the calculation of the buckling load for a partially-braced column, or in other words, he only addresses the calculation of β_i or β_{iF}. He does not address the required bracing stiffness for the geometrically imperfect partially-braced column. Also, he does not consider the strength requirements on the braces for the partially-braced column case.

Similar approximations to those discussed above can be utilized with Yura's approach for the calculation of β_i for a partially braced column. For instance, the AISC factors of $2/\phi = 2/0.75 = 2.67$ (LRFD) or $2\Omega/\alpha = 2(2.0)/1.6 = 2.5$ (ASD) can be applied to the ideal bracing stiffness to obtain the required stiffness. In addition the brace forces

can be estimated as $\beta_{act}\Delta$, where β_{act} is the actual provided stiffness and Δ is obtained from Eq. (2-10), as in Lutz and Fisher (1985).

2.3.5.6 General-Purpose Nodal Bracing Model

All of the above solutions involve various approximations. Tran (2009) and Griffis and White (2011) clearly show that good performance can be obtained with much smaller values of the required stiffness, in specific cases, if the detailed nodal bracing characteristics are analyzed using general purpose second-order analysis software. This type of general-purpose nodal bracing model can include member flexural continuity where it exists, rotational end restraints where they exist, actual brace locations where they exist, and equal or unequal brace stiffnesses.

For general column bracing requirements, the end restraint plays an important role in system strength and bracing requirements. In columns having flexural end restraints Yura (1995) and Helwig and Yura (1999) have pointed out specific cases where the bracing demands increase substantially when the column axial load is larger than the elastic buckling load associated with $K = 1$. However,

1. Although it is certainly correct that a column loaded beyond its Euler buckling load based on $K = 1$ can induce substantially larger demands on its braces, the bracing demands are certain to be reduced at any given axial load level if the column has rotational end restraints.
2. The uniformly loaded prismatic column, subjected to uniform axial force $P > P_{e(K=1)}$, is one of the worst cases where flexural continuity (column bending) effects can dramatically increase the brace forces. However, for nonprismatic columns subject to non-constant axial load, and where the members are designed

based effectively on $K = 1$, the demands are certain to be smaller due to continuity and end restraint effects.

These considerations also extend to warping and lateral bending end restraint in general bracing of beams and beam-columns.

Section 12.2.2 of Ziemian (2010) summarizes the results from a number of additional general purpose second-order analysis solutions, including experimental validation in a few specific cases, which have explored the influence of member inelasticity on bracing requirements both for columns and beams.

Section 2.2.2 of this report explains the proper calculation of the brace point displacements and the bracing forces in relative (shear panel) bracing for the general situation where the bracing must resist both primary (applied) forces as well as forces required to develop the brace locations given unavoidable member imperfections. All of the above nodal bracing equations address only the stability bracing response for cases where the primary forces in the braces are zero. One would expect that when nodal braces are subjected to primary forces, the actual brace point displacements and the required strengths can be estimated similarly by amplifying the first-order forces and transverse displacements on the structure due to the applied loads and adding these to the forces and displacements obtained from the stability bracing equations. Also, one would expect that the amplifier in Eq. (2-3), with $\alpha\Sigma P/L$ replaced by the estimated ideal bracing stiffness, β_i, gives a sufficient estimate of the corresponding amplifier. Alternatively, of course, one can employ an explicit second-order analysis as noted above.

2.4. Key Differences between Column Relative and Nodal Bracing

Given the above discussions, it is useful to summarize the key differences between the fundamental relative and nodal column bracing models applied in the AISC Specification Appendix 6. These differences are as follows:

1. The relative bracing requirements address the *shear force* that must be resolved in *a given panel* of a bracing system.
2. The relative bracing requirements *neglect* the help from the *EI* of the columns, i.e., pins are inserted at all of the brace points in the relative bracing model.
3. The nodal bracing requirements address the absolute or *direct force* that must be transferred to the bracing system *at a brace point*.
4. The nodal bracing requirements include the help from the *EI* of the column(s) in an approximate fashion, via the L_q parameter.

The following section discusses the fundamental requirements for beam bracing. Many of these requirements are direct extensions of the column bracing requirements. Emphasis is placed on the locations where key differences exist.

2.5 Fundamental Beam Bracing Requirements

2.5.1 Beam Lateral Bracing

Winter (1958) proposed lateral bracing requirements for beams that are simple extensions of his column full bracing requirements. For beam lateral bracing, the stability behavior can be quantified in many respects by treating the compression flange as an analogous column. However, beam bracing is much more complicated than column bracing due to load height effects, cross-section distortion, moment gradient effects, and the influence of brace position through the cross-section depth.

Yura (1993 and 2001) provides numerous refinements to the base model developed by Winter. These refinements have served as the primary basis for the beam lateral bracing provisions in the AISC Appendix 6. The AISC beam lateral bracing stiffness and strength requirements are summarized later in Section 2.6.

In addition, Yura et al. (1992) present the following equation for the elastic lateral buckling moment of an I-section member with discrete bracing along its length

$$M_{cr} = \sqrt{[(C_{bu}M_o)^2 + (C_{bb}P_{ef}h_o)^2 A_d](1 + A_d)} \tag{2-11}$$

where

C_{bu} = Moment gradient factor assuming the beam is unbraced

M_o = Elastic buckling moment for the beam under uniform moment, assuming it is unbraced

C_{bb} = Moment gradient factor assuming the beam discrete braces are fully effective

P_{ef} = elastic lateral buckling load of the compression flange idealized as an isolated column = $\pi^2 EI_{yc}/L^2$

I_{yc} = moment of inertia of the compression flange about the weak-axis of the beam

L = total beam span length between rigid lateral end braces

h_o = distance between the flange centroids

$$A_d = \frac{L^2}{\pi}\sqrt{\frac{0.34\overline{\beta}_L}{C_{tL}EI_{yc}}}$$

$C_{tL} = 1 + 1.2/n_L$ for top flange loading

$C_{tL} = 1$ otherwise

n_L = number of intermediate discrete nodal lateral braces along the beam length

$\overline{\beta}_L$ = equivalent continuous lateral bracing = $\beta_L \, n_L / \alpha L$

β_L = stiffness of equally-spaced equal stiffness intermediate discrete nodal braces

α = 0.75 for one intermediate mid-span brace

α = 1.0 otherwise

When used with discrete braces, the value of M_{cr} from Eq. (2-11) is limited to the moment corresponding to buckling between the braces. Furthermore, Yura et al. (1992) state that Eq. (2-11) is not valid beyond the yield moment of the beam.

2.5.2 Beam Torsional Bracing

The fundamental requirements for beam torsional bracing come from Taylor and Ojalvo (1966). These researchers investigated the elastic buckling strength of beams with continuous elastic torsional bracing. Yura and Phillips (1992) and Yura et al. (1992) expanded upon this research and developed detailed design requirements for both continuous and nodal (discrete grounded) beam torsional bracing. Their studies addressed the effects of cross section distortion, position of loading, and location of the torsional brace relative to the member depth on the buckling behavior of I-section beams. Yura (1993 and 2001) provides a synthesis of the recommendations based on this research.

The detailed torsional brace stiffness and strength requirements developed by the above researchers can be summarized as follows. The central equation in these developments is the following expression for the elastic lateral-torsional buckling resistance of a general I-section member with continuous torsional bracing along its length:

$$M_{cr} = \sqrt{(C_{bu} M_o)^2 + \frac{C_{bb}^2 EI_{eff} \overline{\beta}_T}{C_{tT}}} \qquad (2\text{-}12)$$

where

C_{bu} = C_b factor for the unbraced beam, i.e., the factor applied to M_o to account for moment gradient effects if there were zero intermediate bracing

M_o = buckling capacity of the beam subjected to uniform moment if zero intermediate bracing were present

C_{bb} = C_b factor for the critical unbraced segment of the braced beam

I_{eff} = I_y for doubly symmetric sections

$= I_{yc} + \frac{t}{c} I_{yt}$ for singly symmetric sections

c = distance between cross section centroid and centroid of compression flange

t = distance between cross-section centroid and centroid of tension flange

I_{yc} = moment of inertia of the compression flange

I_{yt} = moment of inertia of the tension flange

C_{tT} = torsional bracing factor accounting for the effects of transverse load height

= 1.2 when the transverse loading is applied at the flange level in a way that is detrimental to the member stability (this occurs when the transverse loading is applied at the flange level and is directed toward the member shear center from the point of application)

= 1.0 otherwise

$\overline{\beta}_T$ = actual or equivalent continuous torsional bracing stiffness

$= \frac{\beta_T n_T}{\alpha L}$ for equal-stiffness equally-spaced intermediate discrete nodal torsional braces

β_T = intermediate nodal torsional brace stiffness

n_T = number of intermediate nodal torsional braces

L = total beam span length between rigid end lateral braces

α = 0.75 for a single mid-span torsional brace in beams subjected to centroidal loading (i.e., for beams with a single mid-span torsional brace in which there are no load height effects)

= 1.0 for all other cases

The torsional brace stiffness and strength requirements recommended by Yura (2001) are derived from this equation and may be summarized as follows:

Stiffness Requirement

- The ideal discrete torsional bracing stiffness may be estimated as

$$\beta_{Ti} = \left(M_{cr}^{\ 2} - C_{bu}^{\ 2} M_o^{\ 2}\right) \frac{C_{tT}}{C_{bb}^{\ 2} EI_{eff}} \frac{\alpha L}{n_T} \tag{2-13}$$

  This equation is obtained simply by solving Eq. (2-12) for the required discrete torsional bracing stiffness required to develop a desired critical moment M_{cr}.

- The required effective stiffness of the total torsional bracing system recommended by Yura (2001) for LRFD building design is

$$\beta_T = \frac{2\beta_{Ti}}{\phi} \tag{2-14a}$$

  where ϕ = 0.75 and β_{Ti} is based on the governing LRFD strength load combination. For ASD building design, the recommended equation is

$$\beta_T = 2\,\Omega\,\beta_{Ti} \tag{2-14b}$$

where $\Omega = 3.0$. However, in this case β_{Ti} is based on the allowable or working loads. The large value of Ω is due to the fact that the moment terms are squared in Eq. (2-13). The safety factor $\Omega = 3.0$ is obtained as $(1.5)^2/0.75$.

- It is essential to note that the distortional flexibility of the member web as well as any influence of slip or local deformation on the tangent stiffness of the torsional brace connections must be included when calculating the torsional stiffness of the bracing system. These deformations increase the effective torsional bracing flexibility (they decrease the effective torsional bracing stiffness), and generally increase the required stiffness of the actual torsional bracing necessary for the total effective torsional bracing system to satisfy Eq. (2-14). Basically, all the contributions to the torsional bracing flexibility combine additively to obtain the total flexibility of the discrete torsional braces. That is, they work as springs in series. For example, if the only contributors are the actual torsional bracing and the beam web flexibility, then one can write

$$\frac{1}{\beta_T} = \frac{1}{\beta_{Tb}} + \frac{1}{\beta_{\text{sec}}} \tag{2-15}$$

to obtain the minimum required bracing stiffness β_b, where

β_{Tb} = torsional stiffness of the actual torsional bracing

β_{sec} = web distortional stiffness contribution to the torsional bracing stiffness

$$= \frac{3.3E}{h_o}\left(\frac{1.5h_o t_w^{\,3}}{12} + \frac{t_s b_s^{\,3}}{12}\right) \tag{2-16}$$

(i.e., $1/\beta_{sec}$ is the torsional rotation due to the web cross-*sec*tion distortional flexibility for a unit applied torsional moment at the brace location)

t_w = beam web thickness

t_s = web stiffener thickness

and

b_s = stiffener width for one-sided stiffeners

= two times the individual stiffener width may for double-sided stiffeners; alternatively, the sum of the stiffener widths plus the member web thickness is justified for this dimension.

It should be noted than when flange diagonal braces are directly connected to the member flanges from girts or purlins, the web distortional flexibility is zero. However, it is again emphasized that any other contributions to the flexibility of the torsional bracing (connection slip, local connection deformation at the connections of diagonal braces, diagonal brace axial stiffness, girt or purlin flexural stiffness, etc.) must be included to ensure that the total stiffness of the bracing system β_{Tb} is greater than or equal to β_T. (It may be possible to consider slip of connections into bearing by increasing the effective geometric imperfection Δ_o within limits; this question is not addressed in this research, but is discussed in Section 9.3, "Recommendations for Further Research").

- Given Eq. (2-15), the required stiffness of the actual torsional bracing may be solved for as

$$\beta_{Tb} = \frac{\beta_T}{\left(1 - \frac{\beta_T}{\beta_{\text{sec}}}\right)} \tag{2-17}$$

Hence, for cases where the web distortional stiffness, β_{sec}, is relatively small, the required stiffness of the rest of the torsional bracing system, β_{Tb}, has to be much

larger than β_T. In the limit that β_{sec} is reduced to β_T (from above), all the torsional bracing stiffness has been "eaten away" by the web distortional flexibility. When β_{sec} is less than β_T, β_{Tb} in Eq. (2-17) is a negative number, indicating that it is impossible to torsionally brace the beam without stiffening the cross-section to reduce the web distortional deformations.

Strength Requirement

- Given the total bracing system stiffness required at a given torsional brace (β_T), an estimate of the torque that must be resisted by this system is obtained by multiplying this required stiffness (but without ϕ or Ω) by the initial layover of the cross-section at the critical torsional brace point, assumed as $\theta_o = (L_b/500)/h_o$. This is based on the underlying assumption that the additional rotation at the critical torsional brace θ is equal to θ_o. The resulting estimate of the required brace strength is

$$M_{br} = \frac{\beta_T}{\psi}\theta_o = \frac{\beta_T}{\psi}\frac{L_b}{500h_o} \tag{2-18}$$

where $\psi = 1/\phi$ for LRFD or Ω for ASD.

AISC Appendix 6 uses simplified versions of these equations as its recommendations for brace strength and stiffness design. These equations are discussed further in the following Section 2.6. Specific bracing design concepts and rules for columns and beams are discussed independently in this section. The aim of Section 2.6 is to summarize all the various enhancements to the base AISC Appendix 6 equations detailed in the Appendix 6 commentary. By doing this, the best application of the AISC Appendix 6 rules can be evaluated more easily and potentially improved.

As a final note, as stated at the end of Section 1.2, this research focuses predominantly on the stability bracing requirements, neglecting any potential primary forces that the bracing components must resist. Section 2.2 explains how the relative bracing equations can be extended to handle primary (applied) loading effects combined with stability bracing effects and Section 2.3.5.6 explains how these relative bracing calculations can be extrapolated to handle combined primary loading and stability bracing effects on nodal braces. Unfortunately, the situation is much more complex when beam bracing systems are subjected to primary forces. For example, suppose that one wishes to determine the combined primary loading and stability bracing effects on the purlins and flange diagonals on a roof girder, where the primary loading effects come from the application of snow, wind and/or other loads to the roof system. In this case, it is expected that the amplifier

$1 / (1 - \beta_i / \beta)$

where β_i is the ideal bracing stiffness of the beam bracing system may provide a relatively conservative estimate of the second-order amplification of the primary loading effects. The following discussions in Section 2.6 address only the stability bracing effects.

2.6 Overview of 2010 AISC Appendix 6 Bracing Requirements

The requirements for the strength and stiffness of relative (shear panel) and nodal (discrete grounded) column braces are summarized below in Section 2.6.1. The requirements for relative and nodal beam braces are then summarized in Section 2.6.2.1. This is followed by a summary of the AISC Appendix 6 nodal torsional bracing requirements in Section 2.6.2.2. These summaries include all of the refinements provided

in the Appendix 6 Commentary as well as interpretations of the Specification and Commentary provisions important for their most effective implementation. The main AISC Specification Appendix 6 provisions are based on a number of simplifying assumptions that tend to increase their conservatism for certain cases. It is useful to include the various enhancements from the Specification Commentary when evaluating potential improvements for stability bracing design.

It should be noted that the 2010 AISC Appendix 6 provisions are largely the same as in the 2005 Specification. The primary changes in 2010 are the addition of a Section 6.4 on beam-column bracing, the addition of several user notes, and the refinement and streamlining of the discussions in the Commentary. The Appendix 6 equations in the 2010 Specification are identical to those in 2005. However, due to several refinements in the commentary, the equation numbers are different in the 2010 Commentary. All the AISC commentary equation numbers in the following section correspond to the 2010 Commentary.

2.6.1 Bracing of Columns

The 2010 AISC Appendix 6 addresses only two types of column bracing: relative and nodal. The recommended equations are summarized in the following subsections.

2.6.1.1 Relative Bracing

The base AISC Appendix 6 requirements for the strength and stiffness of a column relative brace are as follows:

Strength Requirement

$$V_{br} = 0.004\,\Sigma P_r \qquad \text{(2-19, AISC A-6-1)}$$

where

ΣP_r = required axial strength in the unbraced length under consideration (in a single column or in a set of columns braced by the shear panel), determined from the LRFD or ASD load combinations, taken as the largest value of the total column axial force stabilized by the shear panel at any cross-section cut along the corresponding unbraced length.

V_{br} = required shear strength in the bracing panel (the notation V_{br} is used here rather than the notation P_{br} from AISC Appendix 6, to emphasize the fact that this is panel shear force, not a brace axial force).

Stiffness Requirement

$$\beta_{br} = \psi\left(\frac{2\Sigma P_r}{L_b}\right) \qquad \text{(2-20, AISC A-6-2)}$$

where

$\psi = 1/\phi = 1/0.75 = 1.33$ for LRFD

$= \Omega = 2.00$ for ASD

L_b = distance between brace points for the shear panel under consideration

β_{br} = required stiffness of the shear panel, defined as the shear force required to generate a unit relative transverse deflection of the unbraced length ends.

If the actual provided brace stiffness is larger than that required by Eq. (2-20), the AISC Commentary indicates that the required brace strength may be determined as

$$V_{br} = \frac{0.004\Sigma P_r}{2 - \dfrac{\beta_{br}}{\beta_{act}}} \qquad \text{(2-21, AISC C-A-6-1)}$$

where β_{act} is the actual provided shear panel stiffness. Griffis and White (2011) give a derivation of Eq. (2-21) based on the use of the AISC Direct Analysis Method. For design by ASD, Eq. (2-21) gives exactly the same result as Eqs. (2-1) or (2-2). The term in the denominator of Eq. (2-21) is basically an adjustment to the base AISC Appendix relative bracing force, $V_{br} = 0.004P_r$, accounting for the influence of brace stiffnesses different from the required value β_{br}.

For the relative bracing model (i.e., pins implicitly included at all of the brace points), Eq. (2-21) gives the correct solution for any value of β_{act}. However, as noted above, the commentary indicates that this equation should only be used for $\beta_{act} > \beta_{br}$. One can observe that in the limit that $\beta_{act} = \beta_{br}/2$, the brace force given by Eq. (2-21) becomes unbounded. This corresponds to the amplification factor becoming unbounded in the reduced stiffness analysis model of the DM (see Eqs. (2-1) and (2-3)).

One should note that in the case of multiple columns tied together and braced by a single shear panel, the flexibility of the components tying the individual columns back to the shear panel is not considered in the above equations. These tie components, and their connections to the members being braced and to the bracing system, may be modeled as individual axial struts. If this flexibility is an important contributor to the brace point displacements, the bracing problem effectively involves a combination of relative and nodal bracing, i.e., relative bracing from the shear panel, and nodal bracing from the ties linking the columns to the shear panel. Actually, the ties must be designed for strength as nodal braces in any case, but if they are effectively rigid, the shear panel bracing can be designed without considering their flexibility.

The AISC Appendix 6 provisions do not address the design of bracing where the ties back to the relative bracing system have significant flexibility. This situation can occur where the columns being braced are tied to the relative bracing system via a long length of horizontal members. However, this case can be addressed easily by using the DM, as discussed in White et al. (2007).

The following are key points that should be kept in mind when applying the AISC Appendix 6 relative bracing equations (Griffis and White 2011):

- The relative bracing requirements give the shear force that must be resisted by as well as the shear stiffness that must be provided in a given panel of the bracing system.
- The relative bracing model neglects any help from the flexural rigidity *EI* of the column(s). That is, the columns are modeled as bar chains, with pins at the brace points, in the development of the relative bracing equations. Therefore, the L_q concept (discussed previously in Section 2.3.5.3) is not applicable for relative bracing. This idealization is conservative relative to the physical behavior when there are substantial flexural continuity effects through the brace points or at the member ends. However, in many practical relative bracing situations, the shear panel bracing stiffness dominates over the other bracing contributions.

In addition, it is useful to note that the adjacent unbraced lengths along the same member need not be equal to one another for the relative bracing idealization to be applicable. Given the pin and shear spring idealizations discussed in Section 2.2.2, the adjacent unbraced lengths are effectively independent of one another in the AISC relative bracing model.

2.6.1.2 Nodal Bracing

The AISC Appendix 6 requirements for nodal column bracing are as follows:

Strength Requirement

$$P_{br} = 0.01\, P_r \qquad \text{(2-22, AISC A-6-3)}$$

Stiffness Requirement

$$\beta_{br} = \psi\left[2\left(4 - \frac{2}{n}\right)\right]\left(\frac{P_r}{L_q}\right) \qquad \text{(2-23, AISC A-6-4)}$$

where

$\psi = 1/\phi = 1/0.75 = 1.33$ for LRFD

$= \Omega = 2.00$ for ASD

n = number of intermediate brace points within the column length between the "end" rigid bracing locations (not including the end points). The term $(4 - 2/n)$ gives an approximation of the coefficients in the first column of Table 2.2. This term accounts for the benefit of having rigid end supports close to the intermediate braces when n is small. It accounts for the fact that the buckling displacements at each of the adjacent brace points are actually the same but in opposite directions in the idealized situation where n approaches infinity, as shown in Figure 2.11. That is, as n approaches infinity for a given P_r, L_b, and β, the buckling rotation of the unbraced length chords approaches two times the rotation associated with the movement of any of the individual intermediate braces. As such, two times the $n = 1$ nodal bracing stiffness requirement is required to develop the same buckling strength as n approaches infinity.

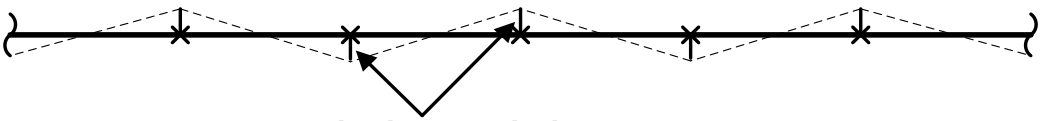

Fig. 2.11. Buckling displacements at adjacent brace points as *n* approaches infinity

It should be emphasized that the variation of $(4 - 2/n)$ from the value of 2 for $n = 1$ to the value of 4 for $n = \infty$ is due to the beneficial effect of the nodal braces having close proximity to the rigid end braces for small n and the fact that the rigid end braces have a limited influence on the interior brace responses for large n.

P_r = required axial strength, taken as the largest value of the column axial force along the member length.

L_q = the maximum unbraced length for which the member can support the required axial load using $K = 1$.

If the actual provided brace stiffness is larger than that required by Eq. (2-23), the AISC Commentary indicates that the required brace strength may be determined as

$$P_{br} = \frac{0.01P_r}{2 - \frac{\beta_{br}}{\beta_{act}}} \qquad \text{(2-24, AISC C-A-6-1)}$$

where β_{act} is the actual provided brace stiffness. This equation is based on an ad hoc extension of Eq. (2-21) to the nodal bracing problem.

The axial load term is written without a summation in Eqs. (2-22) through (2-24). Where multiple columns are tied together in series by lines of braces extending to a fixed (grounded) brace point, these equations can be used with the sum of the axial forces to

check the brace between the last of the members tied together in series and the fixed point, assuming the flexibility of the ties between the members is negligible. These equations do not directly address the influence of the flexibility of the ties between the members though, if this flexibility is a significant contributor to the brace point displacements.

Key points that should be kept in mind when applying the AISC Appendix 6 nodal bracing equations are (Griffis and White 2011):

- The nodal bracing requirements address the absolute or direct force that must be transferred from a brace point back to an effectively rigid structure, assembly or grounded location, as well as the discrete stiffness that must be provided by the ties back to the grounded location.
- The nodal bracing requirements include the help from the *EI* of the column(s) in an approximate fashion via the L_q parameter. For columns where the smallest possible effective length factor is $K = 1$ for the ideal case of rigid bracing, the resistance to brace point movement from the column flexural rigidity diminishes to zero in the limit that the bracing system stiffness approaches the full bracing value. For cases having rotational end restraint of a critical unbraced length such that the "actual" K is less than one, the help from the column flexural rigidity and the end rotational restraint can substantially reduce the bracing demands at loads less than or equal to the member capacity associated with $K = 1$ (as well as somewhat higher than that load level). This beneficial effect is not included in the Appendix 6 nodal bracing equations.

It should be emphasized that AISC (2010) Appendix 6 uses the *applied load* P_r to estimate the brace stiffness and strength requirements as shown by the above equations. This is in contrast to Winter's (1958) equations, which are derived based on the assumption that the column is loaded at the *critical buckling load* P_e. The switch from P_e to P_r is based on two important concepts and assumptions:

1. It is assumed that when the required (i.e., applied) axial load P_r reaches the design resistance, $\phi_c P_n$ in LRFD or P_n/Ω_c in ASD, the elastic or inelastic column is effectively at a state of incipient buckling and responds in the same fashion as the ideal elastic imperfect column in Winter's model.
2. It is assumed that for $P_r < \phi_c P_n$ (LRFD) or P_n/Ω_c (ASD), it is conservative to use the smaller load P_r in specifying the column strength and stiffness requirements. This assumption is certain to be true because of the nonlinear reduction in the effective column stiffness due to distributed yielding and second-order effects as the column axial load is increased.

If $L_q > L_b$ is used in Eq. (2-23), it is important to recognize that the relaxed β_{br} is sufficient only to develop $\phi_c P_n = P_u$ (LRFD) or $P_n / \Omega_c = P_a$ (ASD). If the unbraced length is also subjected to major-axis bending moment, the combined loading should be considered. The 2010 AISC Specification Appendix 6 Section 6.4 provides some limited guidance for this common situation.

Lastly, it should be noted that Eqs. (2-22) and (2-23) may be applied in an ad hoc manner to cases with unequal axial load and/or unbraced length L_b by using the largest P_r /L_b, as long as the P_r in any of the unbraced lengths does not exceed the design capacity based on $K = 1$ for that segment. As such, the bracing is designed assuming an

effective column subjected to constant axial load and having a total length of $(n + 1)L_b$. This solution is conservative since the flexural end restraint from less critical adjacent unbraced lengths tends to reduce the bracing demands.

In the above case, it is not appropriate to use L_q. If L_q were considered for each unbraced length, the bracing design is governed simply by the largest P_r. However, the use of the largest P_r along with the corresponding L_q does not recognize the influence of variable brace spacing along the member length. The brace requirement would be the same for unequal and equal spacing of braces if the rule were applied in this way.

It should be noted that the equations from Lutz and Fisher (1985) are recommended by the 2005 and 2010 AISC Commentary to Appendix 6 as a more accurate calculation of the bracing stiffness and strength requirements for nodally-braced columns. Savings in the bracing stiffness requirements of more than a factor of two can be obtained in some cases by using the corresponding Eqs. (2-8a) through (2-9d) as an alternative to the above refined AISC nodal bracing equations. However, similar to many of the other equations that have been discussed, the Lutz and Fisher equations are strictly applicable only to prismatic columns with equal-stiffness equally-spaced braces, subjected to constant axial load.

2.6.2 Bracing of Beams

The behavior of beam bracing systems is more complicated than that of column flexural buckling bracing systems. This is because the beam buckling resistance involves both bending and torsion while the column flexural buckling capacity depends only on the column flexural rigidity and the resistance of the braces to transverse displacements

due to column bending. The 2010 AISC Appendix 6 beam lateral bracing requirements are summarized in the following section.

2.6.2.1 Lateral Bracing Requirements

2.6.2.1.1 *Relative Bracing*

The 2010 AISC Appendix 6 requirements for relative lateral bracing of beams are as follows:

Strength Requirement

$$V_{br} = 0.004\,(M_r/h_o)\,C_{tR}C_d \qquad \text{(2-25, AISC C-A-6-6a)}$$

where:

M_r = required flexural strength in the unbraced length under consideration from the LRFD or ASD load combinations

M_r/h_o = required equivalent flange force from the LRFD or ASD load combinations, taken as the largest value within the unbraced length under consideration

C_{tR} = flange load height factor for relative bracing

= 1.0 for centroidal loading, or if tipping restraint exists at the points of the load application. The value 1.0 often can be justified due to the restoring torque caused by the eccentric bearing of the girt or purlin against the flange of the member when it starts to twist, the rotational stiffness provided by the attachment of the girt or purlin to the member, and the fact that a large percentage of the moment being resisted comes from applied end moments.

= $1 + 1.2/n$ when the transverse load is applied at the flange level and is detrimental to the member stability (this occurs when the transverse load is applied at the flange level normal to the flange and in the plane of the web and is directed toward the shear center from its point of application). Since the unbraced lengths are independent of one another for the fundamental relative bracing model (see Section 2.2.2), it may be possible that n should be taken equal to one in this equation for relative bracing. The background for this equation is explained by Yura (1995) in the context of nodal beam bracing. The use of $n > 1$ here recognizes that the physical member typically is continuous across the intermediate brace points.

C_d = double curvature factor, which accounts for the potential larger demands on the "shear panel" bracing due to flexure in the unbraced lengths near inflection points; applied only to the unbraced length containing the inflection point and the adjacent unbraced length closest to the inflection point. Note that if relative (shear panel) bracing is employed near an inflection point, then effectively one needs to have shear panel bracing for both of the flanges at the inflection point. This is of course not commonly encountered in practice. One can have relative (shear panel) bracing on one flange plus a flange diagonal to the opposite flange. However, strictly speaking, this involves a hybrid combination of shear panel bracing plus discrete nodal bracing. The background to the C_d equation is from the nodal bracing studies discussed by Yura (2001).

= $1 + (M_S/M_L)^2$ for the above two unbraced lengths, where M_S and M_L are defined below

= 1.0 otherwise

M_S = smallest moment within the two unbraced lengths referenced in the definition of C_d

M_L = largest moment within the two unbraced lengths referenced in the definition of C_d

V_{br} = required shear strength in the bracing panel under consideration

h_o = distance between the flange centroids.

A simple interpretation of the equation for C_d factor is as follows (see Fig. 2.12). For the case with fully reversed curvature bending, i.e., $M_S = M_L$, the C_d factor is equal to 2. For the hypothetical case with an inflection point at the far end of one of the two unbraced lengths under consideration, $M_S = 0$ and the factor $C_d = 1$. However, based on the above definition of C_d, the two unbraced lengths on each side of the inflection point (the location where $M_S = 0$ in the middle sketch) would be used in the calculation in this case, not the two unbraced lengths shown in the figure. The bottom sketch in the figure shows the case for the smallest C_d, given the above definition and assuming a linear moment diagram. In this case, the inflection point is at the mid-length of the left-hand unbraced length, $M_S = M_L/3$, and $C_d = 1.11$. For $M_s < M_L/3$, the inflection point would be closer to the left-most brace point in the bottom sketch, and farther away from the unbraced length with the maximum moment M_L. As such, the C_d calculation applies to the left-most brace point in the bottom sketch. Therefore, for linear moment diagrams, C_d

varies between 1.11 and 2. For general multi-linear or nonlinear moment diagrams, C_d varies between 1 and 2.

It should be noted that the AISC Appendix 6 Commentary refers to M_S and M_L as the smallest and largest moment causing compression in each flange. This definition appears to be a mis-interpretation of the statement "M_S and M_L are the maximum moments causing compression in the top and bottom flanges" from Yura (2001). The author believes that the definition should be consistent with that given in the Yura (2001) reference as noted.

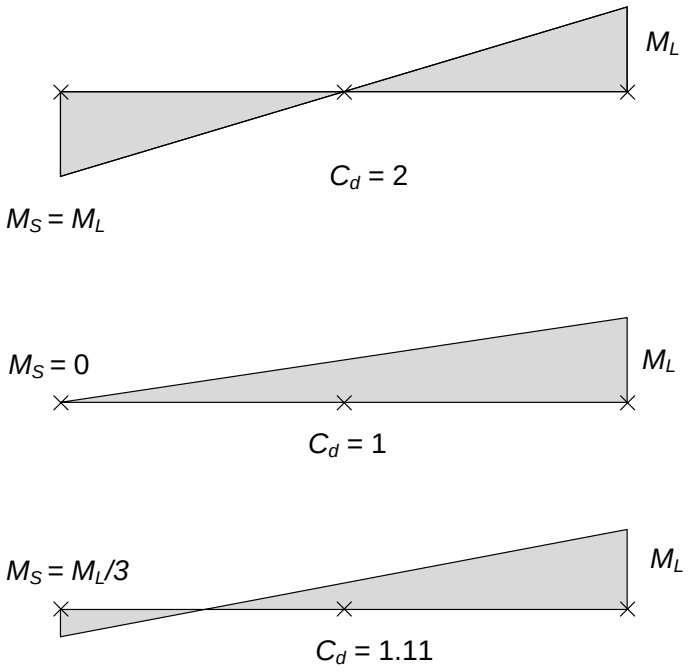

Fig. 2.12. Double curvature factor.

In addition, it should be noted that for web-tapered members,

$$C_d = 1 + [(M_S/h_{oS})/(M_L/h_{oL})]^2$$

may be more representative of the behavior than the previous equation, to account for the influence of web taper. However, neither of these equations has been validated for web-tapered members at the present time (2010).

Stiffness Requirement

$$\beta_{br} = \psi\left(\frac{2(M_r / h_o)}{L_b}\right)C_{tR}C_d \qquad \text{(2-26, AISC A-6-6)}$$

where

ψ = $1/\phi = 1/0.75 = 1.33$ for LRFD

= $\Omega = 2.0$ for ASD

L_b = distance between the brace points for the shear panel under consideration

β_{br} = required stiffness of the shear panel, defined as the shear force required to generate a unit relative transverse deflection of the unbraced length ends.

If the actual provided brace stiffness is larger than that required by Eq. (2-26), the AISC Commentary indicates that the required brace strength may be determined as

$$V_{br} = \frac{0.004(M_r/h_o)}{2 - \dfrac{\beta_{br}}{\beta_{act}}}C_{tR}C_d \qquad \text{(2-27, AISC C-A-6-1)}$$

where β_{act} is the actual provided brace stiffness.

One can observe that all of the above equations are based on the assumption of the equivalency of a relatively braced beam compression flange to a relatively braced column, with the exception of the factors C_{tR}, which accounts for load height effects on the bracing strength and stiffness demands, and C_d, which accounts for higher strength and stiffness demands observed in some cases in the vicinity of beam inflection points.

Therefore, the prior relative column bracing discussions also apply in large part to relative beam bracing.

It should be noted that the beam flange force is actually shown as $P_f = \pi^2 EI_{yc}/L_b^2$ in the AISC Appendix 6 Commentary. However, if designers were to use this expression for the flange force, the beam lateral bracing stiffness requirements would be excessive for most practical problems. In the implementation of the AISC beam lateral bracing requirements, $C_b P_f$ is expressed as M_u/h_o in LRFD, where M_u is the required flexural strength of the beam for the critical LRFD load combination. Similar relationships can be stated for ASD. The maximum permitted value of M_u is $\phi_b M_n$ in LRFD. Hence, the beam lateral bracing stiffness requirements are based on the same type of assumptions as those discussed previously for columns. That is, the bracing stiffness necessary to develop $M_u = \phi_b M_n$ is assumed to be the same as the bracing stiffness necessary to develop the buckling strength in a beam that buckles elastically at this load level. The bracing requirements for $M_u < \phi_b M_n$ tend to be estimated conservatively by this approach, since the beam tends to provide some resistance to the brace point movement for $M_u < \phi_b M_n$.

Where multiple beams are linked effectively by rigid ties back to a single shear panel bracing system, the moment term M_r in the above equations may be replaced by ΣM_r.

2.6.2.1.2 *Nodal Bracing*

The 2010 AISC Appendix 6 requirements for beam nodal lateral bracing are as follows:

Strength Requirement

$$P_{br} = 0.01(M_r/h_o)\, C_{tN} C_d \qquad \text{(2-28, AISC C-A-6-6b)}$$

where

M_r = required flexural strength in the beam from the LRFD or ASD load combinations

M_r/h_o = required equivalent flange force from the LRFD or ASD load combinations, taken as the largest value within the member length

C_{tN} = flange load height factor

= 1.0 for centroidal loading, or if substantial tipping restraint exists at the points of the load application. The value 1.0 often can be justified due to the restoring torque caused by the eccentric bearing of the girt or purlin against the flange of the member when it starts to twist, the rotational stiffness provided by the attachment of the girt or purlin to the member, and the fact that a large percentage of the moment being resisted comes from applied end moments.

= $1 + 1.2/n$ when the transverse load is applied at the flange level and is detrimental to the member stability (this occurs when the transverse load is applied at the flange level normal to the flange and in the plane of the web and is directed toward the shear center from its point of application)

C_d = double curvature factor, which accounts for the potential larger demands on the nodal bracing due to flexure in unbraced lengths containing inflection points; applied only to the brace closest to the inflection point.

= $1 + (M_S/M_L)^2$ when an inflection point occurs within one of the unbraced lengths adjacent to the brace being considered

= 1.0 when neither of the unbraced lengths adjacent to the brace has an inflection point, or when an inflection point exists within a given unbraced

length but is closer to the adjacent brace location (for example, the middle sketch in Fig. 2.12 satisfies this later condition for the middle brace point in the sketch and the bottom sketch in this figure satisfies this condition for its middle brace point if M_S is modified to a value slightly less than $M_L/3$)

M_S = smallest moment within the two unbraced lengths adjacent to the brace under consideration

M_L = largest moment within the two unbraced lengths adjacent to the brace under consideration

h_o = distance between flange centroids

P_{br} = required axial strength of the brace.

The above definitions of C_d, M_S, and M_L are similar to the definitions provided for relative bracing in Section 2.6.2.1.1, but are directed toward the requirements for nodal bracing. Figure 2.12 applies to either of these sets of definitions.

Stiffness Requirement

$$\beta_{br} = \psi\left[2\left(4-\frac{2}{n}\right)\frac{(M_r/h_o)}{L_q}\right]C_{tN}C_d \qquad \text{(2-29, AISC A-6-8)}$$

where

ψ = $1/\phi = 1/0.75 = 1.33$ for LRFD

= $\Omega = 2.0$ for ASD

n = number of intermediate brace points within the beam length between the "end" rigid bracing locations (not including the end braces)

L_q = the maximum unbraced length for which the member can support the required load using $K = 1$.

If the actual provided brace stiffness is larger than that required by Eq. (2-29), the AISC Commentary indicates that the required brace strength may be determined as

$$P_{br} = \frac{0.01(M_r / h_o)}{2 - \frac{\beta_{br}}{\beta_{act}}} C_{tN} C_d \qquad \text{(2-30, AISC C-A-6-1)}$$

where β_{act} is the actual provided brace stiffness.

Similar to the developments in Section 2.6.2.1.1, one can observe that these provisions are a direct mapping of the column nodal bracing provisions to beams, with the addition of the factors C_{tN} and C_d to account for load height and double-curvature effects. Therefore, the prior column nodal bracing discussions also apply in large part to nodal beam bracing.

Where multiple beams are linked effectively by rigid ties back to a nodal brace from the last member to an effectively rigid support, the moment term M_r in the above equations may be replaced by ΣM_r in designing this last nodal brace. If the ties between the members have non-negligible flexibility, a more sophisticated estimate of the demands is necessary.

2.6.2.2 Torsional Bracing Requirements

The complete nodal torsional brace stiffness and strength requirements from the 2010 AISC Appendix 6 Specification and Commentary provisions may be written as follows:

Stiffness Requirement

$$\beta_T = 20\psi h_o^2 \left[\frac{M_r / C_b h_o}{P_{e.eff}} \right] \left(\frac{M_r / C_b h_o}{L_b} \right) \frac{(n_T + 1)}{n_T} C_{tT} \qquad \text{(2-31, AISC A-6-11)}$$

where

$\psi = 1/\phi = 1/0.75 = 1.33$ for LRFD

$= \Omega = 3.0$ (Ω is usually taken equal to $1.5/\phi$, but it is taken as $1.5^2/0.75$ in this case since the moment term appears twice in the equation)

L_b = spacing between the torsional brace points, assumed constant in the development of the equation

M_r/C_b = equivalent uniform moment for a given unbraced length within the member span

M_r / h_o = required effective flange force, taken as the largest value within each unbraced length

C_b = equivalent uniform moment factor for a given unbraced length, based on flange stresses for non-prismatic members (ad hoc extension)

C_{tT} = torsional bracing factor accounting for the effects of height of the transverse loads applied normal to the flanges and in the plane of the web

= 1.2 when the transverse loading is applied at the flange level in a way that is detrimental to the member stability (this occurs when the transverse loading is applied at the flange level and is directed toward the member shear center from its point of application), assuming that substantial tipping restraint does not exist at the transverse loading points. It should be noted that C_{tT} has a different value compared to C_{tR} and C_{tN}.

= 1.0 otherwise; in many cases, this value can be justified due to the restoring torque caused by the eccentric bearing of the girt or purlin against the flange of the member when the it starts to twist, the rotational stiffness provided by the attachment of the girt or purlin to the outside flange of the member, and the fact that a large percentage of the moment being resisted comes from moments applied at the ends of the member.

n_T = number of intermediate nodal torsional brace points within the member length between the rigid"end" brace locations, where both twisting and lateral movement of the beam are prevented. It is interesting to note that the ratio $(n_T + 1)/n_T$ has a maximum value of 2 for $n_T = 1$ and approaches 1 for $n_T = \infty$. This trend is opposite to the trend in the nodal lateral bracing equations as n varies from 1 to ∞. This difference is due to the fact that $(n_T + 1)/n_T$ comes from the mapping of continuous torsional bracing springs to equivalent discrete torsional bracing springs in the development of Eq. (2-31), whereas $(4 - 2/n)$ in the nodal bracing equations is a curve fit to the influence of the rigid end braces on the discrete nodal brace demands. Yura et al. (1992) actually recommend that for $n_T = 1$, the term $(n_T + 1)/n_T$ may be multiplied by 0.75 (see Eq. 2-13).

$P_{e.eff}$ = effective flange buckling load

$= \pi^2 E I_{eff} / L_b^2$

E = modulus of elasticity of steel = 29,000 ksi

I_{eff} = I_y for doubly symmetric sections

= $I_{yc} + \frac{t}{c} I_{yt}$ for singly symmetric sections

c = distance between cross section centroid and centroid of compression flange

t = distance between cross-section centroid and centroid of tension flange

I_{yc} = lateral moment of inertia of the compression flange

I_{yt} = lateral moment of inertia of the tension flange

The above equation (2-31) is derived from Eq. (2-13) by neglecting the unbraced beam buckling term ($C_{bu}M_o$), substituting the applied moment M_r for the critical moment M_{cr}, substituting L_b (n_T + 1) for the term αL, and multiplying the resulting estimate of the ideal bracing stiffness by 2ψ. It is emphasized that Eq. (2-31), with C_{tT} taken equal to 1.2, gives exactly the same result as the AISC Eq. (A-6-11). However, the logical contributions of the various terms can be discerned more clearly in the form shown above.

The similarity of Eq. (2-31) to Eq. (2-9d) should be recognized. Both of these equations are arrived at by extending analytical solutions for continuously-braced members to discretely-braced cases. Both have a term involving a load, P^* or $M_r / C_b h_o$, divided by the brace spacing L_b. In addition, both have a term involving the ratio of P^* or $M_r / C_b h_o$ to an effective buckling load value, $P_{e\tau}$ or $P_{e.eff}$. This ratio captures the resistance provided from the member itself to the brace point displacements.

However, there are also some important differences between Eqs. (2-31) and (2-9d). A term similar to the bracketed expression in Eq. (2-9d) does not appear in Eq. (2-31). This is simply due to the simplification of dropping the $C_{bu}^2 M_o^2$ term in Eq. (2-13) in the development of Eq. (2-31), based on the practical recognition that weak partial bracing of beams is non-typical. Conversely, Eq. (2-9d) does not have any term such as (n_T + 1) / n_T,

involving the number of intermediate braces. This is because the bracketed expression in Eq. (2-9d) is an approximate curve fit to all the analytical solutions for $n > 2$. However, more importantly, Eq. (2-31) does not include any inelastic stiffness reduction whereas Eq. (2-9d) can be affected substantially by the column inelastic stiffness reduction factor τ. Bishop et al. (2010) show that both:

- The AISC torsional bracing equation (Eq. (2-31)) as well as
- A form of Eq. (2-9d), *with τ taken equal to 1.0*, intended for beam nodal lateral bracing,

provide an accurate characterization of the knuckle stiffness values from virtual test simulation for various practical beam benchmarks. In addition, Bishop et al. (2010) show that the ratio between the above torsional bracing stiffness equation, written as an equivalent lateral bracing stiffness by dividing by h_o^2, and the recommended beam nodal bracing equation developed as an extension of Eq. (2-9d) is

$$5\left[\frac{n_T+1}{n_T}\right]\left[\frac{C_{tT}}{C_{tN}C_d}\right]\frac{P_{ef}}{P_{e.eff}}$$

where P_{ef} is the elastic lateral buckling load of the compression flange in the nodally-braced beam, $\pi^2 EI_{yc}/L_b^2$. From this expression, one can observe that the estimated torsional bracing stiffness requirements (β_T) are on the order of $5h_o^2$ times the corresponding nodal lateral bracing stiffness requirements. This value is similar to conversion factors between torsional and lateral bracing stiffness requirements recommended by Yura et al. (1992), which range from πh_o^2 to $2\pi h_o^2$ for practical beam geometries.

Generally, it is recommended that Eq. (2-31) should be evaluated for each unbraced length within the span. The largest resulting value is the required minimum torsional brace stiffness for all the braces. For problems having unbraced lengths with different brace spacing L_b, equivalent uniform moment M_r / C_b, effective lateral bending rigidity EI_{eff}, or member depth h_o, one can still apply AISC Appendix 6 by evaluating Eq. (2-31) for each unbraced length and using the largest resulting value as the required minimum bracing stiffness. The logic behind this ad hoc application of the AISC provisions is that the restraint from less critical adjacent unbraced lengths tends to make the calculation from Eq. (2-31) conservative. This type of ad hoc application of Eq. (2-31) is compared to the results of rigorous virtual test simulation analyses in Chapter 4. It should be noted that there is already precedent for this type of ad hoc application when one uses M_b / C_b in the AISC Appendix 6 torsional bracing equations.

In many situations involving moment gradient, unequal brace spacing L_b, changes in EI_{eff} along the member length, and/or changes in the depth h_o along the member length, it appears that the brace stiffness and strength demands decrease dramatically as one moves away from the most critical member unbraced length. Therefore, it may be possible in many cases to calculate a reduced requirement for the individual braces by applying Eq. (2-31) only considering the unbraced length(s) adjacent to each brace. In addition, there appears to be some potential for use of an effective unbraced length KL_b in the calculation of $P_{e.eff}$ in Eq. (2-31) to account for the interactions between adjacent unbraced lengths, as well as the influence of beam end conditions on the brace demands. For instance, if warping and flange lateral bending are fully restrained at one member

end, a K value of 0.7 might be used in the calculation of $P_{e.eff}$. This would effectively reduce the bracing demands from this unbraced length by a factor of two.

In some situations, member continuity effects can lead to increased bracing demands. In addition, if the bracing stiffnesses are reduced too extensively in the unbraced lengths of a beam where the demands from Eq. (2-31) are small, it is possible that an overall stability failure of the beam could be precipitated, akin to the behavior in benchmark problems with weak partial bracing. Therefore, the above type of ad hoc application of Eq. (2-31) needs careful scrutiny prior to application in design practice. The examples in Chapters 4 through 8 are intended to provide some insight into these considerations.

In any case, the flange bracing must be designed for the internal force envelopes corresponding to all the appropriate load combinations. This tends to limit the savings that can be achieved by recognizing that the braces more remote from a critically loaded section are subjected to substantially smaller demands.

It should be noted that as a result of its origin in the elastic LTB resistance equation for an I-section member with continuous torsional bracing, the stiffness requirement from Eq. (2-31) is proportional to $(M_r /C_b)^2$ and inversely proportional to EI_{eff} /L_b. It is interesting to contrast this rule with Eq. (2-29) for beam lateral bracing, which indicates that the lateral bracing stiffness requirement is proportional to M_r /L_q, or M_r /L_b in the limit that $M_r = \phi_b M_n$ (LRFD) or M_n / Ω_b (ASD). It is particularly interesting to contrast each of these equations with the result from Eqs. (2-8) and (2-9) in the limit that $L_e = L_b$, if one infers that the column analogy can be applied to arrive at the beam lateral bracing requirements using this equation as an alternative to Eq. (2-29). This is because Eqs. (2-8) and (2-9) are derived from the buckling resistance (but inelastic rather than elastic) of

a continuously braced column. Equations (2-8) and (2-9) indicate that the lateral bracing stiffness requirement is proportional to $\tau EI / L_b^3$, or P_{cr} / L_b, in the limit that $L_e = L_b$. An important question that can be asked is the following: Which of these relationships give a better characterization of the stiffness requirements for a given type of bracing? Another question that may be asked is: Does the inelastic member response have any significant effect on the torsional bracing stiffness requirements?

In the application of the AISC torsional bracing equations, the web distortional stiffness should be taken as

$$\beta_{sec} = \frac{3.3E}{h_o}\left(\frac{1.5h_0 t_w^{\ 3}}{12} + \frac{t_s b_s^{\ 3}}{12}\right) \qquad \text{(2-32, AISC A-6-12)}$$

where

t_w = beam web thickness

t_s = web stiffener thickness

b_s = stiffener width for one-sided stiffeners (two times the individual stiffener width is recommended for double-sided stiffeners; two times the individual stiffener width plus the web thickness is also legitimate)

This equation is the same as the corresponding Eq. (2-16) from Yura and Phillips (1992) and Yura et al. 1992). In addition, this equation has origins in the research by Milner and Rao (1978).

The required stiffness that must be provided by the remainder of the torsional bracing system, accounting for the influence of web distortion, is

$$\beta_{Tb} = \frac{\beta_T}{\left(1 - \frac{\beta_T}{\beta_{sec}}\right)} \qquad \text{(2-33, AISC A-6-10)}$$

The derivation of this equation is explained previously in Section 2.5.2.

Interestingly, it should be noted that there is no C_d term in the torsional bracing equations. Apparently there are no significant additional demands on torsional bracing at beam inflection points, whereas if only lateral bracing is provided, both flanges have to be braced near the inflection point and the calculated demands can be significantly larger. This does not appear to be logical, but specific investigation of this consideration is beyond the scope of the present research.

Lastly, Yura and Phillips (1992) point out that the height of the torsional braces is not an important factor as long as the beam cross-section does not distort. Yura (1993 and 2001) handles this attribute by providing a generalized equation for β_{sec} that depends on the height at which the torsional bracing is attached to a full-depth or partial depth beam transverse stiffener.

Strength Requirement

Given the required total bracing stiffness β_T from the AISC torsional bracing requirements and the assumed layover at the brace point of $\theta = \theta_o = 0.002L_b/h_o$, the strength required for the brace can be calculated as

$$M_{br} = \frac{\beta_T}{\psi}\theta_o = \frac{\beta_T}{\psi}\frac{L_b}{500h_o} \qquad \text{(2-34, AISC C-A-6-8)}$$

This equation is identical to Eq. (2-18). However, the AISC requirement for β_T is a simplification of the more refined estimate of the required β_T given by Yura and Phillips (1992). The refined β_T is substantially smaller in some situations.

The AISC Appendix 6 Eq. (A-6-9) for M_{br} combines a separate form of Eq. (2-31) with Eq. (2-34). This AISC form of Eq. (2-31) uses L rather than $(n_T + 1)L_b$, resulting in

the length ratio L/L_b appearing in the final AISC expression for M_{br}. In addition, C_{tT} is taken equal to its maximum value, 1.2, and $(M_r/C_b h_o)/P_{e.eff}$ is taken equal to ½ to obtain AISC Eq. (A-6-9).

AISC Appendix 6 states that when L_b is less than L_q, L_b in the equation for M_{br} may be replaced by L_q. There appears to be little rationale for this substitution. All the other uses of L_q in the AISC provisions involve reductions in the required lateral bracing stiffnesses to approximate the partial bracing stiffness requirements. However, for torsional bracing, the origin of the bracing stiffness requirement in the continuously braced model (Eq. (2-13)) already accounts for the partial bracing characteristics of the problem. The use of L_q in the calculation of M_{br} appears to be an ad hoc addition for which no validation has been published. Therefore, L_q is not used with the torsional bracing calculations in this research.

2.7 Example Ad Hoc Application of the Current AISC Appendix 6 Requirements to Metal Building Frame Systems

This section presents sample calculations showing an example application of the AISC Appendix 6 requirements to a non-Appendix 6 type bracing system similar to that shown in Fig. 1.1. The purpose of this section is to demonstrate *a representative example application* of the Appendix 6 equations. As such, these calculations are intended to aid in identifying where potential improvements are needed as well as where current provisions adequately address stability bracing considerations. It should be noted that since the Appendix 6 equations do not apply directly to the bracing design for a system such as the one in Fig. 1.1, it is possible that these equations can be refined to obtain better estimates of the demands on the bracing system than those provided here. Other

interpretations may be required when addressing various other non-Appendix 6 characteristics.

There are two essential contributors to the flange bracing of the main frame members in the type of structure shown in Fig. 1.1:

1. Lateral relative ("shear panel") bracing of the member outside flanges, via the attachment of the girts and purlins to the outside flange of the members, the attachment of diagonals parallel to the plane of the wall or roof, near the outside flange, and/or the attachment of wall or roof diaphragms to the outside of the girts or purlins. This type of bracing is required to:
    - Define the brace points corresponding to the X-bracing panels for development of the nominal axial resistances P_n required to support the axial forces ΣP_r, where ΣP_r is the total axial force in the members stabilized by a given X-bracing panel.
    - Define the brace points to develop the P_n values necessary to support the ΣP_r in the main frame members by wall or roof panels between the outset girt/purlin locations, wherever the girt or purlin locations are considered as brace points along a "constrained axis" for calculation of the constrained axis torsional (CAT) buckling column axial resistances.
    - Define the brace points to develop the P_n values necessary to support the ΣP_r in the main frame members by the panels between girt/purlin locations, when out-of-plane column flexural buckling is to be restrained at these girt/purlin locations (typically by a combination of the attachment of the girts/purlins to the outside flange as well as the attachment of a diagonal flange brace to the

inside flange, so that both flanges are restrained against out-of-plane movement). This permits calculation of the column axial resistance based on flexural buckling using the length between these panel points.

- Develop $\Sigma M_r / h_o$ in main frame members by the shear panels (either X-bracing panels or panels between girt/purlin locations) where the members are subjected to flexural compression on the outside flange, *unless* torsional bracing is provided at these brace points. It should be noted that flange diagonal bracing affects a single frame only, whereas lateral relative bracing can be used to develop the brace points for multiple frames (hence the term $\Sigma M_r/h_o$).

Lateral relative bracing of the outside flange of the main structural members is not effective (and should not be counted upon) to restrain beam lateral-torsional buckling at any brace point where the flexural compression is on the *inside* flange (unless flange diagonals are provided). However, if the flexural compression occurs on the outside flange at the opposite end of the unbraced length, "shear panel" bracing can be designed to develop that point as a brace point. In this case, some type of restraint to the inside compression flange is required at the end of the panel where this flange is in compression.

2. Discrete ("point") torsional bracing of the member inside flanges via the attachment of flange diagonals between the girts or purlins and the inside flange of the main members. This type of bracing is required to:

   - Develop M_r at any location assumed as a lateral-torsional buckling (LTB) brace point for the design of the member, *with the exception of* cases where:

     a. Lateral relative bracing is provided on the outside flange, *and*

b. The outside flange is subjected to flexural compression at the corresponding brace point.

- Develop $P_r h_o/2$ at any location assumed as a column flexural buckling brace point for the design of the member. The value $P_r h_o/2$ is an ad hoc "equivalent moment" intended to ensure that the inside flange is adequately braced at those locations, since the column relative bracing is attached to the outside flange.

The discrete torsional braces are assumed to be attached to the flange or to the web at a location very close to the web-flange juncture in this research. Hence, the web flexibility does not affect the stiffness provided by the flange diagonal for the members and frames considered in this work. If the brace is attached other than the web-flange juncture, the web distortional flexibility must be taken into account when calculating the stiffness needed from the brace itself (see Eq. 2-33).

Discrete torsional braces need not be provided at girt or purlin locations that are:

- Counted upon only as a brace point along a constrained axis at the depth of the girts or purlins for calculation of the P_n associated with the constrained axis torsional buckling limit state,
- Not considered as a brace point for lateral torsional buckling, or
- Tied to outside flange "shear panel" relative bracing, *unless* the inside flange is subjected to flexural compression at this location.

Figure 2.13 shows an elevation view of the clear span frames illustrated in Fig. 1.1. These frames are assumed to be an interior spans within a metal building. The bracing for these frames is evaluated extensively in subsequent studies (see Chapter 6). This

frame has been studied in the prior research by Kim (2010) and White and Kim (2006) based on the assumption that all the brace points effectively function as immovable supports. The original design of the frame was performed by Mr. Duane Becker of Chief Industries. Figure 2.14 shows additional information about the layout of the roof system between two of these internal frames. The complete geometric attributes of this frame are provided subsequently in Chapter 6.

The following calculations assume that the X bracing is placed longitudinally in every fifth bay along the length of the building. The frame spacing in the out-of-plane direction is 25 ft. The load case considered in this example is the ASD load combination Dead + Collateral + Uniform Snow. The second-order moment and axial force diagrams determined by Kim (2010) at $\alpha = 1.6$ times the ASD load level are shown in Figure 2.15.

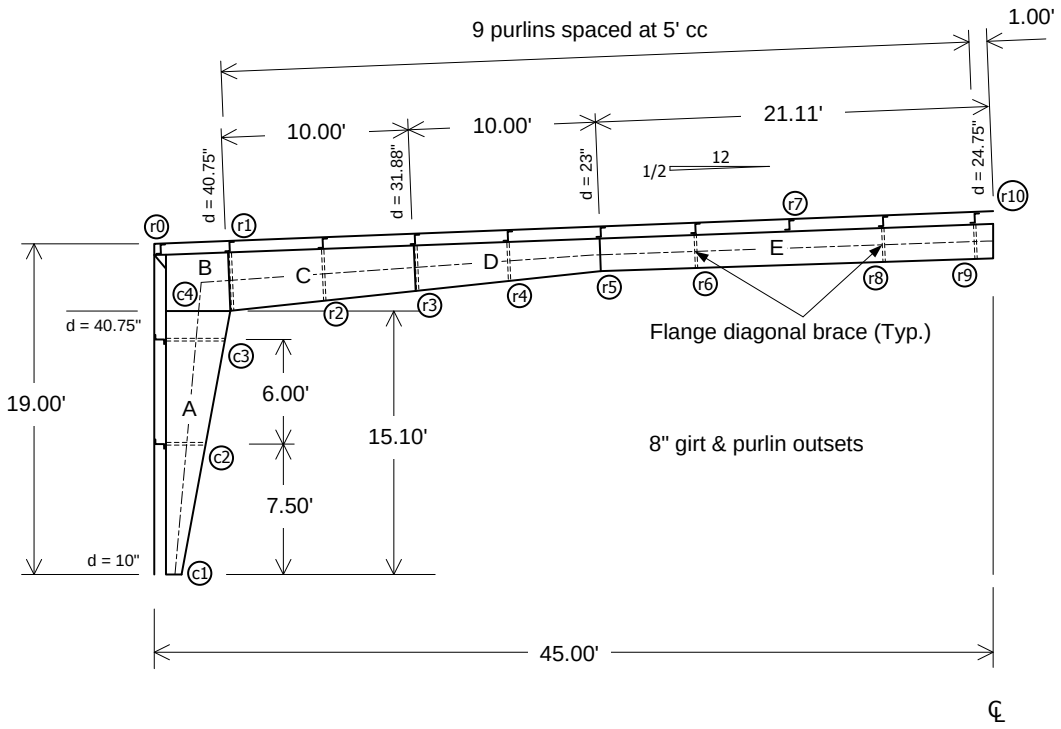

Fig. 2.13. Elevation view of an example clear span frame from Kim (2010).

The specific bracing systems for this building are as follows:

- The wall and roof diaphragm shear stiffness and allowable strengths are shown in Table 2.4. These values are representative of typical R panels.

Table 2.4 Wall and roof diaphragm strength and stiffness representative of typical R panels

	G' (kips/inch)	v_a (lb/ft)
Wall	3.52	61.2
Roof	4.19	122

- The X-bracing system consists of 5/8 in rods. As noted in the prior discussions at the end of Sections 1.2 and 2.2.2, the X-bracing typically plays a relatively minor role in developing the girt and/or purlin locations as brace points. Therefore, the contributions from these rods do not enter into any of the following calculations.
- The girts and purlins are 8 inch deep, 16 gage cold formed Z-sections framed continuously over the frames in the out-of-plane direction. These sections have a moment of inertia of I = 8.15 in^4. Any increase in the moment of inertia by overlapping of these sections is neglected for simplicity in the example calculations. These girt/purlin sizes are considered to be representative minimum sizes for the loadings and 25 ft out-of-plane frame spacing on this structure (Becker, personal communication).
- The flange diagonal braces are 1.5 inch dia. x 15 gage tubes with a 0.5 inch diameter bolt at each end. These diagonal braces are provided on both sides of the main frame members and they are attached directly to the inside flange of the

primary members near the web-flange juncture at all of the diagonal bracing locations. Flange diagonal braces are provided at all the girt and purlin locations except r5 and r7 as shown in Fig. 2.13. Angles are most commonly used for the flange diagonal braces. However, the type of diagonal brace is of minor importance in this study since the flexibility of the system is dominated by the purlin or girt.

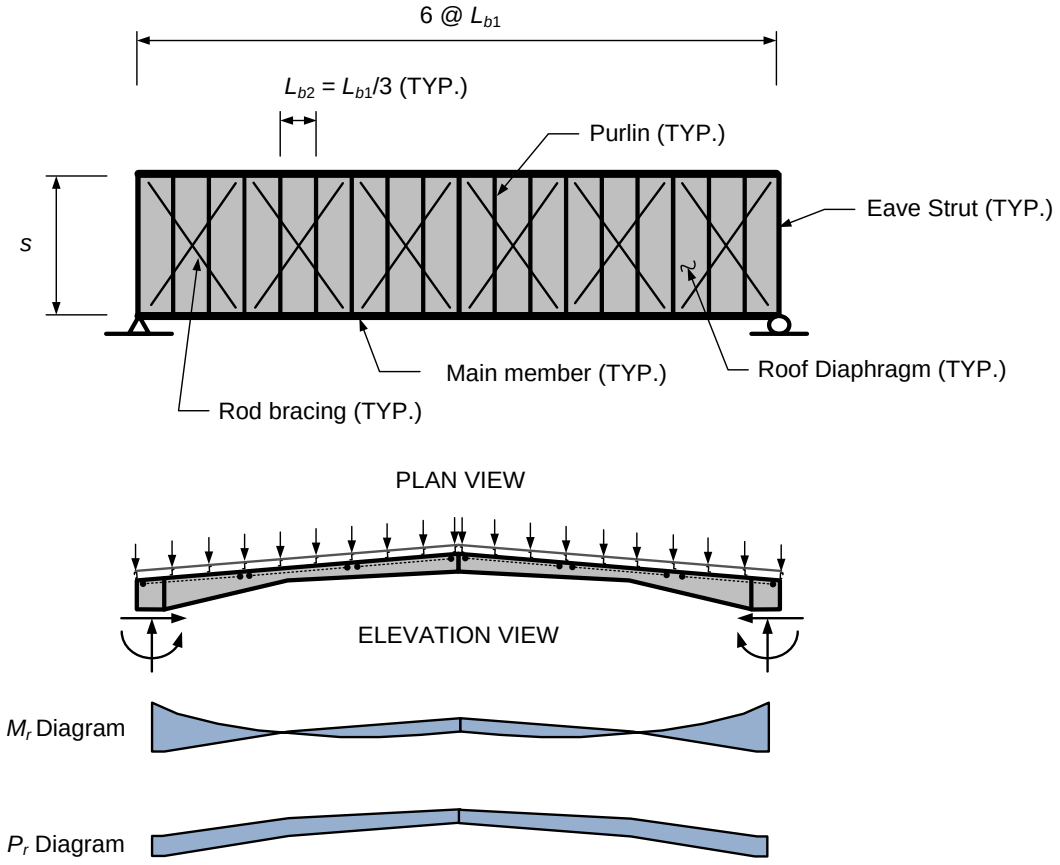

Fig. 2.14. Representative roof girders and roof system for a basic idealized clear span metal building structure having only two main frames.

Selected bracing design checks based on the above idealizations are presented below. The shear-panel bracing by the wall panels is checked first, followed by a check of the flange diagonal torsional brace at location c3 near the top of the columns (see Fig. 2.13).

Next, the roof diaphragm bracing is checked in the negative moment region between the locations r0 and r2. This is followed by a check of the roof diaphragm bracing in the positive moment region between locations r6 and r8. Lastly, the torsional brace at r1 is checked.

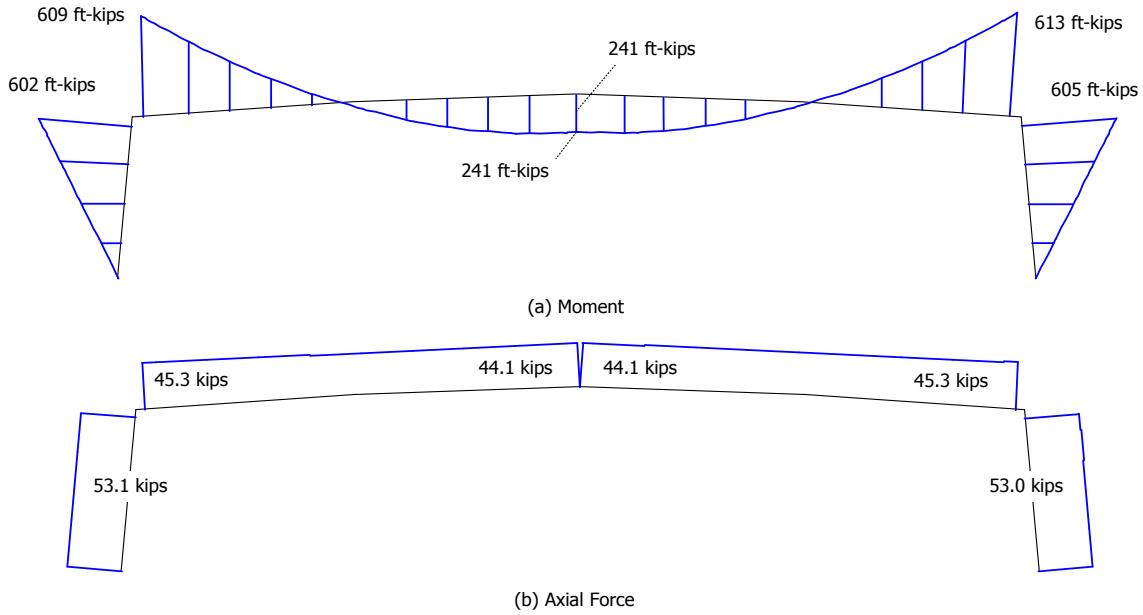

Fig. 2.15. Moment and axial force distributions, clear-span frame Dead + Collateral + Uniform Snow (Kim 2010).

2.7.1 Wall Diaphragm Bracing

The columns are subjected to flexural compression on their inside flange along their entire length. Therefore, the bracing of the inside flanges is accomplished by flange diagonals framed from the girts. These components are designed as torsional braces. Thus, the wall diaphragms are designed solely to brace the members against out-of-plane flexural buckling at each of the girt locations, using the relative bracing provisions detailed in Section 2.6.1.1.

2.7.1.1 Relative (Shear Panel) Bracing Stiffness

The shear panel stiffness check may be written as follows:

$$\left[\beta_{diaphragm} = \frac{G'\sum s}{L_b}\right] \geq \left[\beta_{br} = 2\Omega\left(\frac{\sum P_r}{L_b}\right)\right] \qquad (2\text{-}35)$$

where

Σs = 25 ft x 5 bays = 1500 inches

ΣP_r = (53.0 k /1.6) x 5 bays = 165.5 k

Ω = 2.0

L_b = shortest unbraced length for the shear bracing panels

= 5.5 ft = 66 inches between r0 and c3

By multiplying both sides of Eq. (2-35) by $L_b/\Sigma s$, this check may be written more directly in terms of the specified panel shear stiffness as

[G' = 3.52 k/in] > [G'_{reqd} = 2(2.0)(165.5/1500) = 0.44 k/in] **OK**

2.7.1.2 Relative (Shear Panel) Bracing Strength

The shear panel strength is checked as follows:

$$\left[V_a = v_a \sum s\right] \geq \left[V_{br} = 0.004 \sum P_r\right]$$

where all the terms are defined in Section 2.7.1.1 except

v_a = allowable diaphragm strength = 61.2 lb/ft

This check may be written in terms of the shear panel allowable design strength as follows:

$[v_a = 61.2 \text{ lb/ft}] > [v_{br} = 0.004(165{,}500)/125 \text{ ft}) = 5.3 \text{ lb/ft}]$ **OK**

2.7.2 Torsional Bracing at c3 (Girt Closest to the Top of the Column)

The combination of the girts and flange diagonals at c3 is designed as a torsional brace to restrain the column against lateral-torsional buckling due to the moment causing flexural compression on the inside flange, as well as to prevent twisting of the column at the brace point due to the column axial compression plus the moment. The design equations are detailed in Section 2.6.2.2. The flexure of the column out of the plane of the frame is restrained by the bracing from the wall panels, but the wall panels do not effectively restrain the twisting of the column. The torsional brace is designed for an ad hoc additional moment of $P_r h_o/2$ to account for the influence of the axial load on the tendency for twisting about the girt location. The potential beneficial influence of the combined torsional and lateral bracing is neglected. Location c4 at the top of the column (i.e., the bottom of the panel zone) is assumed to act effectively as a rigid brace point due to the torsional resistance from the roof girder plus the diagonal brace at r1, the flange continuity plate at the bottom of the panel zone, the out-of-plane restraint from the eave strut, the bending stiffness of the outside flange of the column within the panel zone, and the shear panel restraint from the roof panels between r0 and r1.

2.7.2.1 Torsional Brace Stiffness

The torsional brace stiffness check may be written as

$$\beta_{T.provided} \geq \left\{ \beta_T = 20\psi h_o^2 \left[\frac{M_{r.equiv} / h_o}{P_{e.eff}} \right] \left(\frac{M_{r.equiv} / h_o}{L_b} \right) \frac{(n_T + 1)}{n_T} C_{tT} \right\} \tag{2-36a}$$

where

$$M_{r.equiv} = \frac{P_r h_o}{2} + \frac{M_r}{C_b} \tag{2-36b}$$

For the specified continuous girt and flange diagonal braces, the *provided* torsional bracing stiffness is taken as the following coarse approximation:

$$\beta_{T.provided} \approx 2(4EI/s) = 8(29000 \text{ ksi})(8.15 \text{ in}^4)/300 \text{ in} = 6380 \text{ in-kips/rad}$$

This is a rough *upper-bound* estimate of the stiffness provided by the girt and flange diagonal braces for the situation where the frames adjacent to the critical frame do not buckle, but instead offer substantial rotational restraint to the opposite end of the girt spans, where *s* is the frame spacing and *I* is the moment of inertia of the girts about the major-axis (see Fig. 2.16). More refined estimates of this type of stiffness are discussed subsequently. The flexural stiffness contribution from the girt on each side of the critical frame is approximately *4EI/s*, since the opposite end of the girt is assumed to be attached to (and continuous over) an adjacent frame that is idealized as fixed point.

It should be noted that if the adjacent frames are also at their buckling load limit, the rotational stiffness provided by the girt or purlin reduces essentially from *4EI/s* to *2EI/s*, a 50% reduction in stiffness. As shown subsequently in Chapters 4 and 5, stability bracing

experts have spanned the full range of assumptions regarding the restraint conditions from adjacent frames. The appropriate choice of values depends greatly on engineering judgment. In the view of the author, it is probably rare that one can safely assume that one frame is critical while the adjacent frames are not loaded close to their critical load levels. However, it is extremely pessimistic to assume that three adjacent frames are all loaded in an equally critical fashion. Therefore, for cases where flange diagonals are provided on both sides of all the frames, possibly the value $2EI/s + 4EI/s = 6EI/s$ is a reasonable intermediate approximation. This is the value effectively used in the original design problem in Chapter 5.

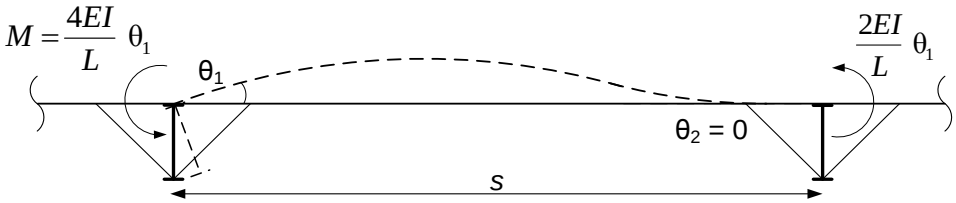

Fig. 2.16. Idealized model used to estimate girt or purlin stiffness.

Because of the short length of only 1.6 ft from c3 to c4, the longer unbraced length c2-c3 governs the brace stiffness and strength calculations for c3. Therefore, the other parameters to be entered into Eqs. (2-36a) for location c3 are:

Ω = 3.0 (= $1.5^2/0.75$, since the moment term appears twice in Eq. (2-36a))

C_{tT} = 1 (negligible tipping effects from any transverse loads)

L_b = 6 ft = 72 inches

$$M_{r.equiv} = \left(\frac{P_r h_o}{2} + \frac{M_r}{C_b} \right)$$

= equivalent uniform moment within the governing unbraced length

C_b = 1.02 for the middle unbraced length of the column, c2-c3, based on flange stresses

M_r = 542 ft-kips/1.6 = 339 ft-kips = 4070 in-kips (largest moment in the unbraced length c2-c3)

$P_r h_o$ /2 = equivalent moment estimate for determining the torsional brace stiffness needed to prevent constrained-axis torsional buckling of the column about the girt at c3

h_o = 37.0 inches, largest value in c2-c3, located at c3 (see Table 6.1)

$P_r h_o$ /2 = (53.0 kips/1.6)(37.0 in)/2 = 613 in-kips, (note that this equivalent moment is relatively small compared to M_r/C_b, typical of metal building frames)

$$M_{r.equiv} = \left(\frac{P_r h_o}{2} + \frac{M_r}{C_b} \right) = 4610 \text{ in-kips}$$

$M_{r.equiv}$ /h_o = 124 kips

$$I_{eff} = I_{yc} + \frac{t}{c} I_{yt}$$

$$I_{yc} = \frac{b_{fc}^3 t_{fc}}{12} = 9 \text{ in}^4 \text{ for } b_{fc} = 6 \text{ inches and } t_{fc} = 0.5 \text{ inches (see Table 6.1)}$$

$$I_{yt} = \frac{b_{ft}^3 t_{ft}}{12} = 6.75 \text{ in}^4 \text{ for } b_{ft} = 6 \text{ inches and } t_{ft} = 0.375 \text{ inches}$$

t/c = 19.6 inches / 17.5 inches = 1.12 at c3

t/c = 13.3 inches / 11.6 inches = 1.15 at c2

Using the smaller of these t/c values,

I_{eff} = 9 in^4 + 1.12 (6.75 in^4) = 16.6 in^4

Therefore,

$$P_{e.eff} = \frac{\pi^2 EI_{eff}}{L_b^2} = 917 \text{ kips}$$

$n_T = 2$, number of intermediate torsional brace points within the member length.

Substituting these values into Eq. (2-36a), one obtains:

$$\beta_{T.provided} < \left\{ \beta_T = 20\text{x}3x37^2 \left[\frac{124}{917}\right]\left(\frac{124}{72}\right)\frac{(2+1)}{2}1.0 \right\}$$

or (β_T =28,600 in-kips/rad) >> ($\beta_{T.provided}$ = 6,380 in-kips/rad) **NG**

It is informative to convert this torsional bracing check to an "equivalent" lateral bracing stiffness check by dividing by h_o^2, where h_o = 37.0 inches at c3. This gives

(β_{br} = 20.9 kips/inch) >> ($\beta_{provided}$ = 4.66 kips/inch) **NG**

It should be noted that the phrase "equivalent" as used here does not mean that torsional bracing having the same equivalent stiffness as a physical lateral brace is equally effective as the lateral brace. This phrase means that the combination of a grounded spring on the compression flange with a stiffness of $\beta_{provided}$ along with a hinge on the tension flange, as shown in Figure 2.17, or a grounded spring on the tension flange with a hinge on the compression flange, gives a resistance to rotation about the hinge equal to the corresponding torsional bracing stiffness $\beta_{T.provided} = \beta_{provided} h_o^2$. However, it should be emphasized that an actual torsional brace theoretically does not provide any resistance to gross lateral movement of the beam cross-section at the brace point. The torsional brace only restrains twisting of the member at the brace point.

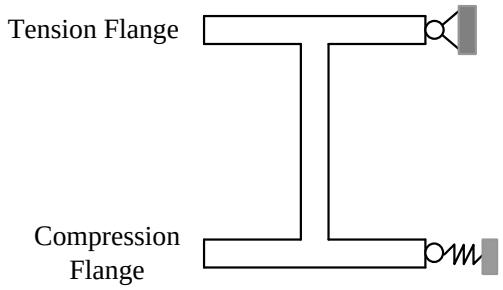

Fig. 2.17. Equivalent lateral bracing stiffness

Since torsional bracing is not required to provide any resistance to overall lateral movement, it is generally not as efficient as lateral bracing. Torsional bracing only restrains the twisting of the member cross-section.

As noted previously in Section 2.6.2.2, one possibility for relaxing the above stiffness requirement at c3 is to base the calculation of $P_{e.eff}$ on an effective unbraced length. Ozgur et al. (2010) recommend a simple procedure for calculating beam LTB effective length factors in general tapered I-section members. Segment c2-c3 potentially receives substantial end restraint from the short segment c3-c4 and from the more lightly loaded segment c1-c2, and therefore, one can calculate a $K < 1$ for this critical unbraced length. If a lower-bound estimate of $K = 0.5$ is utilized, one obtains $P_{e.eff} = 3670$ kips and $\beta_T =$ 7,150 in-kips/rad. It is unlikely that such a small effective length can be justified for segment c2-c3, but it is believed that a K value slightly larger than this, such as $K = 0.65$ (consistent with case (a) in Table C-C2.2 in the AISC (2005) Commentary, is justifiable. Ultimately, the result of either of these calculations can be compared to the virtual test simulation results detailed in Chapter 6.

It should be noted that, when included, K is used only in the calculation of $P_{e.eff}$ in Eq. (2-36a) (or Eq. (2-31)). Note that there are two terms containing L_b in Eq. (2-36a), the

$P_{e.eff}$ term and the term ($M_{r.equiv}$ /h_o)/L_b. The occurrence of L_b in the second of these terms comes from the overall description of the geometry and is not interpreted as an effective buckling length.

2.7.2.2 Torsional Brace Strength

The required strength for the torsional brace is

$$M_{br} = \frac{\beta_T}{\psi} \frac{L_b}{500 h_o} = \frac{28600}{3} \frac{72}{500 x 37} = 37.1 \text{ in - kips}$$

where h_o is taken as the depth between the centroids of the flanges at c3, 37.0 inches. Similar to the above, it is informative to convert this torsional brace moment requirement to an equivalent lateral force by dividing by h_o = 37.0 inches. This gives

P_{br} = 1.00 kips

This is 0.88 % of the maximum equivalent flange force in the unbraced lengths on each side of c3, which is $\left(\frac{P_r h_o}{2} + \frac{M_r}{C_b} \right) \frac{1}{h_o}$ = 114 kips based on h_o = 40.3 inches at c4.

2.7.2.3 Brace Point Movement at the Strength Condition

Given the above P_{br} and β_{br} values, the relative lateral displacement between the flanges at c3 at the strength condition (i.e., the layover, or twist, of the column cross-section at the brace point) may be estimated as

$\Delta = P_{br} / \beta_{br}$ = (1.00 kips) / (20.9 kips/inch) = 0.048 inches

One can observe that, assuming that the adjacent brace points do not move and the rotation is about the tension flange, the corresponding additional out-of-alignment of the column flange within the unbraced lengths is

0.048 inches / 72 inches = 1/1500 in c2-c3 and

0.048 inches / 19.2 inches = 1/400 in c3-c4.

2.7.3 Roof Diaphragm Bracing Between r1 and r2

The segment between r1 and r2 is the most critical unbraced length in the negative bending region of the roof girder. The bracing of the inside flange of the roof girder is accomplished by flange diagonals framed from the purlins, and these components are designed as torsional braces. Thus, the roof diaphragm is designed solely to brace the girder against out-of-plane flexural buckling at each of the purlin locations using the relative bracing provisions detailed in Section 2.6.1.1.

2.7.3.1 Relative (Shear Panel) Bracing Stiffness

The shear panel stiffness check for segment r1-r2 is similar to the wall diaphragm check in Section 2.7.1.1:

$$\left[\beta_{diaphragm} = \frac{G'\sum s}{L_b}\right] \geq \left[\beta_{br} = 2\Omega\left(\frac{\sum P_r}{L_b}\right)\right]$$

where

Σs = 25 ft x 5 bays = 1500 inches

ΣP_r = (45.3 k/ 1.6) x 5 bays = 141.6 k

L_b = 5 ft = 60 inches

Ω = 2.00

Similar to Section 2.7.1.1, this stiffness check may be written directly in terms of the specified panel shear stiffness as

$[G' = 4.19$ k/in$] > [G'_{reqd} = 2(2.0)(141.6/1500) = 0.38$ k/in$]$ **OK**

2.7.3.2 Relative (Shear Panel) Bracing Strength

Similar to Section 2.7.1.2, the shear panel strength is checked as follows:

$$\left[V_a = v_a \sum s\right] \geq \left[V_{br} = 0.004 \sum P_r\right]$$

where all the terms are defined in Section 2.7.3.1 except

v_a = allowable diaphragm strength = 122 lb/ft

This gives

$[\ v_a = 122$ lb/ft$] > [v_{br} = 0.004(141600$ lbs$)/125$ ft$) = 4.53$ lb/ft$]$ **OK**

2.7.4 Roof Diaphragm Bracing Between r7 and r8

The roof girder is subjected to the largest compression force in its outside flange, from combined positive bending moment and axial force, roughly between locations r7 and r8. Furthermore, no flange diagonal braces are used at r7. Therefore, the roof diaphragm is relied upon to provide shear panel bracing for both axial load and bending moment between r7 and r8. The relative bracing provisions from Sections 2.6.1.1 and 2.7.1.1 are combined for this purpose as shown below.

2.7.4.1 Relative (Shear Panel) Bracing Stiffness

The shear panel stiffness check for segment r7-r8 may be expressed as:

$$\left[\beta_{diaphragm} = \frac{G' \sum s}{L_b}\right] \geq \left[\beta_{br} = 2\Omega\left(\frac{\sum P_r + \Sigma C_{tR} C_d M_r / h_o}{L_b}\right)\right]$$

where

Σs = 25 ft x 5 bays = 125 ft = 1500 inches

ΣP_r = (44.1 k / 1.6) x 5 bays = 138 k

Ω = 2.00

ΣM_r = 241 ft-kips/1.6 x 5 frames = 753 ft-k = 9040 in-k

h_o = 24.3 inches

C_{tR} = 1.0, assuming sufficient tipping restraint exists at the points of load application.

If load height effects were considered, one would calculate

$C_{tR} = 1 + 1.2/n$

where the following definition is recommend for n:

n = number of intermediate brace locations between "hard" brace points (the "hard" brace points are located at the column base, the eave, and at the panel points of the X bracing in structures such as the one in Fig. 1.1). In effect, this amounts to assuming that these locations are rigidly-braced beam ends in the model underlying the equations.

= 2 (see Fig. 2.14)

Therefore,

$C_{tR} = 1 + 1.2/2 = 1.6$

It is assumed that sufficient tipping restraint exists in the following calculations.

C_d = 1 since the unbraced length being considered does not have an inflection point

L_b = 5 ft = 60 in

Similar to the previous diaphragm stiffness checks, this stiffness check may be written directly in terms of the specified panel shear stiffness as

$[G' = 4.19$ k/in$] > [G'_{reqd} = 2(2.0)(138+1x1x9040/24.3)/1500 = 1.36$ k/in$]$ **OK**

2.7.4.2 Relative (Shear Panel) Bracing Strength

The combination of the relative bracing strength equations from Sections 2.6.1.1 and 2.6.2.1.1 gives

$$\left[V_a = v_a \sum s\right] \geq \left[V_{br} = 0.004\left(\sum P_r + \Sigma C_{tR} C_d M_r / h_o\right)\right]$$

where all of the above terms are defined in Section 2.7.4.1 except

v_a = allowable diaphragm stiffness = 122 lb/ft

Written directly in terms of the specified diaphragm shear strength, this check becomes

$[v_a = 122$ lb/ft$] > [v_{br} = 0.004(138{,}000 + 9{,}040{,}000/24.3)/125$ ft$) = 16.4$ lb/ft **OK**

2.7.5 Torsional Bracing at r1 (Purlin Closest to the Knee)

Similar to the torsional brace at c3, the purlin and flange diagonals at r1 are designed as a torsional brace to restrain the roof girder against lateral-torsional buckling due to the moment causing flexural compression at the end of the roof girder, as well as to prevent twisting of the rafter at the knee due to the axial compression plus moment in the roof girder. The design equations are taken from Section 2.6.2.2. The flexure of the roof girder out of the plane of the frame is restrained by the bracing from the roof panels, but these panels are not effective at restraining the twisting of the rafter at r1. The torsional brace is designed for an ad hoc additional moment of $P_r h_o/2$ to account for the influence of the

axial thrust in the roof girder on the tendency for twisting about the purlin location. The potential beneficial influence of the combined torsional and lateral bracing is neglected. Location r0 at the side of the panel zone is assumed to act effectively as a rigid brace point due to the resistance from the wall panel at r0 and c3 and the bending stiffness of the outside column flange between r0 and c3. However, any out-of-plane resistance provided to the inside flange of the rafter at r1, from the inside column flange plus the connection plates between c3 and r1, is neglected.

2.7.5.1 Torsional Brace Stiffness

The torsional brace stiffness check is given by Eq. (2-36a). In addition, the purlins and girts are the same section in this example, and therefore the upper-bound estimate of the provided torsional brace stiffness at r1 is the same as that for location c3 detailed in Section 2.7.2.1. The other parameters that need to be entered into Eq. (2-36a) for the check at r1 are:

C_{tT} = 1 at r1, assuming sufficient tipping restraint from the purlins, due to the restoring torque caused by the eccentric bearing of the purlin against the flange of the roof girder when the roof girder starts to twist, the rotational stiffness provided by the attachment of the purlin to the outside flange of the roof girder, and the fact that a large percentage of the moment being resisted at r1 is comes from the beam-to-column joint,

ψ = 3.0

L_b = 5 ft = 60 inches

M_r = 613 ft-kips/1.6 = 380 ft-kips = 4560 in-kips at r1

C_b = 1.08, based on the flange stresses in the tapered member

P_r = 28.3 kips

h_o = 40.4 inches

$$M_{r.equiv} = \left(\frac{P_r h_o}{2} + \frac{M_r}{C_b} \right) = \frac{28.3 \text{x} 40.4}{2} + \frac{4560}{1.08} = 4790 \text{ in-kips}$$

$I_{eff} = 2I_c = 2I_t = 2(0.375 \text{ inches})(6.0 \text{ inches})^3 / 12 = 13.5 \text{ in}^4$

$$P_{e.eff} = \frac{\pi^2 E I_{eff}}{L_b^2} = 1{,}070 \text{ kips}$$

n_T = 2, number of torsional braces between the hard brace points, taken as the X bracing panel points at r0 and r3, i.e., these points are effectively assumed as rigid beam end brace points in the model underlying the equations.

Substituting these values into Eq. (2-36a), one obtains

$$\beta_{T.provided} \geq \left\{ \beta_T = 20 \text{x} 3 x 40.4^2 \left[\frac{4790 / 40.4}{1070} \right] \left(\frac{4790 / 40.4}{60} \right) \frac{(2+1)}{2} 1.0 \right\}$$

(β_T =32,200 in-kips/rad) >> ($\beta_{T.provided}$ = 6380 in-kips/rad) **NG**

As in Section 2.7.2.1, it is informative to convert the above torsional bracing stiffness check to an "equivalent" lateral bracing stiffness check by dividing by h_o^2, where h_o is 40.4 inches at r1. This gives

(β_{br} = 19.7 kips/inch) >> ($\beta_{provided}$ = 3.91 kips/inch) **NG**

Similar to the discussion at the end of Section 2.7.2.1, if a lower-bound *K* factor of 0.5 is utilized to calculate the above estimate for the required torsional bracing stiffness is reduced to β_T = 8000 in-kips/rad.

2.7.5.2 Torsional Brace Strength

The required strength for the torsional brace at r1 is

$$M_{br} = \frac{\beta_T}{\psi}\frac{L_b}{500h_o} = 31.7 \text{ in-kips}$$

If one converts this to an equivalent lateral bracing force applied at the center of each flange, one obtains

$P_{br} = M_{br} / h_o = 31.7/40.4 = 0.78$ kips

This is 0.66% of $\left(\frac{P_r h_o}{2} + \frac{M_r}{C_b}\right)\frac{1}{h_o}$ = 119 kips.

2.7.5.3 Brace Point Movement at the Strength Condition

Given the above P_{br} and β_{br} values, the relative lateral displacement between the roof girder flanges at r1, at the strength condition, may be estimated as

$\Delta = P_{br} / \beta_{br}$ = (0.78 kips) / (19.6 kips/inch) = 0.040 inches

Assuming the adjacent brace point at r2 does not move and that the rotation is about the top (tension) flange, the corresponding additional out-of-alignment of the inside (compression) flange within the unbraced length r1-r2 is

0.040 inches / 60 inches = 1/1510

2.7.6 Summary

From the above interpretations of the 2010 AISC Appendix 6 provisions, it can be summarized that:

- The wall and roof diaphragms have ample stiffness and strength.
- The strength demands on the flange braces and purlins are moderate.

- The upper-bound (large) estimate of the stiffness provided by the girts or purlins combined with the flange diagonal braces is only one-fifth to one-sixth of that required by the ad hoc application of the AISC Appendix 6 torsional bracing stiffness requirements.

At location r1, one can argue that the column may provide substantial additional resistance to twisting of the roof girder, as well as resistance to out-of-plane displacement at the bottom flange of the roof girder. However, the bottom of the roof girder and the panel zone are also considered as a brace point at the top of the column. Therefore, without a more detailed evaluation of the various interactions at the knee joint, it is difficult to suggest a more liberal check than the one provided in Section 2.8.4.1. Furthermore, the torsional bracing requirement at r2 typically would be taken the same as the one calculated at r1 using the previously suggested interpretations of the AISC equations. If one assumes a lower-bound effective length factor of $K = 0.5$ in calculating $P_{e.eff}$ on the critical unbraced length r1-r2, then the upper-bound estimate of the torsional bracing stiffness from the representative minimum size purlins nearly satisfies the stiffness requirement.

At location c3, one can observe that the assumption of $L_b = 6$ ft = 72 inches likely leads to conservatism in the torsional bracing check. However, again, it is difficult to suggest a more liberal check at c3 than the one provided in Section 2.7.2.1 without accounting more rigorously for the differences in the properties of the two adjacent unbraced lengths. Similar to the above, if one assumes a lower-bound effective length factor of $K = 0.5$ on the critical unbraced length c2-c3, the upper-bound estimate of the

torsional bracing stiffness from the representative minimum size girts nearly satisfies the stiffness requirement.

2.8 Simplified Brace Strength and Stiffness Requirements

The ad hoc interpretation of AISC Appendix 6 discussed in the previous section gives reasonable estimates of the brace strength requirements; however, without the use of effective length factors in the form of the AISC equation for the torsional bracing stiffness discussed in Section 2.7, the torsional brace stiffness demand obtained from these equations is roughly five times larger than the upper-bound estimate of the stiffness provided using representative minimum purlin sizes. For other designs, potentially with longer spans, etc., the bracing demands may be even larger relative to the capacity of the secondary elements. Therefore, if further economies can be realized in calculating the estimated torsional bracing stiffness demands, the benefits could be very useful.

The "true" performance of the torsional bracing in this problem is evaluated rigorously in Chapter 6. However, prior to considering virtual simulation results, it is useful to consider other potential simplified estimates of the bracing demands.

Based on the prior research discussed in this chapter, the research by Tran (2009) and the results presented in this study, several fundamental observations can be used to arrive at further simplifications in the AISC brace strength and stiffness requirements. The suggested simplifications are based on the recognition that:

- The maximum brace force demands at the static strength limit of steel members and structures, determined from virtual simulation studies, are often much larger than the AISC strength requirements (although the AISC torsional bracing rules give larger brace strength requirements in some cases). The upper-bound values

for these demands are approximately 4 % for nodal lateral and torsional braces and approximately 1.5 % for relative braces. Although these are approximate upper-bound limits, the brace forces in a wide range of problems with different bracing configurations and stiffnesses approach these percentages at the member or structure strength limit. The reason for these larger strength requirements is often due to the onset of inelasticity prior to the member or structure reaching its maximum strength condition. However, certain cases that fail largely by elastic buckling can also see much larger brace forces than estimated by the AISC brace strength requirements.

- Although the brace strength requirements are relatively large at the limit load of a wide range of problems, the applied load level versus the brace force tends to be relatively flat as structures and their bracing systems approach their maximum capacity. As a result, the traditional 2 % rule for the brace force is a reasonable maximum limit for the sizing of nodal lateral and torsional braces directly for strength, and indirectly for stiffness to develop the strength of the members. A 1 % force rule appears to be sufficient for relative bracing. That is, the bracing can be designed for less than the true maximum strength demand at the overall structure's limit load without adversely affecting the overall resistance of the structure.
- One avenue for improvement of bracing design requirements is to develop more rigorous buckling load estimates for the complex bracing arrangements and structure boundary conditions than utilized in the current AISC Appendix 6 rules. However, improvement of bracing design requirements by calculation of refined

eigenvalue buckling loads and/or second-order load-deflection responses, using structural system models much more sophisticated than the models used in the development of the AISC Appendix 6 equations, would be difficult for ordinary practice.

- As long as the bracing system develops member or structural system strengths approximately equal to the full-bracing strength, or in the context of knuckle curves such as the one illustrated in Fig. 1.3, as long as the bracing stiffness is larger than the knuckle value, the largest bracing demands for a given loading case are often highly localized at the overall strength limit. As such, it appears that the bracing stiffnesses and strengths can be designed largely based on the structure internal forces in the vicinity of each brace. There is already a similar precedent for this in the recommendations by Wang and Helwig (2005) for determining the critical imperfections pertaining to the stability bracing of fully-braced I-section beams. These authors recommend that only a local brace point imperfection need be considered in calculating the beam nodal lateral or torsional brace forces by second-order analysis.
- One potential alternative to working from sophisticated eigenvalue buckling estimates as the underlying basis for improved bracing requirements is to identify tolerable maximum brace point displacements under the applied design loads for different types of bracing systems. Given the above bracing forces and the corresponding tolerable deformation limits, the required stiffnesses can be calculated by simply dividing the maximum expected brace forces by the maximum permitted brace point displacements.

From preliminary studies, the brace point displacement for nodal and relative lateral braces can be allowed to be as high as $2\Delta_o$ (where $\Delta_o = L_b/500$) without significantly impacting the member resistance. Torsional braces without incidental lateral restraint are more sensitive to the brace point displacements. Hence, the brace point rotation for torsional braces that do not have any associated incidental lateral restraint is limited to Δ_o/h_o. If incidental lateral restraint of at least 10% of the lateral bracing stiffness requirement is present, then the brace point rotation limit may be taken as $2\Delta_o/h_o$.

Other considerations such as top flange loading, and special requirements near inflection points in certain cases, can be important when estimating strength and stiffness demands for beam braces. Although it is possible to base these additional demands on a corresponding load-deflection model, the simplest way to address these considerations is to utilize the C_t and C_d factors already adopted in the AISC Appendix 6 provisions, or where the need may arise, to utilize refined versions of these equations.

Based on the above considerations, the following simplified versions of the AISC bracing strength and stiffness requirements are suggested. The final forms of the stiffness requirements are actually very close to the AISC relative and nodal lateral bracing stiffness equations. However, they are arrived at by considering the maximum brace force requirements and the corresponding maximum limit on the brace point displacements as described above. For torsional bracing, the stiffness requirements are arrived at in the same fashion as in the development of the simplified relative and nodal bracing equations. Therefore, the final form of the simplified torsional bracing requirements is somewhat different than the AISC Appendix 6 equations.

2.8.1 Relative Bracing

For column relative bracing, the simplified relative bracing strength requirement is

$$V_{br} = 0.01\,\Sigma P_r \tag{2-37a}$$

As mentioned above, this is a more realistic estimate of the actual brace force demand necessary to develop member or system limit loads for both full-bracing and partial bracing situations close to full bracing. The corresponding displacement limit is

$$\Delta_{max} = L_b\,/250 \tag{2-37b}$$

If one divides the required bracing strength at the ultimate strength level, by Δ_{max}, the following relative bracing stiffness requirements are obtained:

$$\beta_{br} = \frac{\alpha V_{br}}{\Delta_{\max}} = 2.5\frac{\alpha\Sigma P_r}{L_b}$$

$$= 2.5\frac{\Sigma P_r}{L_b}\ \text{(LRFD)} \quad \text{or } 4\frac{\Sigma P_r}{L_b}\ \text{(ASD)} \tag{2-37c}$$

where $\alpha = 1.0$ for LRFD and 1.6 for ASD. This stiffness requirement is identical to the AISC Appendix 6 requirement (Eq. 2-20) for ASD, and is 6 % smaller than the AISC Appendix 6 requirement for LRFD. This 6 % difference between ASD and LRFD is consistent with the results from the underlying Direct Analysis Method (DM) analysis solutions discussed previously in Section 2.2.2. Therefore, the suggested simplified requirements for relative column bracing are actually not simpler than the current AISC requirements at all. The recommended strength requirement is larger than in AISC, but the stiffness requirement is essentially unchanged.

The presentation of these requirements in terms of a maximum potential brace force, and a maximum allowable bracing movement (or deformation) under this force gives the engineer another easily understood criterion, or reason, for providing sufficient relative

brace stiffness. For relative bracing, the bracing movement or deformation being considered is the increase in the out-of-alignment or out-of-plumbness of the unbraced length, or the increase in the relative displacement between the ends of the unbraced length, under the applied loads. This deformation must be limited for the bracing to adequately perform its job.

For beam relative bracing, the equivalent flange force ($\Sigma M_r / h_o$) is used in place of ΣP_r, and the parameters C_{tR} and C_d are included as explained in Section 2.6.2.1.1.

2.8.2 Nodal Lateral Bracing

For column nodal lateral bracing, the maximum brace strength requirement is

$$P_{br} = 0.02\, P_r \tag{2-38a}$$

in the recommended simplified procedure. The corresponding displacement limit is

$$\Delta_{max} = L_b / 250 \tag{2-38b}$$

If one divides the required bracing strength at the ultimate strength level by Δ_{max}, the following nodal bracing stiffness requirements are obtained:

$$\beta_{br} = \frac{\alpha P_{br}}{\Delta_{\max}} = 5\frac{\alpha P_r}{L_b}$$

$$= 5\frac{P_r}{L_b} \text{ (LRFD)} \quad \text{or } 8\frac{P_r}{L_b} \text{ (ASD)} \tag{2-38c}$$

where $\alpha = 1.0$ for LRFD and 1.6 for ASD. For columns with one intermediate nodal brace ($n = 1$), this stiffness requirement is double the relative bracing requirement and is effectively identical to the current AISC Appendix 6 full-bracing stiffness requirement. As n increases, the AISC nodal full-bracing stiffness requirement approaches two times the values in Eq. (2-37c). However, as n increases, the decrease from the fully-braced

strength associated with decreases in the partial bracing stiffness becomes more and more gradual (see Fig. 2.8). For inelastic buckling, the reduction is particularly small near the full bracing limit. This is largely the reason why Tran (2009) found that stiffnesses as small as 1.3 times the ideal bracing limit ($1.3\beta_i$) worked well for columns having multiple intermediate brace points. Therefore, it is possible to simplify the AISC stiffness requirements (Eq. (2-23)) to the values shown in Eq. (2-38c).

Similar to the relative bracing recommendations, the above requirements are actually not much of a simplification at all compared to the requirements given by Eqs. (A-6-3) and (A-6-4) in the AISC Specification. The strength requirement of Eq. (2-38a) is doubled relative to the corresponding AISC equation (Eq. 2-22), based on the recognition that the actual brace forces at the member or overall system strength limits are often much higher than the AISC strength requirements. However, the base recommended stiffness requirement of Eq. (2-38c) is one-half of the base ASD version of Eq. (A-6-4) and 5/8 of the LRFD version of this equation.

It should be noted that the deformation limit for nodal bracing corresponds directly to the brace point displacements (rather than to the relative displacements between the ends of the unbraced length). Therefore, the member out-of-alignment between the brace points can be as much as two times the value in Eq. (2-38b), for the case where two adjacent braces are loaded in opposite directions at the strength requirement given by Eq. (2-38a). This type of failure mode is common for large n. In cases where the brace forces approach 4 % at the limit load, the actual additional out-of-alignment can be as high as 4 x $L_b/250 = 0.016L_b$, giving a total worst case out-of-alignment of $\Delta_o + \Delta = L_b/500 + 4L_b/250 = 0.018L_b$ (1.8 % of the unbraced length). However, more than 90 % of the

member or system overall strength is developed commonly at the smaller recommended bracing strength requirement (Eq. 2-38a).

For beam nodal bracing, the equivalent flange force (M_r/h_o) is used in place of P_r, and the parameters C_{tR} and C_d are included as explained in Section 2.6.2.1.2. It should be noted that there is no division by the equivalent uniform moment factor C_b in the above AISC or simplified nodal bracing expressions. The factor C_b is included in a recommended refined estimate of the beam nodal bracing stiffness requirements developed by Bishop et al. (2010). The equations proposed by Bishop et al. (2010) are based on an adaptation of the Lutz and Fisher (1985) procedures to beams (see Section 2.3.5.4).

2.8.3 Beam Torsional Bracing

For torsional bracing with *no* incidental lateral restraint, the recommended strength requirement is

$$M_{br} = 0.02\, M_r C_{tT} \tag{2-39a}$$

and the targeted corresponding displacement limit is the cross-section twist rotation

$$\theta_{max} = \frac{L_b}{500 h_o} \tag{2-39b}$$

at the brace points. If one divides the required strength at the ultimate strength level by this displacement, the following torsional bracing stiffness requirements are obtained:

$$\beta_T = \frac{\alpha M_{br}}{\theta_{max}} = 10 C_{tT} \frac{M_r h_o}{L_b} \text{ (LRFD)} \quad or \quad 16 C_{tT} \frac{M_r h_o}{L_b} \text{ (ASD)} \tag{2-39c}$$

where α = 1.0 for LRFD and 1.6 for ASD. It should be noted that this stiffness requirement is effectively only about two times the corresponding nodal bracing, whereas, as noted in Section 2.6.2.2, accurate full bracing limits for torsional bracing tend

to fall more within the range of πh_o^2 to $2\pi h_o^2$ of accurate full bracing limits for nodal bracing (Yura et al. 1992), when written in terms of flange forces. Therefore, the bracing stiffness limit of Eq. (2-39c) may indeed be a lower-bound to the true torsional full-bracing requirements. However, the drop in strength with decreases in stiffness is typically very gradual for torsional bracing near the full bracing limit (in fact, the torsional full bracing limit can be difficult to discern because of the asymptotic nature of the strength gain as this limit is approached). Furthermore, some type of small incidental lateral bracing restraint typically exists at any torsional bracing location. Even a very small lateral restraint is effective in providing some reduction in the torsional bracing stiffness requirements.

Even for a relatively small degree of lateral restraint, the torsional bracing stiffness demands are reduced significantly (Yura et al. 1992; Tran 2009). It is suggested that with a lateral bracing stiffness of only 10 % of the lateral bracing strength requirement of Eq. (2-38c), the above displacement limit of Eq. (2-39b) may be doubled and the torsional bracing stiffness requirement of Eq. (2-39c) may be reduced by one-half. Therefore, in this case, the recommended strength requirement is

$$M_{br} = 0.02\, M_r C_{tT} \tag{2-40a}$$

the targeted cross-section twist rotation at the brace points is

$$\theta_{\max} = \frac{L_b}{250 h_o} \tag{2-40b}$$

and the torsional bracing stiffness requirements are:

$$\beta_T = \frac{\alpha M_{br}}{\theta_{\max}} = 5 C_{tT} \frac{M_r h_o}{L_b} \text{ (LRFD)} \quad or \quad 8 C_{tT} \frac{M_r h_o}{L_b} \ (ASD) \tag{2-40c}$$

where α = 1.0 for LRFD and 1.6 for ASD.

In the above equations, P_r and M_r are taken as the largest force and moment in the adjacent unbraced lengths for the brace being designed. For torsional bracing, the equivalent moment at the torsional brace from the axial load needs to be considered. In this case, the equivalent moment is taken as

$$M_{r.equiv} = M_r + P_r h_o/2 \quad (2\text{-}41)$$

The above equations are preliminary. They require further scrutiny via research before any form of them can be recommended for design. Further refinement of these simple rules and/or the consideration of other concepts may be worthwhile. However, these simple rules can serve to provide insight into the behavior and potential directions for improvement of the simplicity and accuracy of stability bracing design rules.

Example simplified design checks for the clear span frame discussed in the previous section are presented in the next several sub-sections. These and the AISC checks are compared to refined full nonlinear virtual simulation analysis results in Chapter 6.

2.8.4 Wall Diaphragm Bracing

2.8.4.1 Relative (Shear Panel) Bracing Strength Requirement

The shear panel strength requirements for the wall panels of the frame in Fig. 2.13 are:

$V_{br} = 0.01\Sigma P_r$

$\Sigma P_r = 165.5$ kips

$V_{br} = 1.66$ k

$\Sigma s = 125$ ft

$[v_a = 61.2$ lb/ft$] > [v_{br} = V_{br} / \Sigma s = 13.3$ lb/ft$]$ **OK**

In comparison, the ad hoc application of the AISC Appendix provisions gives a strength requirement of v_{br} = 5.3 lb/ft (see Section 2.7.1.2)

2.8.4.2 Relative (Shear Panel) Bracing Stiffness Requirement

The shear panel bracing stiffness requirements for the wall diaphragms are

L_b = 5.5 ft = 66 inches

$$\beta_{br} = \frac{4\Sigma P_r}{L_b} = 10.0 \text{ kips/in}$$

$G'_{reqd} = \beta_{br} L_b / \Sigma s$ = 0.44 kips/in

[G' =3.52 kips/in] > [G'_{reqd} = 0.44 kips/in] **OK**

Note that G'_{reqd} = 0.44 kips/in is also obtained from the ad hoc application of the AISC Appendix 6 provisions (see Section 2.7.1.1).

2.8.5 Torsional Bracing at c3 (Girt Closest to the Top of the Column)

2.8.5.1 Torsional Bracing Strength Requirement

The torsional brace strength requirement at c3 is

M_{br} = 0.02 ($M_{r\ equiv}$)x 1.0 = 92.2 in-kips

Based on

$$M_{r.equiv} = \left(\frac{P_r h_o}{2} + \frac{M_r}{C_b} \right) = 4610 \text{ in-kips}$$ (see Eq. 2-41), and

C_{tT} = 1.0

If one converts this torsional brace strength requirement to an equivalent lateral force, by dividing by h_o = 37.0 inches (at c3), one obtains

$P_{br} = M_{br} / h_o$ = 2.50 kips

The corresponding AISC-based strength requirement is P_{br} = 1.00 kips (see Section 2.7.2.2).

2.8.5.2 Torsional Bracing Stiffness Requirement

Since diaphragm bracing is provided to the outside flange at c3 by the wall panels, it is assumed that Eqs. (2-40) apply. Therefore,

$$\theta_{max} = \frac{L_b}{250 h_o}$$

and

$$\beta_T = \frac{\alpha M_{br}}{\theta_{max}}$$

The input values to these equations are

L_b = 72 inches and

h_o = 37.0 inches

giving

β_T = (1.6 x 92.2 x 37.0 x 250) / 72 = 19,000 in-kips/rad.

(β_T = 19,000 in-kips/rad) >> ($\beta_{Tprovided}$ = 6,380 in-kips/rad) **NG**

Note that the base ad hoc application of the AISC provisions indicates that a brace stiffness of 28,600 in-kips/rad is required. Therefore, the suggested simplified rules indicate that the bracing stiffness requirement can be reduced by a factor of 19,000/28,600 = 0.66. However, the simplified estimate of the required torsional bracing stiffness is still three times the upper-bound (large) estimate of the provided stiffness.

Conversion of this torsional bracing stiffness to an "equivalent" lateral stiffness check gives (using h_o = 37.0 inches at c3)

(β_{br} = 13.9 kips/inch) >> ($\beta_{provided}$ = 4.66 kips/inch)

2.8.6 Roof Diaphragm Bracing Between r1 and r2

2.8.6.1 Relative (Shear Panel) Bracing Strength Requirement

The shear panel strength requirements for the roof panels are

$V_{br} = 0.01\Sigma P_r$

$\Sigma P_r = 142$ kips

$V_{br} = 1.42$ kips

$\Sigma s = 125$ ft

$[v_a = 122$ lb/ft$] > [v_{br} = V_{br} / \Sigma s = 11.4$ lb/ft$]$ **OK**

In comparison, the ad hoc application of the AISC Appendix provisions gives a strength requirement of $v_a = 4.53$ lb/ft (see Section 2.7.3.2)

2.8.6.2 Relative (Shear Panel) Bracing Stiffness Requirement

The shear panel bracing stiffness requirements for the roof diaphragms are

$L_b = 5$ ft $= 60$ inches

$$\beta_{br} = \frac{4\Sigma P_r}{L_b} = 9.46 \text{ kips/in}$$

$G'_{reqd} = \beta_{br} L_b / \Sigma s = 0.38$ kips/in

$[G' = 4.19$ kips/in$] > [G'_{reqd} = 0.38$ kips/in$]$ **OK**

$G'_{reqd} = 0.38$ kips/in is also obtained from the ad hoc application of the AISC Appendix 6 provisions.

2.8.7 Torsional Bracing at r1 (Purlin Closest to the Knee)

2.8.7.1 Torsional Brace Strength Requirement

The torsional brace strength requirements at r1 are taken as

$M_{br} = 0.02\ (M_r + P_r h_o/2) = 95.8$in-kips

based on

$$\left(\frac{P_r h_o}{2} + \frac{M_r}{C_b} \right) = 4790 \text{ in - kips} \text{ (see Eq. 2-41)}$$

If one converts this torsional brace strength requirement to an equivalent lateral force, by dividing by h_o = 40.4 inches (at r1), one obtains

$P_{br} = M_{br} / h_o = 2.40$ kips

The corresponding AISC-based strength requirement is P_{br} = 0.78 kips (see Section 2.7.5.2).

2.8.7.2 Torsional Brace Stiffness Requirement

Since diaphragm bracing is provided to the outside flange at r1 by the roof panels, it is assumed that Eqs. (2-40) apply. Therefore,

$$\theta_{\max} = \frac{L_b}{250 h_o}$$

and

$$\beta_T = \frac{\alpha M_{br}}{\theta_{\max}}$$

The input values to these equations are

L_b = 60 inches and

h_o = 40.4 inches

giving

β_T = (1.6 x 92.2 x 37.0 x 250) / 72 = 19,000 in-kips/rad.

(β_T = 19,000 in-kips/rad) >> ($\beta_{Tprovided}$ = 6,380 in-kips/rad) **NG**

Therefore, the simplified stiffness requirement at r1 is obtained as

$$\beta_T = \frac{\alpha M_{br}}{\theta_{\max}}$$

L_b = 60 inches

h_o = 40.4 inches

β_{br} = (1.6 x 95.8 x 40.4 x 250) / 60 = 25,800 in-kips/rad.

(β_{br} = 25,800 in-kips/rad) >> ($\beta_{Tprovided}$ = 6,380 in-kips/rad) **NG**

Note that the base ad hoc application of the AISC provisions indicated that a brace stiffness of 32,200 in-kips/rad was required. Therefore, the suggested simplified rules indicate that the bracing stiffness requirement can be reduced by a factor of 25,800/32,200 = 0.80. However, the simplified estimate of the required torsional bracing stiffness is still four times larger than the upper-bound (large) estimate of the provided stiffness. Conversion of this torsional bracing stiffness check to an "equivalent" lateral stiffness check gives (using h_o = 40.4 inches at r1)

(β_{br} = 15.8 kips/inch) >> ($\beta_{provided}$ = 3.91 kips/inch)

As indicated above, the ad hoc interpretation of the AISC Appendix 6 places substantial stiffness demands on the torsional braces for metal building systems. The motivation behind the current development of the suggested simplified equations is to provide reasonable alternative estimates of the bracing demands. Unfortunately, the simplified calculations also indicate a substantial demand on the stiffness of the torsional braces.

As discussed previously, virtual test simulation finite element analysis can serve as a very useful tool to determine more rigorous estimates of the brace stiffness and strength demands. The following chapter discusses the virtual test simulation approach utilized in this research.

CHAPTER 3

APPLICATION OF VIRTUAL TEST SIMULATION FOR THE ASSESSMENT OF STABILITY BRACING

Appendix 1 of the 2010 AISC Specification has been revised extensively relative to previous specifications to more comprehensively address design by inelastic analysis. The general provisions of Appendix 1 basically indicate that any inelastic analysis utilized for design must account for:

1. All deformations (significantly) contributing to the structural displacements,
2. Second-order effects.
3. Geometric imperfections,
4. Strength reduction from inelasticity including the effect of residual stresses and partial yielding, and
5. Uncertainty in system member and connection strength and stiffness.

These requirements parallel the requirements stated for any method of design provided in Chapter C of the Specification.

The virtual test simulation procedures used in this research follow the general guidelines stated in the Appendix 1 provisions and focus on determining the brace requirements at the maximum strength condition for a given geometry and loading. For structures designed by ASD, the ASD loads may be increased by the factor $\alpha = 1.6$ to achieve an equivalent maximum strength loading. Appendix 1 of AISC actually does not consider the use of ASD, since the maximum strength loads (rather than the working or

allowable strength loads) are the only rational ones appropriate for a virtual test simulation strength analysis. That is, the basic ASD approach of increasing the ASD loads by a factor of $\alpha = 1.6$ for the structural analysis, and then dividing the resulting internal forces by α to reduce them back to allowable or working load levels does not serve any purpose if one is using the Appendix 1 procedures to directly evaluate the member or system strength. Also, the LRFD load combinations generally provide a better characterization of the maximum strength loading requirements, and in many cases actually give smaller load effects than the comparable ASD load combinations multiplied by $\alpha = 1.6$. For structures designed by LRFD, the LRFD load combinations are applied directly (i.e., $\alpha = 1.0$).

The members and frames considered in this research generally are analyzed up to their *actual* maximum load resistance and into their post-peak response, which is generally different than the targeted strength design load combination. Depending on various factors, the maximum strengths may be larger or smaller than the strength load level for the corresponding ASD or LRFD load combination. This is not an issue. This research is aimed at evaluating the brace behavior before, at, and after the true maximum strength condition of the structures, at whatever level this may be. If the reader is concerned about the ratio of the "true" maximum strengths to the ASD or LRFD load combination values, he or she can consider that the nominal loads could be changed for

the underlying designs such that the unity checks for the modified ASD or LRFD loadings are approximately 1.0 at the true strength limit.

It should be noted that the virtual test simulations applied in this research aim to capture the behavior of the structure under the specified loading as would occur in laboratory testing or in the field. If applied for design, Appendix 1 specifies that one way of satisfying the general design requirements is that the virtual simulation model must be analyzed using a reduced elastic stiffness of $0.9E$ and a reduced yield resistance of $0.9F_y$. The 0.9 factor on these stiffness and strength terms is consistent with the use of ϕ_c and $\phi_b = 0.9$ on the axial and flexural strengths P_n and M_n by an ordinary design. However, Appendix 1 specifies that "Strength limit states detected by an inelastic analysis that incorporates all of the above requirements are not subject to the corresponding provisions of the Specification when a comparable or higher level of reliability is provided by the analysis." That is, if a virtual simulation analysis is conducted, there is no need to return to the Specification for checking any of the limit states fully captured by the analysis model.

The virtual test simulation capabilities applied in this research satisfy the Appendix 1 requirements for capturing all the member stability and general yielding limit states, with the exception that the 0.9 factor is not included on F_y and E. This is because the results from the virtual simulation analyses are intended to represent a direct prediction of the response measured in the laboratory or field, given the specified nominal residual stresses

and geometric imperfections in the structure. In other words, the maximum strengths predicted by the virtual simulation models represent the *nominal* strength of the structures and members being considered, for the given strength load combinations.

With respect to LRFD member design requirements, one can move the 0.9 resistance factor to the load side of the limit states design equation. Therefore, the designs can be said to satisfy the LRFD design requirements if they reach a load level of 1/0.9 = 1.11 of the corresponding strength load combination in the virtual test simulation. For ASD, the equivalent factor to 1/0.9 = 1.11 is $\Omega/\alpha = 1.67/1.6 = 1.04$. The members and frames considered do not necessarily reach this load level, mainly because many of them were originally designed to other criteria. This fact is somewhat immaterial to the current study however. The important questions investigated in this research are:

1. What are the strength demands on the bracing system at the "true" maximum load limit of the structure?

2. What is the influence of the bracing system stiffness on the load carrying capacity of the overall structural system?

This chapter is organized as follows. First, Section 3.1 gives a detailed description of the modeling of members and frames used in this research for the virtual test simulations. Next, Section 3.2 presents the nominal residual stress pattern utilized throughout this research. After that, Section 3.3 discusses the geometric imperfections (magnitude and pattern) that should be considered in an inelastic analysis of general members and frames

and their bracing systems. Lastly, Section 3.4 discusses the modeling of the building frame bracing systems employed in this work and the rationale behind the modeling procedures.

3.1 Full Nonlinear Shell FEA Modeling of Members and Frames

3.1.1 Finite Element Discretization

The finite element models developed in this research are constructed using the ABAQUS 6.9 analysis system using the S4R element for the web and flanges. The S4R element is a general purpose four-node quadrilateral displacement-based shell element with reduced integration. A five point trapezoidal rule is used for numerical integration through the thickness of the shell elements.

For all the studies, twenty shell elements are used through the depth of the web. The number of elements across the flange varies with the width of the flanges. These values are chosen to facilitate the modeling of the nominal residual stresses selected in this work. That is, enough elements are employed across the flange widths to capture the transitions in the selected nominal piecewise linear flange residual stress pattern (see Section 3.2). This basically entails the use of 8 to 12 elements across the width of each of the flanges. This number of elements across the flange width is also sufficient to capture the influence of the spread of plasticity across the widths of the flanges with good accuracy in general.

The elements in the web of prismatic members have an aspect ratio of one. In tapered members, the elements at the deeper end have an aspect ratio of one while the elements in the shallower end of the column have an aspect ratio greater than one (i.e., their dimensions along the length of the member are larger than their dimensions through the

web depth). The discretization of the flanges along the member length matches with the discretization of the web. This mesh density generally is sufficient to capture web distortion and flange local bending effects with good accuracy.

3.1.2 Load and Displacement Boundary Conditions

For the individual member studies conducted in this research, the members are modeled as torsionally simply supported, that is:

- Both ends of the member are prevented from twisting,
- Both ends of the member are prevented from transverse displacement,
- One point on the cross-section at one of the member ends is prevented from displacement along the direction normal to the cross-section,
- Both ends of the member are free to bend about both the strong- and weak-axes of the cross-section,
- Both ends of the member are free to warp, i.e., the flanges are free to bend about the weak axis of the member.

In addition, open-section thin-walled beam theory kinematic constraints are imposed at the member ends. In other words, the cross-section profile is constrained against any distortion within its plane, but otherwise the above unconstrained displacement conditions from open-section thin-walled beam theory are permitted.

To achieve the desired kinematic conditions at the ends of the beams, the following multi-point constraints are required. Figure 3.1, from Kim (2010), shows the multi-point constraints used to enforce the open-section thin-walled beam kinematics at the ends of the members as well as the specific constraints used to model the flexurally and torsionally simply-supported boundary conditions in the beam analysis problems. In the

figure, points *a* and *e* represent any nodes on the top and bottom flanges respectively except the nodes at the web-flange juncture. Similarly, point *c* represents any nodes on the web except the nodes at the web-flange juncture. Points *b* and *d* are the nodes at the top and bottom web-flange junctures respectively. In addition, Axis 1 is the longitudinal axis of the members, taken normal to the cross-section, and Axes 2 and 3 are the major and minor bending axes of the I-sections respectively.

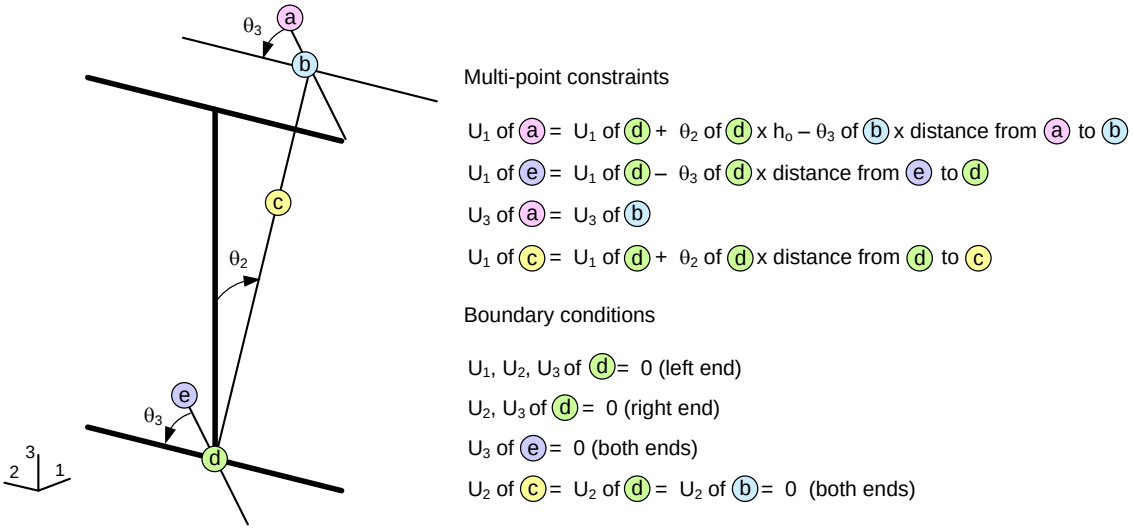

Fig. 3.1. Geometric constraints and end conditions for modeling of beam members, adapted from Kim (2010).

The multi-point constraints shown in Figure 3.1 enforce the following:

- The web remains straight while it is allowed to rotate about the 2 axis at the bottom web-flange juncture node, point *d*.
- The flanges remain straight while they are free to rotate about 3-axis at the web-flange juncture nodes, points *b* and *d*.

Therefore, open-section thin-walled beam kinematics is enforced at the member ends without restraining warping. It should be noted that these multi-point constraints involve a linearization of the finite rotation kinematics. This linearization gives an acceptable

representation of the finite rotation displacement fields as long as θ_2 and θ_3 are less than approximately 0.04 radians. This limit is satisfied generally at the strength limit load of the problems considered in this research.

Regarding the specific constraints used to model the flexurally and torsionally simply-supported boundary conditions, all the displacement degrees of freedom are restrained at point *d* to model a "pin" support at the left end. In addition, the vertical and lateral displacements u_3 of all the bottom flange nodes are restrained. The "roller" support at the right end is modeled similarly except there is no longitudinal constraint at point *d*. Lastly, the lateral displacements of all the nodes in the web, including the web-flange juncture nodes, are restrained at both ends.

All of the frames studied in this research are modeled with ideally simply supported base conditions, that is, the bases of the columns are restricted against twisting and displacement of the cross-section centroidal axis in all three directions. However, the cross-section at the base is free to rotate about its strong- and weak-axis and the flanges of the column are free to warp at the base. These boundary conditions are implemented in a manner similar that described above for the modeling of beam members.

The boundary conditions associated with the modeling of other bracing systems are discussed in Section 3.4.

3.1.3 Material Properties

Figure 3.2 shows a typical multi-linear idealization of the stress-strain curve for a steel with a yield strength F_y of 55 ksi (such as A529-55 or A572-55), which is assumed in all the virtual test simulations. An ultimate strength F_u of 70 ksi is assumed based on the minimum ultimate strength for A572 Grade 55 material as indicated by Table 2-5 in

the 2005 AISC Manual. In addition, it is assumed that the strain hardening strain ε_{st} is ten times the yield strain, and that the engineering stress-strain curve is completely flat (zero slope) between the yield strain ε_y and the strain hardening strain ε_{st}. The strain hardening modulus E_{st} is taken as 700 ksi, for the engineering stress-strain curve. The stress at the end of the initial strain hardening range F_{st} is then calculated as

$$F_{st} = F_y + 2/3(F_u - F_y) = 55 + 2/3(70\text{-}55) = 65 \text{ ksi} \quad (3\text{-}1)$$

Finally, the engineering strain at the ultimate strength ε_u is taken as

$$\varepsilon_u = 70\varepsilon_y = 70 \times (55/29000) = 0.133 \text{ in/in} \quad (3.\ 2)$$

These values fully define the engineering stress-strain curve shown in Fig. 3.2.

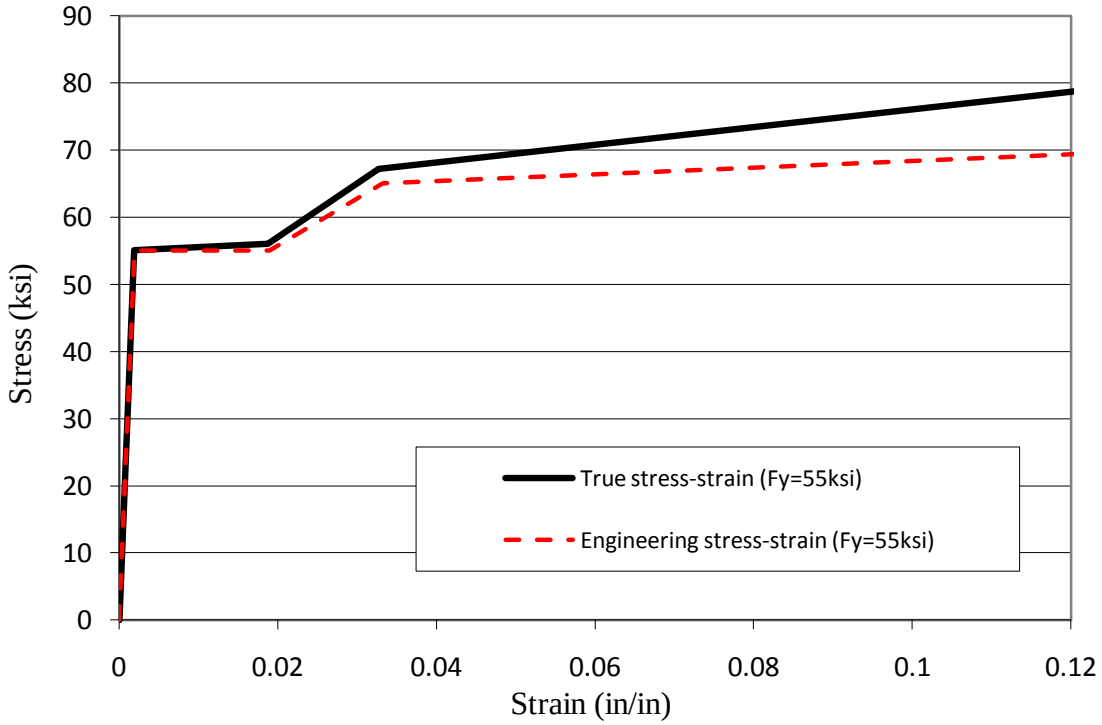

Fig. 3.2. Typical stress-strain curve (F_y = 55 ksi).

Because the four-node (S4R) shell element used in this study is a general large strain formulation, the material properties in the finite element models are based on the true

stress-strain curve. From the engineering stress-strain curve generated as discussed above, the true stress-strain curve is obtained using the following equations:

$$\sigma_{true} = \sigma_{eng} (1 + \varepsilon_{eng}) \quad (3.3)$$

$$\varepsilon_{true} = \ln(1 + \varepsilon_{eng}) \quad (3.4)$$

For purposes of simplicity, these equations are applied only at the four transition points shown in the figure.

At the ultimate strength, the values of σ_{true} and ε_{true} are 79.3 ksi and 0.125 in/in. The maximum strains are smaller than 0.04 until well past the limit load of the structures considered in this work.

3.2 Nominal Residual Stresses

Figure 3.3, adapted from Kim 2010, shows the nominal residual stress pattern selected in this research. This pattern is representative of welded I-section members. It is self-equilibrating for each of the cross-section components and is a fit to the data reported from sectioning of a typical tapered member by Prawel et al. (1974). Because of the tapered geometry of the web panels, it is important to use a self equilibrating residual stress pattern for each of the cross-section plates. Otherwise, the residual stress patterns need to be varied for each cross-section throughout the beam unbraced lengths.

In the residual stress pattern shown in Fig. 3.3, the maximum compressive residual stress in the flanges is $0.25F_y$ at the tip of the flanges. The maximum compressive stress decreases linearly within the one-third of the flange width, $b_f/3$, from the flange tips. In the vicinity of the web-flange juncture, the maximum tensile residual stress is taken as $0.5F_y$. In the web, the maximum tensile residual stress is taken as F_y within the length

h/20 from the web flange juncture, where *h* is the clear web depth. In the middle of the web, there is a constant compressive residual stress of $0.176F_y$.

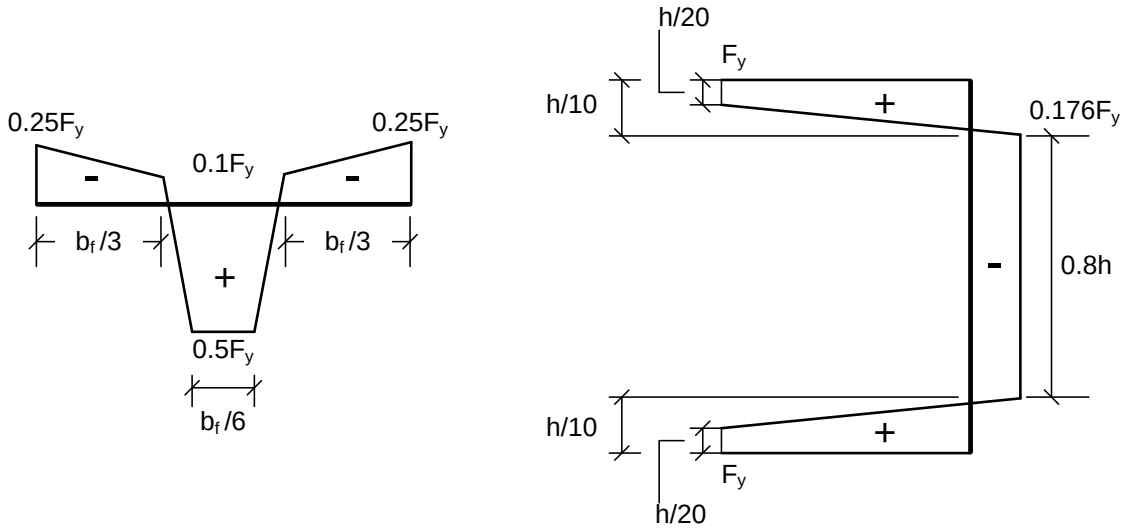

(a) flange distribution (b) web distribution

Fig. 3.3. Nominal residual stress pattern, from Kim (2010).

For members in which the compressive residual stress $0.176F_y$ is larger than the web plate buckling stress for uniform axial compression, assuming singly-supported boundary conditions, these residual stresses are reduced such that they are equal to this idealized web plate buckling stress. This avoids the specification of unrealistically high residual compression stresses that the web plates would have difficulty resisting.

As noted above, the residual stress pattern shown in Figure 3.3 is fit to residual stress measurements provided by Prawel et al. (1974). A number of virtual test simulations were conducted by Kim (2010) for experimental tests performed by Prawel et al. (1974). These simulations show that this residual stress pattern provides a reasonable estimate of the experimental test results.

3.3 Nominal Geometric Imperfections

The selected nominal geometric imperfections are central to the calculation of the strength and stiffness demands on stability bracing systems. Generally, the imperfections applied to the system should be within the tolerance limits of the AISC Code of Standard Practice (COSP). If one uses just the base COSP fabrication and erection tolerances for purposes of simplicity, this entails a limit on out-of-straightness of the members of $\delta_o = L/1000$ between the points that are laterally supported and a limit on out-of-alignment of $\Delta_o = L/500$ between the member working points. In steel construction, the working points are typically taken as the mid-depth of the member for non-horizontal members and the centerline of the top flange for horizontal members at the ends of the shipping pieces. However, the above limits are commonly applied as an assumed tolerance of $L/500$ on the out-of-plumbness or out-of-alignment between adjacent brace points when assessing the demands on stability bracing components. This approach is employed in this work.

The Commentary of the COSP points to other specifications and codes incorporated by reference in Contract Documents for any additional geometry requirements. Neither the COSP nor any of the other prevalent documents provides a tolerance on member twist. However, the AISC Appendix 6 provisions for torsional bracing are based on an assumed initial twist of $\theta_o = (L_b/500)/h_o$ at a given brace location, where h_o is the distance between the flange centroids. If one considers the twist in a member with a relatively large value of L_b/h_o, the resulting θ_o at a given cross-section potentially can be quite large. For instance, if $L_b/h_o = 5$, a value which is not all that unreasonable for some frame or member configurations, the equation $\theta_o = (L_b/500)/h_o$ gives $\theta_o = 1/100$ radians (0.57^o).

In this research, the cross-section twist is limited to 1/100 as a maximum practical limit unless noted otherwise.

Local buckling type imperfections also can be a very important contributor to the stability bracing behavior for members having noncompact or slender plate components. The COSP does not provide any explicit guidance with respect to initial imperfections affine to local buckling modes. However, the AWS D1.1 Specification (AWS 2000) specifies a tolerance on the tilt of the flange plates of min(b_f /100, 0.25 inches). Also, the AWS Specification specifies various tolerances on the out-of-flatness of the web plates ranging from h/150 for unstiffened webs to a maximum of h/67 for stiffened webs.

Section 9 of the MBMA Metal Building Systems Manual (MBMA 2006) gives specific limits on the flange tilt of 3^o, with a maximum limit of 0.25 inches relative tilt displacement between the flange tips. For most flange widths, the 0.25 inch maximum limit governs. In addition, MBMA (2006) specifies a maximum tolerance of h/72 inches on the web out-of-flatness, irrespective of the type of stiffening of the cross-section, where h is the web height.

Section 2a of Chapter C of the 2010 AISC Specification states that the nominal initial geometric imperfections generally must be oriented to produce the greatest destabilizing effect, and that their magnitude shall be the "maximum amount considered in the design." The meaning of this last phrase is basically that the initial imperfections should be based on permissible construction tolerances, and that if tighter tolerances are specified in the Contract Documents, then the strength can be evaluated using these tighter tolerances. Chapter C focuses predominantly on out-of-alignment of the points of intersection of the members in a frame from their ideal locations. However, the requirements for a virtual

simulation analysis model, capable of capturing both local and overall member stability effects per Appendix 1 of the 2010 AISC Specification, are more demanding. This type of analysis model generally must consider the out-of-alignment and out-of-straightness of the flanges, since these imperfections tend to have an important effect on the lateral or torsional bracing demands, as well as the tilt of the flange plates affine to calculated flange local buckling modes, and the out-of-flatness of the web plates affine to calculated web local buckling modes.

3.3.1 Types and Magnitudes of Critical Imperfections

In general, both member out-of-straightness between adjacent braces, member ends, or points of interconnection, as well as out-of-plumbness, i.e., the angular out-of-alignment of the member axis with respect to the ideal member working line must be considered in any analysis of members and frames and their bracing systems. Both of these imperfections can have a significant effect on the bracing demands for members and frames. According to the AISC Specification, the magnitudes of these imperfections should match the tolerances in the AISC Code of Standard Practice unless smaller tolerances are specified for a given structure. As noted above, the Code of Standard Practice for Steel Buildings and Bridges (AISC 2010) specifies these limits as 1/1000 of the length along the member axis between points that are laterally supported for the flange out-of-straightness, and 1/500 angular misalignment relative to the member working line for the member out-of-plumbness.

In addition to these imperfections, web and flange out-of-flatness imperfections need to be considered for systems with members having slender webs, such as typical metal building frames. Since metal building frames typically have slender webs, especially

close to the knee regions, the eigenvalue buckling modes are dominated by web buckling. The most critical pattern of potential web geometric imperfections is generally a combination of web elastic eigenvalue buckling modes that produces an out-of-flatness in the different "critical" locations of the structure, i.e., typically the locations where the members are most highly stressed, or where the member unity checks from an ordinary design are the largest. These imperfections can also have a significant influence on the key response quantities being investigated in this work, i.e., the brace forces, although the specific interaction between local buckling type deformations and brace forces is not well understood at the present time. In addition, not including these imperfections may result in convergence difficulties in the virtual simulation analysis, since the load-deflection solution must then navigate the near bifurcation response of the web panels.

Fig. 3.4 shows the buckling modes for the 90 ft. clear span frame discussed in Section 2.7 and shown in Fig. 2.12. Typically, for metal building frames such as the one shown in Fig. 2.12, it is common that hundreds of modes can be extracted from an elastic eigenvalue buckling solution, all dominated by web buckling. This is due to the slender webs, particularly where the cross-sections have the largest depths. Some of these modes will also show significant flange tilt rotations. As noted above, the Metal Building Systems Manual (MBMA 2006) specifies a tolerance on the web out-of-flatness of $h/72$, where h is the clear depth of the web, and a tolerance on the flange tilt that is typically 0.25 inches from tip to tip. Generally, a linear combination of scaled flange out-of-straightness, flange out-of-plumbness, and web and flange local buckling modes, satisfying the above limits on the overall resulting geometric imperfections, should be applied to the system being analyzed.

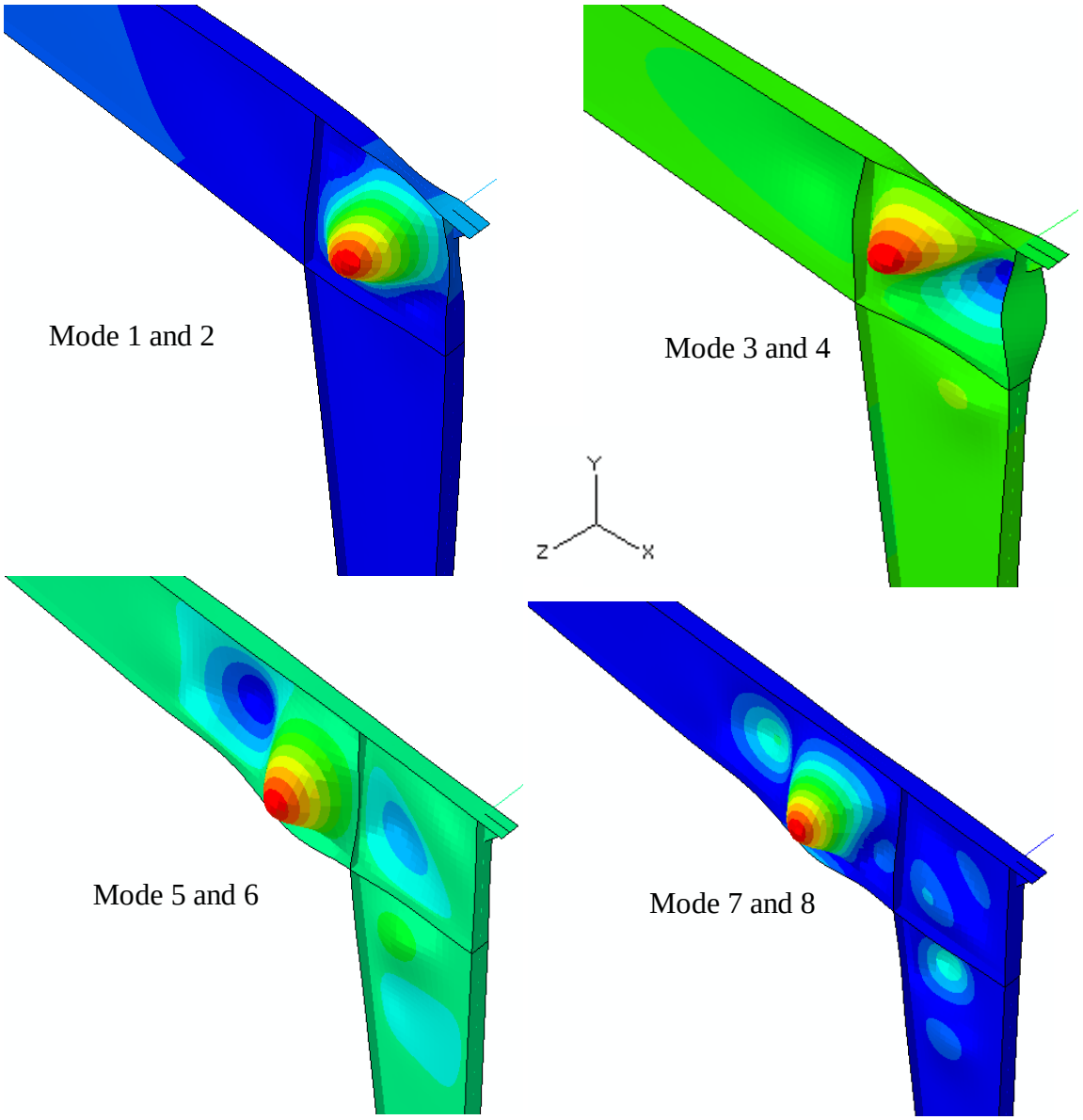

Fig. 3.4 First eight buckling modes for the 90 ft clear span frame.

3.3.2 Selection of the Critical Combination of Geometric Imperfections

The above discussions address the types of imperfections that should be considered for member and frame analysis, as well as the recommended magnitude of these imperfections. However, there is one additional decision that must be addressed in any analysis that explicitly determines the physical stability behavior and strength of a

geometrically imperfect structure and its bracing system. Generally, one must also select the distribution (i.e., the + and – directions) of the out-of-straightness (δ_o) and out-of-plumbness (Δ_o/L_b) from unbraced length to unbraced length throughout the system, as well as the directions of the scaled eigenvalue buckling modes (typically local buckling modes) that are applied as imperfections. When conducting a design check of any bracing components, the distribution of these geometric imperfections must be selected to generate the maximum strength demand on a given brace or set of braces, as well as to produce the maximum "destabilizing" effect on the system as a whole (similar to the way that different ASD or LRFD load combinations are applied to produce the maximum strength requirement on any given component). The following discussion focuses first on generation of the patterns for the nominal flange sweep and out-of-alignment imperfections.

Unfortunately, similar to the fact that different ASD or LRFD load combinations generate the maximum strength requirements on different members or components, different patterns of δ_o and Δ_o create the maximum strength demands on different braces and on the member as a whole. Furthermore, for determining the demands on a given brace, or for determining the strength of the structural system as a whole, the critical distributions of δ_o and Δ_o/L_b along a member length depend in general on the stiffness of the bracing relative to the stiffness of the structure. In addition, characteristics such as non-uniform brace stiffness and strength along the columns or rafters, and/or non-constant brace spacing along the columns or rafters, can have an important influence on which δ_o and Δ_o/L_b distributions are the most critical.

In order to generate the proper distribution of the above imperfections, i.e., the distribution that maximizes the destabilizing effects, two approaches are considered in this research. These are termed as the single brace out-of-alignment approach and the influence line approach.

The single brace out-of-alignment approach can be applied to maximize the brace force at a particular location if the system has very stiff or rigid bracing, i.e., bracing stiffnesses approaching the full-bracing requirements. The brace point where the strength and stiffness demands are to be maximized is displaced out-of-plane by $L_b/500$ while the adjacent brace points are held at zero displacement, where L_b is the unbraced length of that segment. For cases where the response is dominated by beam lateral-torsional buckling, the geometric imperfection is applied only to the compression flange. The prior research by Wang and Helwig (2005) has addressed imperfection requirements for beams with full bracing, and has recommended this approach.

In addition, a flange out-of-straightness with a maximum displacement of $L_b/1000$ is applied relative to the chord between the brace points in each of the adjacent unbraced lengths in this research. These out-of-straightness displacements typically are applied in the direction that the flange tends to bend due to the above out-of-alignment displacement of the brace point. They are implemented by directly applying the desired displacements to the flange at the brace points and at the middle of the unbraced lengths in a pre-analysis, allowing the other nodes of the model to deflect based on the elasticity of the structure. The corresponding nodal displacements from the pre-analysis are then input to the virtual simulation analysis as initial nodal strain-free geometric imperfections.

In many situations, an out-of-straightness between the brace points nearly equal to $L_b/1000$, relative to the chord between the brace points, is obtained simply by displacing the flange at the brace points as shown in Fig. 3.5. One may decide to just use this geometric imperfection based on judgment. In this work, unless noted otherwise, both the out-of-alignment of $L_b/500$ and the out-of-straightness of $L_b/1000$ are applied to the compression flange in the virtual simulation models.

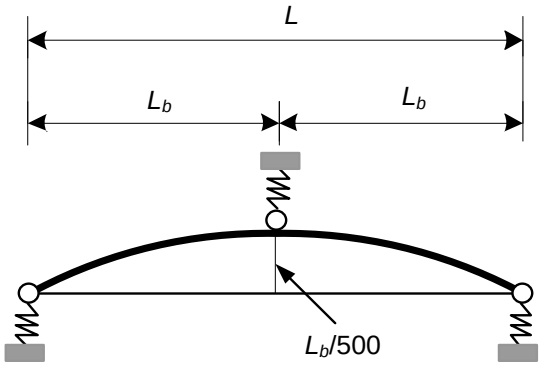

Fig. 3.5 Single brace out-of-alignment imperfection.

The other approach considered in this research is an influence line based procedure. In this approach, influence lines for the brace force (for lateral bracing) or brace moment (for torsional bracing) are generated using a geometric nonlinear pre-analysis using the ideal geometrically-perfect geometry. Unit transverse loads are applied to the flanges in the out-of-plane direction, in addition to the loads from the design load combination being considered, and the corresponding brace forces or brace moments are collected to generate the influence lines. It is sufficient to apply these unit loads just at the brace points and at the middle of unbraced lengths (a larger number of points simply give a greater resolution of the influence line). To generate the influence line, multiple (separate) geometric nonlinear analyses are conducted with each analysis corresponding

to the total load from the design load combination plus a single unit transverse lateral load. The ordinate of the influence line for a given brace force is obtained as the force, in that particular brace, caused by the unit out-of-plane loads applied successively at the different locations along the member or frame. The abscissa corresponds to the positions of the unit loads. By using an elastic second-order analysis to determine influence lines, the elastic out-of-plane stability behavior of the frame and its bracing system is included in the brace force assessment.

Fig. 3.6 shows the influence lines for the torsional brace moment at r1 for the rafter inside flange and the column inside flange for the clear span frame shown in Fig. 2.12. The stiffness contributions from the wall and roof diaphragms are neglected in this particular analysis (the stability bracing behavior without the participation of wall and roof diaphragms is considered as one of the subsequent case studies in Chapter 6). The details of the brace system modeling for this frame are discussed in Sections 3.4 and 6.3.

The influence lines are used generally to determine the brace point out-of-alignment and the flange out-of-straightness between the brace points in the out-of-plane direction that maximizes a given brace force. If these imperfections are represented in a chorded fashion, the change of slope between the chords at a given position is equivalent to an out-of-plane concentrated force, *F*, as shown in Fig. 3.7.

Given the influence lines and the above concept of an equivalent lateral load to a kink in the member flange, the worst case geometric imperfections are determined to maximize the sum of the products of the equivalent lateral forces, *F*, and the corresponding ordinates from the brace force influence line throughout the frame subject to the following constraints:

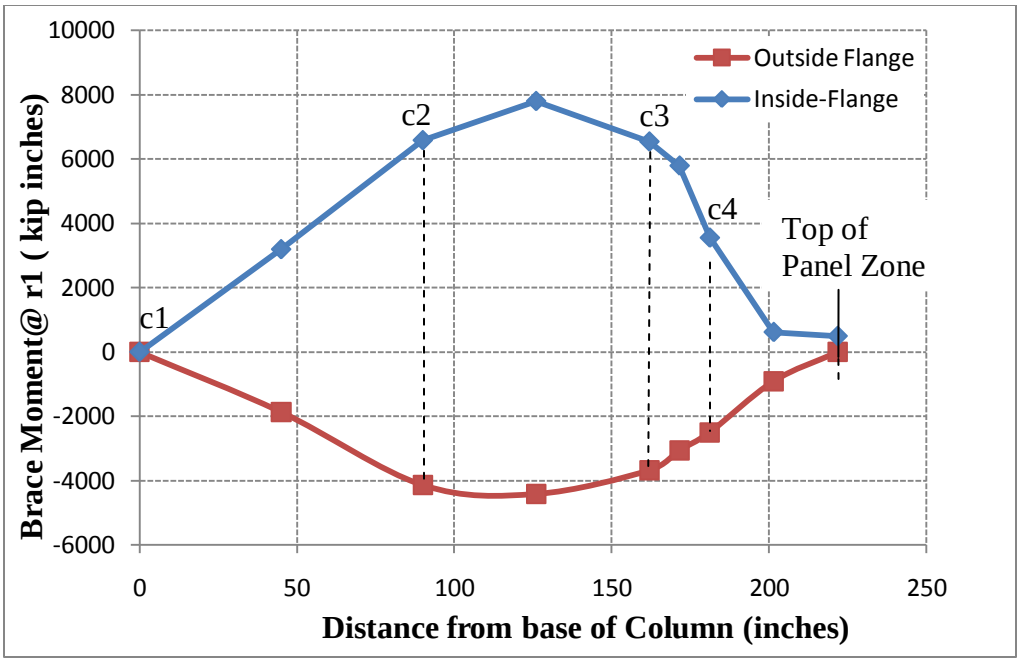

(a)

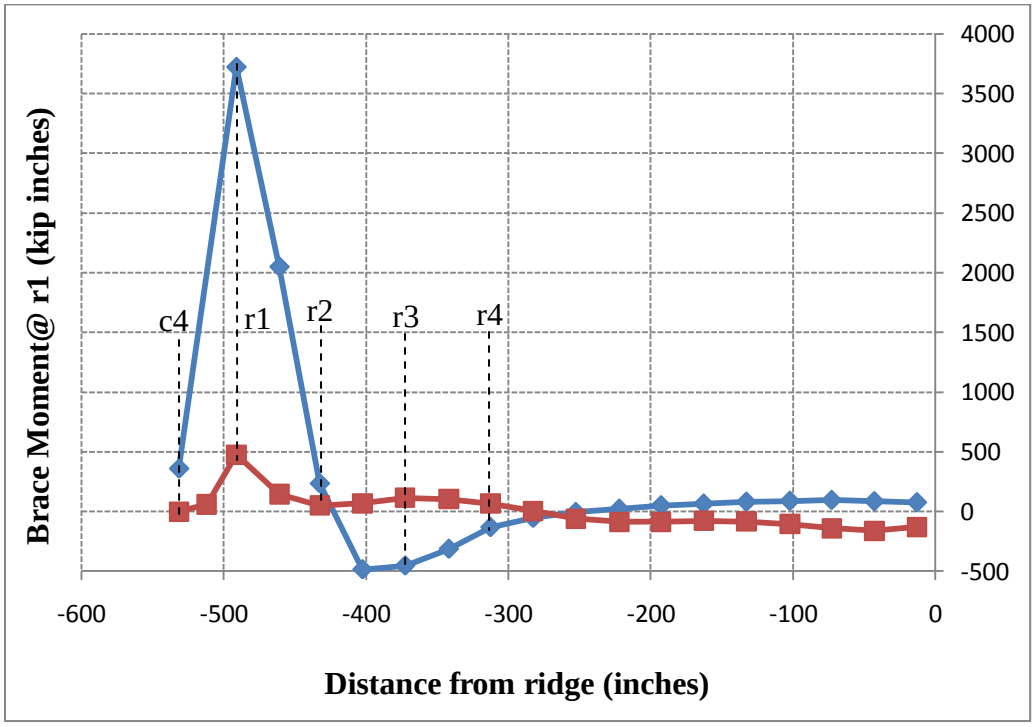

(b)

Fig. 3.6. Influence lines for torsional brace moment at r1 obtained by unit lateral load on the (a) column flange, and (b) the rafter flange.

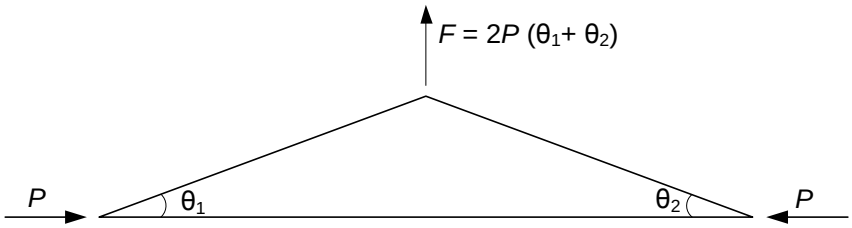

Fig. 3.7. Equivalent lateral force corresponding to a chorded representation of out-of-plumbness and/or out-of-straightness imperfections.

i. The out-of-plumbness of the flanges in any unbraced length should be equal to $L_b/500$.

ii. The out-of-straightness of the flanges in any unbraced length should be equal to $L_b/1000$.

If the above imperfections are applied to both flanges of the columns and the rafters in the 90 ft clear-span frame example, the largest net cross-section twist is approximately 1/50 radians for the clear span frame. Since this violates the maximum limit on the total cross-section twist, stated previously, the imperfections are applied to the compression flange only, producing a maximum net twist of approximately 1/100 radians. The resulting imperfections are shown in Fig. 3.8. It should be noted that the out-of-plane movement of the top flange of the rafter at r1 is 0.166 inches in Fig. 3.8(a). Correspondingly, the entire length of the rafter is shifted out-of-plane from r1 at one knee to r1 at the other knee. The out-of-alignment imperfections in Fig. 3.8(b) are applied relative to this position.

To complete the definition of the initial geometric imperfections, the nodal displacements associated with the selected scaled eigenvalue buckling modes are added to the above displacements, with the overall flange tilt and web out-of-flatness limited to

the previously specified limits. Generally, the scaled eigenmodes are not capable of matching the maximum tolerances for both the flange tilt and the web out-of-flatness. These modes are scaled such that the more critical imperfection tolerance is matched.

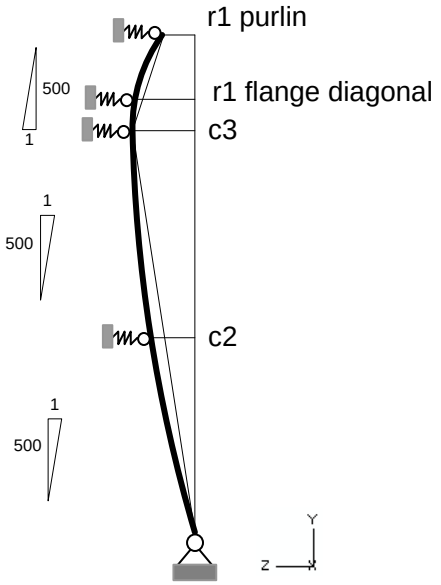

(a) column compression flange imperfections

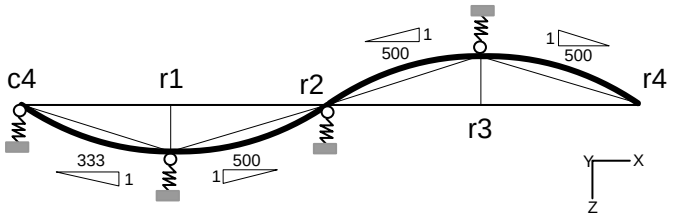

(b) rafter compression flange imperfections

Fig. 3.8. Imperfections corresponding to the influence line approach.

Unless noted otherwise, web out-of-flatness dominates the buckling modes of the problems considered in this research. Hence, the buckling modes are combined and scaled to match the web out-of-flatness tolerance at all the potentially critical locations in the structure. The direction of the local buckling modes is applied to produce the greatest

destabilizing effect along with the other flange sweep and out-of-alignment initial displacements. This direction is not always obvious. Typically several trial directions of the local buckling modes need to be tested to identify the critical pattern.

In summary, for the flexible bracing case on the 90 ft clear span frame, the linear combination of imperfections used to obtain the final imperfect geometry for this frame is

$$0.29 \times \Sigma_1^6 \text{ Mode } i + 0.29 \times (\text{Mode } 9 + \text{Mode } 10) + 0.25 \times (\text{Mode } 11 + \text{Mode } 12) +$$

compression flange out-of-alignment + compression flange out-of-straightness

where *"Mode"* refers to the corresponding buckling mode for the structure and the compression flange out-of alignment and out-of-straightness are shown in Fig. 3.8.

For the rigid bracing case, the influence line approach generally leads to the selection of a single brace point out-of-alignment for the compression flange out-of-alignment and out-of-straightness imperfection. Therefore, the above combination also applies to the rigid bracing case, but with the use of just a single brace point out-of-alignment at r1. In addition to the single brace point out-of-alignment at r1, a single brace point out-of-alignment is also placed at r9 in the rigid bracing model. This allows for easy assessment of the maximum brace demands at both of these locations.

3.4 FEA Representation of the Bracing Components and Systems

Two basic idealizations have been considered when analyzing the bracing systems for the members and frames studied in this research: rigid bracing and flexible bracing.
In the rigid bracing model, the brace points (i.e., the points where the girts or purlins attach to the outside flanges and the points where the diagonal bracing attaches to the inside flanges) are simply constrained to have zero displacement in the out-of-plane direction.

The modeling of the flexible bracing systems presents a greater challenge. In this research, these systems are idealized generally as shown in Fig. 3.9. This figure corresponds to the frame shown previously in Fig. 2.12. The approach implemented in this figure aims to characterize the elastic properties of the bracing system in a way that is easily parameterized and varied to study the fundamental questions of this research:

1. What are the demands on the bracing system, and what are the key factors that influence these demands?
2. How does the bracing system stiffness influence the overall strength of the structure being braced?

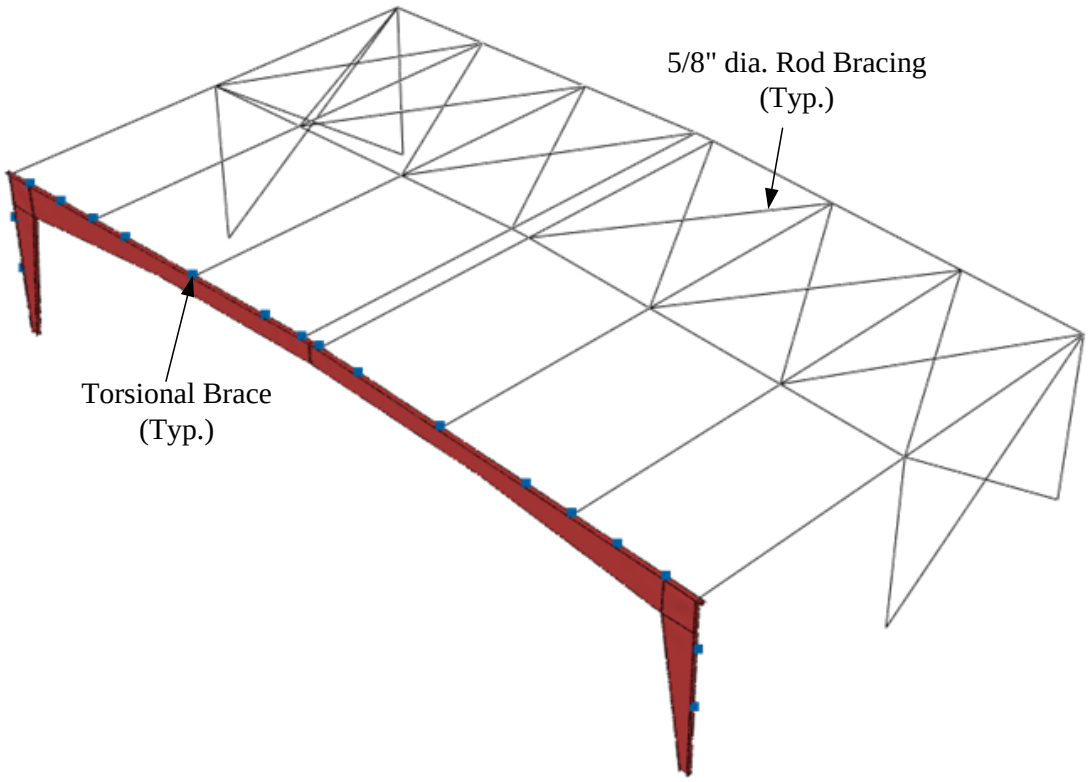

Fig. 3.9. Representative flexible bracing system model for metal building frames with outset girts and purlins, a longitudinal X-bracing system, and flange diagonal torsional braces.

Early on in this research, it was realized that a comprehensive virtual simulation model of the entire metal building primary and secondary structural systems would be prohibitive in terms of answering these fundamental questions. Since a simplified elastic model of the bracing system is employed in the virtual simulations, the strength of the bracing system components needs to be checked in general based on the demands obtained from the analysis. However, since the analysis includes a virtual simulation of the main frame, the calculated strength demands are considered rigorous.

3.4.1 Model of the Building Longitudinal X Bracing System

In the flexible bracing system model shown in Fig. 3.9, the "primary" main frame is modeled using shell finite elements. Furthermore, for the basic situation shown in Fig. 3.9, where the contributions from the roof and wall diaphragms are not included, it is assumed that the out-of-plane lateral restraint comes only from the panel points of the longitudinal X-bracing system. The purlins and eave struts at the "hard" brace points, i.e., at the panel points of the building longitudinal X bracing system, are modeled as elastic struts, using truss elements. The areas of the cold-formed purlin sections are input for these truss areas. The building longitudinal bracing system is also represented using truss elements. This system is assumed to be comprised of two other main frames, the purlins and eave struts attached to these frames, and the X bracing diagonals. The "primary" main frame is separated from, and tied back to the longitudinal bracing system by truss elements (axial struts) at each of the purlin and eave strut locations. This eliminates any contribution of the longitudinal bracing system to the in-plane response of the primary main frame. In other words, this avoids any incidental "stressed skin" action of the longitudinal bracing system with the primary frame. For the X bracing, 5/8 in diameter

rods are assumed. Only 50% of the cross-section area is used for the rods to approximate zero-compression strength of the rods. The chords of the longitudinal bracing system are modeled using truss elements and are assumed to have a cross-sectional area equal to the area of the top flange of the main frame members. In addition, the main frame models of the longitudinal bracing system are pinned at the foundation level, i.e., the displacements are restrained in all three directions at these locations. Lastly, the longitudinal truss system is constrained to deflect only in the plane of the roof and the walls at all of its nodal locations. That is, all the nodal locations above the base in the adjacent frames are restrained in the plane of those frames and are free to deflect in the direction out-of-plane of those frames. As such, the longitudinal X bracing system flexibility is modeled essentially as this system's shear flexibility based solely on the axial flexibility of the bracing diagonals. The chords of the longitudinal X bracing truss are effectively modeled as rigid components. This is believed to be a good approximation since the majority of the longitudinal X bracing system's flexibility is due to the deformation of its diagonals.

3.4.2 Modeling of Torsional Braces

The torsional braces are modeled as grounded rotational springs in the flexible bracing system model shown in Fig. 3.9 and in all of the other related member and frame studies conducted in this research. These torsional springs are placed at each of the purlins and girts where diagonal braces are indicated (see Fig. 2.12). At these locations, multi-point constraints are used to tie the centroidal location of the girt or purlin to the nodes at the corresponding flange-web junctures of the member being braced. These constraints have the same effect as a rigid bar attached from the rotational springs to idealized pinned connections to the flanges of the main frame members. One end of the

rotational spring is grounded and the other end is attached to the node at the top and the bottom of the cross section at the web-flange juncture via the constraints. The rigid bar effect is achieved by using multi-point constraints as shown in Fig. 3.1. Since the springs model only the torsional stiffness, the multi-point constraints applied activate the spring only if there is differential movement of the flanges in the out-of-plane direction. The longitudinal and vertical deflections at the brace points are not restrained by the torsional springs. This idealized model provides a single valued torsional stiffness resisting the twisting of the cross section at the brace points. Other multiple degree of freedom idealizations are possible, but the corresponding results would be much more complex to interpret.

3.4.3 Modeling of Wall and Roof Shear Diaphragms

For situations where the stiffness contributions from the roof and wall diaphragms are considered, the diaphragm stiffness is modeled using a shear spring attached between girts, purlins and eave struts. These shear springs resist the displacement of one brace point relative to the adjacent brace point in the out-of-plane direction of the primary frame, thus representing a shear diaphragm between the two points.

CHAPTER 4

ROOF GIRDER EXAMPLE

4.1 Introduction

This chapter presents a variation of a roof girder example originally presented as "Example 6" by the Ad hoc Committee on Stability Bracing (AISC 2002) and included in the stability bracing short course notes by Yura and Helwig (2009). In the current research, the bracing demands for this girder are estimated using the AISC torsional bracing equations detailed in Section 2.6.2.2 as well as the simplified equations presented in Section 2.8.3. These estimates are then compared to the results obtained from virtual test simulation. First, Section 4.2 gives a broad overview of the geometry and loading for this problem and Section 4.3 discusses the specific bracing configuration being considered. Sections 4.4 and 4.5 then present the AISC-based and simplified estimates for the bracing demands at several load levels ranging from the specified LRFD loading up to the ultimate strength capacity of the girder. This is followed by Section 4.6, which explains the calculation of the provided brace stiffnesses and strengths for this problem. Section 4.7 begins the presentation of the virtual test simulations by discussing the critical geometric imperfections applied in these studies. Section 4.8 then presents the virtual test simulation results using the AISC-based torsional brace stiffness required to develop the specified LRFD design load. Section 4.9 completes the presentation of the virtual simulation results by showing the effect of varying the torsional brace stiffness on the strength of the roof girder. Lastly, Section 4.10 summarizes the important attributes and observations from this example.

4.2 Geometry and Loading

Figure 4.1 shows a roof girder of an industrial building structure. This member has outset purlins attached to its top flange at 5 ft intervals. The LRFD wind uplift load combination, shown in the figure, produces compression on the bottom flange over the majority of the girder length. Three diagonal braces are provided near the mid-span to stabilize the bottom flange of the member under this loading. The bottom flange is loaded in tension at the ends of the girder. Figure 4.1 shows the moment diagram from the LRFD wind uplift load combination and the configuration of the flange bracing. Steel of yield strength F_y = 50 ksi is assumed for the design. The girders are placed 25 ft apart in the out-of-plane direction and the purlins are assumed to frame continuously across the girder top flanges. The diagonal braces are assumed to be attached directly to the bottom flange of the girder.

It should be noted that the committee example (AISC 2002) also considers the beam bracing requirements for the maximum downward LRFD gravity load combination, producing compression in the top flange over the majority of the beam length. This chapter considers solely the wind uplift loading and the associated bracing demands and requirements.

4.3 Bracing Configuration

For this study, the ends of the roof girder are modeled as flexurally and torsionally simply supported. Open-section thin-walled beam theory kinematics is enforced at these end points, as explained in Section 3.1.2. Positive end moments are applied at these locations. The member is assumed to be braced rigidly against twisting and lateral translation at its ends, but warping and lateral bending of the flanges are unrestrained at

these locations. This is consistent with the derivation of all the beam bracing rules in Appendix 6 of the AISC Specification.

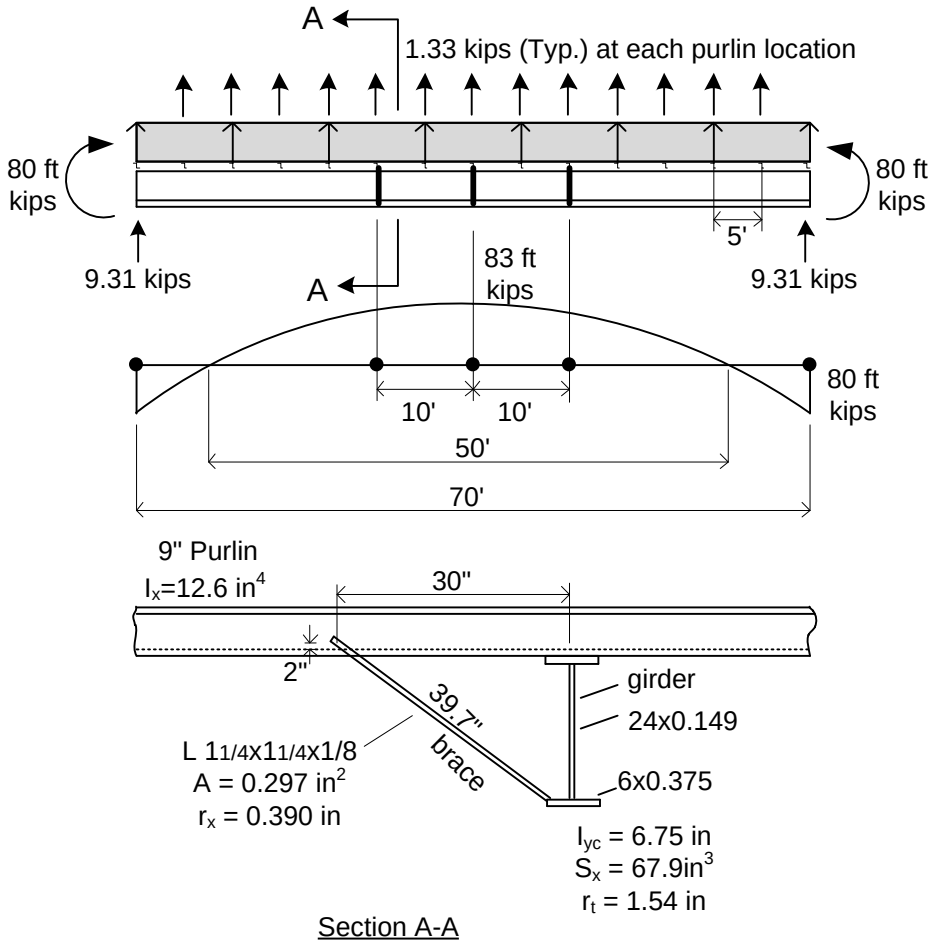

Fig. 4.1. Roof girder description.

In the current study, the torsional bracing from the flange diagonals and purlins is modeled by torsional springs located at the centroidal depth of the purlins and tied to the two flanges of the girder as explained in Section 3.4. The combined flexibility from the axial deformation of the flange diagonal braces and the flexure of the purlins is considered in determining the provided torsional brace stiffnesses. Since the diagonals are assumed to be attached directly to the bottom flange, no additional flexibility due to

cross-section web distortion is considered. In addition, it is assumed that there is no local deformation or slip at the connections at either end of the flange diagonal braces. Furthermore, it is assumed that the purlins are attached to the top flange of the roof girder such that, along with the attachment to the bottom flange, a torsional restraint couple can be developed. However, otherwise the purlins are assumed to not provide any torsional or lateral restraint at the top flange of the member. The torsional restraint from the bracing system comes from the activation of the purlin flexural stiffness via the truss action of the flange diagonals.

The above considerations regarding web distortion and/or connection deformations are very important in general, since web distortion and connection deformations can reduce the effective torsional brace stiffness substantially. Generally, any additional brace flexibility due to web distortion and connection deformations should be incorporated into the torsional spring stiffness calculation.

The committee example (AISC 2002) applies the beam *lateral* bracing provisions of the AISC Specification Appendix 6 to evaluate the three bottom flange braces. As such, the purlins are assumed to be inherently rigidly restrained against movement out of the plane of the page in the AISC (2002) calculations. That is, the axial flexibility of the flange diagonals and the flexural deformation of the purlins are assumed to be the only sources of lateral deflection at the bottom flange brace locations. This is a reasonable assumption if the shear stiffness of the roof diaphragm is relatively large and the diaphragm is rigidly attached to the purlins. However, in the limit that it's stiffness is small, the roof diaphragm may not be sufficient to hold the purlin locations effectively at zero out-of-plane displacement. Even if a substantial finite stiffness is provided by the

roof diaphragm, the lateral stiffness provided at the middle brace will be somewhat different than the stiffness at other two intermediate brace points (see Fig. 1.2 for a comparable generalized explanation of this behavior).

Rather than count on a rigid roof diaphragm, the lateral bracing stiffness from the diaphragm is neglected and the three flange diagonal brace points are considered only as torsional braces in the current study. It is interesting to compare and contrast the bracing requirements based on torsional bracing rules, which assume zero lateral bracing stiffness, to those of the AISC (2002) committee example, which assume a rigid roof diaphragm. Note that in the AISC (2002) example lateral bracing calculations, as well as in the AISC-based torsional bracing calculations provided here, an ad hoc interpretation of the AISC rules is invoked since the flange diagonal braces are not located at constant spacing. As noted previously, equally-spaced equal-stiffness braces are assumed in the development of all the AISC Appendix 6 nodal bracing equations.

4.4 AISC-Based Bracing Requirements

4.4.1 Refined Estimates of the Girder Flexural Resistance for Full Bracing

In the subsequent virtual simulation studies for this problem, the beam and its bracing system are loaded up to their ultimate load capacity. As such, it is useful to determine the nominal moment capacity of the beam (M_n) using the 2010 AISC Specification flexural resistance equations and assuming that the three torsional braces are sufficient to provide full bracing. Note that in the AISC (2002) lateral bracing calculations, as well as in the first set of torsional bracing calculations presented below, the bracing system is designed only for the required moments coming from the LRFD wind uplift load combination.

Therefore, it is possible that the beam is only partially braced and thus unable to develop the fully-braced capacity of the beam under the uplift loading.

Figure 4.2 shows the moment diagram from the uplift load combination on one-half of the overall girder length. Based on the assumption of zero lateral restraint of the top flange by the purlins, that is, assuming that the three flange diagonal (torsional) brace locations are the only brace points within the girder span, one can calculate the moment gradient modifier C_b for the longer 25 ft unbraced length as

$$C_b = \frac{12.5(80)}{2.5(80) + 3(27 + 48) + 4(16)} = 2.04$$

from AISC Eq. (F1-3).

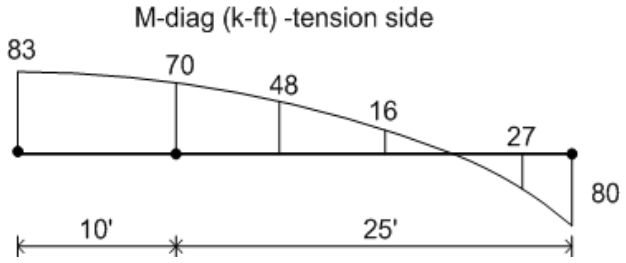

Fig. 4.2. Moment diagram from the LRFD uplift load combination shown on one-half of the girder length.

In addition, although the effective length for lateral torsional buckling is usually taken as $K = 1.0$ in design, it should be noted that the adjacent shorter 10 ft unbraced lengths actually provide substantial warping restraint at the interior ends of the 25 ft outside unbraced lengths in this problem. For estimating the fully-braced beam capacity expected from a virtual test simulation, this warping restraint can be included quite effectively by using a column analogy procedure originally developed by Nethercot and Trahair (1976) and discussed in Ziemian (2010). For this problem, the Nethercot and Trahair approach

gives $K = 0.83$. Since the web is slender and $KL_b = 20.8$ ft is larger than $L_r = 11.7$ ft for the beam section shown in Fig. 4.1, AISC Eq. (F5-4) applies and $M_n = 128$ ft-kips is obtained for the governing 25 ft unbraced length using $C_b = 2.04$ and $K = 0.83$ ($KL_b = 20.8$ ft). Therefore, based on this "best estimate" from the AISC Specification, the fully-braced strength of the girder 25 ft. unbraced length is 128/80 = 1.60 times the load level corresponding to the LRFD wind uplift combination.

As shown subsequently, the virtual simulation limit load of the beam and its bracing system is 1.68 times the required strength associated with the moment diagram of Fig. 4.1, assuming only torsional braces at the three flange diagonal locations along with top and bottom flange rigid lateral bracing at the beam ends, and assuming that the intermediate torsional braces are designed based on the AISC Appendix 6 requirements using this moment diagram. That is, the virtual simulation test capacity is 1.68/1.60 = 1.05 times the best estimate of the corresponding *fully-braced* capacity obtained from the AISC Specification equations (although the braces are designed for substantially smaller beam moments).

Furthermore, if rigid lateral bracing is assumed for the top and bottom flanges at the three interior brace points, the beam supports 2.08 times the required strength and 2.08/1.60 = 1.30 times the best estimate of the capacity from the AISC specification equations in a virtual test simulation. The most likely reasons for the additional capacity in this case are:

1. The existence of some conservatism in the calculation of C_b due to the lower-bound nature of the AISC Eq. (F1-3) as well as the restoring effect of the upward loads applied to the top of the girder flanges at the purlin locations, and

2. Warping restraint provided at the middle brace point due to localization of the buckling deformations on one side of the mid-span at the ultimate strength limit.

Table 4.1 summarizes the different internal moments and the corresponding applied load levels considered in the following sections for this example.

Table 4.1 Summary of girder applied moments and flexural resistances for the LRFD wind uplift load combination.

Calculation Source	Mid-span moment (ft-kips)	End Moment (ft-kips)	Multiple of LRFD Wind Uplift Load Combination	Multiple of AISC Beam Capacity
LRFD Wind Uplift Loading	83	80	1.00	0.625
AISC Ch. F capacity with C_b = 2.04 and K = 0.83 on the outside 25 ft unbraced lengths	133	128	1.60	1.00
Virtual simulation using torsional bracing satisfying the AISC-based requirements to develop the LRFD uplift wind loading	139	134	1.68	1.05
Virtual simulation using rigid lateral bracing of the top and bottom flanges at the torsional brace locations	173	166	2.08	1.30

4.4.2 AISC-Based Torsional Bracing Requirements Using the Moments from the LRFD Wind Uplift Load Combination

4.4.2.1 Required Stiffness

The stiffness for the three torsional braces required by the AISC Appendix 6 provisions is calculated as follows. As noted above, any lateral bracing of the top flange by the purlins and/or the roof diaphragm is neglected in this study. A single required torsional bracing stiffness is calculated, since the AISC equations are based on the assumption of equal-stiffness bracing. The fact that the brace points are not spaced equally is handled in an ad

hoc fashion by evaluating Eq. (2-31) for each of the unbraced lengths and using the largest value obtained as the required stiffness (see Section 2.6.2.2).

Equation (2-31) is

$$\beta_T = 20\psi h_o^2 \left[\frac{M_r / C_b h_o}{P_{e.eff}} \right] \left(\frac{M_r / C_b h_o}{L_b} \right) \frac{(n_T + 1)}{n_T} C_{tT}$$

By considering the longer of the adjacent unbraced lengths adjacent to the outside intermediate torsional braces, the following are obtained as the input parameters to this equation:

ϕ =0.75

h_o = 24.375 inches

M_r = 80 ft-kips = 960 in-kips

C_b = 2.04 (see above)

$M_r / C_b h_o$ = 19.3 kips

E = 29,000 ksi

$I_{eff} = 2I_{yc}$ = 13.5 in^4

L_b = 25 ft = 300 inches

$$P_{e.eff} = \frac{\pi^2 E I_{eff}}{L_b^2} = 42.9 \text{ kips}$$

n_T = 3

C_{tT} = 1.0

This gives

$$\beta_T = \frac{20}{0.75}(24.375)^2 \left[\frac{19.3}{42.9} \right] \left[\frac{19.3}{300} \right] \frac{(3+1)}{3} (1.0) = 611 \text{ in-kips/rad}$$

By considering the shorter of the adjacent unbraced lengths at the torsional brace locations, the following are obtained as the input parameters:

M_r = 83 ft-kips = 996 in-kips

C_b = 1.0 (slightly conservative)

$M_r / C_b h_o$ = 40.9 kips

E = 29,000 ksi

$I_{eff} = 2I_{yc}$ = 13.5 in^4

L_b = 10 ft = 120 inches

$$P_{e.eff} = \frac{\pi^2 E I_{eff}}{L_b^2} = 268 \text{ kips}$$

$n_T = 3$

$C_{tT} = 1.0$

This gives

$$\beta_T = \frac{20}{0.75}(24.375)^2\left[\frac{40.9}{268}\right]\left[\frac{40.9}{120}\right]\frac{(3+1)}{3}(1.0) = 1100 \text{ in-kips/rad}$$

Therefore, the shorter unbraced length governs the bracing stiffness requirement.

Since both flanges are tied to the torsional bracing system, $\beta_{sec} = \infty$ and $\beta_T = \beta_{Tb}$. Therefore, a torsional brace stiffness of 1100 in-kips/rad is required from the above application of the AISC Appendix 6 equations. In Section 4.8, this stiffness is used for the torsional braces in the first of several virtual test simulations.

It is informative to convert the above torsional stiffness requirement to an equivalent lateral bracing requirement at the bottom flange of the roof girder. This is accomplished by dividing β_T by the square of the distance between the girder flanges:

$$\beta_{br} = \beta_T / h_o^2 = 1100 \text{ in-kips/rad} / (24.375)^2 = 1.85 \text{ kips/inch}$$

This value is slightly smaller than the corresponding value for the required lateral brace stiffness of 2.67 kips/inch, using the *base* AISC Appendix 6 beam lateral bracing provisions implemented in the AISC (2002) committee example. It is essentially the same as the corresponding *refined* Appendix 6 beam lateral bracing calculation of 1.78 kips/inch obtained by the committee calculations, using the equations detailed in Section 2.6.2.1.2 of this report.

In Section 2.6.2.2 of this report, it is suggested that Eq. (2-31) a calculated effective length factor K potentially could be used in determining $P_{e.eff}$. For this example, $K = 0.83$ for the longer unbraced length adjacent to the outside intermediate braces, which gives

$$P_{e.eff} = 42.9 / 0.83^2 = 62.3 \text{ kips}$$

for this unbraced length. However, the shorter unbraced length is the critical one in this case. Furthermore, the longer unbraced length tends to destabilize the shorter unbraced length. The corresponding effective length factor for this length is $K = 1/0.83 = 1.20$, and the corresponding $P_{e.eff}$ of the shorter unbraced length is

$$P_{e.eff} = 268 / 1.20^2 = 186 \text{ kips}$$

If one uses this value for the $P_{e.eff}$ of the middle unbraced lengths, the required β_T of the outside intermediate braces is 1580 in-kips/rad. The β_T determined using $K = 1.0$ is retained in the following calculations, for purposes of simplicity. However, all the different potential calculations of β_T are compared to the requirements indicated by virtual test simulation in the subsequent sections.

4.4.2.2 Required Strength

Using the AISC Appendix 6 procedures, the required strength of the torsional braces is determined by simply multiplying the *required* stiffness by a twist rotation equal to the assumed initial twist imperfection at a given brace point, $(L_b/500)/h_o$, where L_b is taken as the unbraced length of the segment governing the required brace stiffness:

$$M_{br} = \frac{\beta_T}{\psi}\frac{L_b}{500h_o} = 1100(0.75)\frac{120}{500(24.375)} = 8.12 \text{ in-kips}$$

Note that the *required* stiffness must be used in this equation, not the actual provided stiffness. If the actual provided stiffness is larger than the required stiffness, the physical brace moment tends to be decreased, not increased. It should be noted that the above brace moment is 100{8.12/[(83)(12)]} = 0.82 % of the maximum required moment in the beam. The corresponding equivalent lateral force at the bottom flange is

$P_{br} = M_{br}/h_o = 8.12/24.375 = 0.33$ kips

This can be compared to the base lateral force estimate of 0.82 kips and to a refined estimate of the lateral bracing force of 0.41 kips in the AISC (2002) committee example. However, the AISC (2002) calculations are based on the implicit assumption that the purlins are rigidly restrained against out-of-plane displacement and that only the purlin flexural deformations and the diagonal brace axial deformations contribute to the brace point displacements at the bottom flange.

4.4.3 AISC-Based Torsional Bracing Requirements Based on the AISC LRFD Beam Design Capacity Assuming Full Bracing Stiffness and Strength

As noted above, the roof girder in this example is able to develop 128/80.0 = 1.6 times the required resistance obtained from the LRFD load combination for wind uplift based on the AISC flexural resistances and the assumption of full bracing. It is interesting

to evaluate what bracing stiffness demand is required using the AISC Appendix 6 equations if one recognized this additional capacity and wished to design the bracing to ensure that the fully-braced strength of the beam is obtained. It should be emphasized that the actual strength obtained in the subsequent virtual simulation studies, using only the AISC required torsional bracing stiffnesses determined with the moments from the wind uplift combination (β_T = 1110 in-kips/rad from Section 4.4.2.1, not the AISC required bracing stiffness corresponding to the fully-braced beam flexural capacity), is already 1.05 times larger than the AISC fully-braced capacity.

The AISC-based estimate of the torsional brace stiffness required to develop the refined AISC fully-braced beam LTB flexural resistance is:

$$\beta_T = 1100(128/80)^2 = 2820 \text{ in-kips/rad}$$

which corresponds to an equivalent lateral brace stiffness of

$$\beta_{br} = 2820 / 24.375^2 = 4.75 \text{ kips/inch}$$

The AISC-based estimate of the torsional brace strength required to develop the refined AISC LTB fully-braced beam flexural resistance is

$$M_{br} = \frac{\beta_T}{\psi}\frac{L_b}{500h_o} = 2820(0.75)\frac{120}{500(24.375)} = 20.8 \text{ in-kips}$$

It should be noted that this is 100{20.8/[(83)(1.6)(12)]} = 1.31% of the maximum major-axis bending moment in the beam at the estimated fully-braced strength condition. The corresponding equivalent lateral force at the bottom flange is

$$P_{br} = M_{br}/h_o = 20.8/24.375 = 0.85 \text{ kips}$$

4.4.4 AISC-Based Torsional Bracing Requirements Based on the Maximum Moments from Virtual Test Simulation

As noted at the end of Section 4.4.1, the actual load capacity of the girders in this problem, obtained from a virtual test simulation using torsional braces satisfying the AISC-based requirements to develop the LRFD uplift load capacity of the girders, is 1.68 times the applied loading from the LRFD uplift load combination, or 1.68/1.60 = 1.05 times the load level corresponding to the above "best estimate" of the beam strength from the AISC Specification equations assuming full bracing stiffness and strength.

If the bracing were sized to fully brace the beam at this load level, the required bracing stiffness would be

$\beta_T = (2820)(1.05^2) = 3110$ in-kips/rad ($\beta_{br} = 3110 / 24.375^2 = 5.23$ kips/inch

and the required torsional brace strength would be

$M_{br} = (20.8)(1.05^2) = 22.9$ in-kips ($P_{br} = 22.9/24.375 = 0.94$ kips)

or 100{(22.9)/[(83)(1.68)(12)]} = 1.37 % of the maximum major-axis bending moment.

Lastly, for the case of rigid lateral bracing at the top and bottom flanges, the corresponding ratio of the load capacity from the virtual test simulation to the LRFD uplift load combination level is 2.08, or 2.08/1.60 = 1.30 times the load level corresponding to the above AISC beam flexural strength assuming full bracing. For full bracing at this load level, the required bracing stiffness is

$\beta_T = (2820)(1.30^2) = 4770$ in-kips/rad ($\beta_{br} = 4770 / 24.375^2 = 8.02$ kips/inch

and the required torsional brace strength is

$M_{br} = (20.8)(1.30^2) = 35.2$ in-kips ($P_{br} = 35.2/24.375 = 1.44$ kips)

or 100{(35.2)/[(83)(2.08)(12)]} = 1.70 % of the maximum major-axis bending moment.

4.5 Simplified Bracing Requirements

Using the simplified bracing stiffness and strength requirements discussed previously in Section 2.8, the required torsional bracing strength is

M_{br} = 0.02 (83 k ft)(12) = 19.9 in-kips (P_{br} = 19.9/24.375 = 0.82 kips)

to develop the applied load corresponding to the LRFD wind uplift load combination,

M_{br} = 19.9 x 1.6 = 31.8 inch-kips (P_{br} = 1.31 kips)

to develop the maximum strength of the fully-braced beam based on the AISC Chapter F provisions with C_b = 2.04 and K = 0.83,

M_{br} = 19.9 x 1.68 = 33.4 inch-kips (P_{br} = 1.37 kips)

to develop the maximum strength obtained by virtual simulation, using the AISC-based brace stiffnesses for full bracing, and

M_{br} = (19.9)(2.08) = 41.3 in-kips (P_{br} = 1.68 kips)

to develop the maximum strength obtained by virtual simulation using rigid bracing. All of these estimates of course correspond to 2.0 % of the maximum internal moment in the beam within the unbraced lengths adjacent to the brace under consideration.

The corresponding torsional brace stiffness requirements, based on the simplified approach, are respectively

$$\beta_T = \frac{0.02(83.0)(24.375)}{0.002(25)} = 809 \text{ in-kips/rad} \quad (\beta_{br} = 809/24.375^2 = 1.36 \text{ kips/inch})$$

$$\beta_T = \frac{0.02(83.0)(1.6)(24.375)}{0.002(25)} = 1300 \text{ in-kips/rad} \quad (\beta_{br} = 2.18 \text{ kips/inch})$$

$$\beta_T = \frac{0.02(83.0)(1.68)(24.375)}{0.002(25)} = 1360 \text{ in-kips/rad} \quad (\beta_{br} = 2.29 \text{ kips/inch})$$

and

$$\beta_T = \frac{0.02(83.0)(2.08)(24.375)}{0.002(25)} = 1680 \text{ in-kips/rad} \quad (\beta_{br} = 2.84 \text{ kips/inch})$$

Obviously, depending on how one approaches this bracing problem, a wide range of stiffness and strength requirements can be estimated. Therefore, it is important to compare these various estimates to rigorous calculations based on virtual simulation. This is accomplished subsequently in Section 4.8. The next section addresses the calculation of the provided brace stiffness and strength in this problem, and compares these values to a summary of the various estimates of the requirements

4.6 Calculation of the Provided Brace Stiffness and Strength and Comparison to Required Values

Assuming that only one girder fails and the adjoining girders remain elastic, an upper-bound estimate of the torsional bracing stiffness provided by the purlins and flange diagonal bracing system can be estimated coarsely as *8EI/s* in this problem, as explained in Section 2.7.2. As shown in Fig. 4.1, the purlins in the AISC (2002) committee example have a moment of inertia of 12.6 in^4. Therefore, given the 25 ft spacing of the frames, this estimate of the torsional stiffness is 9740 in-kips/rad, and the equivalent lateral bracing stiffness is $9740/24.375^2 = 16.4$ kips/inch.

In the committee example, a more conservative estimate of the lateral bracing stiffness at the level of the bottom flange was calculated as $\beta = 9.47$ kips/inch, as shown in Fig 4.3. This stiffness estimate is based on the following assumptions:

- Two adjacent girders buckle simultaneously,
- The diagonal braces are connected to the purlins such that the corresponding work point is located at 10 % of the spacing of the frames (2.5 ft from the main frames),

- The diagonal braces are connected to the purlins on only one side of the main frames,
- The diagonal braces are connected to the main frames in the direction toward the other adjacent frame that is buckling,
- The purlins frame continuously over one additional frame on each side of the critically loaded span of the purlins, and
- The bracing diagonal axial flexibility is the only other important contributor to the brace point flexibility in addition to the purlin flexural deformations.

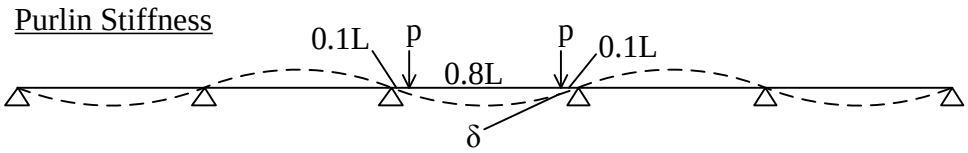

$p/\delta = 569\ EI/L^3 = 569(29000)12.6(25x12)^3 = 7.7$ k/in

Equivalent horizontal stiffness $= 7.7/\tan^2\theta = 10.2$ k/in

Angle Stiffness

$(30^2 + 26^2)^{0.5} = 39.7$ in

$$\frac{0.297(29000)}{39.7}\cos^2\theta = 124 \text{ k/in}$$

$(1/10.2)+(1/124) = 1/\beta$: $\beta = 9.47$ k/in

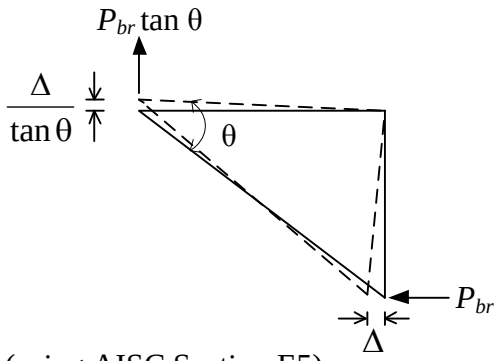

Brace Strength

$F_y = 50$ ksi $\quad L/r_x = 39.7/0.390 = 102$ (using AISC Section E5)

$KL/r = 32 + 1.25(L/r_x) = 160$: $\phi_c F_{cr} = 8.82$ ksi

$\phi_c R_n = 8.82(0.297)\cos\theta = 2.62\cos\theta = 1.98$ k

Fig. 4.3. Calculation of bracing stiffness and strength, adapted from AISC (2002).

The above lateral bracing stiffness may be converted to an equivalent beam torsional bracing stiffness by multiplying by h_o^2:

$\beta_{T(act)} = 9.47\ (24.375)^2 = 5630$ in-kips/rad

This value is 58 % of the above upper-bound, coarse estimate of the provided torsional bracing stiffness. It can be argued that both estimates are relatively coarse values, and that some variation in the AISC committee value can be expected depending on any changes in the above list items. However, the AISC committee value is considered a reasonable lower-bound estimate of the provided stiffness for this problem.

It should be noted that the AISC committee example uses an estimate of the vertical height of the flange diagonal bracing system of 26 inches, which is equal to *h* plus the 2 inch distance from the inside of the purlin bottom flange to the centerline of the attachment of the diagonal brace to the purlin as shown in Fig. 4.1. It can be argued that a vertical distance equal to 24.56 inches + 9 inches /2 (one-half the purlin depth) = 29.06 inches is a more appropriate estimate of the vertical height of the flange diagonal bracing system, since the diagonal brace force has to be transferred to the mid-depth of the purlin to avoid the need to calculate an additional moment on the purlin due to the eccentricity of its horizontal component. However, in this case, we should use a horizontal length of the bracing system of approximately 32.2 inches rather than 30 inches as shown in Figs. 4.1 and 4.3. The distance between the flange centroids on the member being braced (h_o) is used as a reasonable constant approximation in all the conversions between the torsional and equivalent lateral brace properties in this report. However, the stiffness estimate from the AISC committee example is summarized in Fig. 4.3 without any modifications.

One can observe that the above stiffness estimate is more than enough to satisfy any of the estimated stiffness requirements from the prior sections.

Furthermore, the lateral bracing design strength is calculated in the AISC committee example as

$$\phi_c R_n = (2.62 \text{ kips}) \cos (40.9^o) = 1.98 \text{ kips}$$

as shown in Fig 4.3, based on the assumption that the bracing diagonal governs the provided strength (note that the above value is the design lateral load capacity given the column axial design strength of 2.62 kips for the diagonal brace). This can be converted to an equivalent torsional bracing strength by multiplying by h_o:

$$\phi M_{n(br)} = 1.98 \text{ x } 24.375 = 48.2 \text{ in-kips}$$

This strength is sufficient to satisfy the all of the prior estimated strength requirements, with the exception that the requirement to develop the virtual simulation strength for the rigid bracing case is larger than the above value.

Table 4.2 summarizes the above estimates of the provided stiffness and strength in terms of the equivalent lateral bracing properties, and compares these to the various estimated requirements from the previous sections. Also, the required lateral bracing stiffnesses and strengths obtained by implementing the AISC (2002) refined calculations at the beam ultimate strength load levels are shown in the table. Similar to the comparisons in Section 4.4.2.1, the equivalent lateral bracing stiffnesses are very close to one another for all the loadings. However, the AISC (2002) required lateral bracing strengths are significantly smaller than those obtained using the torsional bracing rules.

Table 4.2 Summary of provided versus required brace strengths and stiffnesses, expressed in terms of the equivalent lateral brace properties.

Criterion or condition		Stiffness β_{br} (kips/in)	Strength P_{br} (kips, %)[a]
Provided		9.47	1.84 kips
Required to brace the beam for the loading from the LRFD wind uplift load combination, M_{max} = 83 ft-kips	AISC	1.85	0.33, 0.82
	Simplified	1.36	0.82, 2.0
	AISC (2002) base nodal	2.67	0.82, 2.0
	AISC (2002) refined nodal	1.78	0.41, 1.0
Required to brace the beam for the "best estimate" of the capacity from AISC Ch. F using C_b = 2.04 and K = 0.83 (1.60 times the LRFD uplift loading), M_{max} = 133 ft-kips	AISC	4.75	0.85, 1.31
	Simplified	2.18	1.31, 2.0
	AISC (2002) refined nodal	4.83	0.65, 1.0
Required to brace the beam for the capacity obtained from virtual simulation using the AISC-based torsional brace stiffnesses for full bracing (1.68 times the LRFD uplift loading), M_{max} = 139 ft-kips	AISC	5.23	0.94, 1.37
	Simplified	2.29	1.37, 2.0
	AISC (2002) refined nodal	5.07	0.69, 1.0
Required to brace the beam for the capacity obtained from virtual simulation using rigid lateral bracing at the top and bottom flanges (2.08 times the LRFD uplift loading), M_{max} = 173 ft-kips	AISC	8.02	1.44, 1.70
	Simplified	2.84	1.68, 2.0
	AISC (2002) refined nodal	6.28	0.85, 1.0

(a) Percent values are M_{br} /M_{max} written as a percentage.

4.7 Critical Geometric Imperfections for Virtual Simulation Analysis

The critical geometric imperfections for this problem are determined below using the influence line approach discussed in Section 3.3.2. These imperfections are applied to the girder bottom flange in a pre-analysis. The corresponding influence line for the left-most intermediate brace is shown in Figure 4.4 and the corresponding out-of-alignment and out-of-straightness applied to the girder bottom flange are shown in Figure 4.5. In addition to the out-of-alignment of the brace points of $L_b/500$, an out-of-straightness of $L_b/1000$ is applied to the girder bottom flange at the middle of the larger unbraced lengths to obtain the final imperfect shape. The dotted line in the figure is a representation of the lateral deflection of the bottom flange under the imposed lateral displacements at the brace points and at the middle of the longer unbraced lengths.

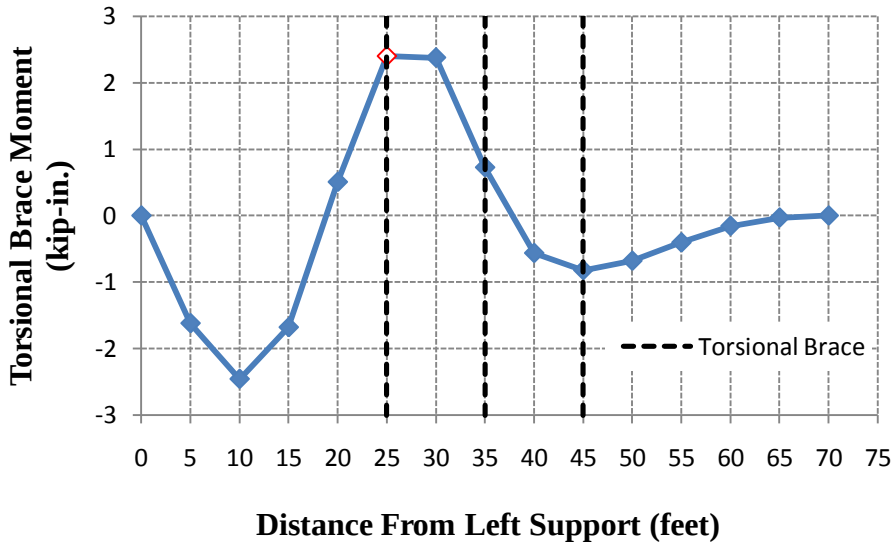

Fig. 4.4. Influence line for the left torsional brace, roof girder example.

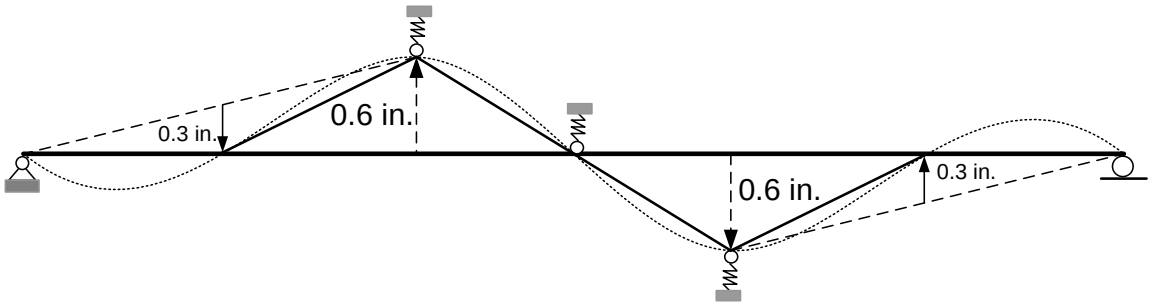

Fig. 4.5. Out-of-alignment and out-of-straightness applied to the girder bottom flange.

No local buckling mode imperfections were applied to the girder in this example. Lateral torsional buckling dominates the buckling modes from the fundamental mode, which has an eigenvalue of 1.8, to the 50th mode, which has an eigenvalue of 3.10.

The out-of-alignment in the two middle unbraced lengths is actually greater than L_b/500 given the above imperfections. Strictly speaking, the out-of-alignment should be limited to L_b/500 in all the unbraced lengths. However, if this limit were implemented in this problem, the end brace points also should be moved laterally so that the flange out-of-alignment is maintained at L_b/500 in the outside unbraced lengths. Also, an explicit out-of-straightness of L_b/1000 should be applied to the shorter middle unbraced lengths in the directions they are bent in Fig. 4.5, to maximize the demands on the targeted brace. Therefore, it is expected that the resulting critical brace force demands would be comparable to those obtained with the imperfection shown in Fig. 4.5

No out-of-alignment is applied to the top flange in this study. Similar to the situation for the 90 ft clear span frame discussed in Section 3.3, the resulting cross-section twists would tend to be excessive if imperfections were also applied to the top flange. Given the bottom flange out-of-alignment values shown in Fig. 4.5, the initial twist rotation of the girder cross-section is 1/40 radians at the outside intermediate brace points.

The influence line shown in Fig. 4.4 is generated by applying a unit load in the out-of-plane direction on the bottom flange at each purlin location in a second-order elastic analysis of the beam subjected to the applied design uplift loads. The AISC-based torsional brace stiffnesses of 1100 in-kips/rad are used in this development. Strictly speaking, the influence line varies with different values of the brace stiffnesses. However, typically the sensitivity of the influence line to the brace stiffness values is relatively small when the bracing stiffnesses are in the vicinity of the full-bracing requirements.

The torsional brace locations are marked on the influence line plot. The influence line corresponds to the brace force demand at the left torsional brace. From symmetry, the right torsional brace has the same influence line. Figure 4.5 shows the out-of-alignment and out-of-straightness that maximize the brace force at the left torsional brace.

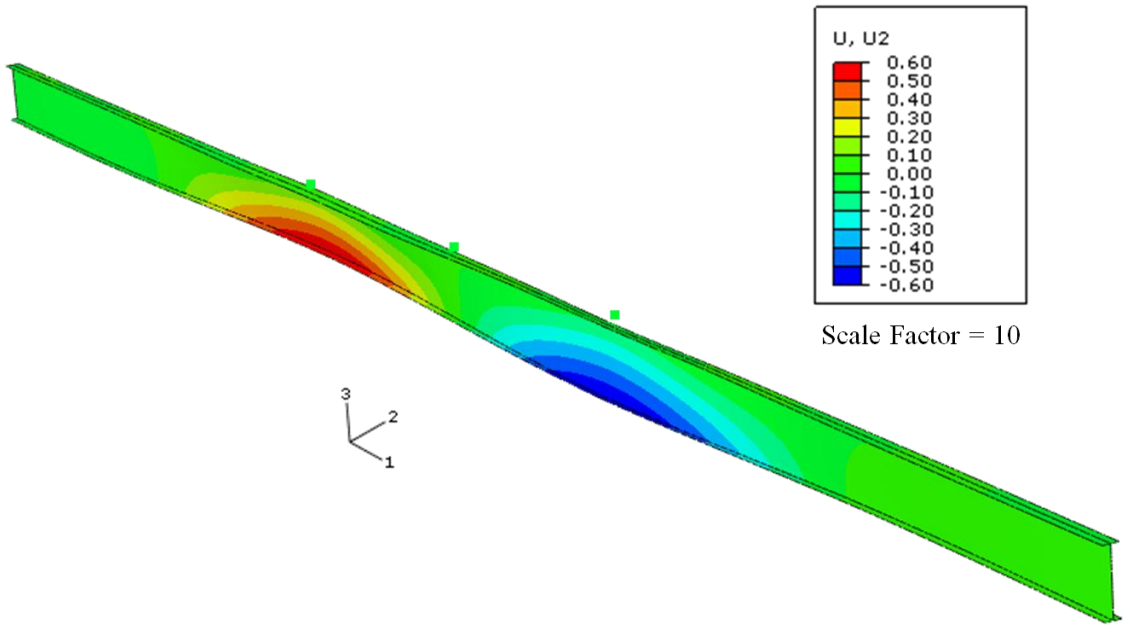

Fig. 4.6. Imperfect geometry of the girder with contours of the corresponding out-of-plane displacements (units = inches).

The corresponding out-of-plane bending displacements throughout the member, determined by imposing the above displacements at the targeted locations in a pre-

analysis, are applied as initial geometric imperfections in the virtual test simulation. Figure 4.6 shows the resulting deformed shape and out-of-plane displacement contours.

4.8 Virtual Simulation Results Using the AISC-Based Torsional Brace Stiffness Required to Brace for the LRFD Wind Uplift Loading

Figure 4.7 shows the load-vertical displacement response for the roof girder using intermediate torsional braces with a stiffness of β_T = 1100 in-kips/rad, the required AISC-based torsional stiffness to brace the beam for the LRFD wind uplift loading, calculated in Section 4.4.2 (equivalent lateral brace stiffness β_{br} = 1.85 kips/inch). The horizontal axis shows the vertical deflection at the midspan and the vertical axis shows the ratio of the applied load to the load from the LRFD wind load combination (i.e., the load producing the moment diagrams in Figs. 4.1 and 4.2). The system reaches its load capacity of 1.68 times the design load at a vertical deflection of 5.43 inches. After this point, the system becomes unstable and the load drops off.

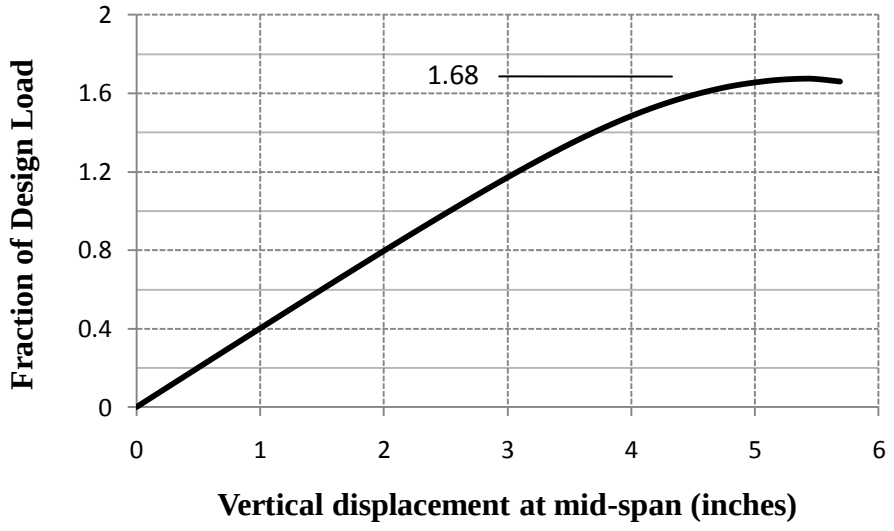

Fig. 4.7. Load-deflection response of the roof girder with β_T = 1100 in-kips/rad (β_{br} = 1.85 kips/inch) subjected to the LRFD wind uplift load combination.

The above limit load corresponds to a maximum moment of 80 ft-kips x 1.68 = 134 ft-kips at the beam ends. This moment can be compared to the refined estimate of the fully-braced capacity of M_n is 128 ft-kips determined previously using C_b = 2.04 and K = 0.83 (based on Winter's definition of full bracing corresponding to effective immoveable supports). Therefore, the beam is able to reach 134.5/128 = 1.05 of the best estimate of its fully-braced load capacity with $K < 1$, even though the torsional bracing is sized only for 1/1.68 = 0.60 of the corresponding internal moments.

Figure 4.8 shows the variation of the brace forces at the three torsional braces versus the applied load level. The vertical axis shows the fraction of the design load applied to the girder and the horizontal axis shows the torsional brace strength demand as a percentage of the moment at the midspan of the beam at the above AISC-based beam moment capacity, M_n^* = (83)(128)/(80) = 133 ft-kips. This value is used to normalize the torsional brace moments in a number of the subsequent plots.

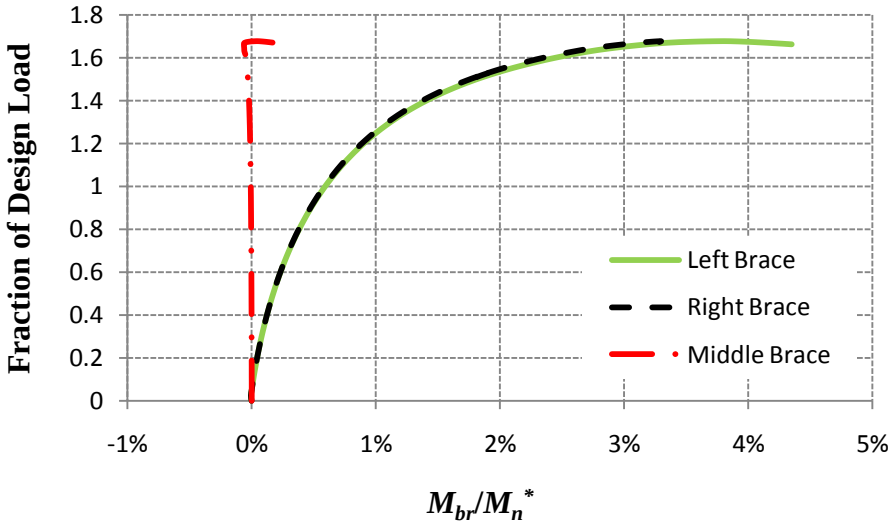

Fig. 4.8. Brace force demand on the torsional braces of the roof girder with β_T = 1100 in-kips/rad (β_{br} = 1.85 kips/inch) subjected to the LRFD wind uplift load combination (M_n^* = moment at mid-span based on refined AISC estimate of the beam flexural capacity).

From the above figure, it can be seen that the maximum strength demand on the braces is approximately 0.6 % of M_n^* at 1.0 of the LRFD wind uplift load combination. This corresponds to 1.0 % of the mid-span moment of 83 ft-kips at this load level. Therefore, the AISC torsional bracing strength requirement (1.06 %, see Table 4.2) is an excellent estimate of the virtual simulation requirements at the design load in this problem. Conversely, the simplified estimate of 2.0 % is somewhat conservative, but it should be noted that this estimate is based on providing a torsional brace stiffness of only 809 inch-kips/rad (or an equivalent lateral brace stiffness β_{br} = 1.36 kips/inch, see Table 4.2).

As the maximum load capacity of the beam is approached, the brace moment percentage increases substantially in Fig. 4.8. This should not be a surprise, since Fig. 4.8 is based on β_{br} = 1.85 kips/inch, but both the AISC and the simplified estimates indicate that larger stiffness values of β_{br} = 5.14 kips/inch (AISC) or 2.29 kips/inch (simplified) should be used to develop this load capacity (again, see Table 4.2). However, it may be a bit of a surprise to some readers that the bracing satisfying the AISC torsional bracing stiffness requirement for the LRFD wind uplift load combination is actually able to develop 1.05 times the best estimate of the beam capacity from AISC Chapter F using accurate C_b and LTB effective unbraced length calculations (1.05 = 1.68/1.60). One caveat to this statement is that the most heavily loaded braces would need to withstand a 3.8 % of M_n^* (3.6 % of the maximum mid-span moment at the actual virtual simulation limit load).

It can be observed from Fig. 4.8 that the demand on the middle torsional brace is significantly less than that for the outer two braces, while the demands for the outer two braces are essentially the same. This behavior can be attributed to the specific initial imperfection applied to the system in this virtual test simulation, which places little

demands on the midspan brace. The bottom flange imperfection in this analysis (see Fig. 4.5) maximizes the brace force in the outer torsional brace on the left-hand side to obtain the maximum strength demand for all the braces.

Figure 4.9 illustrates the failure mode of the girder by showing contours of the lateral displacements on the deformed geometry at the peak load level. It can be observed that the lateral displacement in the vicinity of the critical brace location is quite large (up to 6.07 inches at the bottom flange in this region).

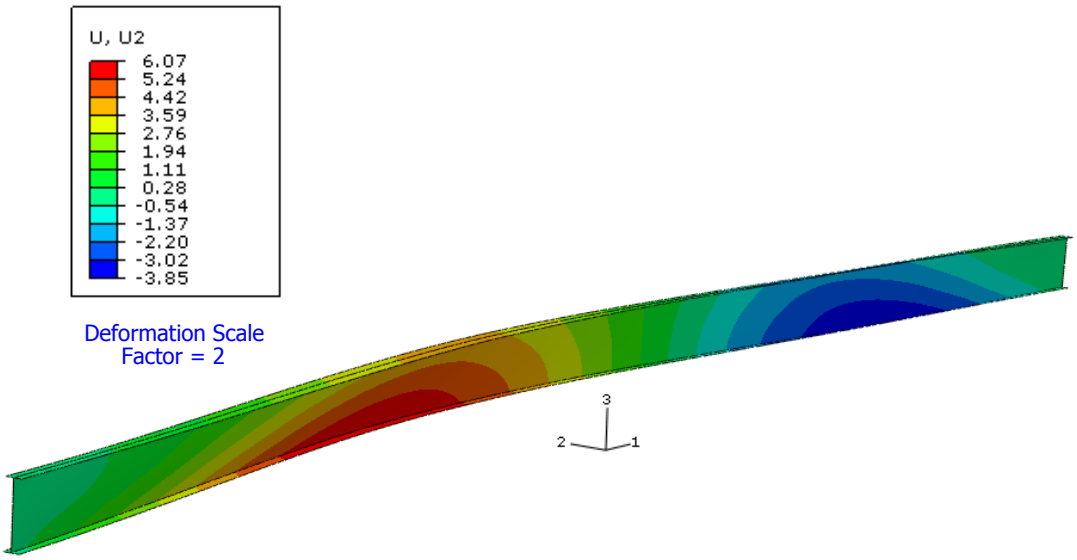

Fig. 4.9. Deformed shape of the roof girder at the maximum applied load with β_T = 1100 in-kips/rad, β_{br} = 1.85 kips/inch (units=inches).

Figure 4.10 gives a better perspective of the deflections in this region by plotting the lateral displacement of the top and bottom flanges at the critical brace location. Although the lateral deflection at the bottom flange at the critical brace location is 5.13 inches at the limit load, the corresponding top flange lateral deflection is 3.84 inches. Therefore, the majority of the movement illustrated by the contours in Fig. 4.9 is due to lateral translation of the entire cross-section at the two outside brace locations. Nevertheless, the

overall twist rotation at the critical torsional brace is reasonably large at 0.053 radians, the additional out-of-alignment of the bottom flange in the adjacent 25 ft unbraced length is 1/58, and the additional out-of-alignment of the adjacent 10 ft unbraced length is 1/25.

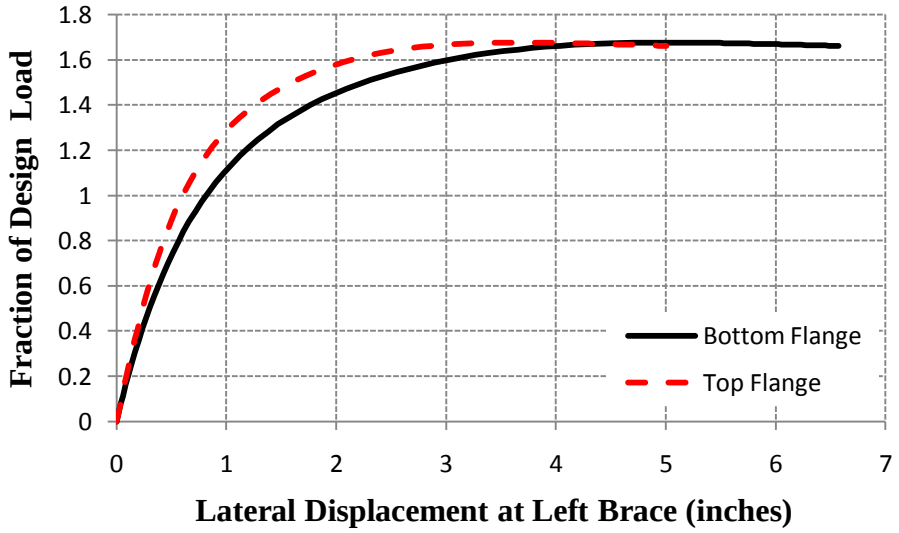

Fig. 4.10. Lateral displacement at the left brace for AISC estimate of torsional brace stiffness based on the applied load (β_T = 1100 in-kips/rad)

It is interesting to check whether the use of a larger torsional brace stiffness will substantially reduce the out-of-plane movement at the critical brace location in this problem. Figure 4.11 shows the lateral displacement at the left brace for a torsional brace stiffness ten times greater than the AISC-based torsional bracing stiffness requirement. One can observe that the twist rotation of the cross-section is essentially zero in this case, but prior to and at the limit load, there is still substantial lateral movement of the beam cross-section even with this very large torsional bracing stiffness.

The above presentation focuses on the stability behavior for torsional bracing sized to brace a beam for a loading substantially smaller than its maximum capacity assuming full bracing. Obviously, it is useful to also evaluate the behavior for the different brace stiffnesses intended to provide full bracing. The results from the virtual simulation analysis of

these systems are presented in the next section in the context of determining the knuckle curve for the torsional brace stiffnesses for the beam of Fig. 4.1. The reader is referred to the discussion at the end of Section 1.3 for an introduction to these types of curves.

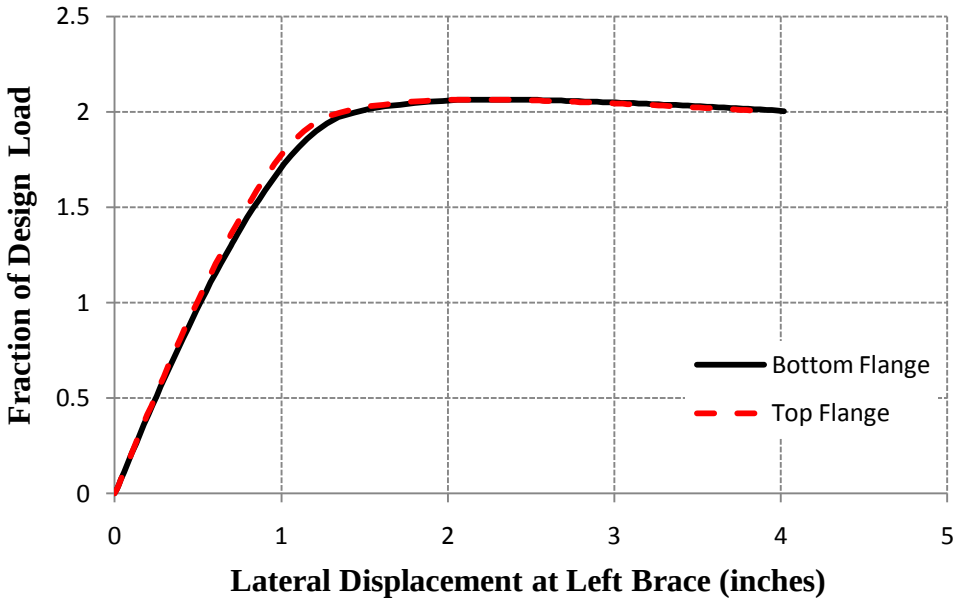

Fig. 4.11. Lateral displacement at the left brace when a torsional brace stiffness equal to ten times the AISC-based torsional stiffness to brace for the LRFD uplift load is employed.

4.9 Effect of Varying the Brace Stiffness

Figure 4.12 shows the knuckle curve for the roof girder example. The vertical axis shows the normalized maximum moment in the roof girder, M_{max}/M_n^*, where M_{max} is the midspan moment at the girder limit load and M_n^* = 133 ft-kips is the moment at the midspan of the girder when the outside unbraced lengths reach their maximum flexural resistance based on the refined application of Ch. F of the AISC Specification with C_b = 2.04 and K = 0.83. The value of M_{max}/M_n^* at the load level corresponding to the LRFD wind uplift load combination, 80/128 = 0.625, is highlighted by the horizontal blue line in the figure.

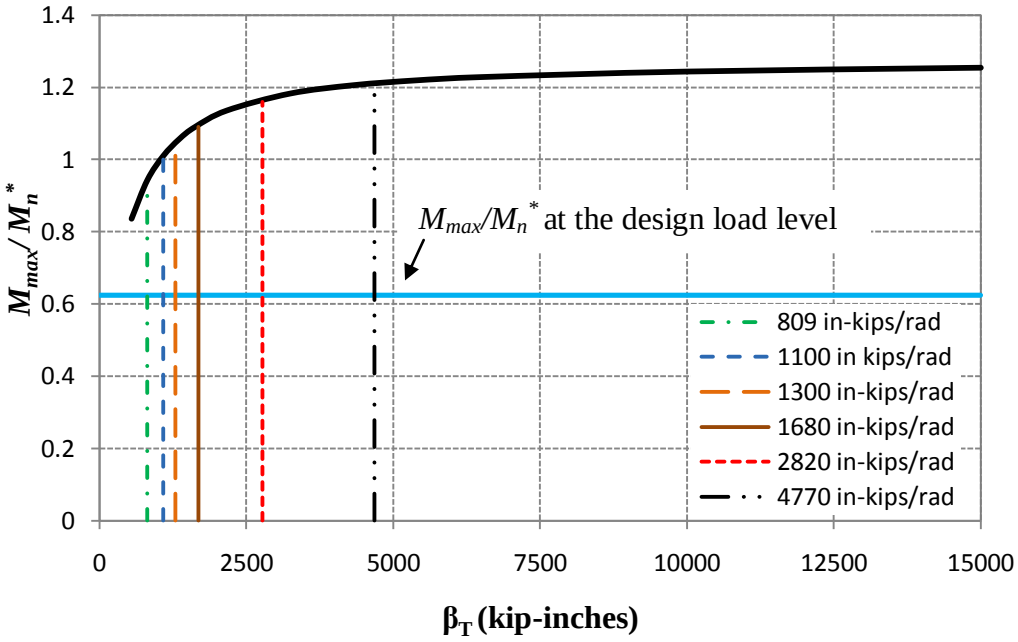

Fig. 4.12 Member strength knuckle curve, roof girder example (M_n^* = moment at mid-span based on refined AISC estimate of the beam flexural capacity).

The use of M_{max}/M_n^* as the ordinate in Fig. 4.12 is informative as an alternative to plotting the basic ratio of the system strength to the LRFD uplift wind load level, since the ratio M_{max}/M_n^* allows the reader to assess the impact of the different bracing stiffness values relative to the refined estimate of the beam LTB capacity based on AISC Ch. F using accurate C_b and K values.

The different bracing stiffness values calculated previously are highlighted in the figure. These stiffnesses are, from smallest to largest:

i. The required stiffness β_T = 809 in-kips/rad (β_{br} = 1.36 kips/inch), determined from the *simplified* equations based on the LRFD wind uplift loading,

ii. The *AISC* estimate of the required stiffness β_T = 1100 in-kips/rad (β_{br} = 1.85 kips/inch) based on the LRFD wind uplift loading,

iii. The required stiffness β_T = 1300 in-kips/rad (β_{br} = 2.18 kips/inch) calculated using the *simplified* equations at the beam strength condition corresponding to the AISC Specification Ch. F beam strength with C_b = 2.04 and K = 0.83,

iv. The required stiffness from the *simplified* equations, β_T = 1680 in-kips/rad (β_{br} = 2.84 kips/inch) based on the virtual simulation limit load of the beam for the case of rigid lateral bracing,

v. The *AISC* estimate of the required stiffness β_T = 2820 in-kips/rad (β_{br} = 4.75) based on the load level corresponding to the AISC Specification Ch. F beam strength with C_b = 2.04 and K = 0.83, and

vi. The *AISC* estimate of the required stiffness β_T = 4770 in-kips/rad (β_{br} = 8.02 kips/inch) based on the virtual simulation limit load of the beam for the case of rigid lateral bracing.

One can observe that the smallest brace stiffness (β_T = 809 inch-kips/rad) is not successful in developing the refined AISC Ch. F beam strength, whereas the smallest AISC estimate, β_T = 1100 inch-kips/rad, studied in detail in the previous section, is able to develop the refined AISC Ch. F resistance. *Nevertheless, neither of these stiffness values are intended to achieve* $M_{max}/M_n^* \geq 1.0$. Both of these bracing stiffnesses were intended to ensure $M_{max}/M_n^* \geq 0.625$. Therefore, both of these limits are successful at achieving their objectives. However, it is clear from the knuckle curve that the beam is only partially braced with these stiffness values.

The simplified and AISC estimates of the required bracing stiffnesses needed to reach the refined AISC Ch. F strength, β_T = 1300 and 2820 in-kips/rad, are also successful at

achieving their objectives. However the simplified estimate gives a stiffness much closer to the "true" required value from the virtual simulation.

Lastly, if the objective is to develop say 90 % of the beam resistance obtained for the case of rigid lateral bracing, then M_{max}/M_n^* must be greater than or equal to 2.08 x 0.625 = 1.17. The simplified estimate of β_T = 1680 falls short of this objective, since it develops an M_{max}/M_n^* of only 1.09, or only 84 % of the virtual simulation strength of the rigidly-braced beam. However, the AISC-based estimate of β_T = 4770 develops an M_{max}/M_n^* of 1.22, which is 94 % of the maximum virtual simulation strength.

It should be noted that in the vicinity of the simplified estimate of the stiffness needed to develop $M_{max}/M_n^* = 1.0$, β_T = 1300 inch-kips/rad, the system strength becomes significantly more sensitive to changes in the brace stiffness. This is indicative of the fact that the beam is no longer fully-braced. However, the strength becomes relatively insensitive to brace stiffness, for stiffness values somewhat larger than β_T = 1300 inch-kips/rad.

Figure 4.13 shows a particularly interesting result related to the knuckle curve behavior in Fig. 4.12. This figure shows how the brace forces at the maximum strength limit vary as a fraction of M_n^* with changing torsional brace stiffness. It should be noted that M_n^* corresponds to the actual maximum beam moment at the limit load only for β_T slightly less than 1100 in-kips/rad (see Fig. 4.12). However, it is easier to understand the actual variation in the brace moments when they are expressed as a fraction of a constant beam moment value, rather than plotting them as a function of the increasing maximum moment capacity of the beam with increasing brace stiffness.

Interestingly, the maximum brace force occurs for a brace stiffness in the vicinity of β_T = 1100 in-kips/rad. For brace stiffnesses smaller than this value, the brace moment

drops off rapidly with decreasing stiffness, whereas for brace stiffnesses larger than this value, the brace moment decreases more gradually. This type of behavior may be useful in defining an appropriate "knuckle" value for the brace stiffness, although the corresponding reduction in the system strength relative to the rigidly-braced virtual simulation value is slightly more than 10 % at this stiffness value (see Fig. 4.12).

Also, from Fig. 4.13, it can be seen that at high stiffness values, the brace force tends to decrease, but only very slightly. One can observe that at the largest value of β_T considered in Figs. 4.12 and 4.13, $M_{br}/M_n^* = 3.0$ % and $M_{max}/M_n^* = 1.25$, so that the brace force as a percentage of the maximum moment is $M_{br}/M_{max} = 2.4$ %. The brace forces gradually increase toward the maximum percentage value $M_{br}/M_n^* \cong M_{br}/M_{max} \cong$ 3.8 % at $\beta_T = 1100$ in-kips/rad.

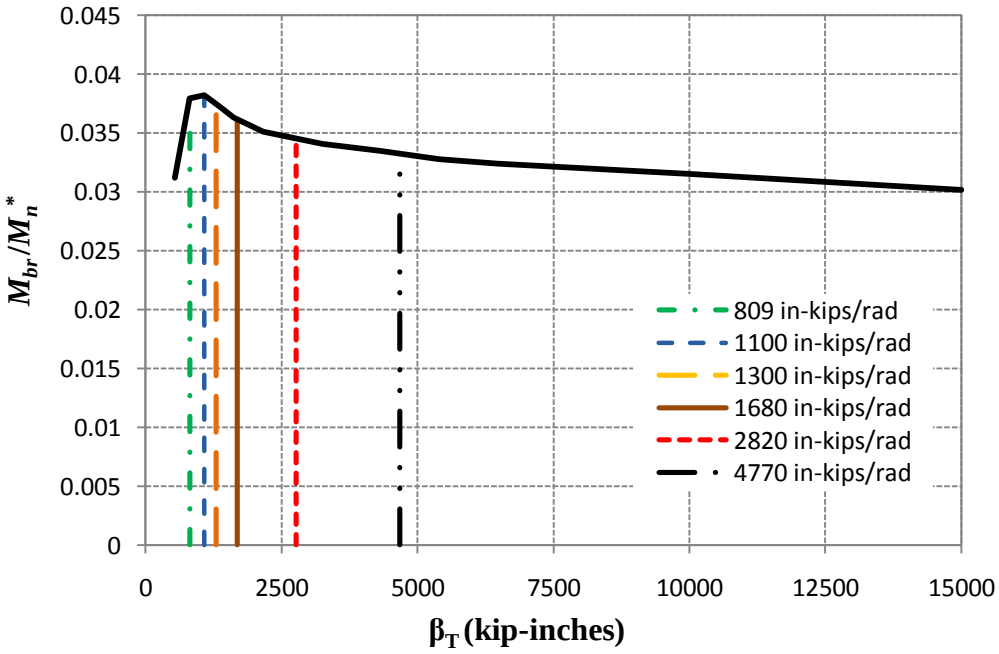

Fig. 4.13 Brace force demand at the beam maximum strength limit versus brace stiffness, roof girder example (M_n^* = moment at mid-span based on refined AISC estimate of the beam flexural capacity).

It should be noted that the percentage brace force is M_{br}/M_n^* = 3.3 %, or M_{br}/M_{max} = 2.7 % corresponding to the AISC-based torsional bracing requirement to develop the virtual simulation capacity of the rigidly-braced beam (β_T = 4770 in-kips/rad, or β_{br} = 8.02 kips/inch). This value can be compared to the AISC-based strength requirement of 2.2 % at the rigidly-braced virtual simulation limit load level of M_{max}/M_n^* = 0.625 x 2.08 = 1.30, calculated in Section 4.4.4. It can also be compared to the more basic value of 2.0 % used for all the cases in the simplified estimates.

One can raise the following important question when evaluating the above results: What are the consequences of underestimating the "true" brace forces at the maximum load limit in both the AISC-based and the simplified strength requirements? Figure 4.14 provides some insight toward answering this question. This figure shows the brace moment demand M_{br}/M_n^* at the left torsional brace, for the beam restrained by torsional braces with β_T = 4770 in-kips/rad, versus the fraction of the LRFD wind uplift design load. The M_{br}/M_{max} = 2.0 % brace moment level is highlighted in the plot. One can observe that by sizing the torsional braces for a brace moment capacity of 2.0 % of the beam moment at the limit load in this problem, the beam would be able to develop a design load fraction of 1.98 before reaching the strength of the most critically loaded brace. This corresponds to 100 x 1.98 /2.01 = 99 % of the system capacity achieved without considering any strength condition being reached in the braces. Therefore, if one adopts a philosophy of allowing the strength to be governed by the braces, as long as the strength condition is reached within a close percentage of the member or system strength that would otherwise be attained, the 2.0 % simplified strength limit may be considered acceptable.

It appears that the use of the AISC-based bracing strength requirements could potentially lead to a significant reduction in the overall system strength for this problem. The torsional bracing equations give a strength requirement of only 1.67 % while the application of the refined nodal equations as in AISC (2002) gives a strength requirement of only 1.0%.

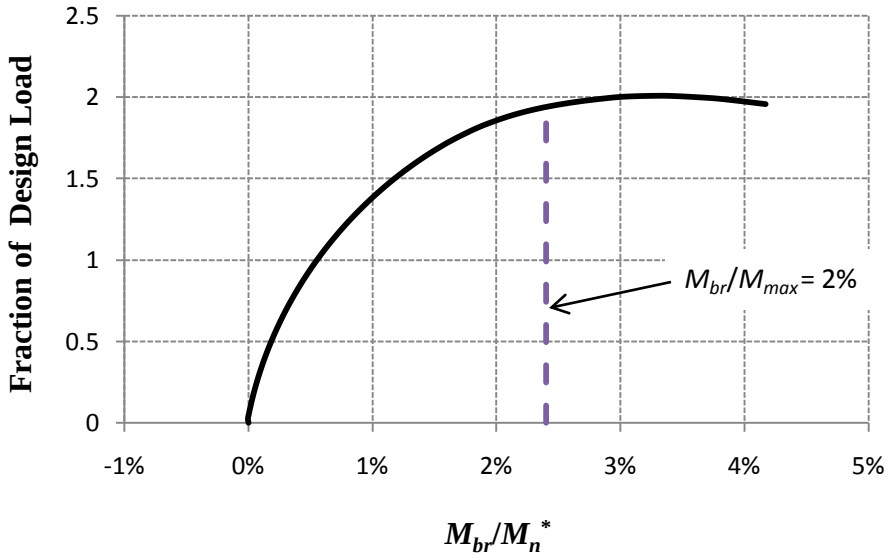

Fig. 4.14. Brace force demand on the left torsional brace of the roof girder for a brace stiffness satisfying the AISC requirement of 4770 in-kips/rad (M_n^* = moment at mid-span based on refined AISC estimate of the beam flexural capacity).

Table 4.3 provides an additional illustration of this behavior by showing the equivalent lateral bracing force values at 90, 95 and 100 % of the maximum moment capacity for three different brace stiffness values. These results indicate that the behavior is similar to the above using the smaller stiffness values of β_T = 1100 in-kips/rad and 1300 in-kips/rad.

It should be emphasized that the above philosophy generally would not be considered appropriate in applications where ductility is a concern, for example for seismic applications. However, this approach is considered to be sufficient for ordinary static

strength applications. It should be noted that if a philosophy were adopted that the strength of the braces should not govern the strength of the structure, much larger force percentages should be used in general for the strength design of the braces than required in the 2010 AISC Specification.

Table 4.3 Summary of strength demand at the critical torsional brace from virtual test simulation using various brace stiffness values.

Criterion or Condition	Strength Demand at 90% of Limit Load P_{br} (kips, %)	Strength Demand at 95% of Limit Load P_{br} (kips, %)	Strength Demand at Limit Load P_{br} (kips, %)
Required to brace the beam for the loading from the LRFD wind uplift load combination using a torsional stiffness of 1100 in-kips/rad. (1.85 kips/inch)	1.23, 1.9	1.60, 2.4	2.50, 3.8
Required to brace the beam for the "best estimate" of the capacity from AISC Ch. F using a simplified estimate based torsional stiffness of 1300 in-kips/rad. (2.18 kips/inch)	1.24, 1.9	1.58, 2.4	2.44, 3.7
Required to brace the beam for the capacity obtained from virtual simulation using the AISC-based torsional brace stiffness of 4770 in-kips/rad. (8.02 kips/inch)	1.21, 1.9	1.44, 2.2	2.20, 3.4

Based on the above discussions, it can be concluded that, for this problem, the simplified estimates provide the best characterization of the torsional brace stiffness and strength requirements both for the partial bracing case, where the bracing is sized to support the beam for a load level substantially smaller than its fully-braced capacity, as well as for the full-bracing case, where the bracing is sized to support the beam for the

load level corresponding to a refined estimate of its capacity from the AISC Ch. F with accurate C_b and K values. For the partial bracing case, the simplified estimate of the stiffness is 25% smaller, and for the full-bracing case, the simplified estimate of the stiffness is 53 % smaller.

For the partially-braced case, β_T = 809 in-kips/rad (or β_{br} = 1.36 kips/inch) and P_{br} = 0.82 kips (or M_{br}/M_{max} = 2.0 %) both work well in that the virtual simulation indicates an actual capacity of M_{max}/M_n^* = 0.94 (design load fraction = 0.94 / 0.625 = 1.50) for this bracing stiffness, with a brace force of M_{br}/M_n^* = 3.6 % (or M_{br}/M_{max} = 3.8 % and P_{br} = 5.36 kips) at this maximum strength level, which is 50 % larger than the required strength. The brace force at the LRFD wind uplift load level is or M_{br}/M_{max} = 0.63 % and P_{br} = 0.4 kips.

For the fully-braced case, β_T = 1300 in-kips/rad (or β_{br} = 2.18 kips/inch) and P_{br} = 1.37 kips (or M_{br}/M_{max} = 2.0 %) both work well in that the virtual simulation indicates an actual capacity of M_{max}/M_n^* = 1.05 (design load fraction = 1.05 / 0.625 = 1.68) for this bracing stiffness, with a brace force of M_{br}/M_n^* = 3.8 % (or M_{br}/M_{max} = 3.6 % and P_{br} = 2.59 kips) at this maximum strength level.

However, if the goal is to develop a minimum of say 90 % of the rigidly-braced strength of the beam in this problem, a stiffness nearly equal to β_T = 4770 in-kips/rad (β_{br} = 8.02 kips/in) is required. As noted previously, M_{max}/M_n^* = 1.22 when β_T = 4770 in-kips/rad. This value is 94 % of the virtual simulation strength of the rigidly-braced member.

4.10 Summary

The following key observations can be gleaned from this roof girder example:

- Both the AISC and the simplified estimates give conservative estimates of the strength and stiffness demands at the LRFD design load level in this problem. This is largely because the beam is well below its strength limit at this stage.

  None of the finite bracing stiffnesses are able to completely develop the virtual simulation strength of the beam based on rigid bracing. However, the virtual simulation strength for rigid bracing is 1.30 times the best estimate from the AISC Chapter F flexural resistance equations, using C_b = 2.04 and an LTB effective length factor of K = 0.83. It can be argued that the bracing should not necessarily be required to develop a beam strength this large, unless a capacity design type of philosophy is to be applied to the bracing. This should not be necessary except possibly in high seismic design applications.

- The bracing sized based on the simplified bracing rules is able to develop 88 % of the beam rigid bracing strength. The beam strength is essentially at the "knuckle" value of the bracing stiffness in this design, where any reductions in the brace stiffness result in significant reductions in the beam strength. Therefore, it can be concluded that the simplified estimate is a good minimum stiffness value for this example problem. The AISC equations give a bracing stiffness requirement that is well into the plateau of the knuckle curve for the system strength versus the bracing stiffness.

- The brace force demand is 3.3% using the AISC estimate of required stiffness to develop the virtual simulation limit load of the beam for rigid lateral bracing (β_T =

4770 in-kips/rad). This stiffness develops 94% of the virtual simulation strength. The simplified stiffness estimate of β_T = 1680 in-kips/rad develops only 84% of the virtual simulation strength of the rigidly-braced beam.

- The bracing strength demand at the system limit load increases to a maximum of approximately 3.8 % as a percentage of the maximum beam moment near the knuckle value for the bracing stiffness in this problem. As the brace stiffness increases, the brace force demand at the system limit load decreases to close to 3 % for very high stiffness values. However, for all stiffnesses larger than the knuckle value, more than 90 % of the corresponding system limit load is developed when the maximum bracing force (or moment) reaches 2 % of the corresponding maximum beam moment.
- The simplified estimates provide the best characterization of the torsional brace stiffness requirements for both the partial and full bracing cases in this problem. For the partial bracing case the simplified estimate of the stiffness is 25% smaller than the corresponding AISC value, and for the full-bracing case, the simplified estimate is 53 % smaller.
- If the AISC stiffness requirements are satisfied, the AISC equation for the torsional brace strength requirement gives a good characterization of the demands from the virtual test simulation at the LRFD load combination level in this problem. However, the AISC strength requirement tends to underestimate the strength demands obtained in the virtual test simulation when the brace is proportioned at the AISC stiffness requirement.

- The simplified estimates of the strength requirements are a good characterization of the stiffnesses needed to develop strengths close to the limit load of the structural system for all torsional stiffnesses greater than or equal to the knuckle value. The simplified estimates are conservative at load levels smaller than the strength limit of the system.

It should be noted that this example is just one of the many possible design cases and hence the results cannot be generalized based on this example alone. Further studies are necessary in order to determine and generalize the bracing demands for such systems and to justify the applicability of various interpretations of the AISC or other simplified equations. This statement applies not only to this example, but also to all of the other examples considered in this research.

CHAPTER 5

SIDEWALL COLUMN EXAMPLE

5.1 Introduction

This chapter presents a specific variation on a sidewall column example from a recent AISC conference session (CSD 2009). The calculations evaluated in this problem are based on Allowable Strength Design (ASD). The torsional and relative bracing demands from the column are estimated using the AISC and simplified equations detailed in Chapter 2 and are compared to the results obtained from virtual test simulation. First, Section 5.2 gives a broad overview of the geometry and loading of the sidewall column and Section 5.3 discusses the specific bracing configuration. Sections 5.4 and 5.5 then present the AISC-based and simplified estimates of the bracing demands for several different system strengths. This is followed by Section 5.6, which discusses the calculation of the provided bracing stiffnesses and strengths.

The critical geometric imperfections applied for the virtual test simulation are discussed in Section 5.7. Section 5.8 then shows a first set of virtual test simulation results by focusing on a case where the required AISC-based torsional brace stiffness for the selected ASD loading is used along with a typical wall-panel relative bracing stiffness. Next, Section 5.9 evaluates the capacity of the column and the corresponding relative bracing demands if the member is constructed with no torsional bracing. Section 5.10 then discusses various virtual simulation test results that evaluate the effect of varying the relative brace stiffness on the member strength. Lastly, Section 5.11 summarizes the key attributes and observations from this example.

5.2 Geometry and Loading

Figure 5.1 shows an elevation view of a sidewall column in a metal building frame. The column section chosen for the design is a W24x84, which has a compact web and compact flanges and a yield strength of F_y = 50 ksi. The columns are spaced at 30 ft in the out-of-plane direction. The brace point spacing is 7.25 ft along the length of the column. The column is subjected predominantly to end moments causing reverse curvature bending, with the larger end moment causing compression on the outside flange at the bottom of the column. Two key but separate considerations exist for the bracing of the column for the selected ASD load combination: (1) compression on the inside flange at the top of the column, and (2) compression on the outside flange at the bottom of the column. The column bracing is designed as follows:

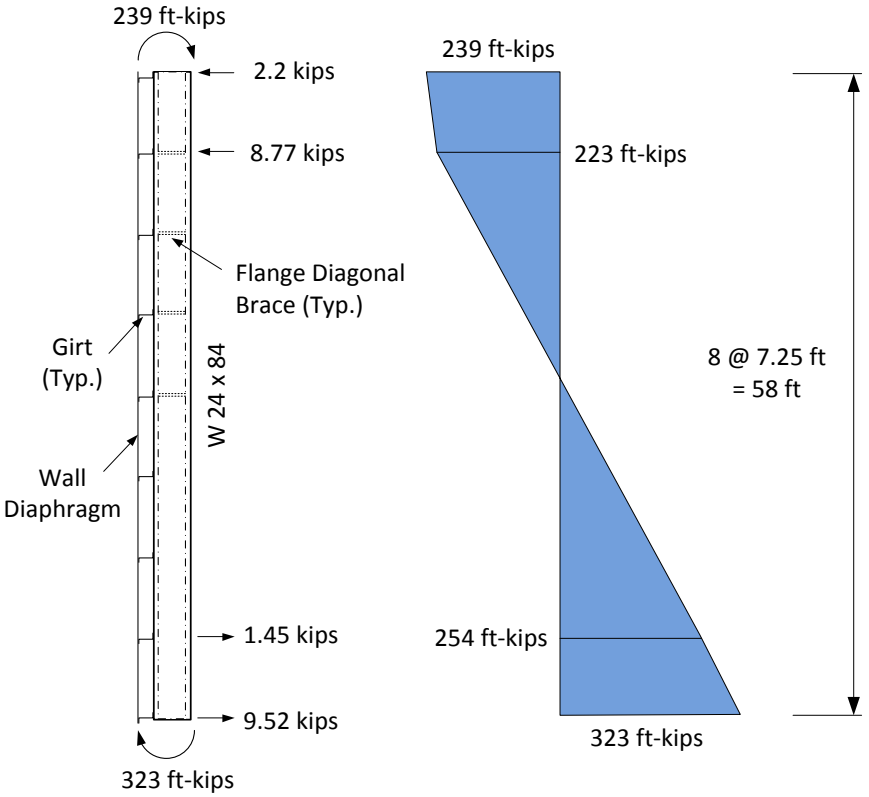

Fig. 5.1. Elevation view of sidewall column with specified ASD loads.

a) For the portion of the column near its top, where the interior flange is in flexural compression, the inside flange is restrained out-of-plane by diagonal braces framing from the girts. The girts and flange diagonals are designed as torsional braces at these locations.

b) For the portion of the column near its bottom, where the exterior flange is in flexural compression, the wall panels are designed to brace the exterior flange via relative (i.e. shear panel) bracing.

Sidewall columns typically function primarily as beams. Therefore, for purposes of simplicity, the demand on the bracing from axial load is neglected here. The column actually has an applied axial load of P_r = 26.6 kips (ASD) in the CSD example, but this loading is also neglected in the CSD calculations.

The geometry of the column and the brace layout have been modified slightly from the CSD (2009) solution to implement a constant brace spacing in this study, thus making the Appendix 6 equations more applicable. However, the Appendix 6 equations strictly do not apply to relative (shear panel) lateral bracing on one portion of a beam, combined with torsional bracing (or torsional bracing combined with relative lateral bracing) on another part of the beam.

5.3 Bracing Configuration

For this example, the sidewall column ends are modeled as flexurally and torsionally simply supported. Warping and lateral bending are assumed to be unrestrained at the member ends. Open-section thin-walled beam theory kinematics is enforced at the end points as explained in Section 3.1, and end moments and concentrated loads are applied to the column to obtain the moment diagram shown in Figure 5.1. The member is

assumed to be braced rigidly against twisting and lateral translation at its ends. The column exterior flange is braced at the girt locations by a continuous wall diaphragm along its entire length. However, diagonal braces to the inside flange are provided only in the top region of the column, where the inside flange is in flexural compression, with the exception of one additional set of diagonal braces just below the point of inflection in the column. Thus, there are a total of four sets of intermediate diagonal braces toward the top of the column. Two-sided L2x2x3/16 diagonal braces (A = 0.715 in^2, r_x = 0.612 inches) are assumed at each of these locations. The girts are 10Z3.25x105 sections with A = 1.88 in^2 and I_x =28.4 in^4.

At the diagonal brace locations, the flange diagonals are assumed to be attached directly to the interior flange of the column. Therefore, no additional flexibility due to cross-section web distortion is considered. In addition, it is assumed that there is negligible local deformation or slip at the connection points on either end of the flange diagonal braces. Also, it is assumed that a rigid offset of the girts is ideally pin connected to the exterior flange of the sidewall column, but the girts do not offer any direct torsional restraint at the exterior flange of the member. The torsional restraint of the column comes predominantly from the activation of the flexural stiffness of the girts via the truss action from the flange diagonals. The specific modeling of the torsional braces is discussed in Section 3.4.

The CSD example calculations use the beam relative bracing provisions of the AISC Specification Appendix 6 to evaluate the diaphragm strength for the condition where the exterior flange is in compression. The shear stiffness specified for the wall diaphragm in the CSD example (G' = 40 kips/inch) is relatively large. For the calculations

considered in this research, CS wall panels with 12 inch screw spacing at the base and eave are assumed. These panels have a stiffness of G' = 3.52 kips/inch and a strength of v_a = 61.2 lb/ft. These are also the properties assumed for the roof diaphragm in the 90 ft clear span frame example presented in Section 2.7.

The CSD example also uses the AISC beam relative (shear panel) bracing provisions to evaluate the demands on the bracing near the top of the column where the interior flange is in compression. However, the example calculates the stiffness provided to the inside flange at the bracing diagonals assuming the girts and the bracing diagonals act as discrete nodal braces. As such, the resistance and demand parts of the CSD calculations are not compatible. This type of error is expected to be common in practice, since the AISC Appendix 6 provisions do not clearly identify the relative bracing stiffness and strength demands as *shear demands*.

In actuality, since the girts are restrained by the wall panels against translation out of the plane of the column in this problem, the bracing system at the bracing diagonal locations is in fact a hybrid one, involving:

1. Relative (shear panel) bracing between the girt locations at the outside flange,
2. Discrete nodal torsional bracing of the column via the axial stiffness of the four sets of bracing diagonals and the flexural stiffness of the corresponding girts at the four locations of the bracing diagonals, and
3. Discrete nodal lateral bracing of the inside flange of the column at the four locations of the bracing diagonals. However, the lateral bracing of the inside flange at these locations is achieved by the torsional resistance from the bracing diagonals and girts, which work as torsional springs at the brace points, acting in

series with the wall panels, which work as shear springs between the brace locations.

The AISC Appendix 6 provisions strictly do not provide any guidance for designing bracing systems involving nodal and relative bracing components in parallel or in series, such as in the above case. In the next section, the AISC Appendix 6 calculations are applied in a manner similar to the approach taken with the clear span frame considered previously in Section 2.7. The flange diagonal braces and purlins are checked as torsional braces. This neglects the additional benefits of the lateral relative bracing of the outside flange. Nevertheless, it is interesting that in some cases, these torsional bracing calculations can give smaller requirements than the AISC nodal lateral bracing equations, which assume fully-fixed lateral restraint at the level of the girts.

As discussed previously in Chapter 4, any use of nodal lateral bracing equations for this type of problem is inherently based on the assumption that out-of-plane brace point movement at the inside flange occurs only due the flexure of the girts (or purlins) and the axial deformation of the flange diagonal braces. The girts or purlins are assumed to be rigidly restrained against out-of-plane movement at their centroidal axis. Conversely, the torsional bracing equations, applied in this Chapter as well as in Chapter 4, assume zero restraint of overall translation out-of-plane at the brace points. The torsional braces are assumed to only restrain twisting of the cross-section at the brace points.

5.4 AISC-Based Bracing Requirements

5.4.1 Refined Estimate of the AISC Flexural Resistance for Full Bracing

In the subsequent virtual simulation studies for this problem, the beam and its bracing system are loaded up to the system limit load. As such, it is useful to determine the

nominal load capacity of the member using the 2010 AISC Specification flexural resistance equations and assuming full bracing.

Given that we have equal brace spacing in this example, and given that the moments are largest at the bottom of the column, the maximum load capacity is governed by the unbraced length at the bottom of the column. The C_b factor for this unbraced length may be calculated most accurately as

$$C_b = 1.75 - 1.05\,(254/323) + 0.3\,(254/323)^2 = 1.11$$

using Eq. (C-F1-1) of the 2010 AISC Commentary (since the moment diagram is nearly linear). This equation provides a larger, more liberal, lower-bound C_b estimate than the Specification Eq. (F1-1) for linear or nearly linear moment diagrams. Given this value for C_b and assuming $K = 1$, the "plateau" LTB strength $M_n = M_p = 933$ ft-kips is developed at the base of our W24x84 column. Since the beam is already at its maximum potential flexural resistance, there is no need to perform a refined calculation to determine an LTB effective length factor. The beam nominal capacity is 933/323 = 2.89 times the specified ASD loads on the column. Considering that the ASD loads have to be increased by a factor of $\alpha = 1.6$ to reach the ASD ultimate strength load level, the beam nominal capacity is 2.89/1.6 = 1.81 times the ASD *ultimate strength* load level on the column. In summary, the column selected for this design has a high reserve capacity for the given bracing configuration and the selected loading.

As will be shown subsequently, the virtual simulation limit load for the column and its bracing system occurs at 3.00 times the required ASD moments shown in Fig. 5.1 (or 3.00/1.6 = 1.89 of the moments at the ASD ultimate strength load level). That is, the virtual simulation test capacity is 3.00/2.89 = 1.04 times the estimate of the fully-braced capacity

obtained from the AISC Specification equations. The most likely reason for this additional capacity in the virtual simulation model is strain hardening in the vicinity of the maximum moment at the bottom of the column, which is common for compact rolled I-section members with reasonably close brace spacing, subjected to moment gradient loading. In addition, the unbraced length adjacent to the critical bottom unbraced length provides some warping restraint to the critical segment.

It is interesting to check whether the W24x84 column would work without any of the four intermediate flange diagonal braces that have been placed near its top. This hypothetical design can be checked using the following C_b equation from Fig. 5.8 of Ziemian (2010), applicable for a member continuously braced on one flange and with no support on the other flange except at the member ends, loaded by end moments and transverse loads on the outside flange directed toward the section shear center:

$$C_b = 3.0 - \frac{2}{3}\left(\frac{M_1}{M_0}\right) - \frac{8}{3}\left(\frac{M_{mid}}{M_0 + M_1}\right) \tag{5.1}$$

where

M_0 = the negative end moment that gives the largest compression stress on the inside flange, input as a negative value in the above equation,

M_1 = the other end moment, input as a negative number if the moment is negative, i.e., causing compression on the inside flange. If M_1 is positive, this term is to be taken equal to zero in the last term of the C_b expression.

M_{mid} = the moment at the member mid-span, taken as positive for positive bending, i.e., tension on the inside flange

Given the moment diagram of Fig. 5.1, this equation gives

$$C_b = 3.0 - \frac{2}{3}\left(\frac{323}{-239}\right) - \frac{8}{3}\left(\frac{15.5}{-239}\right) = 4.07$$

This C_b factor is applied to the uniform bending resistance of the W24x84 for L_b = 58 ft to obtain a nominal resistance of M_n = 560 ft-kips (from Eq.F2-3, AISC 2010). Therefore, M_n/Ω = 560/1.67 = 335 ft-kips. According to Ziemian (2010), this moment is to be compared to the maximum moment causing compression on the inside flange, i.e., the 239 ft-kip moment at the top of the column. Therefore, the column has ample capacity to support the specified ASD loading without any torsional braces being placed near its top. In these calculations, the corresponding larger moment at the bottom of the column (560 x 323/239 = 757 ft-kips/1.6 = 473 ft-kips, assuming a linear moment diagram) is to be checked only against flange local buckling, if applicable, and general yielding. Since the W24x84 flanges are compact, only the general yielding check, $M_a \leq M_p/\Omega$ or 473 $\leq$ 933/1.67 = 559 ft-kips , applies. The subsequent virtual simulation of this problem, discussed in Section 5.9, shows that the column is able to develop a maximum moment at its top of 478 ft-kips (or 646 ft-kips at its bottom).

Although the W24x84 would actually work for the specified ASD loading without the diagonal braces near its top, the four sets of diagonal braces still are assumed to be framed into the inside flange near the top of the column as shown in Fig. 5.1 throughout most of this chapter. It is interesting to evaluate what sort of forces these non-critical (actually not even needed) braces are subjected to. Section 5.9 focuses on the virtual simulation behavior of the column for the case where no torsional braces are used.

As noted above, if the column in Fig. 5.1 is loaded to its ultimate capacity per the AISC flexural resistance checks, the internal moments are 1.81 times larger than the ultimate strength ASD loads (i.e., the ASD loads times α = 1.6). In this case, M_n/Ω = 335 ft-kips is

less than M_a = 1.81 x 239 ft-kips = 433 ft-kips. Therefore, the AISC design checks indicate that the column needs some type of flange diagonal bracing at its top to reach this load level. The response of the column to this hypothetical strength loading condition is also evaluated in the subsequent discussions.

Table 5.1 summarizes the different internal moments and the corresponding applied load levels considered in this example.

Table 5.1 Summary of applied moments and flexural resistances for the sidewall column.

Calculation Source	Moment at the bottom of the column (ft-kips)	Multiple of ASD Load Combination	Multiple of ASD Ultimate Strength Loading	Multiple of AISC Ch. F Nominal Beam Capacity[(a)]
ASD Load Combination	323	1.00	1/1.6 = 0.625	0.350
AISC Ch. F with C_b = 1.11 and K = 1.0 on bottom unbraced length	933	2.89	2.89/1.6 = 1.81	1.00
Virtual simulation using torsional braces satisfying AISC-based requirements to develop the ASD load combination, β_T = 1730 in-kips/rad. (β_{br} = 3.19 kips/inch) along with shear panels having G' = 3.52 kips/in	969	3.00	1.89	1.04
AISC Ch. F with C_b = 4.07 and L_b = 58 ft on inside flange (assuming no flange diagonal bracing)	757	1.67	1.08	0.81
Virtual simulation without any torsional bracing at the top of the column and using shear panels having G' = 3.52 kips/in	646	2.00	1.25	0.69

[(a)] Calculated assuming torsional bracing near the top of the column such that the nominal strength is governed by $M_n = M_p$ = 933 ft-kips at the bottom of the column (accounting for the moment gradient effects, i.e., C_b = 1.03).

5.4.2 AISC-Based Torsional Bracing Requirements at the Top of the Column

5.4.2.1 Required Stiffness to Develop the Specified ASD Moments in the Column

The AISC Appendix 6 required stiffness for the torsional braces is calculated as follows. As noted above, any assistance from the wall diaphragm relative bracing at the outside flange is neglected in checking the torsional braces at the top of the column. One single torsional stiffness requirement is calculated for all of these brace points, since the AISC equations are based on the assumption of equal stiffness bracing. The AISC torsional bracing stiffness requirement is given by Eq. (2-31):

$$\beta_T = 20\psi h_o^2 \left[\frac{M_r / C_b h_o}{P_{e.eff}} \right] \left(\frac{M_r / C_b h_o}{L_b} \right) \frac{(n_T + 1)}{n_T} C_{tT}$$

where

$\psi = \Omega = 3.0$

$h_o = 23.3$ inches

$M_r = 239$ ft-kips = 2870 in-kips (within the top unbraced segment)

$C_b = 1.75 - 1.05\,(223/239) + 0.3\,(223/239)^2 = 1.03$

$M_r / C_b h_o = 120$ kips

$E = 29{,}000$ ksi

$I_{eff} = I_y = 94.4$ in^4

$L_b = 7.25$ ft = 87 inches

$P_{e.eff} = 3570$ kips

$n_T = 7$

(There are no AISC rules for how one should handle cases in which a portion of the beam is restrained by torsional bracing and another portion is restrained by relative bracing. The ad hoc interpretation applied in this case, when considering the torsional braces, is to consider all of the brace points as torsional.)

$C_{tT} = 1.0$

(It is assumed that there are no significant load height effects from the transverse load at the brace point 7.25 ft below the top of the column. The transverse load at this position is a relatively minor contributor to the overall moment, with the greatest contributions being the two member end moments and the corresponding end shear reactions. Furthermore, it is likely that there is some tipping restraint due to the restoring torque caused by the eccentric bearing of the girt against the flange of the column when it starts to twist, as well as the rotational stiffness provided by the attachment of the purlin to the column.) By substituting the above values into Eq. (2-31), one obtains

$$\beta_T = 20(3.0)(23.3)^2\left[\frac{120}{3570}\right]\left[\frac{120}{87}\right]\frac{(7+1)}{7}(1.0) = 1730 \text{ in-kips/rad}$$

This torsional brace stiffness is used in the first of the virtual test simulations discussed below. Since the flange diagonals are connected directly to the inside flange of the column, $\beta_{sec} = \infty$ and $\beta_{Tb} = \beta_T$. By representing the above torsional stiffness requirement as an equivalent lateral bracing requirement at the interior flange of the column, we obtain

$\beta_{br} = \beta_T / h_o^2 = 1730 / 23.3^2 = 3.19$ kips/inch

This value is much smaller than the corresponding value for the required lateral brace stiffness of 5.7 kips/inch calculated in the CSD (2009) example, which incorrectly uses the 2010 AISC Appendix 6 relative bracing Eq. (A-6-6). If one were to correctly apply

the refined form of the Appendix 6 beam nodal lateral bracing Eq. A-6-8, given by Eq. (2-29) in this report, one obtains

$$\beta_{br} = \psi\left[2\left(4-\frac{2}{n}\right)\frac{(M_r/h_o)}{L_q}\right]C_{tN}C_d$$
$$= 2\left[2\left(4-\frac{2}{7}\right)\frac{(239/23.3)}{26.1}\right](1.0)C_d = 5.84C_d \text{ kips/inch}$$

equal to 5.84 kips/inch at all the flange diagonal braces except for the brace closest to the inflection point, where $C_d = 1 + (15.5/64.3)^2 = 1.06$, and thus $\beta_{br} = 5.84 \times 1.06 = 6.19$ kips/inch. The term L_q in this equation is calculated by setting the elastic LTB equation, Eq. (F2-4) in the 2005 AISC Specification, equal to $M_r \Omega_b/S_{xc}$ = (239 ft-kips x 12 in/ft) x 1.67 / 196 in^3 = 24.4 ksi.

Note that M_r = 239 ft-kips is used in the above equation instead of the moment at the bottom of the column of 323 ft-kips, and L_q is calculated based on the moment diagram in the top unbraced segment of the column. This is an ad hoc interpretation of the AISC beam lateral bracing stiffness equation based on the assumption that the moment at the bottom of the column is not relevant to the nodal bracing demand near the column's top. It is a legitimate question whether the required brace stiffness at the top of this column is influenced in any significant way by the moment at the bottom of the column. However, the AISC nodal bracing equations are based strictly on considering the maximum moment *throughout* the span, and as such, they provide a single constant bracing stiffness that should be satisfied at all the brace points.

It is interesting that the nodal bracing stiffness requirement for this column is 5.84/3.19 = 1.83 to 6.19/3.19 = 1.94 times larger than the equivalent lateral stiffness from the above torsional bracing requirement. That is, the torsional bracing equation gives a smaller stiffness requirement. However, the torsional bracing equation is based on the assumption of zero lateral bracing stiffness at the brace points whereas the lateral bracing equation assumes out-of-plane restraint at the centroid of the girts. Therefore, conceptually, one would expect the lateral bracing equation to give a smaller requirement. The torsional bracing equation gives a smaller requirement in this case because it relies more optimistically on the restraint of brace point displacements provided by the member.

5.4.2.2 Required Stiffness to Develop the Estimated AISC Load Capacity of the Column

Given the above calculations, the torsional brace stiffness necessary to develop the AISC ASD load capacity of the column, i.e., to fully brace the column for the maximum ASD loads it can support, is

$$\beta_T = 1730(1.81)^2 = 5670 \text{ in-kips/rad}$$

giving a corresponding equivalent required lateral bracing stiffness at the inside flange of

$$\beta_{br} = 5670 / 23.3^2 = 10.4 \text{ kips/in}$$

If the AISC nodal bracing requirements are used instead, the required lateral bracing stiffness is

$$\beta_{br} = 4.15 \times 1.81 = 7.51 \text{ kips/in} \quad \text{or } 4.15 \times 1.06 \times 1.81 = 7.96 \text{ kips/in}$$

Therefore, the torsional bracing equations indicate a slightly larger stiffness demand to develop the AISC fully-braced load capacity of the member.

5.4.2.3 Required Stiffness to Develop the Virtual Simulation Capacity of the Column

Continuing with the same logic as in the previous sub-section, if the goal is to develop the load capacity of the column obtained from the virtual test simulation (using the braces designed for the specified ASD load combination), the torsional bracing requirement at the top of the column is

$$\beta_T = 1730(1.89)^2 = 6180 \text{ in-kips/rad}$$

with a corresponding equivalent required lateral bracing stiffness at the inside flange of

$$\beta_{br} = 6180 / 23.3^2 = 11.4 \text{ kips/in}$$

If the AISC nodal bracing requirements are used instead, the required lateral bracing stiffness

$$\beta_{br} = 4.15 \times 1.89 = 7.84 \text{ kips/in} \quad \text{or } 4.15 \times 1.06 \times 1.89 = 8.31 \text{ kips/in}$$

The following sections consider the AISC Appendix 6 strength requirements to develop the different moment levels in the column.

5.4.2.4 Required Strength to Develop the Specified ASD Moments in the Column

Using the AISC Appendix 6 torsional bracing provisions, the required strength of the torsional braces at the top of the column is determined by simply multiplying the *required* stiffness (after removing the effect of ψ) by a twist rotation equal to the assumed maximum initial twist imperfection at the brace points, $(L_b / 500) / h_o$:

$$M_{br} = 1.6 \frac{\beta_T}{\psi} \frac{L_b}{500 h_o} = 1.6 \frac{1730}{3} \frac{87}{500(23.3)} = 6.89 \text{ in-kips}$$

Thus, the equivalent lateral bracing strength requirement at the inside flange is

$P_{br} = M_{br}/h_o = 6.89 / 23.3 = 0.30$ kips

Note that the above values are multiplied by 1.6 so that they correspond to the ASD ultimate strength load level. The 1.6 factor would not be included if the bracing components were being designed by ASD for these requirements. However, for comparison to virtual test simulation results, the brace forces at the ultimate strength load level are needed.

If the AISC beam nodal bracing provisions are used, one obtains

$P_{br} = 1.6 \text{ x } 0.01 (M_r / h_o) C_{tN} C_d = 1.6 \text{ x } 0.01 (239\text{x}12/23.3)(1.0) C_d = 1.96 C_d$ kips

or 1.96 kips except for the brace point closest to the inflection point, where the strength requirement is 2.09 kips.

5.4.2.5 Required Strength to Develop the Estimated AISC Load Capacity of the Column

The required strength to develop the estimated AISC load capacity of the column is calculated as

$$M_{br} = 1.6 \frac{\beta_T}{\psi} \frac{L_b}{500 h_o} = 1.6 \frac{5670}{3} \frac{87}{500(23.3)} = 22.6 \text{ in-kips}$$

corresponding to the ASD Strength condition. The corresponding equivalent lateral bracing strength requirement at the inside flange is

$P_{br} = M_{br}/h_o = 22.6/ 23.3 = 0.97$ kips

If the AISC beam nodal bracing provisions are used, one obtains

$P_{br} = 1.6 \text{ x } 1.81 \text{ x } 0.01 (M_r / h_o) C_{tN} C_d$

$= 1.6 \text{ x } 1.81 \text{ x } 0.01 (239\text{x}12/23.3)(1.0) C_d = 3.57 C_d$ kips

or 3.57 kips except for the brace point closest to the inflection point, where the strength requirement is 3.77 kips.

5.4.2.6 Required Strength to Develop the Virtual Simulation Load Capacity of the Column

The required strength to develop the virtual simulation load capacity of the column is calculated as

$$M_{br} = 1.6 \frac{\beta_T}{\psi} \frac{L_b}{500 h_o} = 1.6 \frac{6180}{3} \frac{87}{500(23.3)} = 24.6 \text{ in-kips}$$

The corresponding equivalent lateral bracing strength requirement at the inside flange is

$P_{br} = M_{br}/h_o = 24.6 / 23.3 = 1.06$ kips

If the AISC beam nodal bracing provisions are used, one obtains

P_{br} = 1.6 x 1.89 x 0.01 (M_r /h_o) $C_{tN}C_d$

= 1.6 x 1.89 x 0.01 (239x12/23.3)(1.0)C_d = 3.72C_d kips

or 3.72 kips except for the brace point closest to the inflection point, where the strength requirement is 3.95 kips.

At this point, the critical relative bracing requirements for the shear panels at the bottom of the column have not yet been considered. The following sections present these checks.

5.4.3 AISC Relative Bracing Design Requirements at the Bottom of the Column

5.4.3.1 Required Stiffness to Develop the Specified ASD Moments in the Column

At the bottom of the column, the bracing is designed as relative bracing on the exterior flange of the column. The AISC beam relative bracing rules are used to evaluate the bracing requirement as follows at the bottom 7.25 ft shear panel:

$$\beta_{br} = 2\psi\left(\frac{\Sigma P_r + \Sigma(C_{tR}C_d M_r/h_o)}{L_{bi}}\right)$$

Neglecting the axial load effects,

C_{tR} = 1.0

C_d = 1.0

ΣP_r = 0 kips

$\Sigma M_r = M_r$ = 323 ft-kips = 3880 in-kips

h_o = 23.3 inches

L_{bi} = 7.25 ft = 87 inches

$$\beta_{br} = 2(2.0)\left(\frac{(1.0)(1.0)(323)/(23.3)}{7.25}\right) = 7.65 \text{ kips/inch}$$

or

$G'_{reqd} = \beta_{br} L_b / \Sigma s$ = 7.65 (87) / 360 = 1.84 kips/inch

The total width of the diaphragm available to brace each sidewall column is assumed to be equal the spacing between the columns, i.e., Σs = 30 ft = 360 inches.

5.4.3.2 Required Stiffness to Develop the Estimated AISC Load Capacity of the Column

As discussed previously, if the column in Fig. 5.1 is loaded to its ultimate capacity per the AISC flexural resistance checks, the internal moments are 1.81 times larger than the ASD ultimate strength load combination level. Hence, the shear panel stiffness required to develop the estimated AISC load capacity of the column is

β_{br} = 7.65 x 1.81 = 13.8 kips/inch (G'_{reqd} = 3.32 kips/inch)

5.4.3.3 Required Stiffness to Develop the Virtual Simulation Capacity of the Column

The subsequent virtual simulation results show that the column attains 1.89 times greater capacity than the moments at the ASD ultimate load combination level (i.e., 1.6 times the ASD load combination). Therefore, the estimated relative bracing stiffness required to reach the virtual simulation load capacity is

β_{br} = 7.65 x 1.89 = 14.5 kips/inch (G'_{reqd} = 3.48 kips/inch)

The following sections address the strength requirements for the wall panels.

5.4.3.4 Required Strength to Develop the Specified ASD Moments in the Column

The required shear panel strength is calculated using AISC equations as follows:

$$V_{br} = 0.004\left(\Sigma P_r + \Sigma(C_{tR}C_d M_r / h_o)\right)\times 1.6$$

V_{br} = 0.004 (1.0)(1.0)(3880)(1.6) / 23.3 = 1.08 kips

or, in terms of the shear strength per unit width of the wall panels,

v_{br} = 1000 x 1.08 / 30 = 35.7 lb/ft

Note that as in Sections 5.4.2.4 to 5.4.2.6, the above values are multiplied by 1.6 so that they can be compared directly with the forces determined in the virtual test simulation.

5.4.3.5 Required Strength to Develop the Estimated AISC Load Capacity of the Column

To develop the estimated AISC load capacity of the column, the strength required from equation above is

V_{br} = 1.08 x 1.81 = 1.95 kips (v_{br} = 64.9 lb/ft)

5.4.3.6 Required Strength to Develop the Virtual Simulation Load Capacity of the Column

Similarly, the strength required to develop the virtual simulation load capacity of the column is

V_{br} = 1.08 x 1.89 = 2.04 kips (v_{br} = 68.0 lb/ft)

5.5 Simplified Bracing Requirements

5.5.1 Required Torsional Brace Strength

Using the simplified rules, the required torsional brace strength may be calculated as

M_{br} = 0.02 M_r x 1.6 = 0.02 (239)(12)(1.6) = 91.8 in-kips

at the load level corresponding to the applied ASD ultimate strength loads, or in terms of the equivalent lateral brace force,

$P_{br} = M_{br} / h_o$ = 91.8 / 23.3 = 3.94 kips

Similarly, at the load level corresponding to the estimated AISC load capacity of the column,

M_{br} = 91.8 x 1.81 = 166 in-kips (P_{br} = 7.12 kips)

and at the load level corresponding to the virtual simulation load capacity,

M_{br} = 91.8 x 1.89 = 174 in-kips (P_{br} = 7.45 kips)

5.5.2 Required Torsional Brace Stiffness

The required torsional brace stiffness is obtained from the simplified rules as

$$\beta_T = \frac{M_{br} h_o}{0.004 L_b} = 6150 \text{ in-kips/rad}$$

to brace the column for the applied ASD ultimate strength loads. By converting this value to an equivalent lateral bracing requirement at the interior flange of the column, one obtains

$\beta_{br} = \beta_T / h_o^2$ = 6150 / 23.3^2 = 11.3 kips/inch

The AISC-based estimates for this stiffness are 3.19 kips/inch from the torsional bracing equations, and 4.15 kips/inch except near the inflection point from the nodal lateral bracing equations, as determined previously in Section 5.4.2.1. The above simplified

equation gives a significantly larger stiffness requirement. This is because it does not contain any implicit recognition of the fact that the W24x84 member actually doesn't even need the torsional braces to support the ASD ultimate strength loads. As noted previously, the AISC lateral bracing stiffness requirements are conservative relative to the torsional bracing requirements because their recognition of the member resistance to brace point movements, via L_q, is generally a conservative representation.

To develop the estimated AISC ultimate strength of the column, the corresponding requirement from the simplified equations is

β_T = 6150 x 1.81 = 11,100 in-kips/rad (β_{br} = 20.5 kips/inch)

and to develop the virtual simulation strength of the column, the required stiffness is

β_T = 6150 x 1.89 = 11,600 in-kips/rad (β_{br} = 21.4 kips/inch)

5.5.3 Required Shear Panel Strength

By applying the simplified bracing stiffness and strength equations discussed previously in Section 2.8, the required shear panel strength for the sidewall column is determined as follows:

$V_{br} = 0.01(M_r/h_o)$ x 1.6 = 0.01 (323x12/23.3) x 1.6

M_r = maximum positive moment in the column

V_{br} = 2.66 kips (v_{br} = 2.66 x 1000 / 30 = 88.7 lb/ft)

at the load level corresponding to the ASD ultimate strength condition. Again, note that the force is multiplied by 1.6 to convert from the ASD working load level to the ultimate strength load level. The required shear panel strength as calculated by the AISC equations discussed above was v_{br} = 35.7 lb/ft at this load level.

Similarly, the required shear panel strength at the load level corresponding to estimated AISC load capacity of the column is

V_{br} = 2.66 x 1.81 = 4.81 kips (v_{br} = 161 lb/ft)

and the required strength at the virtual simulation load capacity of the column is

V_{br} = 2.66 x 1.89 = 5.03 kips (v_{br} = 168 lb/ft)

5.5.4 Required Shear Panel Stiffness

The required shear panel stiffness for the different load levels is obtained as

$$\beta_{br} = \frac{V_{br}}{0.004 L_b}$$

where V_{br} is the required shear force at the ultimate strength load level. Considering the selected ASD load combination, this equation gives

β_{br} = 7.68 kips/inch (G'_{reqd} = 7.68 x 87 / 360 = 1.86 kips/inch)

The AISC estimate for this stiffness is G'_{reqd} = 1.84 kips/inch as shown previously in Section 5.4.3.1. Alternatively, to develop the estimated AISC load capacity of the column, the required stiffness is

β_{br} = 7.68 kips/inch x 1.81 = 13.9 kips/inch (G'_{reqd} = 3.34 kips/inch)

and to develop the virtual simulation load capacity of the column

β_{br} = 7.68 kips/inch x 1.89 = 14.5 kips/inch (G'_{reqd} = 3.51 kips/inch)

5.6 Calculation of Provided Brace Stiffness and Strength and Comparison to Required Strengths

5.6.1 Torsional Bracing at the Top of the Column

5.6.1.1 Provided Torsional Brace Stiffness

The provided torsional brace stiffness is calculated below by paralleling the calculation of the nodal lateral bracing stiffness provided in the CSD (2009) example. The input parameters for this calculation are as follows:

Continuous Z girts (10Z 3.25x105): A = 1.88 in^2, I_x = 28.4 in^4

Two-sided L 2x2x3/16 flange diagonal braces: A = 0.715 in^2, r_x = 0.612 inches

The truss/frame analysis model from the CSD (2009) example calculations is illustrated in Fig. 5.2.

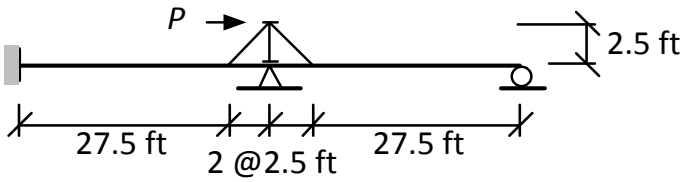

Fig. 5.2. Analysis model for calculation of the bracing stiffness at the flange diagonals, from CSD (2009).

The lateral stiffness at the inside flange brace point is calculated by applying a unit load P = 1 kip at the inside flange location. The corresponding lateral displacement at the load location is

Δ = 0.05 inches

Therefore, the lateral bracing stiffness is obtained as

$\beta_{provided}$ = 1/0.05 = 20 kips/inch

This lateral bracing requirement can be converted to an equivalent torsional stiffness requirement by dividing by h_o^2:

$\beta_{Tprovided} = 20 \times 23.3^2 = 10{,}900$ in-kips/rad

This stiffness is substantially larger than all of the requirements previously calculated in Section 5.4.2, and it is significantly larger than or comparable to the requirements calculated in Section 5.5.2. Table 5.2 compares this provided stiffness to the various stiffnesses calculated in these sections. In addition, it compares the provided strength determined in the next section and the corresponding estimated strength requirements.

Table 5.2 Summary of provided versus required brace strengths and stiffnesses, expressed in terms of the equivalent lateral brace properties for the intermediate torsional braces near the top of the column.

Criterion or condition		Stiffness β_{br} (kips/in)	Strength P_{br} (kips, %)[a]
Provided		20.0	4.83, -
Required to brace the column for the ultimate strength loading from the ASD load combination, M_{top} = 1.6 x 239 ft-kips = 382 ft-kips	AISC Torsional Requirement	3.19	0.30, 0.16
	AISC Nodal Requirement	4.15	1.96, 1.0
	Simplified	11.3	3.94, 2.0
Required to brace the column for its estimated capacity using AISC Ch. F, M_{top} = 2.89 x 239 = 691 ft-kips	AISC Torsional Requirement	10.4	0.97, 0.27
	AISC Nodal Requirement	7.51	3.57, 1.0
	Simplified	20.5	7.12, 2.0
Required to brace the column for the capacity obtained from virtual simulation using the AISC-based torsional brace stiffnesses for full bracing, M_{top} = 3.00 x 239 = 717 ft-kips	AISC Torsional Requirement	11.4	1.06, 0.29
	AISC Nodal Requirement	7.84	3.72, 1.0
	Simplified	21.4	7.45, 2.0

(a) Percent values are M_{br} /M_{top} written as a percentage, where M_{top} is the moment at the top of the column.

The above CSD model assumes that the girt on one side of the sidewall column is fixed at its opposite end and that the girt on the other side of the column is pinned at its opposite end as shown in Fig. 5.2. The $8EI/s$ torsional stiffness suggested as an upper bound estimate in Section 2.7 assumes that the girts on both sides of the member are fixed at their opposite end, where they are assumed continuous across and attached to the adjacent frame. Conversely, in Section 4.6, the provided stiffness for the roof girder example is calculated assuming that the adjacent girder on one side of the member is buckling simultaneously with the critical girder. Other engineers may assume that the members on both sides of the critical member are buckling, effectively resulting in a provided stiffness of roughly $2(2EI/s) = 4EI/s$. One can observe that the estimates of the provided stiffness can vary substantially. The CSD model provides a median estimate of the provided stiffness value.

5.6.1.2 Provided Brace Strength

Similar to the prior calculations shown in Fig. 4.3, flange brace lateral strength based on the L2x2x3/16 flange diagonals is calculated in this example as follows:

L/r_x = (30 inches)(1.414)/0.612 inches = 69

$(KL/r)_{equiv} = 72 + 0.75\,(L/r_x) = 72 + 0.75\,(69) = 124$

(using Section E5 of the AISC Specification)

$F_{cr}/\Omega = 9.55$ ksi

$R_a = (9.55)(0.715)(0.707) = 4.83$ kips

Note that the length of the diagonal used in the above calculations, which is based on the centerline distances between the work points in Fig. 5.2, is more conservative than the length of the diagonal used in Section 4.6.

Based on the assumption that the flange diagonals are the critical component in the bracing system with respect to strength, one can observe from Table 5.2 that the provided strength is significantly larger than all the estimated required strengths except for the simplified estimates of the bracing strength required to develop the ultimate strength load levels for the column. The simplified estimates are as much as 1.5 times larger than the provided strength for the ultimate strength loadings.

This concludes the presentation of the design estimates of the required and the provided stiffnesses and strengths for the torsional braces in this example. The next section discusses the provided and required stiffnesses and strengths for the wall panels in this problem.

5.6.2 Relative (Shear Panel) Bracing at the Bottom of the Column

5.6.2.1 Provided Diaphragm Shear Stiffness

As noted in Section 5.3, the provided diaphragm shear stiffness is assumed as $G' = 3.52$ kips/inch for this example. This is greater than all the required stiffness estimates from Sections 5.4.3 and 5.5.4. However, this stiffness is only slightly larger than the G' value required by the AISC and the simplified equations to develop $M_n \geq M_p$ at the bottom of the column. Table 5.3 summarizes the provided stiffness and the estimated stiffness requirements, as well as the provided and estimated strengths discussed in the next section.

The shear panels above the base are satisfactory by inspection, including the panel where the moment changes sign and $C_d > 1$. The maximum bending moment in this panel is less than a factor of two smaller than the maximum M_r at the base.

Table 5.3 Summary of provided versus required brace strengths and stiffnesses, for the relative (shear panel) bracing at the bottom of the column.

Criterion or condition		Stiffness G' (kips/in)	Strength v_{br} (lb/ft, %)[a]
Provided assuming CS wall panels with 12 inch screw spacing at the base and eave		3.52	61.2
Required to brace the column for the loading from the ASD load combination, M_{bot} = 1.6 x 323 = 517 ft-kips	AISC	1.84	35.7, 0.4
	Simplified	1.86	88.7, 1.0
Required to brace the column for the estimated capacity from AISC Ch. F, M_{bot} = 2.89 x 323 = 933 ft-kips	AISC	3.32	64.9, 0.4
	Simplified	3.34	161, 1.0
Required to brace the column for the capacity obtained from virtual simulation using the AISC-based torsional brace stiffnesses for full bracing, M_{bot} = 3.00 x 323 = 969 ft-kips	AISC	3.48	68.0, 0.4
	Simplified	3.51	168, 1.0

(a) Percent values are V_{br} / (M_{bot} /h_o) written as a percentage, where M_{bot} is the moment at the bottom of the column.

5.6.2.2 Provided Diaphragm Shear Strength

Assuming CS wall panels with 12 inch screw spacing at base and eave, v_a = 61.2 lb/ft, or

$$[V_a = (61.2)(30) = 1.84 \text{ kips}] > [V_{br} = 0.004\ (323\text{x}12/23.33) = 0.67 \text{ kips}]$$

OK

The CSD (2009) example assumes strength of the R panels to be 140 lbs/ft. The simplified equations suggest that a significantly larger bracing force of 1.0 % needs to be developed in the shear panels, whereas the AISC equations require only 0.4 % brace force. The appropriateness of each of these limits is discussed after considering the virtual simulation test results.

5.7 Critical Geometric Imperfections for Virtual Simulation Analysis

All of the above requirements are essentially just coarse simplified design estimates. This section and the following sections evaluate the true demands on the bracing using virtual test simulation. In these studies, the critical imperfection applied to the system to maximize the demand on the intermediate torsional brace at the top of the column is obtained via the influence line approach discussed previously in Section 3.3. Figure 5.3 shows the influence line on the inside flange for the top torsional brace of the column. The top torsional brace point is marked by the open diamond symbol. The corresponding out-of-plumbness imperfection (L_b/500, L_b = 7.25 ft) is shown in Figure 5.4a.

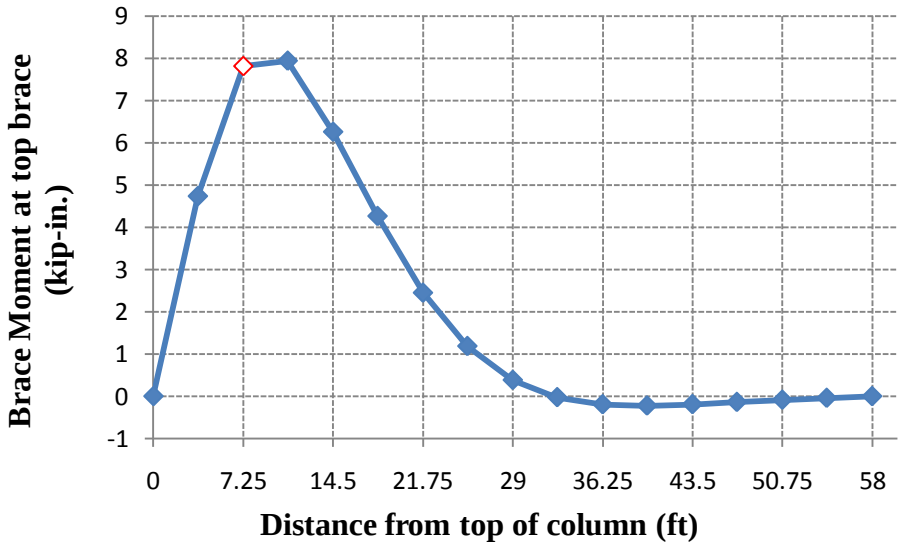

Fig. 5.3. Influence line on the inside flange for the top torsional brace, sidewall column with β_T = 1730 in-kips/rad (β_{br} = 3.19 kips/inch) and G' = 3.52 kips/inch.

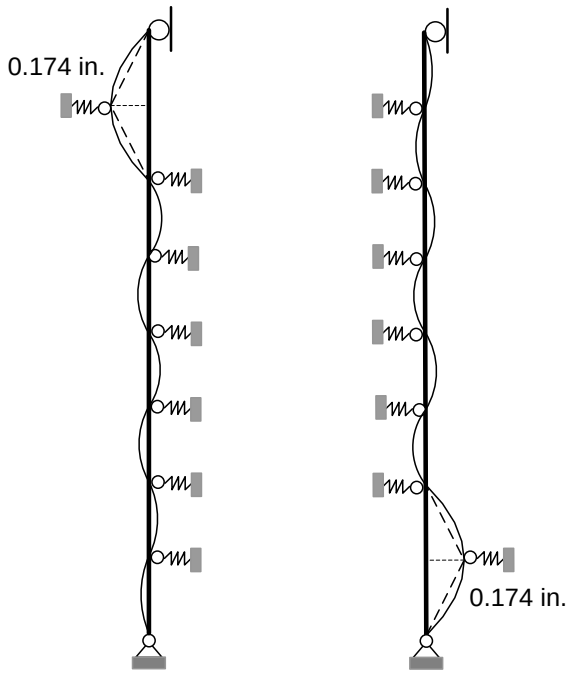

Fig. 5.4. Out-of-plumbness imperfection, sidewall column with β_T = 1730 in-kips/rad (β_{br} = 3.19 kips/inch) and G' = 3.52 kips/inch.

Since the outside flange at the bottom of the column is in compression, the relative bracing demand should be largest there. As such, in addition to the geometric imperfection applied to maximize the demand on the torsional brace at the top, a single brace point out-of-alignment is applied at the first intermediate brace on the outside flange from the bottom of the column, as shown in Fig. 5.4(b). This imperfection maximizes the demand on the relative (shear panel) bracing at the bottom of the column.

5.8 Virtual Simulation Results Using the AISC Required Torsional Brace Stiffness to Develop the Specified ASD Loads and a Representative Wall Panel Stiffness of G' = 3.52 kips/inch

The above applied critical imperfections aim at maximizing the brace force at the top torsional brace of the column as well as in the shear panel (relative) bracing at the bottom of the column. It should be emphasized that the W24x84 column has a large reserve

capacity relative to the applied ASD ultimate strength loads. The capacity of the column, determined using the equations from 2010 AISC Chapter F provisions, is $M_n = M_p$ = 933 ft-kips for the top unbraced length of 7.25 ft.

The torsional brace stiffness used for this virtual test simulation is the AISC value of 1730 kip-in, which is the estimated torsional brace stiffness necessary to develop the specified ASD loads. The "shear panel" bracing stiffness is the stiffness provided by selected wall panels, G' = 3.52 kips/inch as discussed previously. It should be noted that this shear stiffness is sufficient to develop the full capacity $M_n = M_p$ at the bottom of the column according to both the AISC and the simplified bracing rules.

Figure 5.5 shows the shear demand in the bottom wall panel as a percentage of the flange force at the bottom unbraced length. M_{max} is the maximum moment in the column at its limit load in the virtual simulation analysis, which occurs at its bottom. No torsional braces are used at the bottom of the column where the inside flange is in tension.

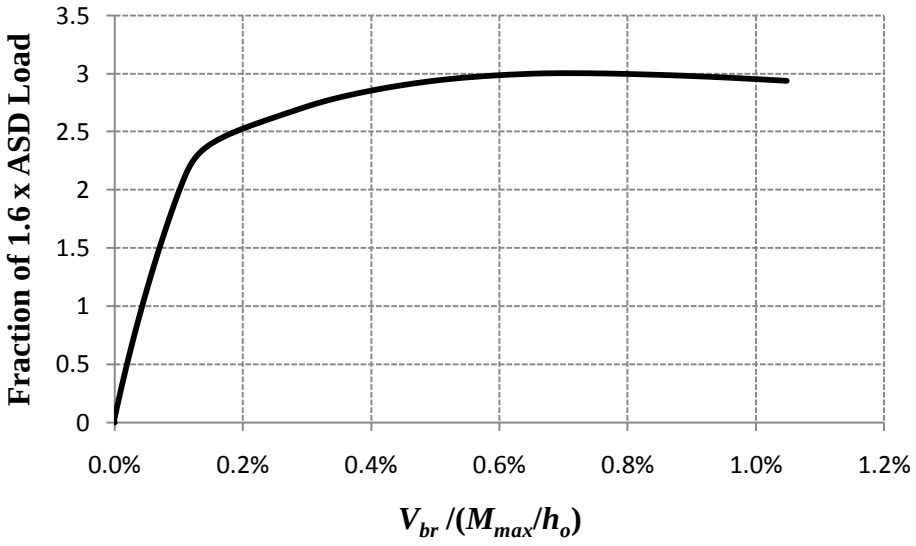

Fig. 5.5. Required shear panel strength versus load level for the sidewall column with β_T = 1730 in-kips/rad (β_{br} = 3.19 kips/inch) and G' = 3.52 kips/inch, M_{max} = moment at column base at the virtual simulation peak load.

Since G' = 3.52 kips/inch is estimated to be sufficient to develop the plastic moment capacity at the bottom of the column, the corresponding strength requirements should be compared to the virtual simulation results at the ultimate strength load level. The relative brace force demand at the bottom unbraced length is 0.71% of M_{max}/h_o or 3.54 kips at the peak load capacity. This corresponds to a shear force per unit width of 3.54x1000/30 ft = 118 lb/ft in the bottom wall panels. The AISC calculations estimate this force to be 2.04 kips (0.40 % of M_{max}/h_o or 68.0 lb/ft in the wall panels) while the simplified equations estimate it to be 5.03 kips (1.0 % of M_{max}/h_o or 168 lb/ft in the wall panels). One can observe that the AISC strength requirements are somewhat low compared to the required critical shear panel strength at the limit load, whereas the simplified strength requirement is a conservative estimate of the required shear panel strength at the limit load. However, similar to the observations in Section 4.9, one can observe from Fig. 5.5 that the AISC bracing strength requirement of 0.4% is not breached until approximately 94 % of the system load capacity is applied to the beam. Figure 5.6 shows the failure mode of the column including the corresponding lateral displacement contours at the end of the analysis.

Figure 5.7 shows the brace force demand at the top torsional brace on the column as a percentage of the moment at the top of the column at the peak load in the virtual test simulation. The low torsional brace force demands may be attributed partially to the fact that the column fails at its bottom. The moments at the top of the column are limited statically by the development of the plastic moment at the bottom of the column.

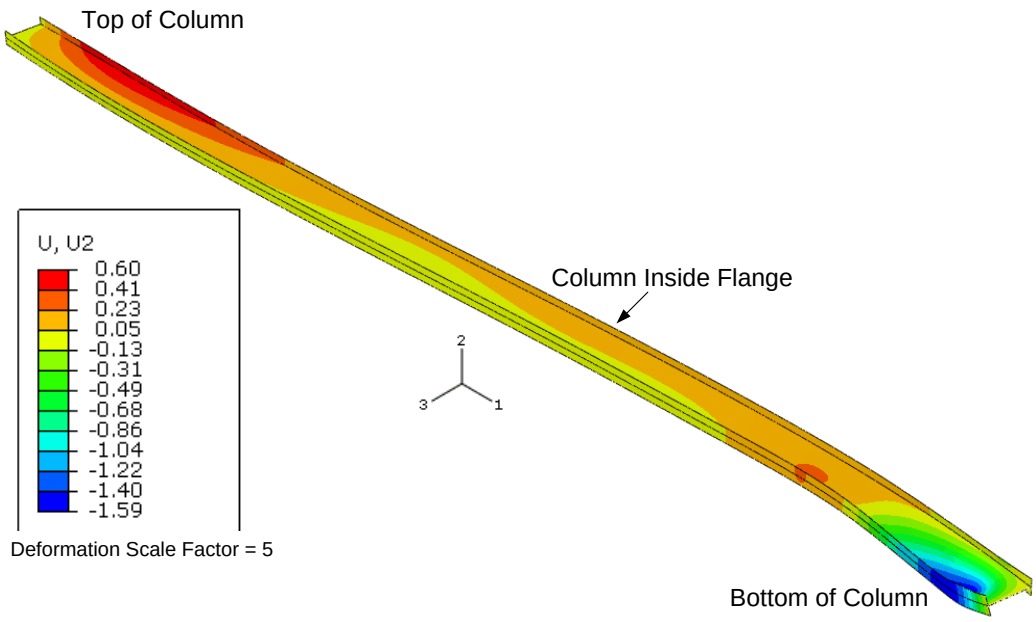

Fig. 5.6 Final failure mode (post-peak at the end of the analysis) for the sidewall column with β_T = 1730 in-kips/rad (β_{br} = 3.19 kips/inch) and G' = 3.52 kips/inch, including contours of the corresponding lateral deflections (units = inches).

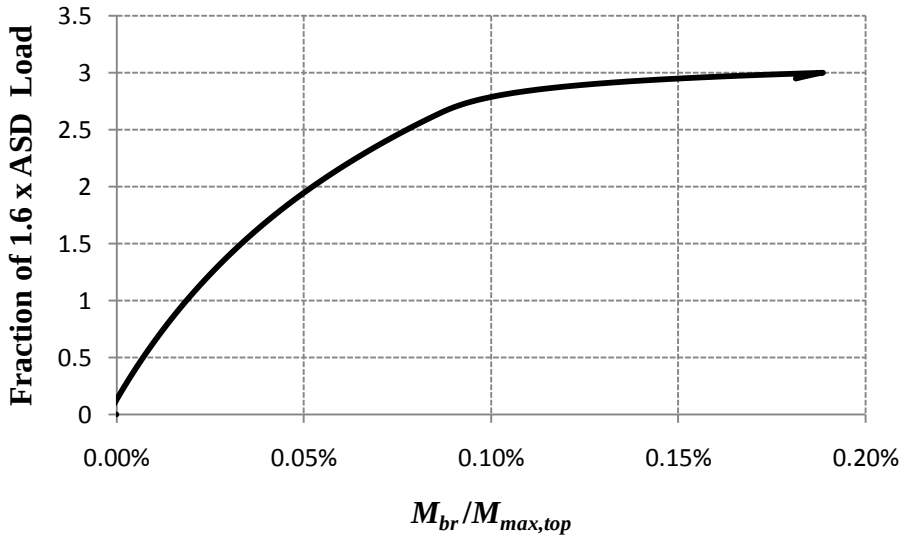

Fig. 5.7. Brace force demand at the top torsional brace of the sidewall column with β_T = 1730 in-kips/rad (β_{br} = 3.19 kips/inch) and G' = 3.52 kips/inch ($M_{max.top}$ = moment at the top of the column at the virtual test simulation limit load).

However, it is apparent that other than the moment at the top of the column being linked to the moment at the bottom by the statics for the selected ASD loading, the stability behavior at the top of the column is largely independent of the stability behavior at the bottom of the column. The member still has ample torsional stiffness to resist the out-of-plane displacement of its inside flange even at its limit load, and it has even more torsional stiffness to resist the out-of-plane movement at the torsional braces at the ASD load level. In addition, the torsional brace moments tend to be reduced by the lateral restraint from the shear panels at the top braces acting in combination with the torsional restraint from the flange diagonals and girts.

One can observe from Fig. 5.7 that the torsional brace moments at the ASD ultimate strength load level (i.e., at an ordinate of 1.0 in the plot) are only on the order of 0.02%.

5.9 Effect of Removing the Torsional Braces

As noted in Section 5.4.1, the capacity of the column is much larger than the ASD ultimate strength load combination in this problem. Also, since the column fails in its bottom unbraced length, the torsional brace stiffness is not expected to affect the system strength significantly. In fact, Section 5.4.1 shows that the column has sufficient capacity to resist the specified ASD load combination without any intermediate torsional braces near its top. However, the AISC flexural resistance checks suggest that the member ultimate strength will be governed by lateral buckling of its inside flange if the torsional braces are removed. This section investigates the virtual test simulation response of the column for the case of zero torsional bracing near its top. The wall panel shear stiffness is still G' = 3.52 kips/inch as in the previous section.

It should be noted that the critical imperfection to be applied for this case is different than the imperfection discussed previously. For this case, the single brace point out-of-plumbness applied to the outside flange at the bottom of the column is the same imperfection as in Section 5.8. However, the fundamental buckling mode of the column involves the constrained-axis twisting of the column about its outside flange, as shown in Figure 5.8. Due to the this attribute, the critical imperfection for this analysis is obtained by directly scaling the fundamental buckling mode such that the maximum cross-section twist is equal to 1/100. This gives a maximum lateral movement of the inside flange of 0.233 inches close to the second intermediate brace from the top of the column, as shown in Fig. 5.9a. It should be noted that scaling the fundamental eigenmode such that the maximum inside flange out-of-straightness between the end brace points is equal to L_b/1000 would give a cross-section twist of 1/120.

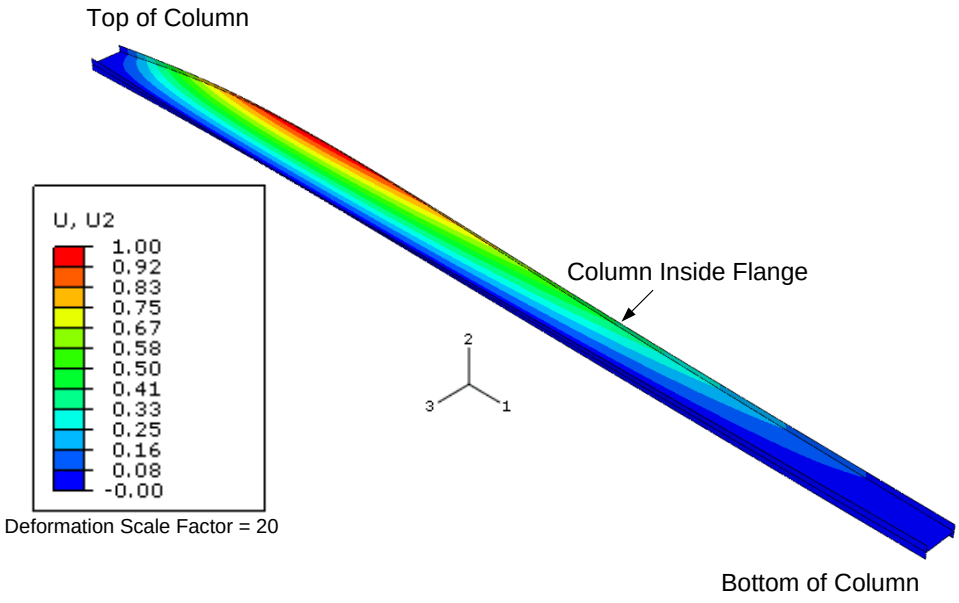

Fig. 5.8 Fundamental buckling mode of the sidewall column with zero torsional bracing and G' = 3.52 kips/inch.

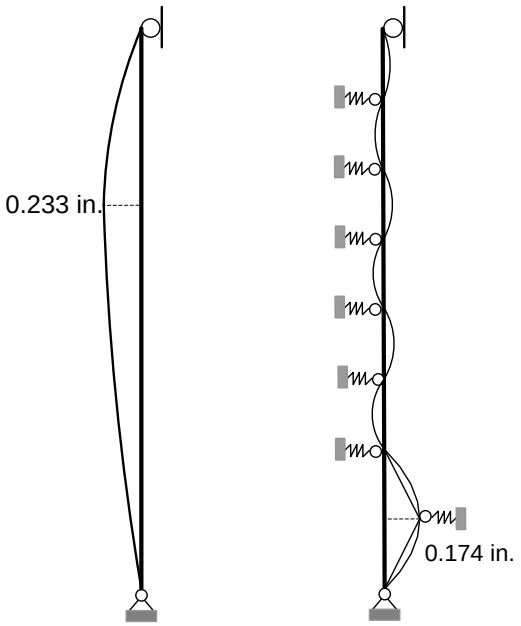

Fig. 5.9. Out-of-plumbness imperfection for the side wall column with zero torsional bracing and G' = 3.52 kips/inch.

In the virtual test simulation of this problem, the moment at the top of the column is 478 ft-kips at limit load. This strength can be compared to the strength estimate from the AISC equations of M_n = 560 ft-kips, causing compression on the inside flange, determined in Section 5.4.1. Hence, in the virtual test simulation, the column reaches a capacity of only 478/560 = 0.85 times the AISC-based prediction of the maximum moment at the top of the column. The corresponding maximum moment at the bottom of the column is 478 x 323/239 = 646 ft-kips.

Figure 5.10 shows the bracing force demand in the wall panel as a percentage of the outside flange force M_{max}/h_o at the bottom unbraced length, where M_{max} is the moment at the bottom of the column at the virtual simulation limit load.

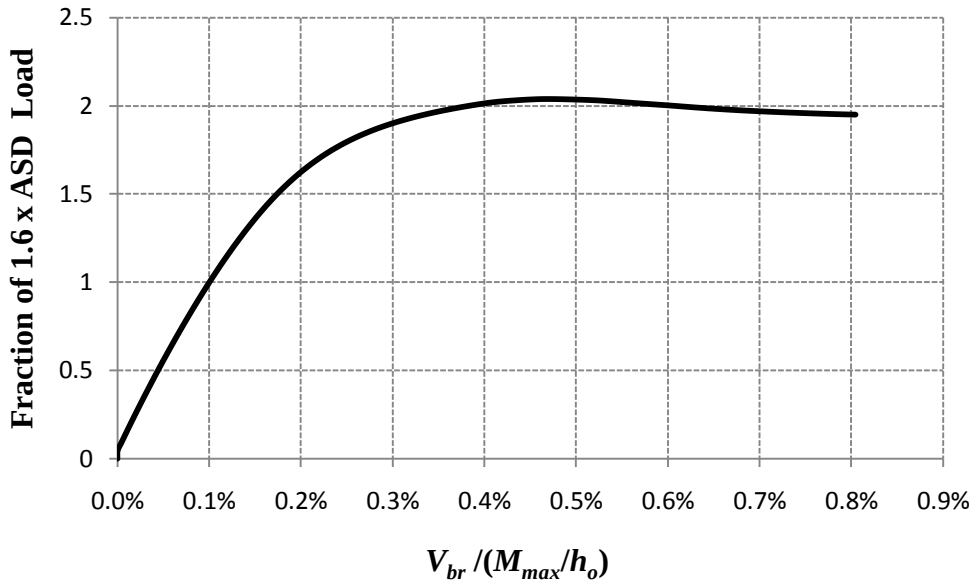

Fig. 5.10. Required relative ("shear panel") strength to brace the bottom unbraced length, sidewall column with zero torsional bracing and G' = 3.52 kips/inch (M_{max} = moment at the base of the column at the limit load in the virtual test simulation).

The relative brace force demand at the bottom unbraced length is 0.46% or 1.6 kips (53 lb/ft) at the peak load. In this case, the column fails at the top unbraced length where the inside flange is in compression. Figure 5.11 shows the failure mode of the column. The figure also shows the lateral displacement contours at the end of the analysis. The fact that the column strength is governed essentially by the lateral buckling of the inside flange causes the critical shear panel forces in the bottom unbraced length of the column to be relatively low.

Since the column fails at the top, it is interesting to see the brace force demand on the shear panel bracing close to the top of the column. Fig. 5.12 shows the maximum brace force demand in the shear panel bracing close to the top of the column as a percentage of the flange force at the top of the column, $M_{max,top}/h_o$, where $M_{max,top}$ is the moment at the top of the column at the peak load from the virtual test simulation.

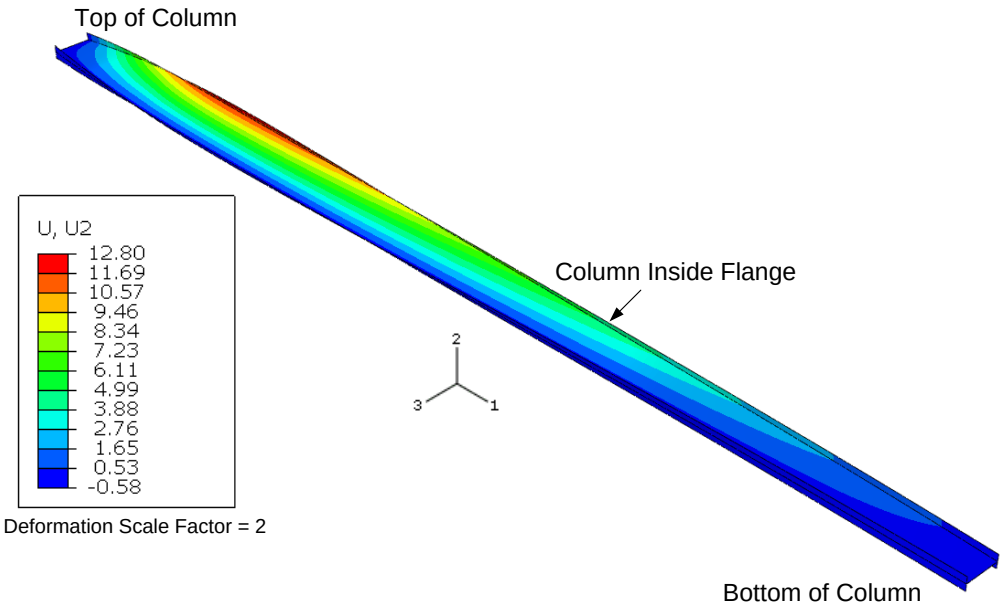

Fig. 5.11 Final failure mode at the end of the analysis for the sidewall column with zero torsional bracing and G' = 3.52 kips/inch.

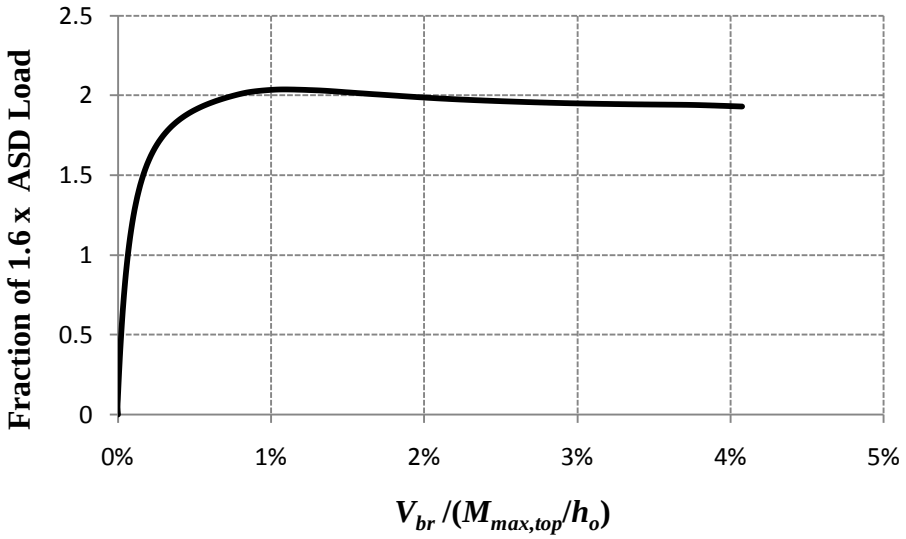

Fig. 5.12. Required relative ("shear panel") strength to brace the top of the column, side wall column with zero torsional bracing and G' = 3.52 kips/inch ($M_{max,top}$ = moment at the top of the column at the limit load in the virtual test simulation).

The maximum relative brace force demand close to the top of the column is 1.0% or 2.7 kips (90 lb/ft) at the peak load. The brace force demand close to the top of the column is higher than that at the bottom for this case as the failure is governed by the lateral buckling of the inside flange close to the top of the column.

5.10 Effect of Varying the Wall Panel Relative Bracing Stiffness

As mentioned earlier, the column fails at the bottom if a torsional brace stiffness of β_T = 1730 in-kips/rad and a wall panel stiffness of G' = 3.52 kips/inch are used. Therefore, it is expected that the column may be more sensitive to changes in the wall panel stiffnesses with the torsional brace stiffnesses held constant at its top. Figure 5.13 shows the knuckle curve for this sidewall column example for the relative bracing at the bottom unbraced length. The vertical axis shows the normalized maximum moment in the sidewall column, M_{max}/M_n, where M_{max} is the moment at the bottom of the column at the limit load and M_n is the corresponding nominal moment capacity of the column, $M_n = M_p$ = 933 ft-kips, based on Ch. F of the AISC Specification with C_b = 1.11 and K = 1.

The AISC and the simplified relative brace stiffness requirements are essentially the same for this check. The two requirements to develop the specified ASD moments in the column are highlighted in the plot.

However, it is important to note that the ASD moments are substantially smaller than the moments corresponding to the beam strength, and that the AISC and simplified stiffness requirements to develop the member fully-braced strength are substantially larger than the stiffness values highlighted in the above plot. The sidewall column is able to reach 1.04 of the best estimate of its fully-braced load capacity using a relative brace stiffness of β_{br} = 7.65 kips/inch, or G' = 1.84 kips/inch (the AISC relative bracing

stiffness estimate to support the applied ASD loading). As noted above, the estimate from the simplified equations (β_{br} = 7.68 kips/inch or G' = 1.86 kips/inch) is essentially the same as this value. Both estimates give a stiffness requirement well into the plateau of the knuckle curve. That is, a substantial reduction in the shear panel bracing stiffness will not lead to any dramatic drop in the capacity of the column. It should be emphasized though that the AISC and simplified relative bracing stiffness requirements to develop the AISC Ch. F fully-braced strength ($M_n = M_p$ = 933 ft-kips at the bottom of the column) are β_{br} = 13.8 kips/inch (G' = 3.32 kips/inch) and β_{br} = 13.9 kips/inch (G' = 3.34 kips/inch) respectively, essentially 180 % of the above values (see Table 5.3).

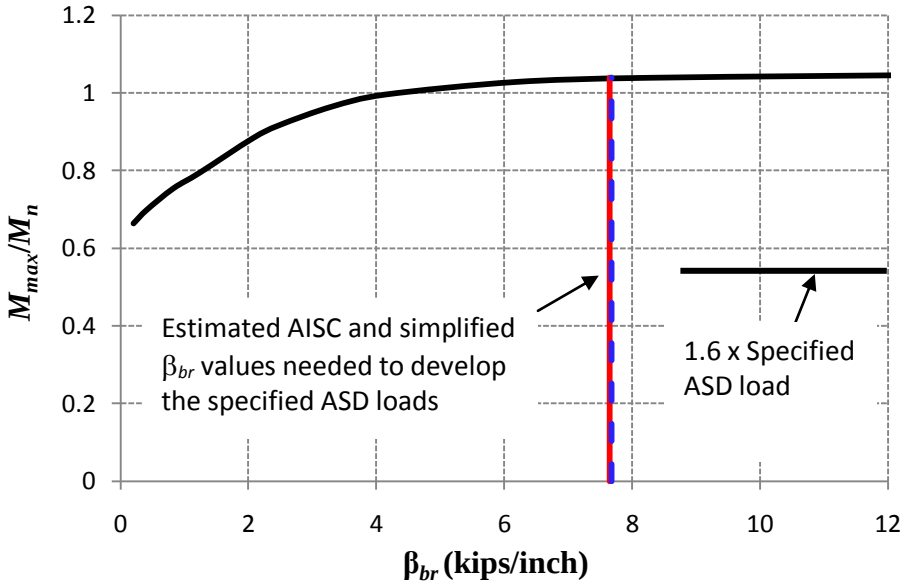

Fig. 5.13 Member strength knuckle curve for relative bracing stiffness, sidewall column example, β_T = 1730 in-kips/rad, M_n = column nominal moment capacity = 933 ft-kips.

Figure 5.14 shows the changes in critical brace force demand, determined at the maximum load capacity of the column, versus changes in the relative bracing stiffness. Similar to the previous curve of this type in Fig. 4.13, the largest shear force occurs essentially at the stiffness knuckle value from Fig. 5.13. The brace forces drop

precipitously for brace stiffnesses smaller than the knuckle value, and they decrease rather gradually with increasing shear stiffnesses larger than the knuckle value. The maximum shear force demand in Fig. 5.14 is 1.36 %. If the stiffness at this limit is used to define the knuckle value, the knuckle value stiffness is β_{br} = 3.31 kips/inch (G' = 0.80 kips/inch), essentially only 24 % of the AISC and simplified requirements. Based on Fig. 5.13, this bracing stiffness is capable of developing 97 % of the beam $M_n = M_p$ in this problem.

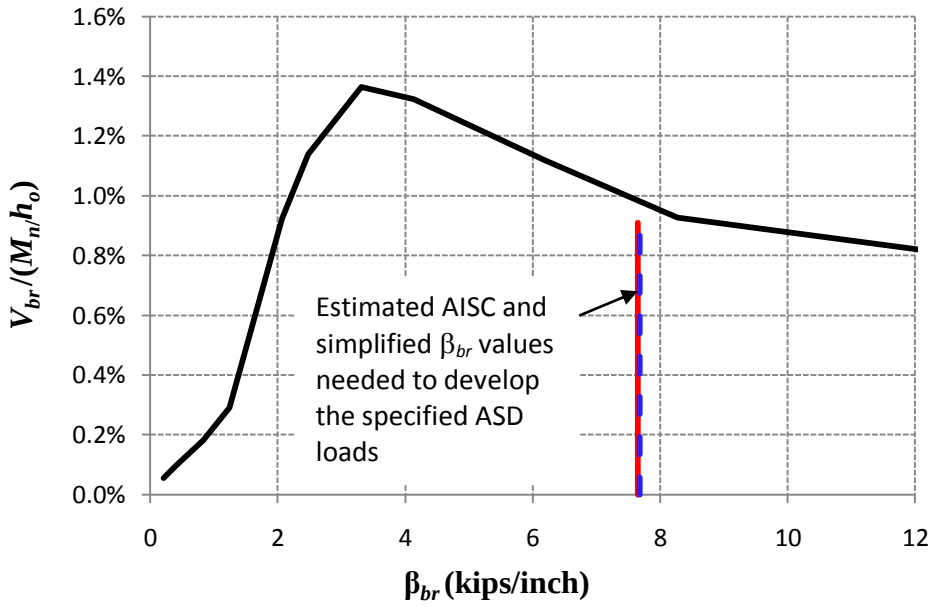

Fig. 5.14 Brace force demand at the column maximum strength limit versus relative brace stiffness, sidewall column example, β_T = 1730 in-kips/rad, **M_n = column nominal moment capacity = 933 ft-kips**.

Obviously both the AISC and simplified estimates of the required relative bracing stiffness are very conservative in this example. It is important to understand that the reason behind this conservatism is the continuity of the W24x84 column across the interior brace points. Neither the relative bracing model nor the simplified relative bracing equations recognize the resistance provided by the member to the brace point

movement due to this continuity. Of course, one must be careful not to infer that the above reduction applies to cases where continuity does not exist or the continuity effects are reduced more substantially than in this problem due to member yielding.

Regarding the AISC and simplified estimates of the required relative bracing strength, Fig. 5.14 shows that even at relatively large stiffnesses compared to the above knuckle value, the shear panel brace force is larger than 0.8 % at the system limit load. Therefore, for the relative bracing stiffness values shown in Figs. 5.13 and 5.14, the AISC strength requirement of 0.4 % appears to be too small. However, one should recall that in the base virtual simulation study presented in Section 5.8, the shear panel brace force is 0.71 % at the limit load (see Fig. 5.5), and the system is able to develop 94 % of the limit load capacity before the relative bracing shear force exceeds 0.4 % (or 98 % of the beam strength at $M_n = M_p$). Furthermore, the wall panel stiffness is G' = 3.52 kips/inch in that study (β_{br}= 14.6 kips/inch), which satisfies the AISC relative bracing minimum stiffness requirement of G' = 3.32 kips/inch (13.8 kips/inch). Therefore, if the AISC or simplified bracing stiffness requirements are met, then it can be argued that the design of the shear panels for a 0.4 % strength requirement is sufficient and that the 1.0 % simplified bracing force requirement is conservative.

Figure 5.15 shows the required shear panel strength versus the load level for the suggested knuckle value stiffness of β_{br} = 3.31 kips/inch (G' = 0.80 kips/inch) from Figs. 5.13 and 5.14. One can observe from this plot that the 1.0 % simplified bracing rule is a good choice for the maximum bracing strength requirement, assuming that system ductility beyond the maximum strength limit is not a key consideration. The beam maximum moment when the brace force reaches the 1.0% is $0.95M_n$, where $M_n = M_p$.

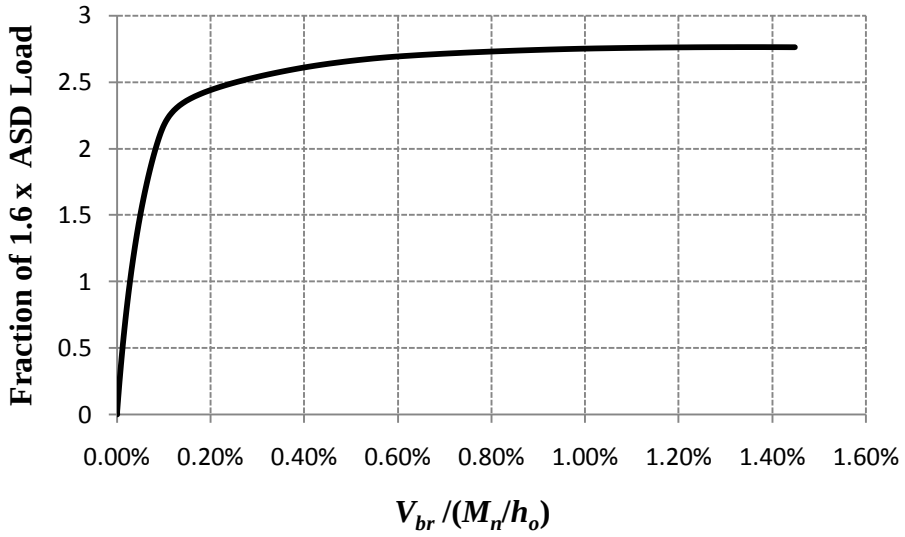

Fig. 5.15. Required relative ("shear panel") strength to brace the bottom unbraced length, side wall column with β_{br} = 3.31 kips/inch (G' = 0.8 kips/inch) (M_n = nominal moment capacity of the column = 933 ft-kips)

If a shear panel stiffness of approximately two times the knuckle value, or β_{br} = 6.6 kips/inch (G' = 1.60 kips/inch) is used, the sidewall column is able to develop a maximum moment slightly larger than $M_n = M_p$ at a brace strength requirement of 1.0%. This shear panel stiffness corresponds to slightly less than one-half of the AISC and simplified estimates for the stiffness requirement.

Based on the above discussions, it can be concluded that, for this problem:

- The AISC relative bracing strength requirement of 0.4 % works sufficiently when the AISC or simplified relative bracing stiffness requirement is satisfied.
- The AISC and simplified relative bracing stiffness requirements, which are effectively the same in value, can be reduced by a factor of two without having any significant impact on the overall strength of the sidewall column and its bracing system. If these reduced stiffnesses are employed, the simplified relative bracing strength requirement of 1.0 % works well.

5.11 Summary

The following key observations can be summarized from the sidewall column example:

- Both the AISC and the simplified equations for relative and for torsional bracing give very conservative estimates of the strength and stiffness demands at the specified ASD load level in this problem. This is largely because the column is well below its strength limit at this stage.
- The demand on the torsional braces near the top of the column is relatively low since the column fails close to its bottom, where the lateral relative bracing of the outside compression flange by the wall panels is very effective. Also, the assistance to the torsional braces from the relative bracing on the outside column flange appears to provide some beneficial effects. Hence, the column strength is not expected to be affected even by substantial reductions in the torsional brace stiffness.
- Although the torsional braces are not needed for the column to support the specified ASD loads, some amount of torsional bracing is necessary near the top of the column if it is desired to develop the member strength $M_n = M_p$ at the column base maximum moment location. Specific reductions in the stiffness, strength and/or number of the torsional braces near the top of the column are not considered in the current study.
- The AISC relative bracing strength requirement of 0.4 % works sufficiently for this problem when the AISC or simplified relative bracing stiffness requirement is satisfied.

- The AISC and simplified relative bracing stiffness requirements, which are effectively the same in value, can be reduced by a factor of two without having any significant impact on the overall strength of the sidewall column and its bracing system. If these reduced stiffnesses are employed, the simplified relative bracing strength requirement of 1.0 % works well. One must be careful in extrapolating these results to other problems however, since the response is heavily influenced by the degree of continuity of the member across the brace points, as well as the ability of the member to resist brace point movement at the load level under consideration.

CHAPTER 6

90 FT CLEAR SPAN FRAME EXAMPLE

6.1 Introduction

This chapter presents a 90 ft clear span frame example from Kim (2010) and White and Kim (2006). The original design of the frame was performed by Mr. Duane Becker of Chief Industries. The design check calculations for this frame can be found in Kim (2010). The estimated bracing demands for this frame, using the AISC and simplified equations, are discussed previously in Sections 2.7 and 2.8. These design requirements are compared to the results obtained from virtual test simulation in this chapter. First, Sections 6.2 and 6.3 give a broad overview of the geometry and loading of the clear span frame. Second, Section 6.4 gives an overview of the specific bracing configuration on the frame. Section 6.5 then compares the AISC-based and simplified estimates for the bracing demands calculated in Sections 2.7 and 2.8 as well as the provided bracing stiffnesses and strengths from Section 2.7.

The critical geometric imperfections applied for the virtual test simulations are discussed in Section 6.6. Section 6.7 presents the results from a virtual test simulation using the provided torsional brace stiffness for representative minimum girt and purlin sizes and assuming zero stiffness contributions from the roof and wall diaphragms. Section 6.8 then discusses the effect of varying the torsional brace stiffness on the overall frame strength and on the brace strength demands for this configuration. This is followed by Section 6.9, which discusses the bracing demands in non-critical regions of the frame.

Section 6.10 presents results for the clear span frame with a simplified bracing layout near the knee and considering the stiffness from the wall and roof panels. This is

followed by Section 6.11, which discusses the effect of increasing the flange width on the bracing demands using the simplified configuration from Section 6.10.

Section 6.13 concludes that studies by considering the effect of roof and wall diaphragm stiffness on the system strength and bracing demands for the original configuration considered in Sections 6.8 through 6.10. Lastly, Section 6.14 summarizes key attributes and observations from this example.

6.2 Frame Geometry

Figure 6.1 shows an elevation view of the 90 ft clear span frame discussed previously in Section 2.7. This figure is a repeat of Fig. 2.13 provided here for convenience of access. Table 6.1 summarizes the specific web and flange geometries for five different member lengths in this structure as well as the panel zone at the knee of the frame. This frame uses a singly-symmetric tapered section for its columns. The column web is nominally 7/32 inch thick and the total column depth tapers from d = 10 inches at the base to d = 40.75 inches at the bottom of the knee joint. This gives a web slenderness ranging from compact at h/t_w = 42 at the column base to slender at h/t_w = 182 at the knee. The outside flange of the columns is 6 x 3/8 inches ($b_f/2t_f$ = 8) while the inside flange is 6 x 1/2 inches ($b_f/2t_f$ = 6). Both of these slenderness values satisfy the AISC (2010) compactness criteria for flange local buckling.

The rafters have doubly-symmetric cross-sections with 6 x 3/8 inch top and bottom flanges ($b_f/2t_f$ = 8) along their entire length. Also, these members have two linear tapers between the knee and the ridge, with the first taper ranging from d = 40.75 inches at the knee to d = 23 inches at 20 ft inside of the knee, and the second taper ranging from d = 23 inches to 24.75 inches at the ridge. The web of the rafter is 1/4 inch thick in the 10 ft

length next to the knee (length C in Fig. 6.1), 3/16 inch thick in the next 10 ft length (length D), and 5/32 inch thick in the remainder of the rafter span (length E). These dimensions result in a range of h/t_w from 119 to 166 in the rafters. Based on the above proportions, the member webs are classified as slender both under flexure and under compression in every unbraced segment of the clear span frame, with the exception of the unbraced length (c1-c2) at the bottom of the column, which is classified as compact or noncompact under flexure.

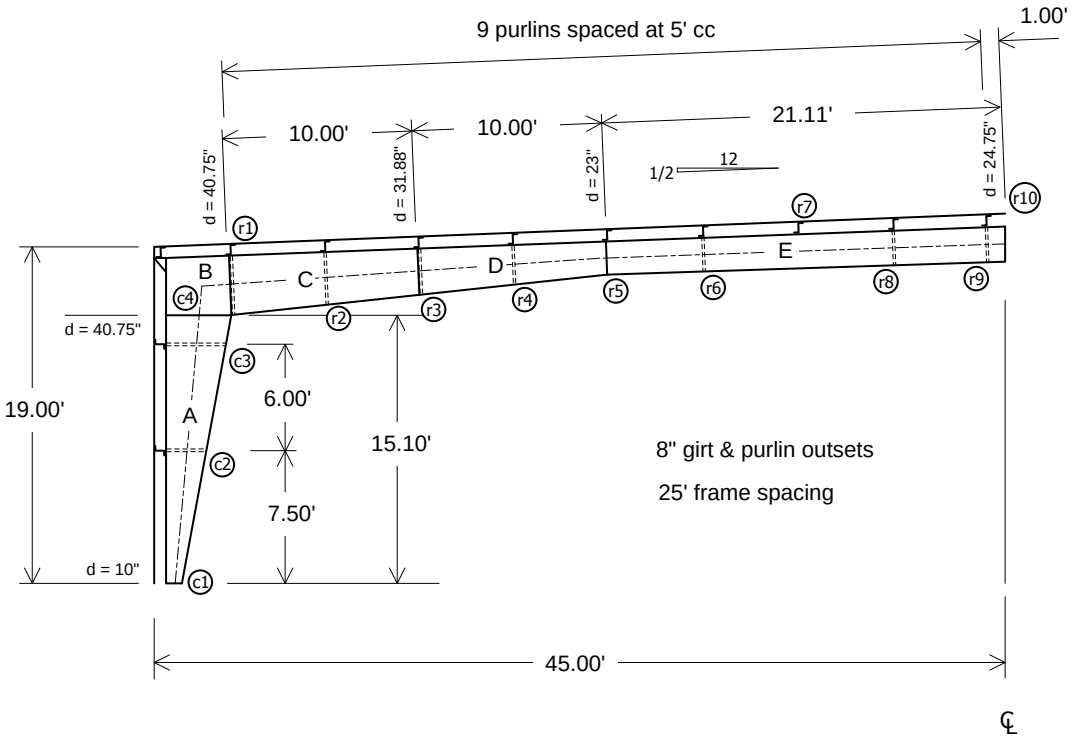

Fig. 6.1. Elevation view of 90 ft clear span frame, from Kim (2010).

Table 6.1. Summary of web and flange geometry, 90 ft clear span frame

Length	Location	Web				Inside Flange			Outside Flange		
		d (in)	t_w (in)	h/t_w*	h_c/t_w	b_f (in)	t_f (in)	$b_f/2t_f$	b_f (in)	t_f (in)	$b_f/2t_f$
A	c1	10.00	7/32	42	36	6.0	1/2	6.0	6.0	3/8	8.0
	c2	25.27		112	103						
	c3	37.49		167	157						
	c4	40.75		182	172						
B			7/32								
C	r1	40.75	1/4	160		6.0	3/8	8.0	6.0	3/8	8.0
	r2	36.31		142							
	r3	31.88		125							
D	r3	31.88	3/16	166		6.0	3/8	8.0	6.0	3/8	8.0
	r4	27.44		142							
	r5	23.00		119							
E	r5	23.00	5/32	142		6.0	3/8	8.0	6.0	3/8	8.0
	r6	23.42		145							
	r7	23.80		148							
	r8	24.25		150							
	r9	24.67		153							
	r10	24.75		154							

*For F_y = 55 ksi, the webs are compact for $h/t_w \leq 86$ and they are slender for $h/t_w \geq 130$.

6.3 Loading

The load case considered for this study is the ASD gravity load combination [Dead + Collateral + Uniform Snow] since it produces the largest moments in the frame. A load factor of $\alpha = 1.6$ is applied to this load combination to increase the ASD loads to the corresponding strength level.

The following are the loadings and load magnitudes for this frame:

i. Dead load: 1.95 psf

ii. Collateral: 3.0 psf

iii. Snow load: 21 psf

The self weight of the main frame members is included in the original design, and in all the frame analysis results from Kim (2010) and White and Kim (2006). However, the self weight of these members is not included in the following virtual test simulations.

6.4 Bracing Configuration

As described in Section 3.1.2, the column bases are idealized as flexurally and torsionally simply supported in all the frames studied in this research. That is, the member cross-section is free to rotate about its strong and weak axes and it is free to warp at the base of the frames. However, translations are restrained in all three coordinate directions and twisting is fully restrained at the column bases. In addition, as described in Section 3.1.2, open-section thin-walled beam kinematics is enforced at the column bases using multi-point constraints

The outside flanges of the columns and rafters are connected directly to outset girts or purlins. Diagonal braces to the inside flanges are indicated by the double dashed lines in Fig. 6.1. The purlins are spaced at 5 ft on center except at the knee of the frame, and the girts are located at 7.5 and 6 ft spacing starting from the base of the frame. If the girts are sufficiently restrained against out-of-plane translation by the wall panels, both of the column flanges are braced laterally at the above girt locations. The bottom flange of the rafters is unsupported at the purlin locations 20 ft and 30 ft from the inside of the knee, and the top flange at these locations is supported only via the roof diaphragm stiffness. However, otherwise both flanges are braced at each purlin location via either torsional bracing or a combination of torsional and lateral bracing.

The bottom of the panel zones at the knee is taken as a brace point for the design of the columns. This is achieved conceptually by the lateral bracing at r1 via the roof purlins and the flange braces to the inside flange at r1, and the weak-axis flexural restraint to twisting of the column from the rafter at r1. The brace points and the section transitions in Figure 6.1 are sufficiently close to one another such that the section transitions are

assumed to be located at the brace points without any significant loss in accuracy in the analysis models. The centroidal axis coordinates of the framing members are determined by working from the building envelope established by the 19 ft eave height, 90 ft span length and 0.5/12 roof slope shown in Fig. 6.1, and subtracting the 8 inch girt and purlin outsets plus the depth from the edge of the outside flange to the cross-section centroids. The total depths of the members (*d*) are shown in Figure 6.1 and in Table 6.1.

The original design of the frame uses cold-formed 16 gage, 8 inch deep Z816 sections for the girts and purlins. In this study, flexible torsional bracing from the flange diagonals and girts/purlins is modeled by torsional springs located at the centroids of the girts/purlins, as explained in Section 3.4. Generally, the combined flexibility from the axial deformation of the flange diagonal braces and the flexure of the girts/purlins should be considered in determining the torsional bracing stiffnesses. However, in this chapter, only a coarse estimate of the provided torsional brace stiffness is utilized. The main focus in this chapter is on the overall strength of the frame and the strength demands on the bracing for different magnitudes and configurations of the bracing properties. Since the flange diagonals are assumed to be attached directly to the bottom flange, no additional flexibility due to cross-section web distortion is considered here. In addition, it is assumed that there is no local deformation or slip at the connection points on either end of the flange diagonal braces. It is assumed that the girts/purlins are "rigidly pinned" to the top flange of the roof girder, i.e., there is no translation of the top flange of the roof girder relative to the bracing system. However, the purlins are assumed to not offer any direct torsional restraint at the top flange of the member. The torsional restraint by the girts/purlins is activated via the truss action of the flange diagonals.

6.5 Comparison of AISC and Simplified Bracing Requirements to Provided Values

The calculations presented in Section 2.7 use one possible interpretation/extrapolation of the AISC Appendix 6 rules to evaluate the brace strength and stiffness requirements. In these calculations, any benefits of the lateral bracing from the roof and wall diaphragms are neglected and the flange diagonal brace points are considered only as torsional braces at all negative moment locations. The relative bracing from the longitudinal X bracing system and from the roof and wall diaphragms is designed to brace the members for axial load and for positive bending moments.

As noted previously, both nodal lateral and nodal torsional braces are assumed to have equal stiffness and are assumed to be placed at constant spacing in the development of the AISC Appendix 6 equations. The torsional brace characteristics vary due to the changes in depth of the nonprismatic members and the brace spacing is not constant throughout the unbraced lengths in the frame considered here.

The required brace strength calculations presented in Section 2.8 target 2.0% of the maximum internal moment in the adjacent segments of the rafter or the column for the calculation of required brace strength of a torsional brace. The required torsional stiffness is based on restricting the brace point displacement to a specified value if the brace is loaded up to this strength requirement.

The required torsional brace strengths and stiffnesses estimated using the AISC simplified equations are summarized in Table 6.2 along with the values provided in the base design (see Section 2.7 and 2.8 respectively for the detailed calculations). Strength and stiffness requirements for the relative bracing from the wall and roof shear panels are summarized with the provided base stiffness values in Table 6.3.

Table 6.2 Summary of provided versus required brace strengths and stiffnesses assuming lateral restraint from diaphragm on the outside flange, expressed in terms of the equivalent lateral brace properties for the torsional braces.

Criterion or condition		Stiffness β_{br} (kips/in)	Strength P_{br} (kips, %)[a]
Provided torsional brace strength and stiffness at c3 (top of column) based on an upper-bound estimate of 8*EI/s*, as discussed in Section 2.7		4.66	-
Required to brace the frame at c3 for the loading from the ASD load combination, $\frac{P_r h_o}{2} + \frac{M_r}{C_b} = 4610\,\text{in - kips}$	AISC	20.9	1.00, 0.88
	Simplified	16.8	2.50, 2.0
Provided torsional brace strength and stiffness at r1 (at the connection of the rafter to the knee) based on an upper-bound estimate of 8*EI/s*, as discussed in Section 2.7		3.91	-
Required to brace the frame at r1 for the loading from the ASD load combination, $\frac{P_r h_o}{2} + \frac{M_r}{C_b} = 4790\,\text{in - kips}$	AISC	19.7	0.78, 0.66
	Simplified	15.8	2.4, 2.0

(a) Percent values are $M_{br}/(P_r h_o/2+M_r/C_b)$ written as a percentage.

As discussed in the previous examples, various simple models can be used to estimate the torsional stiffness provided by the bracing diagonals combined with the girts or purlins. In this study, a basic beam model is used to estimate the stiffness provided by typical flange diagonal braces along with representative minimum size girts and purlins. The actual stiffness provided by the bracing diagonals and the girts or purlins depends to some extent on the restraint provided by the adjacent frames at the opposite ends of the girts and purlins from the frame under consideration (see Fig. 2.16). It should be noted that in this approach, it is assumed that the purlins and the flange diagonals do not fail before a sufficient amount of the frame strength is developed.

Table 6.3 Summary of provided versus required brace strengths and stiffnesses, for the relative (shear panel) bracing at the top of the column and at the knee.

Criterion or condition		Stiffness G' (kips/in)	Strength v_{br} (lb/ft)
Provided assuming CS wall panels with 12 inch screw spacing at the base and eave		3.52	61.2
Required to brace the segment r0-c3 on the column for the ASD load combination	AISC	0.44	5.3
	Simplified	0.44	13.3
Provided assuming CS roof panels with 12 inch screw spacing		4.2	122
Required to brace the segment r1-r2 on the rafter for the ASD load combination	AISC	0.38	4.53
	Simplified	0.38	11.4

6.6 Critical Geometric Imperfections for Virtual Simulation Analysis

The critical imperfections applied to this frame have been discussed in Section 3.3. The influence lines for the compression flange out-of-straightness and out-of-alignment imperfections for the base flexible bracing model are presented in Fig. 3.6, and the corresponding flange out-of-alignment and out-of-straightness are summarized in Fig. 3.8. For the virtual simulation analysis of the frame based on the assumption of rigid lateral bracing, discussed in the next section, a single brace out-of-alignment is placed both at r1 and r9. For both the flexible and rigid bracing cases, the frame is modeled as initially out-of-plumb to the right hand by $0.002h$ in its own plane, where h is the height above the base (i.e., all the points are shifted by $0.002h$ to the right relative to the perfect geometry).

6.7 Base Virtual Simulation Results

In this section, the system response of the 90 ft. clear span frame is analyzed for both rigid bracing and the base flexible bracing conditions described previously. The stiffness contributions from the roof and wall diaphragms are neglected in these analyses. For the base flexible bracing case, the intent is to evaluate how well the frame performs in the absence of any significant restraint from the wall and roof diaphragm panels. For the rigid bracing case, the frame is assumed to be rigidly restrained in the out-of-plane direction at the connection of all the girts and purlins to the outside flanges, as well as at the connection of the flange diagonal braces to the inside flanges of the frame members. Therefore, the stiffness of the wall and roof diaphragms is irrelevant for the rigid bracing case. The imperfections for both of these cases are obtained as described in Sections 6.6 and 3.3 and are aimed at maximizing the brace forces at the knee and at the r9 brace locations.

6.7.1 Rigid Bracing

Figure 6.2 shows the load-deflection response of the frame with rigid bracing under the applied gravity load. The vertical deflection at the ridge is plotted on the horizontal axis whereas the fraction of the reference ultimate strength load combination is plotted on the vertical axis. Since this frame is designed using ASD, the reference ultimate strength loading is taken as $\alpha = 1.6$ of the targeted ASD Dead + Collateral + Snow load combination.

The unity check for this frame is 1.10 using the AISC Design Guide 25 checks (Kaehler et al. 2011) for the selected ASD load combination (Kim 2010). Therefore, the frame is not necessarily expected to support the full ASD strength loading. As discussed

at the beginning of Chapter 3, a structure will satisfy the AISC ASD strength criteria approximately if virtual simulation models that use the nominal elastic stiffness properties (rather than reduced elastic stiffnesses) reach a fraction of the ASD ultimate strength loading (1.6 times the ASD load) of approximately $\Omega/\alpha = 1.67/1.6 = 1.04$. In Fig. 6.2, the maximum fraction reached is 0.95. The ratio of 1.04 to 0.95 is 1.09, which closely matches with the 1.10 unity check value from Kim (2010). Note that because of second-order amplification effects, one cannot in general assume that a frame such as this one would reach its limit load at 1.04/1.10 = 0.95 of the ASD ultimate strength loading. However, this ratio provides an accurate estimate for the structure being examined here because the frame's overall second-order amplification is small.

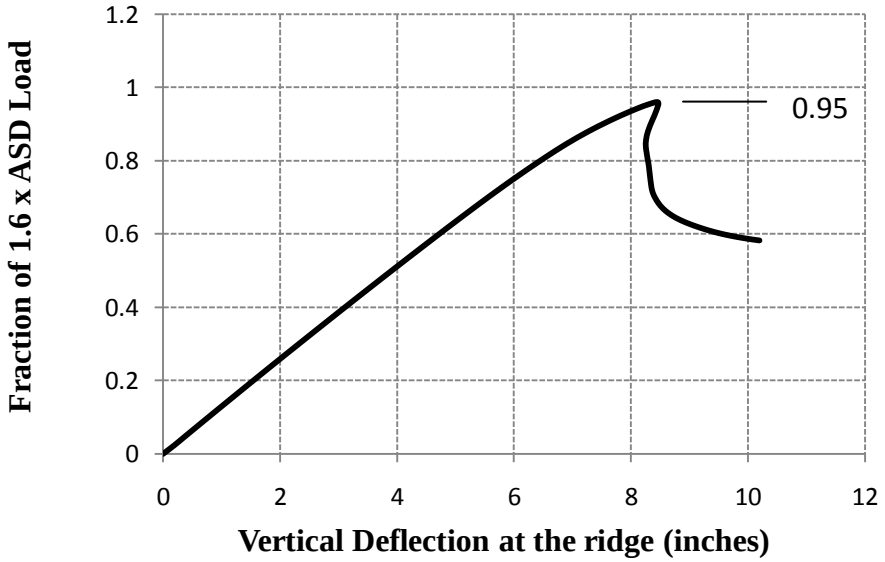

Fig. 6.2. Load-deflection response, 90 ft clear span frame, base rigid bracing condition.

Figure 6.3 shows the brace force demand at the inside flange of the knee (at r1) for the rigid bracing case. The brace force demand is presented as a percentage of the moment at r1 at the peak load for the rigid bracing condition $M_{knee}^{\#}$.

The maximum brace force demand occurs at the system collapse load and is 1.9% of the corresponding moment at r1. It should be noted that this value is close to 2%, the value used in simplified equations to determine brace strength and stiffness demands. If Eq. C-A-6-4b from 2010 AISC Commentary to Appendix 6 is used, the brace force demand at r1 is estimated to be 1% of the internal moment. The brace force demand falls off rapidly away from the critical knee region. It is 0.7% of the internal moment at the brace c3 close to the top of the column and 0.1% at r2 on the rafter. This reduced demand may be attributed in part to the fact that the selected geometric imperfection maximizes the brace forces at the knee. The imperfection that maximizes the brace force at r2 or c3 gives a higher demand at that brace point but gives a smaller brace force demand at the knee.

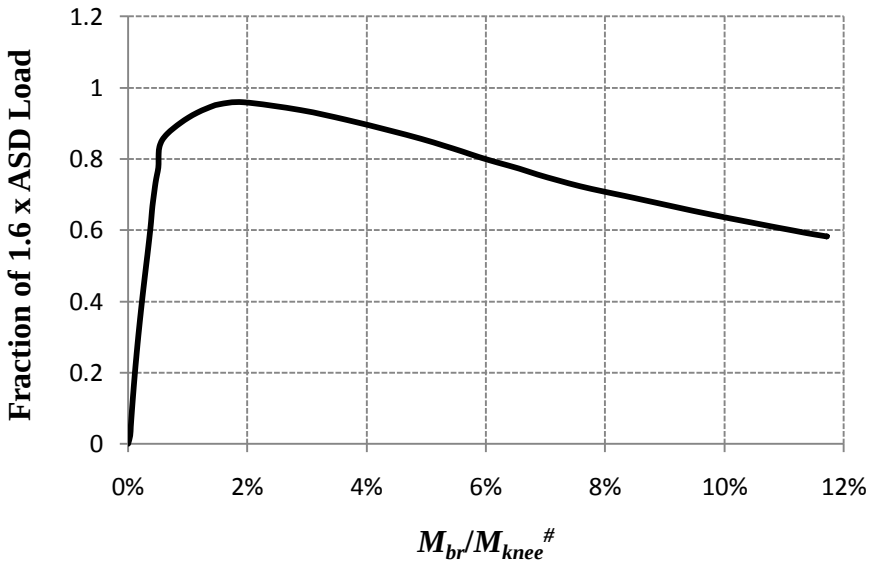

Fig. 6.3. Brace force demand at r1, base rigid bracing condition, $M_{knee}^{\#}$ = corresponding moment at r1 at the peak load.

6.7.2 Flexible Bracing Based on the Specified Girt and Purlin Sizes, Neglecting Wall and Roof Diaphragm Stiffnesses

Figure 6.4 shows the load-deflection response of the frame for the flexible bracing condition, neglecting the stiffness contributions from the wall and roof diaphragms. The fraction of the ASD load applied to the frame is shown on the vertical axis and the vertical deflection at the ridge is shown on the horizontal axis. The stiffness of the torsional bracing is taken as $8EI/s$=6380 in-kips/rad., where s is the frame spacing. The assumptions behind this estimate have been discussed previously in Section 2.7.

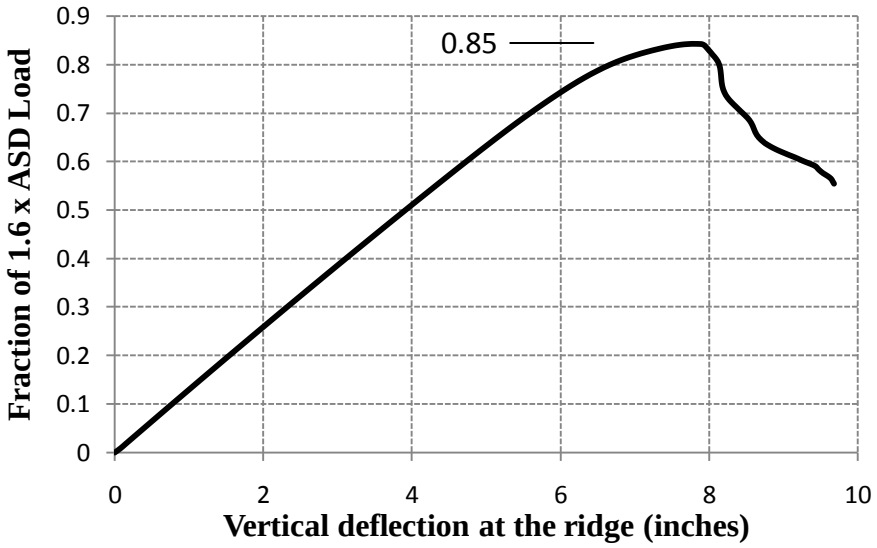

Fig. 6.4. Load-deflection response, 90 ft clear span frame, base flexible bracing condition.

For the flexible bracing case, the frame fails at 0.85 of the design load level, that is, the strength of the frame is reduced by 1 - 0.85/0.95 x 100 = 11 % due to the flexibility of the bracing. The maximum moment at r1 from the virtual test simulation is 490 ft-kips. Figure 6.5 shows the brace force demand at r1 as a percentage of the moment at r1 at the peak load for the flexible bracing condition, $M_{knee}^{\#\#}$.

The brace force demand at r1 is 3.3% of the corresponding moment, which is more than the approximated 2% considered in the simplified equations. Eq. A-6-9 from the

2010 AISC Appendix 6 estimates this to be 2.4% of the member internal moment. Similar to the response for rigid bracing, the brace force demand is significantly smaller as one moves away from the critical knee region.

The stiffness demand for the bracing calculated via the AISC equations is 32,200 in-kips/rad and the demand estimated from the simplified equations is 25,800 in-kips/rad. Both these estimates are well above the stiffness value used for the virtual test simulation, i.e. 6380 in-kips/rad.

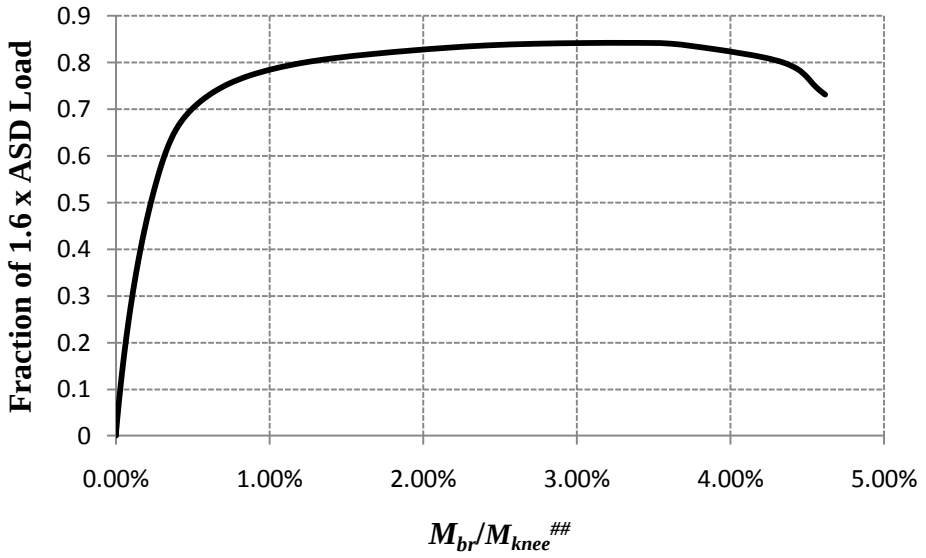

Fig. 6.5. Brace force demand at r1, 90 ft clear span frame, base flexible bracing condition, $M_{knee}^{\#\#}$ = corresponding moment at r1 at the peak load.

For both bracing cases discussed above, the frame has a similar failure mode. The web close to the knee buckles in the out-of-plane direction and the flange at that location buckles locally. This failure mode is illustrated in Figure 6.6.

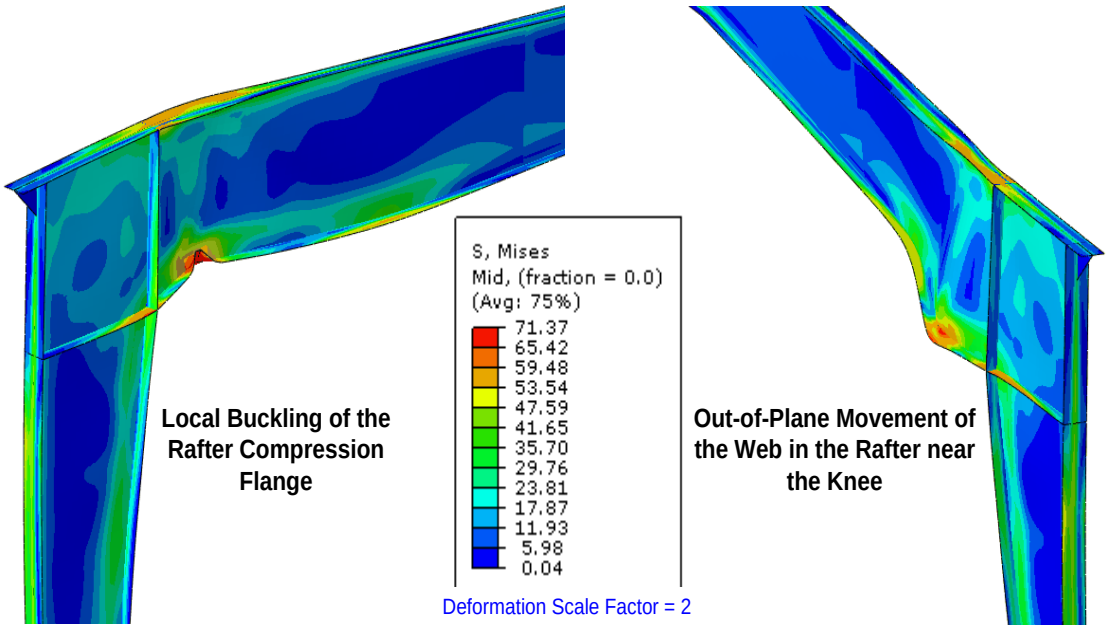

Fig. 6.6. Final failure mode (at the end of the analysis) for the 90 ft clear span frame showing web and flange local buckling and the von-Mises stress contours at the mid-surface of the plates.

For the flexible bracing case, since the stiffness contribution from the diaphragms is not considered, the top flange of the rafter is not braced in the out-of-plane direction at r5 and r7. As a result, the top flange deflects in a clear zigzag pattern involving a lateral displacement at these purlin locations. However, these deflections are secondary to the deflections shown in Fig. 6.6. Out-of-plane restraint from the purlins via the stiffness contributions from roof diaphragm helps keep the top flange of the rafter straight.

The brace force demand at c3 (the brace closest to the top of the column) is 1.7% of the member internal moment at that location, which is essentially the same as the demand at r1. This behavior can be attributed to two factors: (1) the imperfection that maximizes the brace force at r1 is very close to the imperfection that maximizes the brace force at c3, and (2) these braces are located relatively close to each other. These strength demands are slightly lower than those predicted by both the AISC and the simplified equations.

Figure 6.7 shows the maximum brace force demand at r2, obtained from an analysis in which the imperfections are specified to maximize the brace force at r2. These imperfections are obtained by the influence line approach in a similar fashion to the imperfections shown in Fig. 3.8. The brace force demand at r2 at the limit load is 0.8% of the internal moment at the knee. This is significantly smaller than the maximum brace force demand at r1 (3.3%). It should be noted that the system strength for this case is 0.89 of the ASD ultimate strength loading, which is 6% higher than in the virtual simulation where the brace force demand at r1 is maximized.

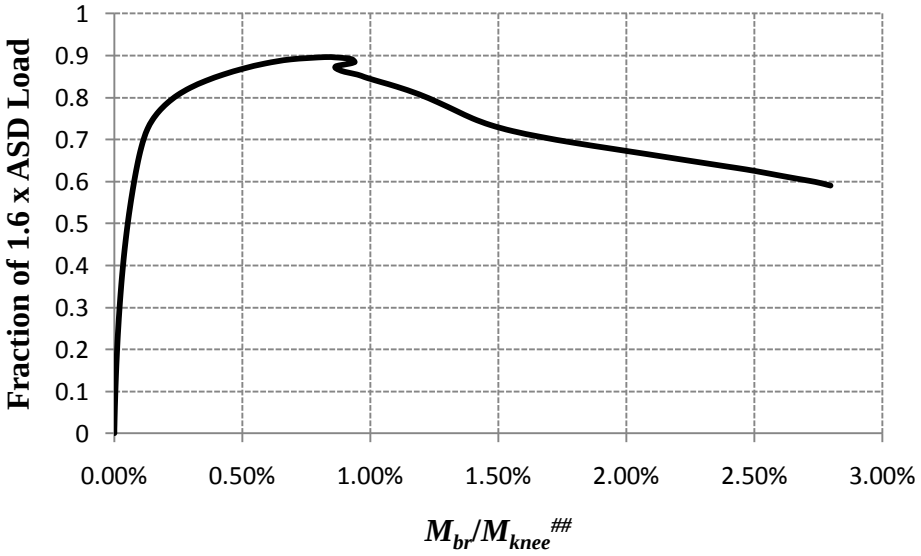

Fig. 6.7. Brace force demand at r2, 90 ft clear span frame, base flexible bracing condition, $M_{knee}^{\#\#}$ = corresponding moment at r1 at the peak load.

It is apparent that the reduction in the strength of this frame relative to the value for rigid bracing (11 %) is rather small given that the provided torsional brace stiffnesses are only 4.66/26.4x100 = 18 % at r1 and 3.91/19.6x100 = 20 % at c3 of the values indicated by the AISC equations and 4.66/16.8x100 = 28 % at r1 and 3.91/15.8x100 = 25 % at c3 of the values indicated by the simplified equations. Therefore, it is important to

understand how the strength of the frame and the strength demands for the braces changes as a function of the magnitude and distribution torsional bracing stiffnesses.

6.8 Effect of Varying Torsional Brace Stiffnesses

Several variations of the 90 ft frame are considered in this section to study the effect on the system behavior due to: (1) changes in the torsional brace stiffness, and (2) the use of unequal torsional brace stiffnesses along the length of the members.

First, the stiffness of the torsional brace is varied just at r1 and the change in the strength of the system is observed. As noted previously, the frame was designed with 16 gage, 8 inch deep Z816 purlins (I = 8.15 in^4). Based on the assumption that the adjacent frames do not buckle, the stiffness provided by these purlins is taken as *8EI/s*. The load-deflection responses for this case are shown in Fig. 6.8 as the 100 % value. In the figure legend, the other values are the percentage of the torsional stiffness provided by the above 8 inch purlins.

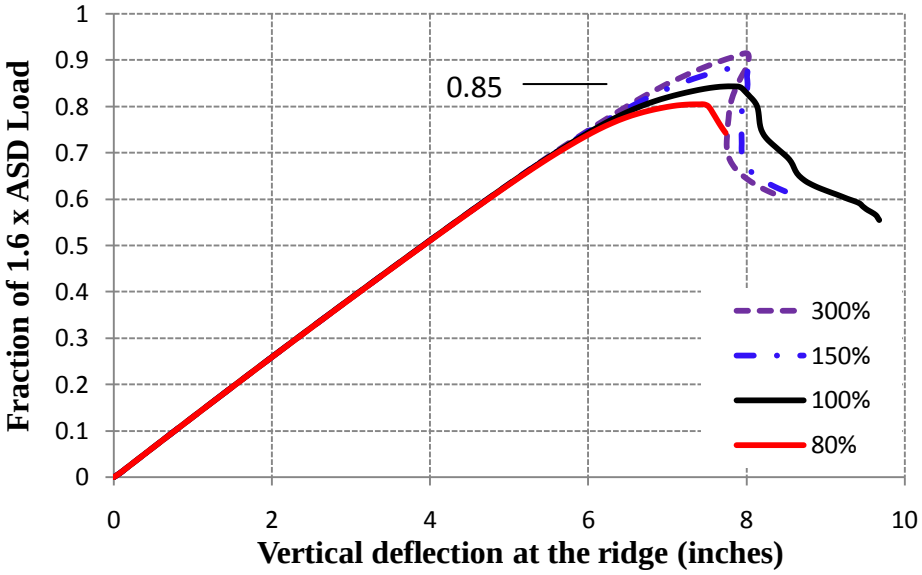

Fig. 6.8. Load-deflection response, 90 ft clear span frame with all the torsional bracing stiffnesses increased or decreased relative to values for the base example.

Figure 6.8 shows that increasing the torsional brace stiffness increases the capacity of the frame, but the increase in capacity is only (1-0.92/0.85)x100 = 8% for a stiffness that is 300 % of the reference value. However, if the stiffness is decreased by only 20 %, the strength of the frame is reduced by nearly the same amount. As noted previously, the estimated stiffness provided by Z816 purlins is sufficient to develop 0.85 of the ASD ultimate strength load level for the frame, which corresponds to 0.85/0.95x100 = 89 % of the rigidly braced frame capacity. However, if the stiffness provided is less than the upper-bound value taken for the Z816 purlins (for example if the adjacent frames buckle simultaneously, in which case the stiffness provided is reduced by approximately 50%), the frame will fail at a significantly smaller load.

It should be noted that the torsional brace characteristics vary slightly due to changes in the depth of the section. In the next frame variation, the specified torsional brace stiffnesses also are varied along the lengths of the members. Specifically, it is observed that the brace forces at the locations removed from the critical knee region are quite small in the above virtual test simulations. Therefore, to observe whether a dramatic decrease in the stiffnesses at the "non-critical" brace locations will have an effect on the overall behavior, the torsional stiffnesses at girts c2 and c3 and at purlins r1, r2 and r3 are kept the same as in the base design, but all of the other torsional stiffnesses are reduced by 50 %. Figure 6.9 shows that these changes have essentially no effect on the frame response. This behavior may be attributed to the following: (1) the imperfection applied to maximize the brace force close to the knee does not have much effect away from that region, (2) the frame moments are smaller away from the critical regions, and (3) for the lengths of the rafters closer to the ridge, the inside flange is in tension.

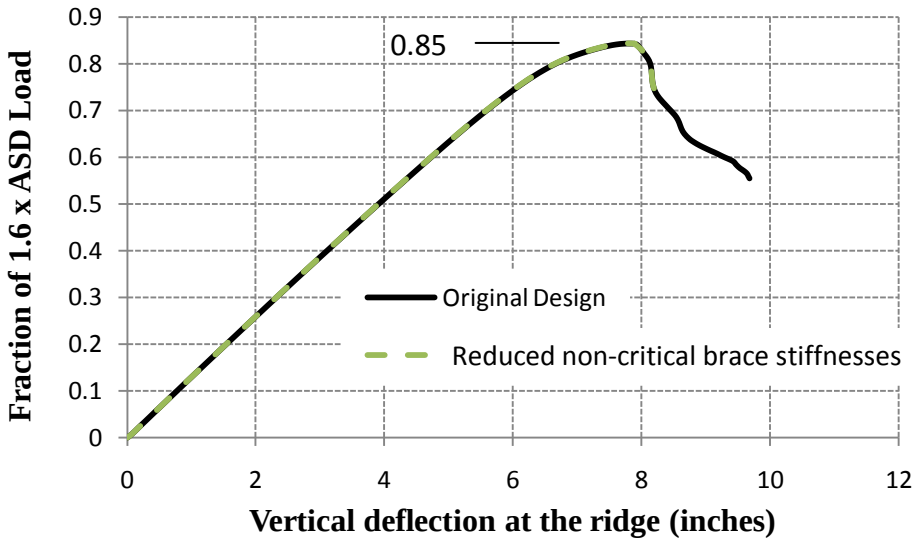

Fig. 6.9. Load-deflection response, base 90 ft clear span frame example with the torsional brace stiffnesses reduced by 50 % at all locations except c2, c3, r1, r2 and r3.

Figure 6.10 shows the knuckle curve for the 90 ft clear span frame obtained by varying torsional brace stiffnesses, keeping all of the stiffness values equal to one another. The vertical axis shows the fraction of load capacity for the rigidly braced frame, expressed as $M_{max}/M_{knee}^{\#}$, where $M_{knee}^{\#}$ is the moment at r1 at the peak load for the rigid bracing condition. This curve shows that the frame strength is relatively unchanged with variations in the brace stiffness at high brace stiffness values but becomes more sensitive at lower brace stiffness. It also shows that the stiffness provided by the representative minimum size girts and purlins for this frame (6380 in-kips/rad) is close to the critical brace stiffness at which a reduction in stiffness relative to this upper-bound prediction would lead to a significant drop in the frame strength. The AISC estimate of the brace stiffness required at r1 for this case is β_T = 32,200 in-kips/rad (or an equivalent lateral brace stiffness at r1 of $32{,}200/40.375^2$ = 19.7 kips/inch) and the simplified equations estimate the required stiffness at r1 as β_T = 25,800 in-kips/rad (15.8 kips/inch).

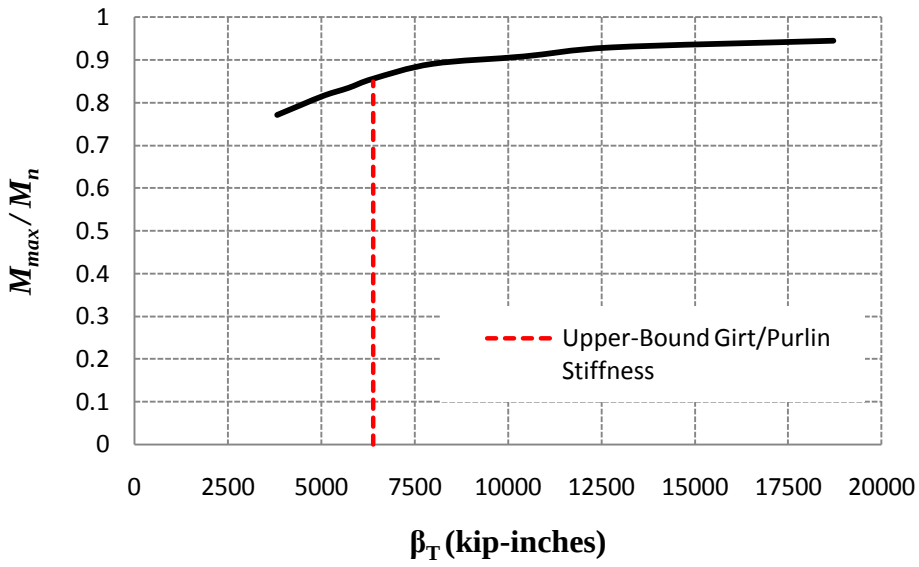

Fig. 6.10 Member strength behavior knuckle curve, 90 ft clear span frame, $M_{knee}^{\#}$ = moment at r1 at the peak load for the rigid bracing condition.

The reason that the estimated stiffness requirements are so high compared to values that would appear to be very close to being sufficient may be attributed to the fact that the AISC and the simplified equations do not adequately account for the resistance from the members (both the column and the rafter) as well as the panel zone to out-of-plane movement at the inside of the knee. As noted in Section 2.7.6, if a lower-bound *K* factor of 0.5 is assumed in calculating $P_{e.eff}$, the estimated stiffness requirements are only slightly larger than the upper-bound torsional bracing stiffness provided by the representative minimum size purlins. More importantly, the corresponding β_T = 8000 in-kips/rad. develops essentially 90 % of the strength of the rigidly-brace frame.

Figure 6.11 shows the maximum brace force demand at r1 versus the brace stiffness. This curve indicates that the brace force is maximum when the brace stiffness is in the vicinity of the "critical" value from Fig. 6.10. This behavior is consistent with the responses associated with the knuckle curves in the previous chapters, and again, it would

appear that the point corresponding to the maximum brace force demand might be considered as a useful indicator of the "true" knuckle value. The brace force tends to decrease dramatically with a reduction in the brace stiffness relative to this value, apparently because the frame capacity is also decreasing dramatically, and it tends to decrease somewhat more gradually as the brace stiffness is increased relative to the knuckle value because of the increased effectiveness of the brace and the associated reduction in the brace point displacement.

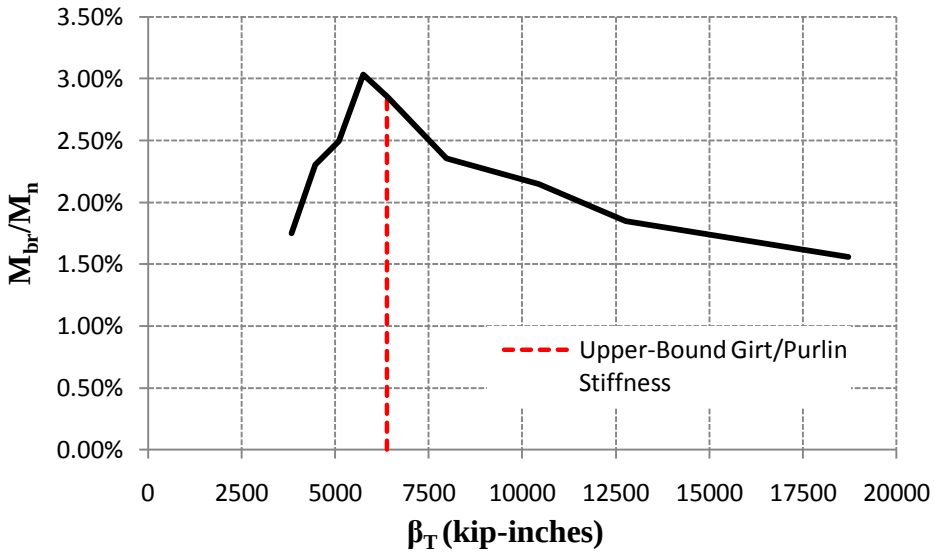

Fig. 6.11 Brace force demand at r1 versus the brace stiffness, 90 ft clear span frame, $M_{knee}^{\#}$ = moment at r1 at the peak load for the rigid bracing condition.

Figure 6.5 previously showed that, when using the provided base torsional bracing stiffnesses in the 90 ft. clear span frame, the brace force at r1 was 3.3 % of the moment $M_{knee}^{\#\#}$ at the limit load of the structural system. However, the curve for the bracing force versus the applied load level is relatively flat as the limit load is approached. Therefore, the limit load of the structural system is nearly achieved when the brace force reaches 2.0 %, the required strength recommended in the simplified bracing design procedure. Table 6.4 supplements this information in Fig. 6.5 by showing the strength demands at r1 and

c3 from the base virtual test simulation at 90, 95 and 100% of the system limit load. One can observe that the strength demand on the braces does not exceed 2 % until more than 95 % of the limit load is applied to the frame.

Table 6.4 Summary of strength demand at the critical torsional braces from the base virtual test simulation, β_T = 6380 in-kips/rad, no consideration of wall or roof diaphragms.

Location	Strength Demand at 90% of Limit Load P_{br} kips, %	Strength Demand at 95% of Limit Load P_{br} kips, %	Strength Demand at Limit Load P_{br} kips, %
r1	1.0, 0.7	1.8, 1.2	4.8, 3.3
c3	0.8, 0.6	1.4, 1.0	3.34, 2.5

6.9 Evaluation of Bracing Demands at Locations Away from the Critical Regions

The above studies focus on the strength and stiffness demands on the braces at the critical locations. The results also show that the demands are significantly lower away from the critical regions. But as mentioned before, the imperfections considered do not maximize the demands at brace points away from the critical region.

In this section, imperfections are applied that maximize the brace demands at the brace r9 closest to the ridge. It should be noted that this brace is located in the positive moment region on the rafter. Figure 6.12 shows the brace force demands at r9 for two cases: (a) Case 1: the imperfection applied maximizes the brace force at r1, and (b) Case 2: the imperfection applied maximizes the brace force at r9. The brace moments are shown as a percentage of the moment at r1, for ease of comparison of the brace force magnitudes.

For the first case, the brace force demand at r9 is 0.05% of the moment at r1 and for the second case, it is 0.07% of this moment. Therefore, it can be inferred that, in general, the brace force demands away from critical regions tend to be significantly lower that the demand at or close to the critical regions. In terms of design, this means that a smaller size brace potentially can be provided at the non-critical regions without affecting the capacity of the frame. Of course, frames generally must be designed for an envelope of forces from various load combinations. However, for the 90 ft clear-span frame, the load combination considered here also produces the largest moment at r9.

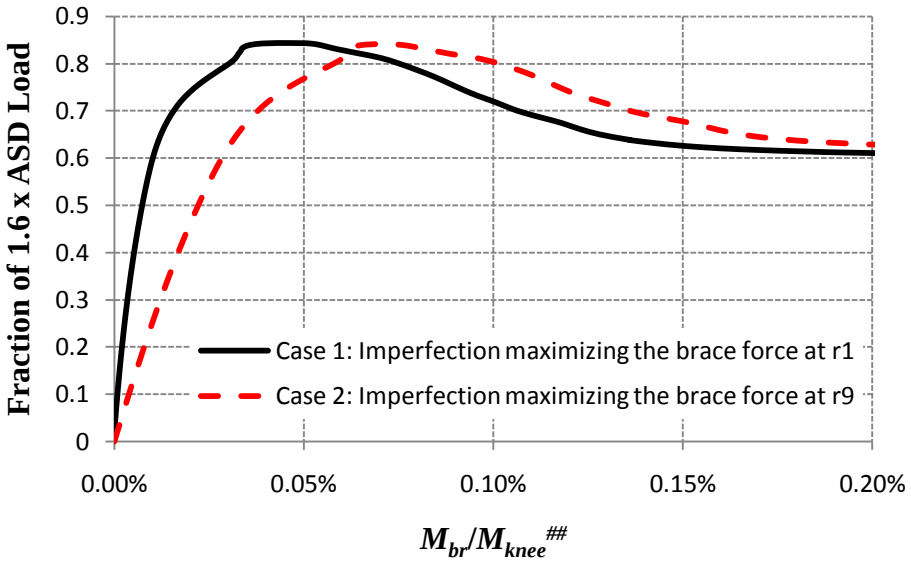

Fig. 6.12. Brace force comparison at r9 for different imperfection cases, $M_{knee}^{\#\#}$ = moment at r1 at the peak load for the flexible bracing condition.

The stiffness demands away from the critical regions are also lower than those close to the critical regions. Reduction of brace stiffness away from the critical regions does not have any effect on the strength of the frame. Hence, lower brace stiffness can be provided in these regions apparently without any significant consequence.

6.10 Effect of Simplified Bracing Layout

It is possible that the location of diagonal braces close to the knee both in the rafter at r1 and in the column at c3 may have a synergistic effect in terms of restraining the out-of-plane movement at the inside corner of the panel zone in the 90 ft clear span frame . To help understand this behavior, this bracing layout is modified such that the out-of-plane movement at the inside corner of the knee is restrained only by a single set of flange diagonal braces at r1. The girt close to the top of the column is moved to the bottom of the panel zone (i.e., the girt at c3 is moved to c4) and the flange diagonal from this girt is removed. Figure 6.13 shows the frame with this modified bracing configuration. To account for the loss of bracing stiffness close to the knee, the stiffness of the brace at r1 is doubled. This can be achieved by either providing two Z816 purlins or one larger purlin with twice the stiffness.

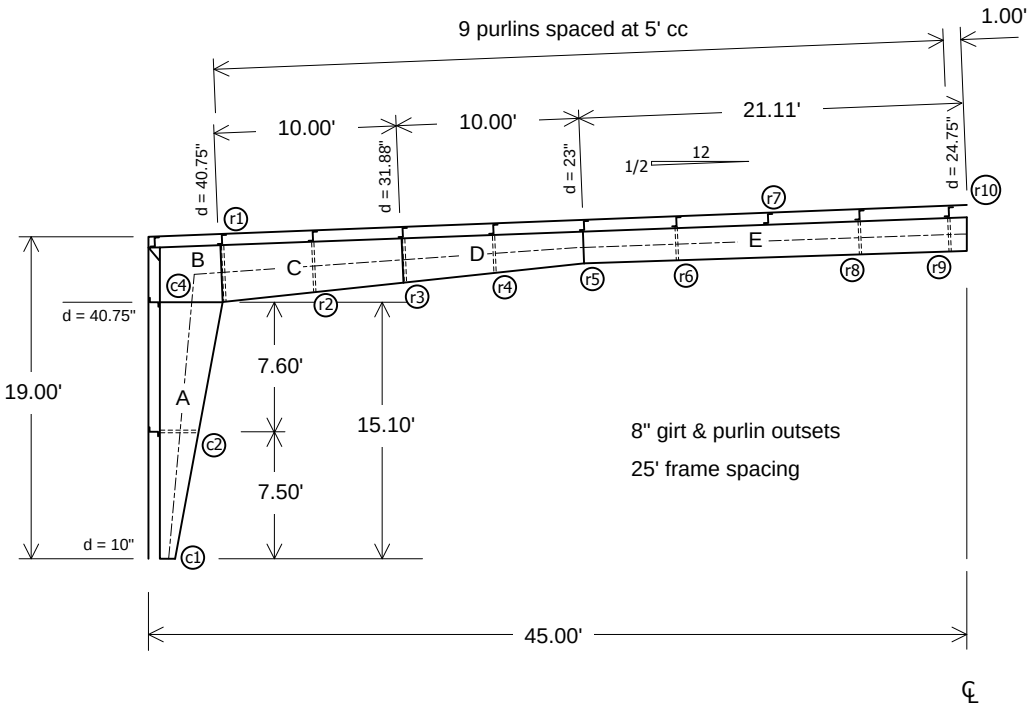

Fig. 6.13., Elevation view of the 90 ft clear span frame with simplified bracing near the knee.

The imperfection pattern applied for the virtual test simulation of this frame again aims at maximizing the brace force at r1 and is developed using the influence line approach. For this frame, the critical imperfection puts a significant twist in the column. Since there is no flange diagonal close to help restrain this twist at the top of the column in the frame with the simplified bracing layout, the diaphragm stiffness from the wall and roof panels is considered in this example. If the girt is removed and no lateral or torsional restraint is added to the column flanges, the column inside flange buckles very early in the loading before the frame reaches the desired strength level. Assuming 12 inch screw spacing at the ridge and eave, the stiffness of the roof panels are taken as $G' = 4.2$ kips/in and assuming 12 inch screw spacing at base and eave, the stiffness of the wall panels are taken as $G' = 3.52$ kips/in.

When analyzed for the rigid bracing condition, the behavior of this frame is similar to that for the base 90 ft frame discussed previously. Figure 6.14 shows the load-deflection response of the modified frame for the flexible bracing condition.

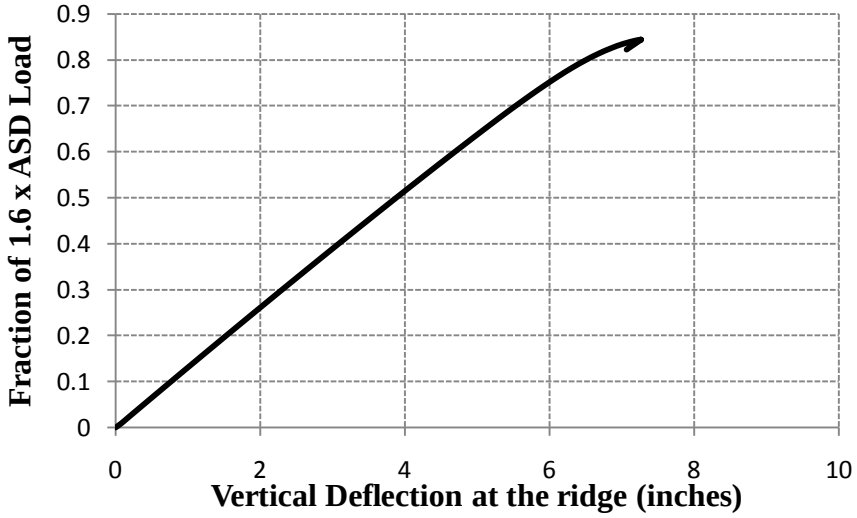

Fig. 6.14 Load-deflection response, 90 ft clear span frame with simplified bracing layout, flexible bracing condition.

The frame reaches its maximum capacity with a maximum moment at r1 at a peak load level of 0.84 of the reference load. Figure 6.15 compares the brace force demand at r1 for the frame with the simplified bracing layout to the base frame with the original bracing layout as discussed in Section 6.2.

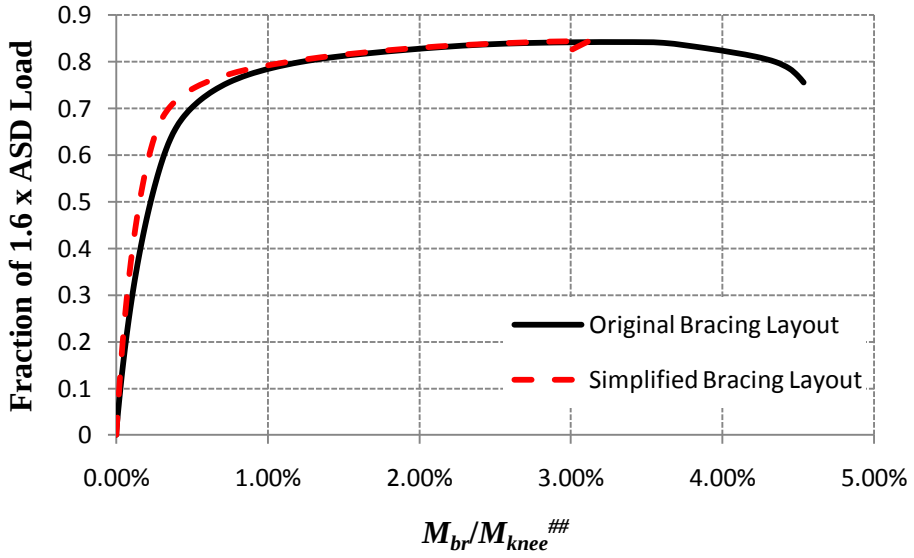

Fig. 6.15. Brace force demand comparison, 90 ft clear span frame with original and simplified bracing layout, $M_{knee}^{\#\#}$ = corresponding moment at r1 at the peak load for the flexible bracing condition.

The system behavior does not change significantly and the brace force demand for the simplified bracing layout is almost the same as the brace force demand for the original bracing layout. The brace force demand at r1 for the simplified bracing layout is 3.1% of the corresponding internal moment at the frame limit load. It is emphasized that the torsional brace stiffness at r1 is doubled to account for the removal of the girt at c3, close to the top of the column, in addition to the adding the wall and roof diaphragms to the model. The brace at r1 restrains the weak axis bending of the column in addition to the bending restraint it provides to the rafter. Also, the diaphragm reacts against the brace at

r1 to provide restraint to the twisting of the column. If the brace at r1 is not doubled in stiffness, the capacity of the frame is only 0.77 of the ASD ultimate strength loading.

Figure 6.16 shows the maximum brace force demand at r2, i.e., the brace force at r2 with the imperfections applied to maximize the demands at this location. The brace force demand at the limit load is 0.7% of the internal moment at the knee. This is significantly smaller than the maximum brace force demand at r1 (3.1%). The frame reaches a load level of 0.88 of the reference load, 5% higher than the case when the brace force at r1 is maximized.

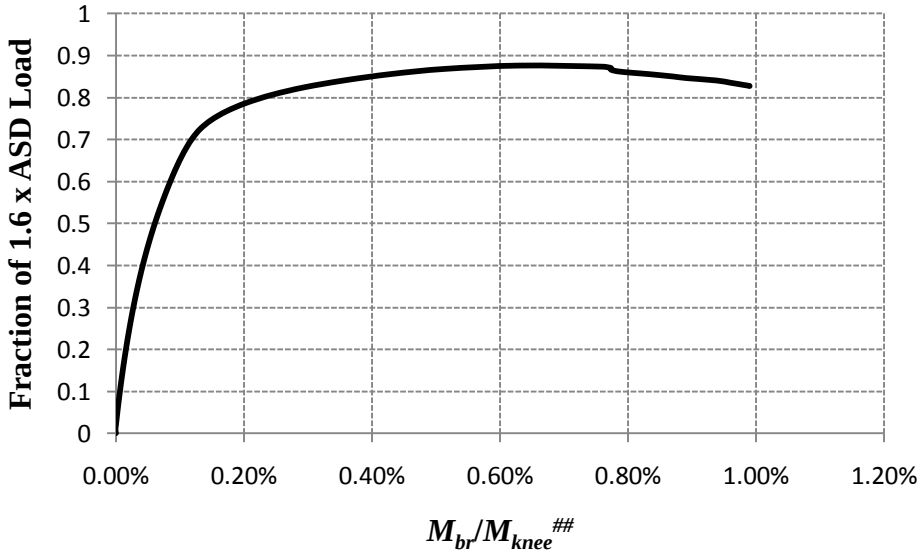

Fig. 6.16. Brace force demand at r2, 90 ft clear span frame with simplified bracing layout, base flexible bracing condition, $M_{knee}^{\#\#}$ = corresponding moment at r1 at the peak load.

Table 6.5 supplements Fig. 6.15 by providing an indication of the brace strength demands at r1 at 90, 95 and 100 % of the limit load for the frame with the simplified bracing layout. One can again observe that the force in the brace at r1 does not exceed 2.0 % until more than 95 % of the limit load is applied.

Table 6.5 Summary of strength demand at the critical torsional brace at r1 for the frame with the simplified bracing layout, from virtual test simulation.

Strength Demand at 90% of Limit Load P_{br} kips, %	Strength Demand at 95% of Limit Load P_{br} kips, %	Strength Demand at Limit Load P_{br} kips, %
0.9, 0.6	1.8, 1.2	4.7, 3.2

6.11 Effect of Increasing the Flange Widths

One of the key attributes of the AISC torsional bracing equations is their ability to include a significant contribution from the resistance of a member to brace point movement, via the I_{eff} term in Eq. (2-31). One can observe from this equation that if the input parameters to this equation, C_{tT}, L_b, M_r, C_b, and n_T, are all the same for two beams, the beam with the larger I_{eff} will have a smaller estimated bracing stiffness requirement, and via Eq. (2-34), a smaller estimated bracing strength requirement. The AISC nodal column and beam bracing equations also work this way to some extent, via L_q. Therefore, in cases where the bracing demands are too large for a given set of flange bracing components, one way of solving the problem is to increase the member I_{eff} or lateral bending rigidity. As such, it is useful to consider the effect of increasing the flange widths in the 90 ft clear span frame.

In this section, all the flange widths of the 90 ft clear span frame with the simplified bracing arrangement are increased from 6 inches to 8 inches to evaluate the influence on the brace force demands. All of the other section dimensions are kept the same as in the previous example. The strength of the frame is of course increased due to the larger flange areas. As in the previous sections, the virtual test simulation focuses on the

behavior of the structure all the way up to its maximum load capacity. Figure 6.17 compares the brace moment at r1 for the design with 8 inch flanges to the one with 6 inch flanges studied in Section 6.10 for the rigid bracing case.

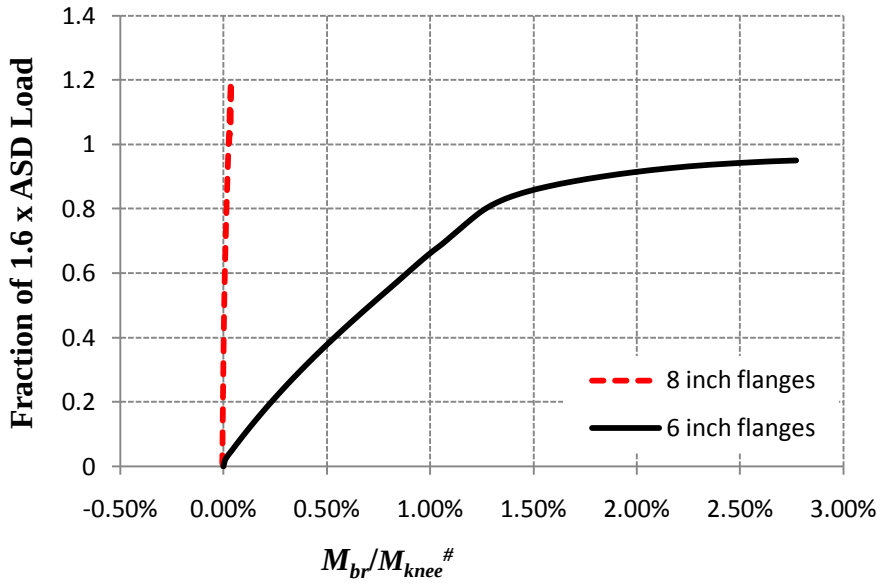

Fig. 6.17. Brace force comparison at r1, 6 inch vs 8 inch flanges, rigid bracing condition, $M_{knee}^{\#}$ = corresponding moment at r1 at the peak load.

For the frame with wider 8 inch flanges, the internal moment at r1 at the limit load is much larger than in the frame with 6 inch flanges. However, the brace moment at r1 decreases substantially as a percentage of the internal moment at this location as the flange width is increased.

Figure 6.18 compares the brace forces at r1 for the flexible bracing cases with the two different flange widths. Again, it can be seen that the brace force demand as a percentage of the internal member moment is substantially smaller for the frame with wider flanges.

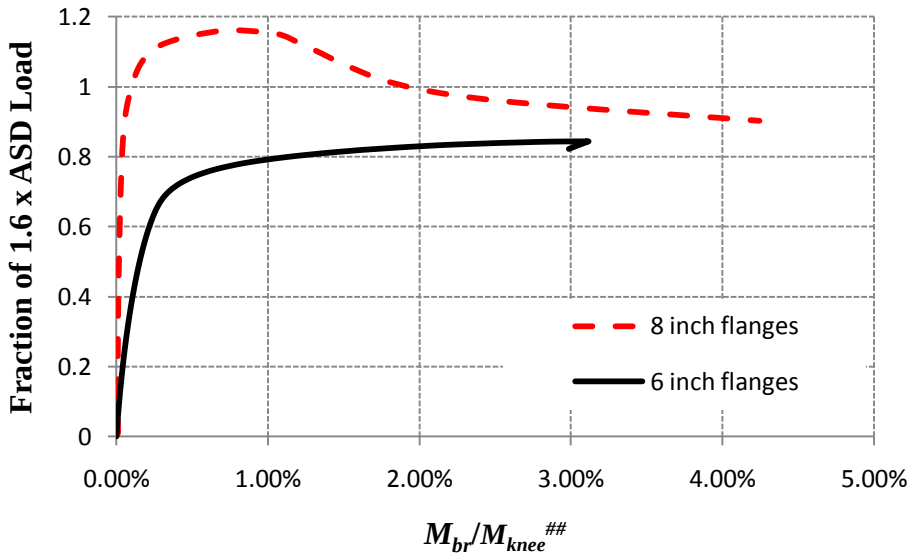

Fig. 6.18. Brace force comparison at r1, 6 inch vs 8 inch flanges, flexible bracing condition, $M_{knee}^{\#\#}$ = moment at r1 at the peak load.

There are several likely reasons for the above behavior:

1. The increased member effective moment of inertias as discussed at the beginning of this section.
2. Local flange buckling. The modified frame clearly fails due to flange local buckling close to the knee. The web out-of-plane displacement is limited and the flange local buckling primarily involves a twisting of the flange about the web-flange juncture. Hence, the brace point displacement at r1 is small, and since the brace forces are proportional to the brace point displacement, the brace forces also are small. In other words, the flange local buckling tends to relieve the bracing demands required to restrain lateral torsional buckling (at least up to the point where the maximum capacity of the frame is reached). Separate preliminary studies of individual beams with similar changes in the flange widths show a significant reduction in the brace forces at the ultimate strength limit, apparently due to this effect.

3. The column and the panel zone provide substantial restraint to lateral bending, twisting, and warping displacements at the end of the rafter, since the predominant failure mode is in the rafter near the knee and the column does not buckle. By increasing the flange widths, as well as the connection plate and continuity plate widths at the panel zones, the resistance provided by the panel zone and the column to the above displacements at the on-set of the local buckling in the rafter is substantially increased.

The above behavior certainly merits further investigation. Figure 6.19 shows the knuckle curve for 90 ft frame with the simplified bracing configuration and the 8 inch flanges. The vertical axis shows the fraction of load capacity of the flexibly braced frames, expressed as $M_{knee}/M_{knee}^{\#}$, where M_{knee} is the moment in the rafter at r1 at the peak load and $M_{knee}^{\#}$ is the moment at r1 at the peak load for the rigid bracing condition.

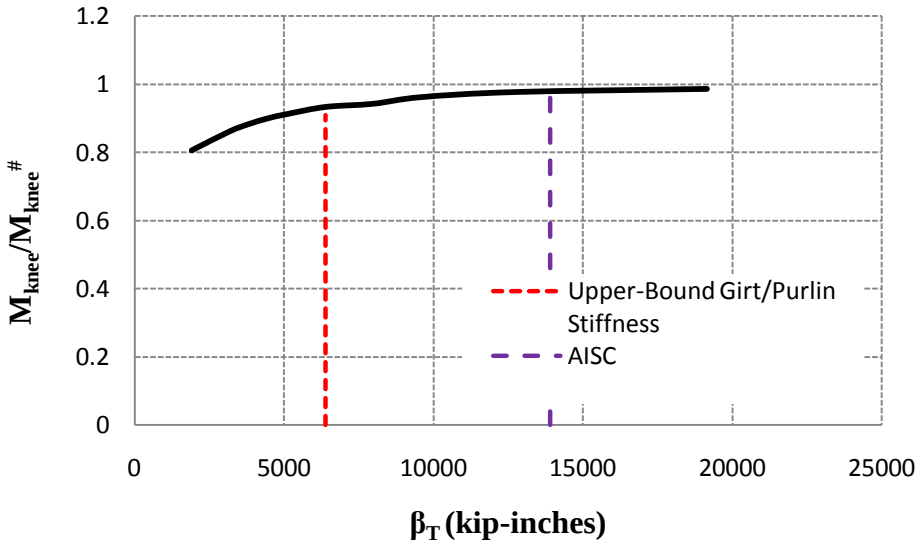

Fig. 6.19. Frame strength behavior knuckle curve for the 90 ft clear span frame with the simplified bracing configuration and 8 inch flanges, $M_{knee}^{\#}$ = moment at r1 at the peak load for the rigid bracing condition.

The above curve shows that the stiffness provided by a typical girt/purlin (6380 in-kips/rad) is located roughly at the knuckle value. It should be noted that the system reaches 90% of the rigidly braced strength for a stiffness only slightly smaller than this value. At higher brace stiffness values, the strength of the frame becomes insensitive to the change in brace stiffness. It is interesting to see that for this frame, the frame reaches 80% of the rigidly braced strength at a relatively low torsional bracing stiffness value compared to the behavior for the base 90 ft. span frame shown previously in Fig. 6.10. Hence, increasing the flange width not only decreases the bracing demands but it also reduces the sensitivity of the frame to changes in the brace stiffness.

Figure 6.20 shows the maximum brace force demand at r1 versus the brace stiffness. This curve does not exhibit the same behavior as that shown by the comparable curve in Fig. 6.11 for the base clear span frame example, or the other curves shown previously in Figs. 5.14 and 4.13. In Fig. 6.20, the maximum brace force occurs at a torsional brace stiffness value approximately 2.0 to 2.5 times the knuckle value. However, there is a definite precipitous drop in the brace force at approximately β_T = 5000 in-kips/rad. This is interpreted as the knuckle value for the torsional stiffness in this frame. The knuckle value in Fig. 6.20 is 5750 in-kips/rad.

It should be noted that the largest brace force demand is less than 1.0% for the full range of stiffness values considered in Fig. 6.20. However, of greater importance for the bracing stiffness design, the overall shape of the knuckle curve in Fig. 6.19 is very similar to the one in Fig. 6.10.

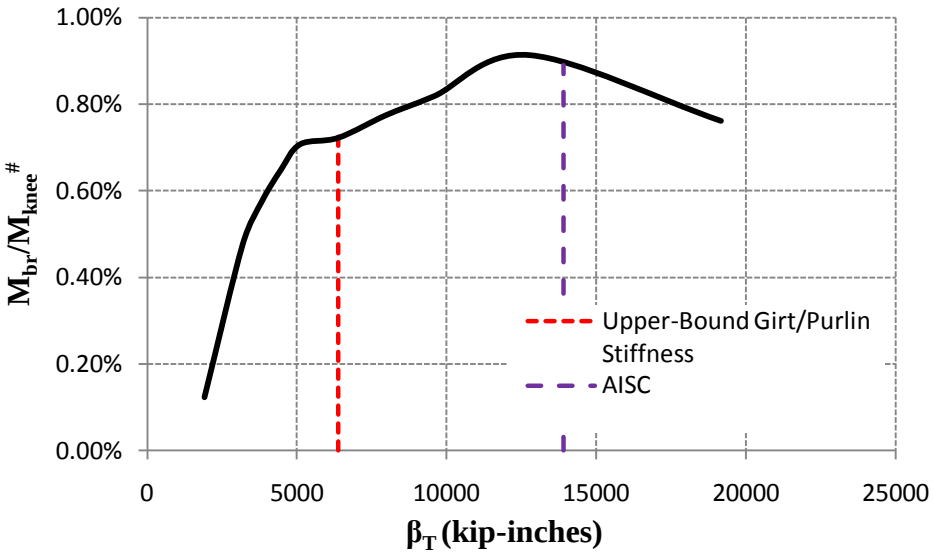

Fig. 6.20. Brace force demand curve, 90 ft clear span frame with simplified bracing configuration and 8 inch flanges, $M_{knee}^{\#}$ = moment at r1 at the peak load for the rigid bracing condition

6.12 Effect of Diaphragm Stiffnesses on System Strength and Brace Forces

As mentioned previously, the relative bracing stiffness provided by the roof and wall diaphragms can help restrain the outside flanges against out-of-plane movement. In general, the wall and roof diaphragms can be sources of substantial bracing strength. This section evaluates the influence of the specified wall and roof diaphragms on the system response for the base 90 ft clear span configuration.

For the rigid bracing case, the system strength and the brace force demands do not change as the brace points are restricted to zero displacement and hence, the relative bracing from the wall and roof diaphragms is not activated. However, for flexible bracing cases, the brace points move out-of-plane, activating the relative stiffnesses provided by the diaphragms. The relative stiffness due to roof and wall panels (R panels) are taken as G' = 4.19 kips/in and G' = 3.52 kips/in respectively in this study.

Figure 6.21 shows the load-deflection response comparison for the 90 ft clear span frame discussed in Section 6.2 with and without diaphragm stiffnesses considered. When the stiffness contribution of the diaphragms is considered, the strength of the frame is increased very slightly.

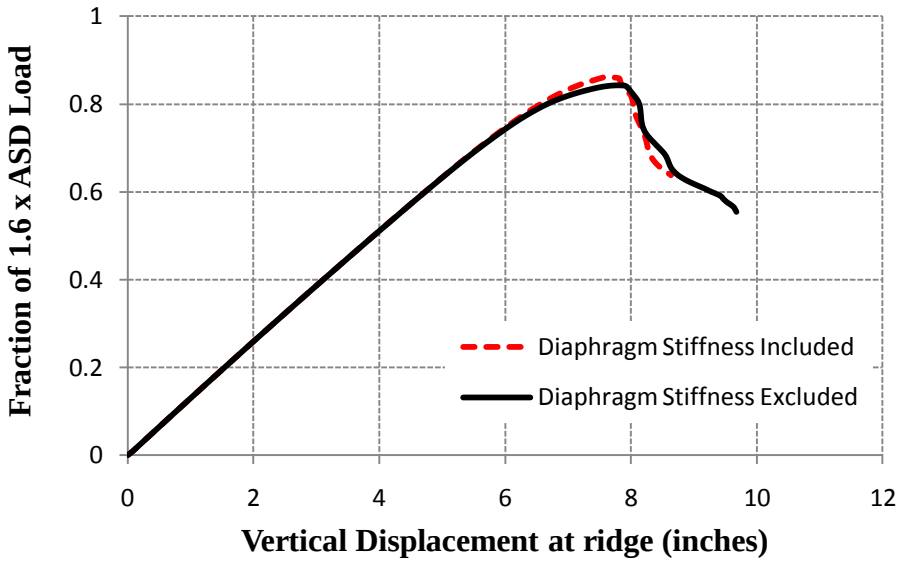

Fig. 6.21. Load-deflection response comparison, 90 ft clear span frame, diaphragm stiffness consideration.

Figure 6.22 compares the torsional brace forces at r1 for the above two cases. The brace force demand decreases significantly from 3.3% to 1.5% for the frame where the diaphragm stiffness is considered. This reduction in the brace force demand is attributable to the restraint provided by the diaphragm, in conjunction with the other bracing components, to the twisting of the column and the rafter at the knees of the frame.

The consideration of the stiffness from more flexible types of diaphragms is sometimes debated by engineers. Specifically, standing seam roof panels allow for thermal expansion by “floating” over the purlins. In addition, concealed fastener wall panels also have limited stiffness. These small stiffness contributions can be quantified,

but for larger structural systems, these stiffnesses may not be large enough to have a significant effect on the overall structural response. The above example shows that even though the 90 ft clear span frame was designed assuming brace points at the outside flanges at each of the girt and purlin locations, and brace points at the inside flanges at each of the flange diagonal locations, the overall frame response is predominantly the same even if the diaphragm stiffnesses are not considered at all.

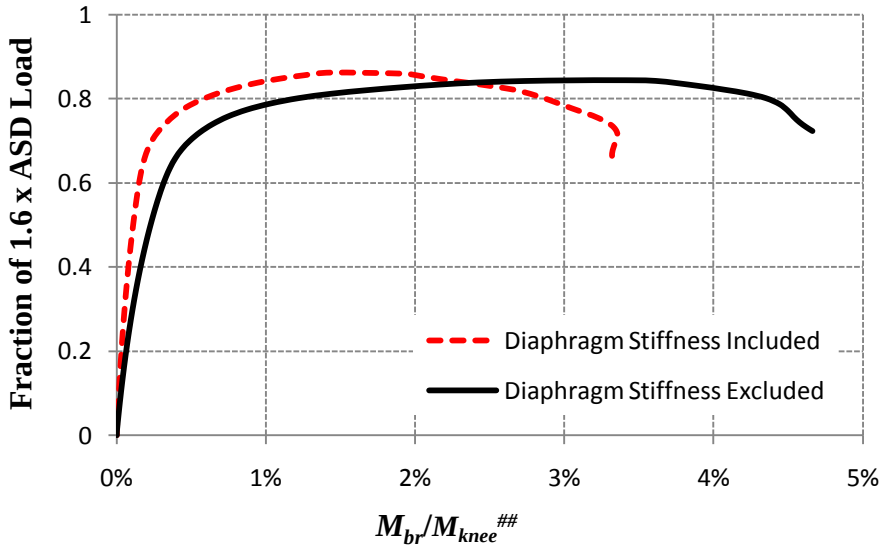

Fig. 6.22. Brace force comparison, base 90 ft clear span frame with and without roof and wall diaphragms, $M_{knee}^{\#\#}$ = moment at r1 at the peak load for the flexible bracing condition.

Table 6.6 summarizes the critical torsional and relative bracing strength demands for the above frame at 90, 95 and 100 % of its limit load. The torsional bracing results in this table can be compared to the previous results for the frame with no diaphragms in Table 6.4.

Table 6.6 Summary of bracing strength demands from virtual test simulation for the 90 ft clear span frame using the original bracing configuration and including the wall and roof diaphragm shear stiffness.

Criterion or Condition	Strength Demand at 90% of Limit Load	Strength Demand at 95% of Limit Load	Strength Demand at Limit Load
Torsional brace strength requirement at r1 using provided torsional brace stiffness required to brace the frame for the loading from ASD load combination, 6380 in-kips/rad	P_{br} = 0.6 kips, 0.4%	P_{br} = 1.0 kips, 0.6%	P_{br} = 2.4 kips, 1.5%
Torsional brace strength requirement at c3 using provided torsional brace stiffness required to brace the frame for the loading from ASD load combination, 6380 in-kips/rad	P_{br} = 0.3 kips, 0.06%	P_{br} = 0.42 kips, 0.09%	P_{br} = 1.1 kips, 0.23%
Relative brace strength requirement at the knee using relative brace stiffness provided by typical CS roof panels with 12 inch screw spacing, G' = 4.19 kips/inch (ν_{br} = 122 lb/ft)	ν = 11.8 lb/ft, 0.2%	ν = 14.84 lb/ft, 0.25%	ν = 29.45 lb/ft, 0.5%
Relative brace strength requirement at the top of column using relative brace stiffness provided by typical CS wall panels with 12 inch screw spacing, G' = 3.52 kips/inch (ν_{br} = 61.2 lb/ft)	ν = 3.1 lb/ft, 0.05%	ν = 4.63 lb/ft, 0.07%	ν = 10.62 lb/ft, 0.2%

6.13 Summary

The following key observations can be summarized from this example:

- Both the AISC and simplified equations give very conservative estimates of the stiffness demands; however, the use of substantially higher brace stiffness does not increase the capacity of the frames significantly. For the base example considered first, if the stiffness provided by a typical girt/purlin (determined using an upper-bound estimate) is available, the system reaches 85% of the specified

ASD load, whereas if rigid bracing is employed, the system reaches 95% of the ASD load. The brace required strength estimates obtained from both the AISC and simplified equations tend to underestimate the bracing strength demands at the limit load at the most critically loaded braces. However, the 2 % strength requirement from the simplified rule is capable of developing frame strengths nearly equal to the system limit load.

- The torsional brace stiffness provided by the representative minimum size purlins lies on the knuckle of the knuckle curves where the frame capacity is sensitive to the change in brace stiffness. If the brace stiffness is increased, the brace force demand at the critical locations reduces significantly, but the frame capacity does not increase considerably.
- If the frame is designed with wider flanges, the brace strength and stiffness demands decrease significantly as a percentage of the moments at the limit load. The causes of these reductions appear to be the greater ability of the members and other components to resist the out-of-plane movement of the brace points, as well as earlier flange local buckling tending to "protect" the bracing system by the response being less influenced by overall lateral buckling at the strength limit.
- The wall and roof diaphragms enhance the frame response by tending to reduce some of the other bracing strength demands. However, the overall load-deflection response of the frame is improved only very slightly.

Additional targeted examples of metal building frame systems are discussed in Chapters 7 and 8.

CHAPTER 7

120 FT CLEAR SPAN FRAME

7.1 Introduction

It is worthwhile to consider one additional clear span frame with a somewhat larger span length to gain some insight into how the flange bracing requirements change as a function of this parameter. In addition, the 90 ft clear span frame considered in Chapter 6 has flange bracing along its columns. It is useful to consider how the flange bracing requirements are affected when the columns need to be designed without any lateral bracing throughout their height. This chapter presents a 120 ft clear span example frame, designed by ASD, that meets these objectives. The original design of the frame was conducted by Mr. Duane Becker of Chief Industries. The torsional bracing demands are estimated using the 2010 AISC Appendix 6 based equations summarized in Section 2.6 as well as the simplified form of the AISC equations discussed in Section 2.8. The flange bracing systems are then evaluated by a range of virtual test simulations.

Sections 7.2 and 7.3 first give a broad overview of the geometry and loading for the selected 120 ft clear span frame. Section 7.4 discusses the configuration of the flange bracing for this structure. Section 7.5 then presents a summary of the AISC-based and simplified estimates for the bracing demands as well as the provided stiffness and strength of typical minimum-size purlins and flange braces for this example.

The critical geometric imperfections applied for the virtual test simulations are discussed in Section 7.6. This is followed by Section 7.7, which presents virtual test simulation results using the provided minimum-size brace stiffnesses. In addition, this

section discusses the effect of torsional brace stiffness on the bracing strength demands. Lastly, Section 7.8 summarizes important attributes and observations.

7.2 Frame Geometry

Figure 7.1 shows an elevation view of the 120 ft clear span frame. Table 7.1 summarizes the specific web and flange geometries for the five member lengths in this structure. This frame is designed without any intermediate braces on the column flanges, to accommodate doors or an open wall on each side of the columns. Ten inch wide column flanges are utilized to offset the large column unsupported lengths. In addition, due to the larger depth of the girders needed for the 120 ft span, and due to the fact that wider flanges tend to reduce the bracing demands, 8 inch wide flanges are used for the roof girders.

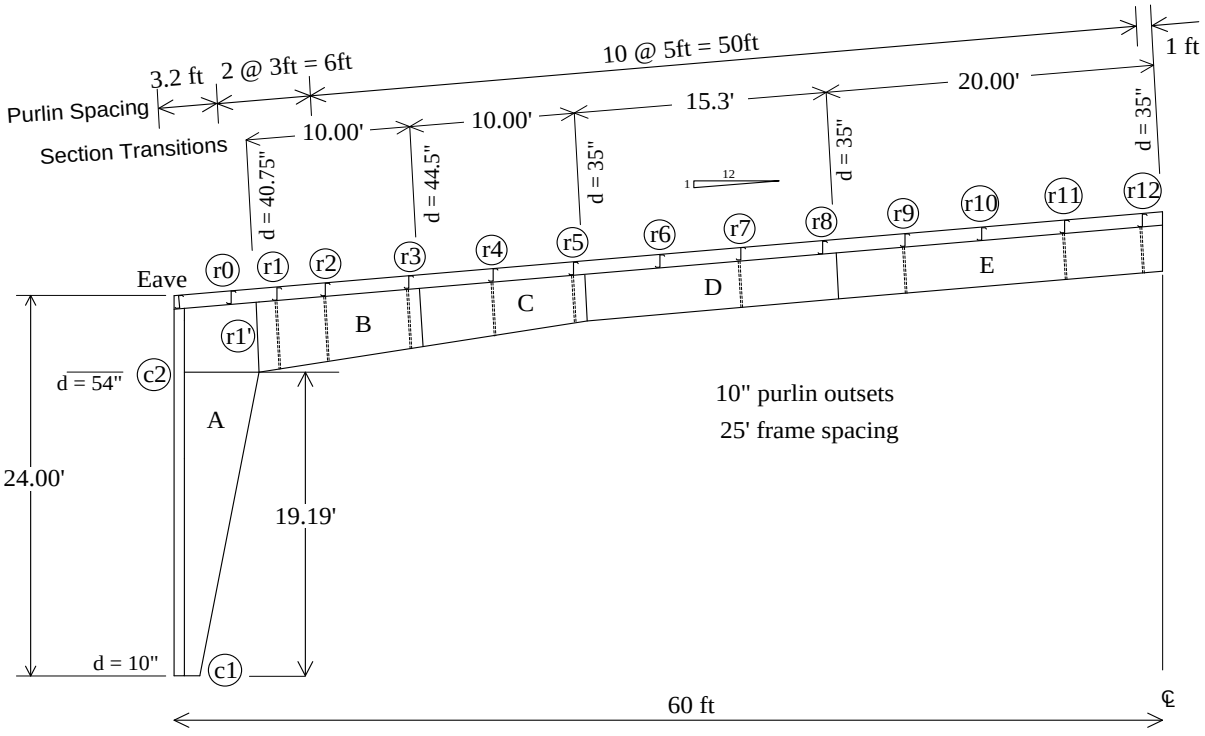

Fig. 7.1. Elevation view of 120 ft Clear Span Frame.

Table 7.1 Summary of web and flange geometry, 120 ft clear span frame

Length	Location	Web			Inside Flange			Outside Flange		
		d (in)	t_w (in)	h/t_w*	b_f (in)	t_f (in)	$b_f/2t_f$	b_f (in)	t_f (in)	$b_f/2t_f$
A	c1	10.00	5/16	27	10.0	3/4	6.7	10.0	3/8	13.3
	c2	54.00		168						
B	r1'	54.00	5/16	170	8.0	1/2	8.0	8.0	1/4	16.0
	r1	53.20		167						
	r2	50.35		158						
	r3	45.60		143						
	r3'	44.50		139						
C	r4	40.85	5/16	128	8.0	3/8	10.7	8.0	1/4	16.0
	r5	36.10		113						
	r5'	35.00		110						
D	r6	35.00	7/32	157	8.0	3/8	10.7	8.0	1/2	8.0
	r7	35.00		157						
	r8	35.00		157						
	r8'	35.00		157						
E	r9	35.00	3/16	183	8.0	3/8	10.7	8.0	1/2	8.0
	r10	35.00		183						
	r11	35.00		183						
	r12	35.00		183						

**For F_y = 55 ksi,* the web is *compact* for $h/t_w \leq 86$) and it is *slender* for $h/t_w \geq 130$.

Singly-symmetric tapered sections are used for the columns. The column web is nominally 5/16 in thick and the total column depth tapers from d = 10 inches at the base to d = 54 inches at the bottom of the knee joint at a height of 19.19 ft above the base. This gives a web slenderness ranging from h/t_w = 32 at the column base to 173 at the knee. The outside flange of the columns is relatively thin ($b_f/2t_f$ = 13.33) while the inside flange is compact ($b_f/2t_f$ = 6.67).

The rafters are composed of four different sets of doubly symmetric cross-sections on each side of the ridge. Rafter length B is tapered and has an outside flange with $b_f/2t_f$ = 16, a compact inside flange with $b_f/2t_f$ = 8, and a slender web with h/t_w = 173 at the knee. Rafter length C is tapered and has an outside flange with $b_f/2t_f$ = 16, an inside flange with $b_f/2t_f$ = 10.67, and a slender web with h/t_w = 130 at its deepest section. Rafter length D is a prismatic section with a compact ($b_f/2t_f$ = 8) outside flange, a noncompact ($b_f/2t_f$ =

10.67) inside flange and a slender web (h/t_w = 158). Rafter section E is another prismatic section with a compact ($b_f/2t_f$ = 8) outside flange, a noncompact ($b_f/2t_f$ = 10.67) inside flange, and a slender web (h/t_w = 184). The locations r1', r3', r5', and r8' in Table 7.1 correspond to the rafter to panel zone connection, and to the section transitions from lengths B to C, C to D, and D to E respectively.

7.3 Loading

The ASD load combination considered for this frame is the same as the one considered for the 90 ft clear span frame presented in Chapter 6, i.e., Dead + Collateral + Uniform Snow. The load magnitudes are as follows:

i. Roof Dead load: 2.56 psf
ii. Collateral: 5.0 psf
iii. Snow load: 21 psf

The self weight of the main frame members is included in the original design. However, the self weight of the members is not included in the following virtual test simulations.

7.4 Bracing Configuration

The outside flanges of the rafters are supported laterally by the purlins but the column is not braced in the out-of-plane direction at any location along its length. Diagonal braces to the inside flanges of the rafters are indicated by double dashed lines in Fig. 7.1. The purlins are spaced at 5 ft on center except at the knee of the frame, where they are placed at 3 ft on center. The bottom flange of the rafters is unsupported at the purlin locations 24 ft, 34 ft and 44 ft from the inside of the knee (locations r6, r8 and r10), but

otherwise both flanges are braced at each purlin location. The base design of the frame uses cold-formed 14 gage, 10 inch deep Z1014 sections for purlins.

In this research, the torsional bracing from the flange diagonals and purlins is modeled by torsional springs located at the centroids of the purlins, as explained in Section 3.4. The upper-bound estimate of the torsional bracing stiffness ($8EI/s$) discussed in the prior chapters is used as a base provided torsional stiffness in this chapter. The underlying assumptions are similar to those made for the 90 ft frame are made for the virtual test simulation, i.e., no local deformation or slip at the connection points and purlins "rigidly pinned" to the top flange of the roof girder.

The roof diaphragm stiffness is neglected in all of the virtual simulation studies for the 120 ft clear span frame. However, relative bracing from the roof diaphragm is considered to establish the purlin locations as brace points for axial load and for positive bending moments on the rafters in the design. The side walls are assumed to not have any wall panels because of a large opening or door. The frame in Fig. 7.1 is assumed to be an interior frame, and X bracing (5/8 inch diameter rods) is assumed in every fifth bay along the length of the building between c1 and the eave, the eave and r3, r3-r6, r6-r9, and r9-r12.

7.5 Comparison of AISC and Simplified Bracing Requirements to Provided Values

Similar to the 90 ft clear span frame, the procedure used in Section 2.7 is used to evaluate the brace strength and stiffness requirements for the 120 ft clear-span frame. At the negative moment locations on the roof girders, the flange diagonal brace locations are considered to be only torsionally braced. Relative bracing from the roof diaphragm is considered to establish the purlin locations as brace points for axial load and for positive bending moments on the rafters in the bracing design checks.

Table 7.2 summarizes the required torsional brace strength and stiffness at r1, as estimated by the AISC Appendix 6 equations outlined in Section 2.6 as well as the simplified equations from Section 2.7. For this frame, the stiffness requirement obtained from the simplified method is excessive. This behavior is due to the relatively large cross-section depth and internal moment in the rafter at its connection to the knee of the frame, as well as the short unbraced length (L_b = 3 ft) at this position. The AISC torsional bracing equation gives a significantly smaller torsional bracing stiffness requirement of β_{br} = 9.66 kips/inch (β_T = 26,900 inch-kips/rad.), by accounting for the ability of the member to assist the bracing system in restraining the brace point displacements in the vicinity of the short unbraced length between r1 and r2.

Table 7.2. Summary of required torsional brace strengths and stiffnesses at r1, expressed in terms of the equivalent lateral brace stiffness, to develop the specified ASD loading.

Criterion	Stiffness	Strength[(a)]
AISC	β_{br} = 9.66 kips/inch	P_{br} = 0.70 kips, 0.38%
Simplified	β_{br} = 74.5 kips/inch	P_{br} = 3.4 kips, 2%

[(a)] The percent values are $P_{br}/((P_r h_o/2 + M_r/C_b)/h_o)$ expressed as a percentage.

If a lower-bound effective length factor of K = 0.5 is used in Eq. (2-36a) for the critical r1-r2 segment of this frame, the required torsional brace stiffness is reduced by a factor of four. This assumption means that the rafter sections adjacent to the critical unbraced length provide close to rigid restraint to the critical segment. Although substantial restraint may occur on the knee-joint side of r1-r2 due to the complexities of the framing interactions between the rafter and the panel zone, the column, the purlins, and the roof system, the subsequent virtual simulations show that there is a tendency for

column lateral-torsional buckling to be the governing failure mode in this frame. Therefore, the assumption of near full flange lateral bending and warping restraint at r1 is suspect in this frame. Furthermore, the adjacent segment r2-r3 is longer than the critical segment; thus, full restraint at r2 is also unlikely. It should be noted that, when included, K is used only in the calculation of $P_{e.eff}$ in Eq. (2-36a) (or Eq. (2-31)). Note that there are two terms containing L_b in Eq. (2-36a), the $P_{e.eff}$ term and the term $(M_{r.equiv}/h_o)/L_b$. The occurrence of L_b in the second of these terms comes from the overall description of the geometry and is not interpreted as an effective buckling length.

The upper-bound estimate of the provided torsional brace stiffness, $8EI/s$, is again used for this example (see Section 2.7). Given the Z1014 purlins specified for this problem (I = 18.4 in^4) and the spacing of the frames s = 25 ft, one obtains

$$\beta_{provided} = 8EI/s = 14{,}200 \text{ in-kips/rad}$$

or in terms of an equivalent lateral bracing stiffness

$$\beta_{br.provided} = \beta_{provided}/h_o^2 = 14{,}200/52.8^2 = 5.09 \text{ kips/inch}$$

This provided stiffness is used for the subsequent virtual test simulation studies.

It should be noted that the AISC-based estimate for the required torsional brace stiffness, using K = 0.5 in the calculation of $P_{e.eff}$, is approximately one-half of the upper-bound estimate of the provided torsional brace stiffness. However, with K = 1.0, the required torsional brace stiffness is approximately double of the upper-bound estimate of the provided stiffness. The subsequent virtual test simulations provide insight into the actual bracing demands.

7.6 Critical Geometric Imperfections for Virtual Simulation Analysis

For the flexibly-braced case of the 120 ft clear span frame, the critical out-of-alignment and out-of-straightness imperfections are generated using the influence line approach detailed in Section 3.3.2. These imperfections are aimed at maximizing the demand on the critical brace at r1. The influence line for the rafter of this frame is similar to that for the rafter of the 90 ft Clear Span Frame (see Fig. 3.6(b)), and hence the imperfections are similar to those shown in Fig. 3.8(b). Figure 7.2 shows the corresponding geometric imperfections applied to the inside flanges of the rafter and column in the 120 ft clear span frame.

No geometric imperfections are applied to the outside (tension) flanges in the column and in the rafter near the knee. As discussed in Chapter 6, this is because the twist rotation of the members tends to be larger than realistic expectations if influence line imperfections are applied to both the tension and compression flanges. Wang and Helwig (2005) recommend applying out-of-plane imperfections only to the compression flange in their studies, so there is precedent for this practice in beam members that are close to fully-braced. The unbraced lengths of the inside flange between r1-r2, r2-r3, and r3-r4 in the rafter all have out-of-alignments of 1/500 between their brace points. The length from the inside flange on the rafter at r1 to the outside flange on the column at c2 is given an out-of-alignment of 1/833 so that there is zero out-of-plane displacement in the imperfection pattern at the tension flange on c2 but compatibility with an out-of-plane movement of Δ_o = 3 ft x 12 in/ft /500 = 0.072 inches is maintained for the compression flange at r1. The corresponding out-of-plane movement at point r1', located at the inside of the knee, is 0.06 inches. The column inside flange is then given an out-of-alignment of

0.06 inches / (19.19 ft x 12 inches/ft) = 1/3840 between its base and r1' also to maintain compatibility with the above out-of-plane displacement at r1'. In addition, a flange sweep of 19.19 ft x 12/ inches/ft / 1000 = 0.23 inches is applied to the column inside flange.

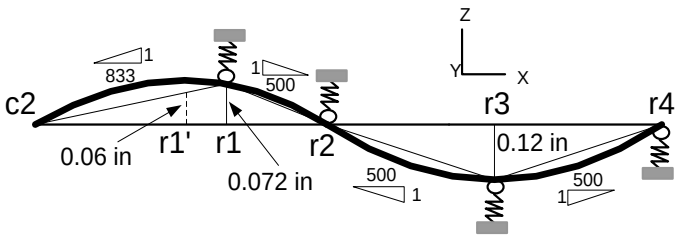

(a) rafter compression flange imperfections close to the knee

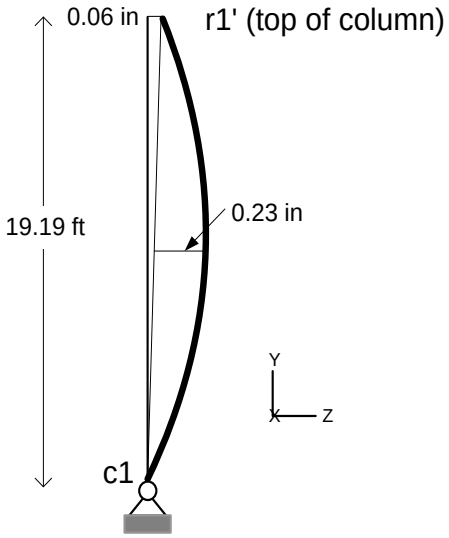

(b) corresponding column compression flange imperfections

Fig. 7.2. Critical geometric imperfection applied to the 120 ft clear span frame

For the rigidly-braced case with the 120 ft clear span frame, a single brace point out-of-alignment is applied to the inside flange of the rafter at r1 to maximize the demands on this brace. This parallels the recommendations by Wang and Helwig (2005) arrived at in their studies of critical imperfections for fully-braced beams. The imperfections for the

rigidly braced case are identical to those described above for the flexibly braced case, with the exception that the inside flange is not displaced out-of-plane at r3.

It should be noted that an out-of-alignment (i.e., out-of-plumbness) of the column inside flange of 1/500 could be achieved by moving the inside flange out-of-plane by an additional 0.40 inches at c1 in Fig. 7.2(b). However, considering that no out-of-plane movement is applied to the tension flange, this would result in an excessive initial twist of the column cross-section at its base. The maximum out-of-plane movement that could be applied to the inside compression flange at c1, without exceeding a cross-section twist of 1/100 radians, is 0.1 inches. Furthermore, applying a twist to the base of the frame causes major complexities in the application of the "pinned" multi-point constraints at the column base (see Section 3.1.2). Therefore, no initial twist is applied to the column cross-section at the base of the frame. In addition, the out-of-plane displacement at r1' could be increased to 0.1 inches by increasing the out-of-alignment of c2-r1' to 1/500. However, this would require the application of an additional out-of-plane displacement of 0.1 inches - 0.06 inches = 0.04 inches to the inside flange at all the brace points along the rafter length in Fig. 7.2(a), to maintain the out-of-alignment of 1/500 in r1-r2, r2-r3, and r3-r4, and to maintain the convention of not applying any initial out-of plane displacements to the outside flange in the negative moment regions. It was decided not to include this additional geometric imperfection in this study.

Similar to the 90 ft frame, this frame is also modeled initially out-of-plumb by $0.002h$ to the right in the plane of the frame (Fig. 7.1), where h is the height above the base.

7.7 Virtual Simulation Results

The 120 ft clear span frame is analyzed for both rigid and flexible bracing conditions in the following sub-sections. The rigid bracing solution is considered first.

7.7.1 Rigid Bracing

Figure 7.3 shows the load-deflection response of the 120 ft clear span frame for the rigid bracing condition. The unity check for this frame is 1.00 for the ASD gravity load combination discussed previously. Hence, the frame supports 28% more load than the ASD ultimate strength load level (i.e., 28% more than 1.6 times the specified ASD loads). This is believed to be due to the existence of significant weak-axis rotational restraint at the top of the column, coming from the rigid out-of-plane restraint of both flanges at r1, the top flange at r0, and at the eave strut, and from the lateral bending and torsional stiffness particularly within the short unbraced length between r1 and r2 and across the width of the panel zone. The rigidly-braced frame fails in local buckling of the web and flange in the rafter close to r1.

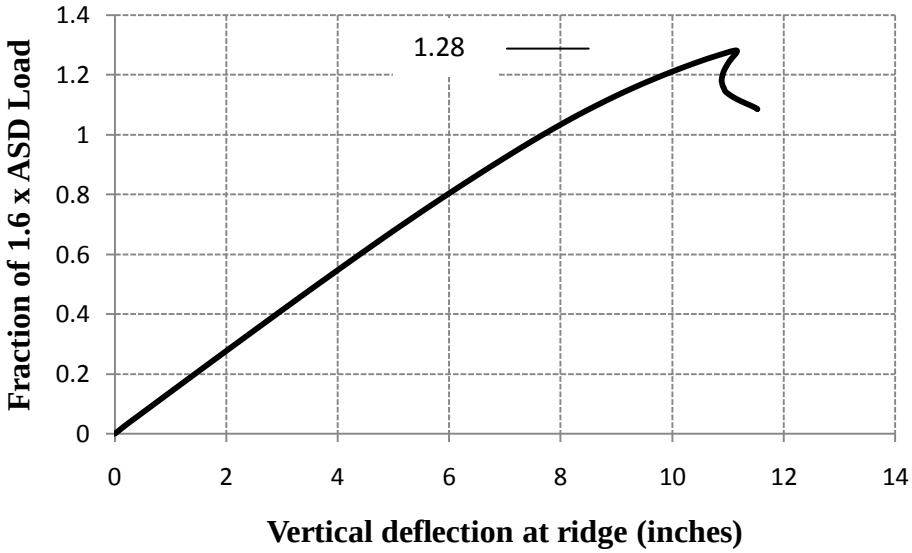

Fig. 7.3. Load-Deflection response, 120 ft clear span frame, rigid bracing condition.

The maximum moment developed in the rafter at r1' (at the structure's limit load), denoted by $M_{knee}^{\#}$, is 1330 ft-kips. Figure 7.4 shows the brace force demand on the inside flange of the rafter at the brace closest to the knee (location r1) as a percentage of $M_{knee}^{\#}$. Note that the internal moment at r1' is used rather than the internal moment at r1 based on the general recommended approach that the bracing requirements should be estimated by applying the corresponding equations with each unbraced length and using the maximum internal force within each length (see Sections 2.6 and 2.8) .

The brace force demand close to the knee is 1.7% of the rafter moment, which is close to the 2.0% estimate considered in the simplified equations (neglecting the contribution to the equivalent moment from the axial load). The AISC-based Eq. (2-34) estimates the strength demand at r1 to be M_{br} = 0.70 kips x 52.8 inches = 37.0 inch-kips at the ASD load condition. This ASD moment may be multiplied by 1.6 x 1.28 to estimate the brace strength requirement as 75.8 inch-kips at the above peak load condition. This brace moment is 0.47 % of the above 1330 ft-kips moment at r1' corresponding to the peak load condition. The base AISC (2010) Eq. (A-6-9) gives a strength requirement of 3.3 % of the member internal moment in this example. This larger percentage is due to conservative assumptions invoked in simplifying from the base Eq. (2-34). These simplifications are explained in the AISC (2010) Commentary. They amount to the assumptions:

- C_{tT} = 1.2, and
- One of the equivalent flange force terms in Eq. (2-31), multiplied by the square-root of ψ, i.e., $\psi^{0.5}M_r/h_o$, is equal to $P_{e.eff}$ /2 (while the other moment term is still interpreted as the applied internal beam moment).

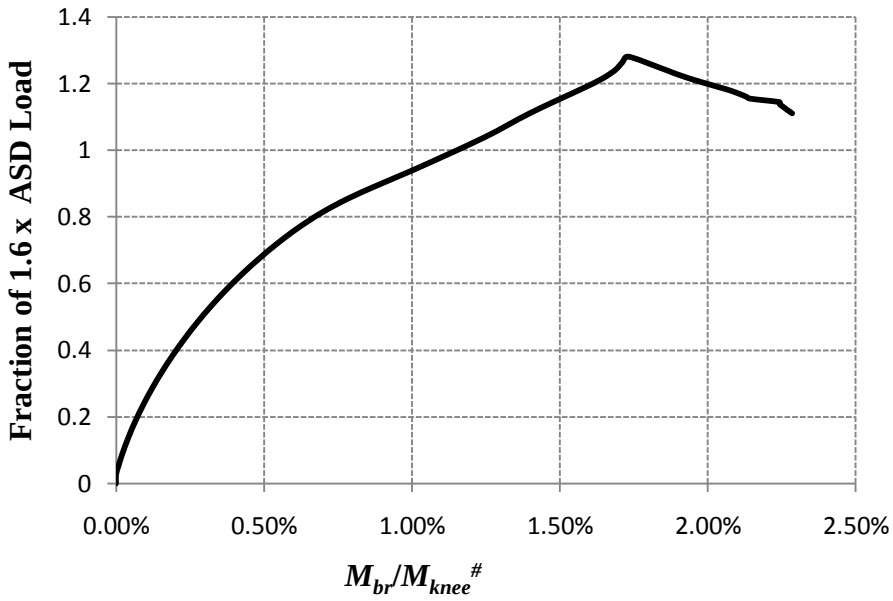

Fig. 7.4. Brace force demand at r1 (close to the knee), 120 ft clear span frame, rigid bracing condition, $M_{knee}^{\#}$ = moment at the connection of the rafter to the knee at the peak load.

Similar to the results for the 90 ft clear span frame in Chapter 6, the brace force demand obtained from the virtual simulation is much smaller for points further away from the critical knee region. One example of this is provided in the next section.

7.7.2 Flexible Bracing

Figure 7.5 shows the load-deflection response of the frame for the flexible bracing condition, utilizing the assumed upper-bound provided torsional brace stiffness of $\beta_{provided}$ = 8*EI*/*s* = 14,200 in-kips/rad ($\beta_{br.provided}$ = 4.94 kips/inch). The maximum moment developed in the rafter at r1' is only 990 ft-kips for this case.

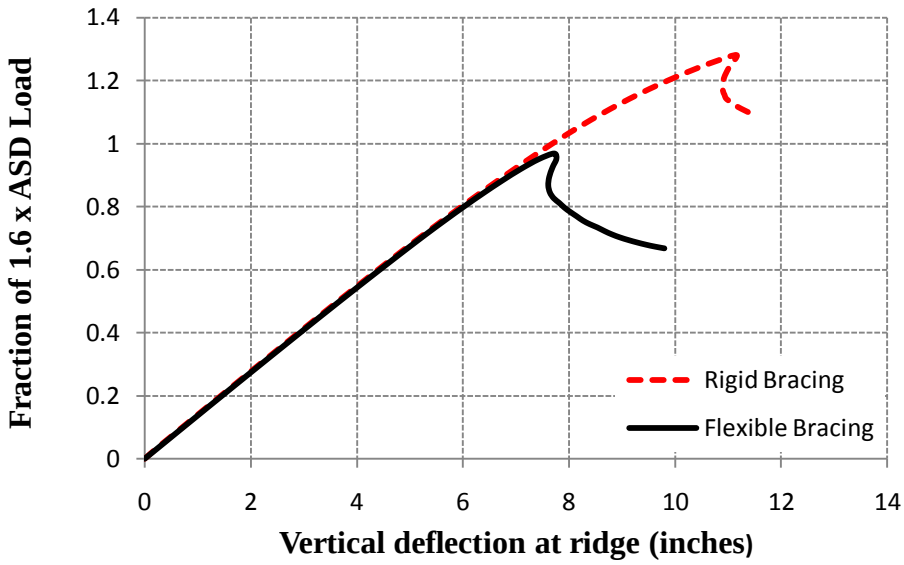

Fig. 7.5. Load-deflection response for rigid and flexible bracing, 120 ft clear span frame.

For the flexible bracing case, the 120 ft clear span frame fails at 97% of the ASD ultimate strength load level, which is a significantly smaller capacity than obtained for the rigidly braced frame. This reduction in the strength of the frame can be attributed to the mode of failure shown in Fig. 7.6. Since the column does not have any bracing along its length, it is susceptible to lateral-torsional buckling.

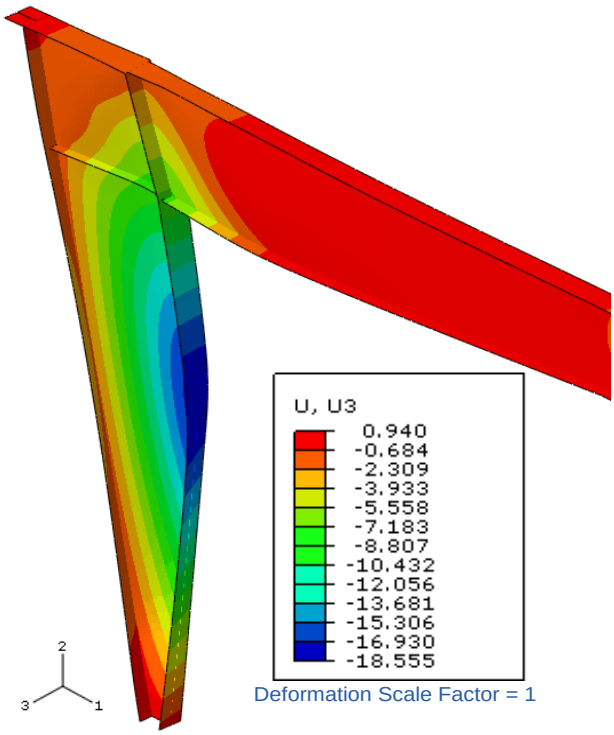

Fig. 7.6. Final failure mode at the end of the analysis for the120 ft clear span frame with flexible bracing, including the corresponding out-of-plane deflection contours.

In this problem, the torsional brace close to the knee is designed to brace the rafter against lateral-torsional buckling. However, in addition to restraining the buckling of the rafter this brace also participates with the rafter, the panel zone region, the eave strut, and the adjacent torsional braces at r2 and r3 in restraining the column against minor-axis bending, warping and twisting displacements at its top. For the rigid bracing case, the corresponding restraint to weak-axis rotation of the top of the column is very large and hence, the column does not buckle in the out-of-plane direction in the failure mode. However, when the torsional brace stiffness is reduced to a practical value, the column becomes weaker and the inside flange of the column buckles in the out-of-plane direction at the strength limit. It should be noted that the purlin location r0 is modeled as a rigid brace point when rigid bracing is assumed. However, this purlin is assumed to offer zero

torsional or lateral resistance for the flexibly-braced case. This is because the roof diaphragm stiffness is not included in the virtual simulation here, and also, the attachment of the purlin at r0 is assumed as a pinned connection (i.e., no rotational compatibility between the purlin and the plate at the top of the column).

Figure 7.7 shows the brace force demands at r1. At the peak load, this demand is 1.5% of the corresponding internal moment at the knee for the flexible bracing case (slightly smaller than the demand of 1.7% for the rigid bracing condition). This value is close to the 2% estimate used in the simplified equations to determine the bracing demands. The 2010 AISC Eq. (A-6-9) estimates this demand to be 3.3% of the maximum internal moment.

Similar to the results for the prior bracing examples in Chapters 4 through 6, the slope of the flexible bracing curve in Fig. 7.7 is very flat in the vicinity of the structure's limit load. Therefore, although the torsional brace moment is 1.5 % of the moment at r1' at the limit load of the structure, the limit load is nearly achieved at a much smaller required bracing strength.

Figure 7.8 shows the maximum brace force demand at r2. In this case, the applied imperfection is aimed at maximizing the brace force at r2 by displacing the compression flange out-of-plane by $L_b/500$ at this brace point. The out-of-plumbness is specified as $L_b/500$ in the unbraced lengths on each side of the brace at r2.

The brace force demand at the limit load is 0.28% of the internal moment at the knee. This is significantly smaller than the corresponding maximum brace force at r1 of 1.5% (note that this is the brace force at r1 for the case where the imperfections are applied to

maximize the brace force at r2). The frame reaches 1.04 of the reference load level, 7% higher than the previous case where the brace force at r1 is maximized.

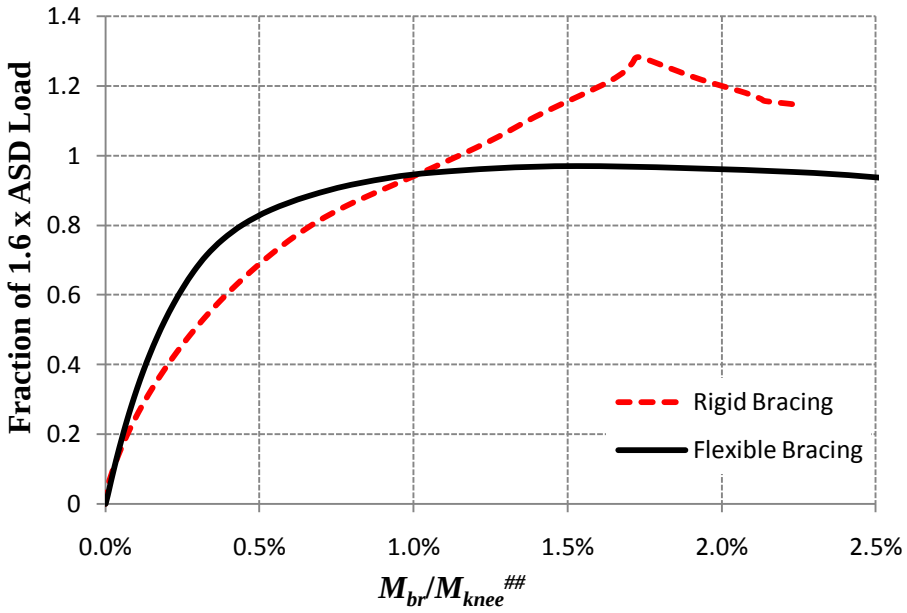

Fig. 7.7. Brace force demand comparison at r1, 120 ft clear span frame, $M_{knee}^{\#\#}$ = moment at the knee at the peak load for the base flexible bracing condition.

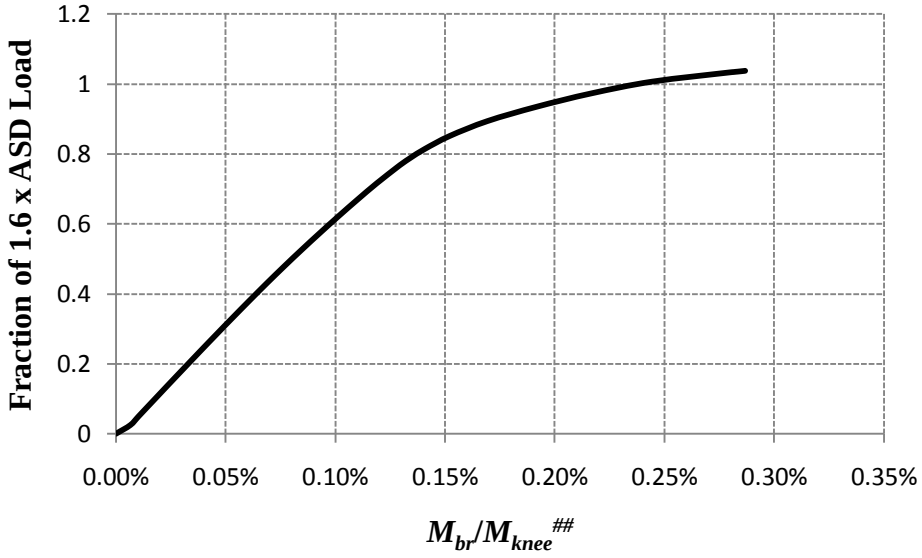

Fig. 7.8. Brace force demand at r2, 120 ft clear span frame, $M_{knee}^{\#\#}$ = moment at the knee at the peak load for the base flexible bracing condition.

Table 7.3 shows the corresponding equivalent torsional brace forces at r1 at 90, 95 and 100 % of the frame's limit load for the analysis where the imperfections are applied to maximize the brace force at r1. It can be observed that even at r1, the brace forces are quite small until the overall structural system is approaching its failure condition.

Table 7.3 Summary of torsional bracing strength demand at r1 from virtual test simulation, for the 120 ft clear span frame with the base flexible bracing condition.

Strength Demand at 90% of Limit Load P_{br} kips, %	Strength Demand at 95% of Limit Load P_{br} kips, %	Strength Demand at Limit Load P_{br} kips, %
1.4, 0.7	1.8, 0.9	3.4, 1.5

7.7.3 Effect of Varying the Torsional Brace Stiffness

Figure 7.9 shows the knuckle curve for the 120 ft clear span frame. The vertical axis shows the ratio of the load capacity to that of the rigidly braced frame, $M_{knee}/M_{knee}^{\#}$, where $M_{knee}^{\#}$ is the girder internal moment at r1' at the peak load for rigid bracing.

This curve shows a very gradual increase in the resistance toward the strength for rigid bracing as the brace stiffness is increased to very large values and through the value for the bracing stiffness provided in this example. The slope of the curve is slightly steeper for the smallest stiffness values, but it is nearly the same for all the stiffnesses shown. As shown in Section 7.5, the AISC estimate of the torsional brace stiffness for this frame is β_T = 26,900 in-kips/rad. (β_{br} = 9.66 kips/inch) and the simplified equations estimate the required stiffness as β_T = 208,000 in-kips/rad. (74.5 kips/inch). However, the frame is capable of developing 97 % of the specified ASD loading for which it was designed (and for which the unity check value was 1.0) using the provided torsional bracing stiffnesses of only 14,200 in-kips/rad (β_{br} = 4.94 kips/inch). If a lower-bound

effective length factor of K = 0.5 is used in Eq. (2-36a), giving β_T = 6,700 in-kips/rad., the limit load of the structure is only 70% of the rigidly braced strength. This confirms that K = 0.5 in segment r1-r2 is too optimistic for sizing the brace at r1 in this problem.

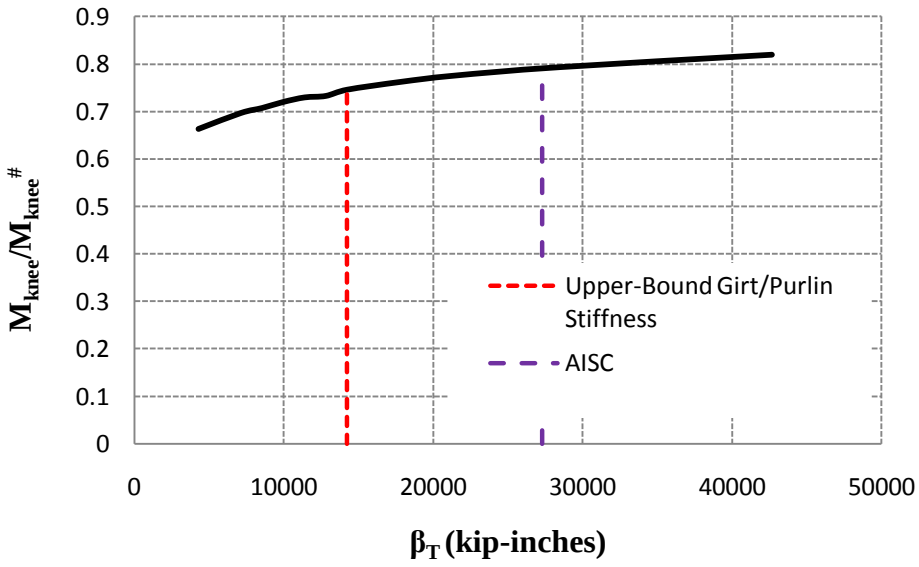

Fig. 7.9 Frame strength behavior knuckle curve, 120 ft clear span frame, $M_{knee}^{\#}$ = moment at the inside of the knee at the peak load for the rigid bracing condition.

It should be noted that the knuckle curve doesn't seem to asymptote to the load capacity of the rigidly braced frame (i.e., a loading parameter of 1.0 on the vertical axis in Fig. 7.9) as the torsional bracing stiffness is increased. This is likely due to the fact that, for the rigid bracing case:

- The top flange of the rafter is restrained rigidly against out-of-plane movement at the eave strut and at all the purlin locations.
- The bottom flange of the rafter is restrained rigidly against out-of-plane movement at each of the diagonal brace locations (see Fig. 7.1).

However, for the flexible bracing case, there is no out-of-plane restraint at all at r0, r1 or r2, and the eave strut and the purlin at r3 are restrained "flexibly" by the X bracing

system. Therefore, the knuckle curve in Fig. 7.8 is asymptoting to the strength corresponding to rigid torsional bracing, but with lateral bracing at the rafter top flange only via the structure's X bracing system.

Figure 7.10 shows a plot of the brace strength requirement, normalized by the moment at r1' for the rigid bracing condition ($M_{knee}^{\#}$) versus the torsional brace stiffness. For this frame, the required brace strength increases gradually until a stiffness approximately equal to the AISC torsional brace stiffness requirement is achieved. For brace stiffnesses larger than that value, the required brace strength is essentially constant. The maximum brace force demand at this level is 1.70%. It should be noted that the brace force demand for the rigid bracing condition is 1.73%. Therefore, it appears that the system is approaching the rigid (torsional) bracing condition at this bracing stiffness. The limit load of the structure is still only about 80 % of the rigidly braced strength though (see Figs. 7.5 and 7.7).

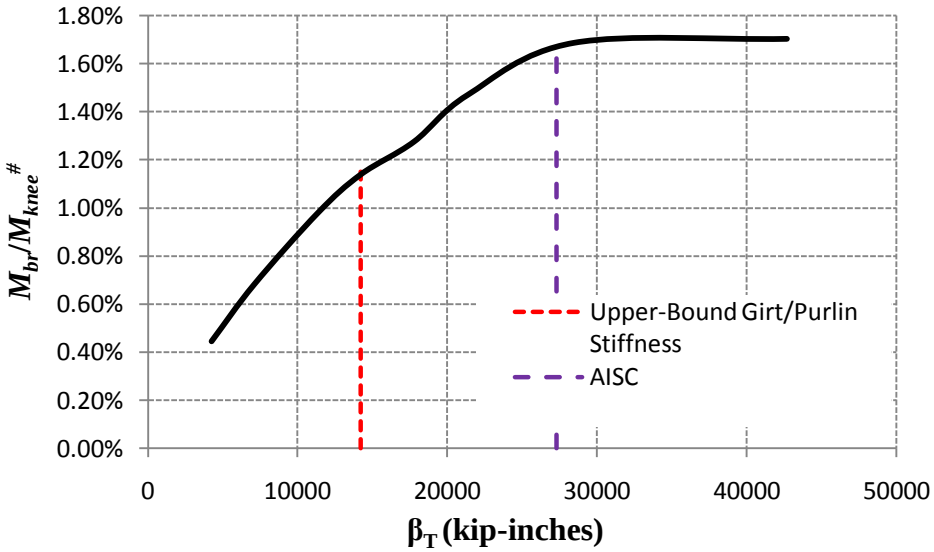

Fig. 7.10 Brace force demand curve at r1, 120 ft clear span frame, $M_{knee}^{\#}$ = moment at the knee at the peak load for the rigid bracing condition.

7.8 Summary

The following observations can be summarized from this example:

- Both the AISC-based equation with $K = 1$ and the simplified equation give higher brace stiffness estimates than that needed to reach the ASD factored load level in the 120 ft clear span frame. The stiffness estimate obtained from the simplified equations is significantly higher. This is due to the fact that the simplified equations do not account for the resistance to brace point displacement provided by the member. The brace strength demand in the virtual test simulation, at the structure's limit load, is close to the 2% estimate used in the simplified equations. However, at the ASD ultimate strength load level, the brace moment is substantially smaller and is better represented by the corresponding prediction from the refined AISC-based Eq. (2-34). The simplified form of this expression, provided as Eq. (A-6-9) in the AISC Specification, gives a significantly conservative estimate of the required brace strength from the virtual simulation even at the limit load of the frame.
- The upper-bound torsional bracing stiffness of $8EI/s$ is able to develop 97% of the ASD ultimate strength load level. However, this stiffness is able to develop only 80% of the rigidly braced strength. The small fraction of the rigidly braced strength is believed to be largely due to the fact that no diaphragm stiffness is included in the virtual simulation results presented in this chapter.
- The brace force demand curve for the flexible bracing condition is flat in the vicinity of the limit load. Hence, the limit load is nearly achieved at a much smaller required bracing strength than the demand at the limit load.

- The frame resistance relative to the rigid bracing strength shows a very gradual decrease as the torsional bracing stiffness is varied from very high to low values. The frame strength is not reduced significantly even if the provided brace stiffness is smaller than the upper-bound estimated value for the minimum-size purlins.
- The brace strength requirement at high stiffness values is essentially constant at 1.7%, close to the 2% value used in the simplified estimate.
- Since the flexibly braced frame fails due to column buckling, the frame doesn't even reach 90% of the rigid bracing strength for high torsional brace stiffness. The strength of the rigidly braced frame is much larger due to the additional restraint provided to the outside flange brace points.

CHAPTER 8

MODULAR FRAME EXAMPLE

8.1 Introduction

This chapter presents a modular frame example. The torsional bracing demands are estimated using the AISC-based and simplified equations presented in Sections 2.6 and 2.8 and are compared to the results obtained from the virtual test simulation. Sections 8.2 and 8.3 first give a broad overview of the geometry and loading for this example. Section 8.4 discusses the bracing configuration. Section 8.5 then presents a summary of AISC-based and simplified estimates of the bracing demands and compares the required stiffness estimates to an upper-bound estimate of the torsional bracing stiffness provided by representative minimum-size purlins. The critical geometric imperfections considered in the virtual test simulations are discussed in Section 8.6. Section 8.7 presents results from the virtual test simulation given the minimum-size purlins and neglecting the roof and wall diaphragm stiffnesses. It also discusses the effect of varying the torsional brace stiffness on the strength and bracing demands and the frame response if the sidesway is restrained. Lastly, Section 8.9 summarizes the important attributes and observations from the modular frame example.

8.2 Frame Geometry

Figure 8.1 shows an elevation view of the modular frame design from Kim (2010) and White and Kim (2006). The frame was originally designed by Mr. Duane Becker of Chief Industries. Table 8.1 summarizes the web and flange geometries for the

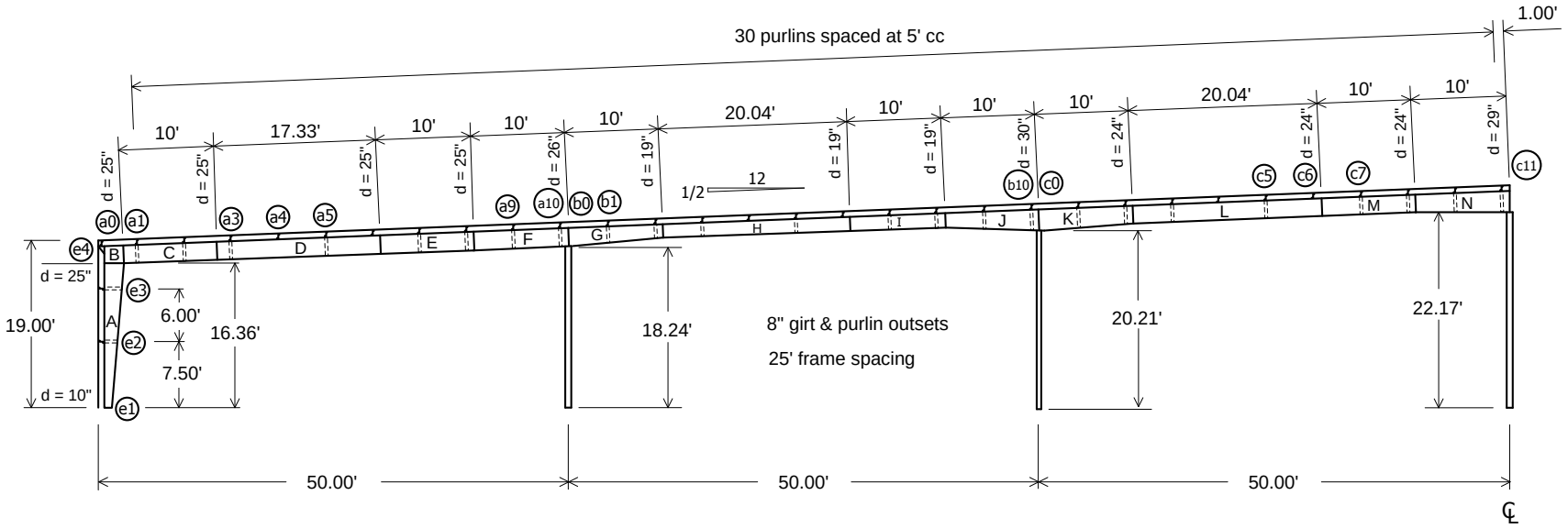

Fig. 8.1. Elevation view of modular building frame, from Kim (2010).

14 different lengths (A-N) in this frame. This frame uses a doubly-symmetric tapered section for its exterior columns. The exterior column web is nominally 1/8 inch thick and the total column depth tapers from d = 10 inches at the base to d = 25 inches at the bottom of the knee joint. This gives a web slenderness ranging from $h/t_w = 76$ at the column base to 196 at the top of the column. The column flanges are 6 x 1/4 in ($b_f/2t_f$ = 12), which makes them noncompact in flexure and slender in uniform axial compression by the AISC (2010) flange local buckling criteria. The rafters are composed mostly of doubly-symmetric cross-sections, but lengths F, G, L and M are singly-symmetric. All the rafter flanges are 6 inches wide.

Lengths C, D and E in the exterior span of the rafters are all doubly-symmetric and prismatic with 1/4 inch thick flanges and 25 inch total depth. Length F is singly-symmetric and has a 5/16 inch top flange ($b_f/2t_f$ = 9.6, noncompact in flexure and slender in uniform axial compression) and a 3/8 in compact bottom flange ($b_f/2t_f$ = 8). Also, this length has a mild linear taper from d = 25 to 26 inches at the first interior column. The webs for lengths C and E are 5/32 inch thick, such that their h/t_w is 157, whereas length D has a thinner 1/8 in thick web (h/t_w = 196) and length F has a thicker 3/16 in web (h/t_w = 130 to 135).

The first interior span starts with length G. This length has a substantial taper from the 26 inches depth at the first interior column to d = 19 inches at 10 ft inside of this column. It has a larger compact bottom (compression) flange (t_f = 3/8 in, $b_f/2t_f$ = 8), a 5/16 inch thick top flange, and a 3/16 inch thick web. Lengths H and I are prismatic and each has 1/4 in thick flanges and 19 in total section depth. Length H uses a 5/32 inch thick web (h/t_w = 118) whereas length I has a 1/8 inch thick web (h/t_w = 148). Length J

completes the first interior span by tapering the depth from d = 19 inches at 10 ft outside the second interior column to d = 30 inches at this column. It has a 3/16 inch web, giving h/t_w from 98 to 157. It has equal-size 5/16 inch thick flanges ($b_f/2t_f$ = 9.6).

Table 8.1 Summary of web and flange geometry, modular frame[(1)].

Length	Location	Web				Inside Flange			Outside Flange		
		d (in)	t_w (in)	h/t_w*	h_c/t_w	b_f (in)	t_f (in)	$b_f/2t_f$	b_f (in)	t_f (in)	$b_f/2t_f$
A	e1	10	1/8	76		6.0	1/4	12.0	6.0	1/4	12.0
	e2	16.88		131							
	e3	22.38		175							
	e4	25		196							
B			5/32								
C	a0-a2'	25	5/32	157		6.0	1/4	12.0	6.0	1/4	12.0
D	a2'-a6'	25	1/8	196		6.0	1/4	12.0	6.0	1/4	12.0
E	a6'-a8'	25	5/32	157		6.0	1/4	12.0	6.0	1/4	12.0
F	a8'	25	3/16	130	124	6.0	3/8	8.0	6.0	5/16	9.6
	a9	25.41		132	126						
	a10	25.91		135	129						
	b0	26		135	129						
G	b0	26	3/16	135	129	6.0	3/8	8.0	6.0	5/16	9.6
	b1	23.13		120	114						
	b2	19.64		101	96						
	b2'	19		98	92						
H	b2'-b6'	19	5/32	118		6.0	1/4	12.0	6.0	1/4	12.0
I	b6'-b8'	19	1/8	148		6.0	1/4	12.0	6.0	1/4	12.0
J	b8'	19	3/16	98		6.0	5/16	9.6	6.0	5/16	9.6
	b9	23.46		122							
	b10	28.96		151							
	c0	30		157							
K	c0	30	3/16	157		6.0	5/16	9.6	6.0	5/16	9.6
	c1	27.57		144							
	c2	24.57		128							
	c2'	24		125							
L	c2'-c6'	24	3/16	123	133	6.0	1/2	6.0	6.0	3/8	8.0
M	c6'-c8'	24	3/16	123	133	6.0	1/2	6.0	6.0	3/8	8.0
N	c8'	24	7/32	107		6.0	1/4	12.0	6.0	1/4	12.0
	c9	26		117							
	c10	28.5		128							
	c11	29		130							

(1) The prime marks on the location symbols indicate positions corresponding to a cross-section transition. The symbols without prime marks represent purlin locations as shown in Fig. 8.1.
**For F_y = 55 ksi*, the web is compact for $h/t_w \leq 86$ and it is slender for $h/t_w \geq 130$.

The inner-most span starts with a taper within length K from d = 30 inches at the second interior column to d = 24 inches at 10 ft inside of this column. Its web is 3/16 inch

thick, giving h/t_w = 157 to 125, and its flanges are the same thickness as those of length J (5/16 inch). Lengths L and M are prismatic singly-symmetric sections with d = 24 inches, t_w = 3/16 inch (h/t_w = 123), and t_f = 3/8 and 1/2 inch for their top and bottom flanges. Lastly, length N has a taper from d = 24 inches at 10 ft from the center column up to d = 29 inches at the center column. It has a 7/32 inch web, giving a range for its web slenderness of h/t_w = 107 to 130. Its flanges are the same size with t_f =1/4 inch.

Based on the above proportions, the member webs are classified as slender both under flexure and under compression within a large number of the unbraced segments in the modular frame; however, the webs within lengths F, G, H and N, and segments b8'-b9 in length J and c2 to c2' in length K are noncompact under flexure.

8.3 Loading

The load case considered for this case is the same as the one considered for the 90 ft clear span frame case discussed in Chapter 6. The load combination, load parameters and magnitudes are presented in Section 6.3.

8.4 Bracing Configuration

The outside flanges of the columns and rafters of the modular frame are assumed to be supported laterally at all the girts and purlins in the design. Diagonal braces to the inside flanges are indicated by double dashed lines in Figure 8.1. The purlins are spaced at 5 ft on center except at the knee and ridge of the frame, and girts are located at 7.5 and 6 ft spacing starting from the base of the exterior columns. Both exterior column flanges are braced laterally at the two girt locations. The flange diagonal braces at a10, b10 and c10 are located slightly off the centerline of the corresponding interior columns. Location a10 is 0.912 ft from the centerline of the first interior column, location b0. The bottom

flanges of the rafters are unsupported at two of the purlin locations within the positive moment region of each of their spans (at locations a4, a6, b4, b6, c4 and c6), but otherwise both flanges are laterally restrained at each purlin. The exterior spans of the rafters and the tops of the exterior columns are assumed to be braced laterally at the panel zone edges of the knee of the frame (locations a0 and e4) in the design calculations.

The total depths of the main frame members (d) are shown in Figure 8.1 and in Table 8.1. Cold-formed 16 gage, 8 inch deep Z816 sections are assumed for the girts and purlins in this frame. These are taken as representative minimum-size purlins commonly used for structure geometries similar to this one.

As with the previous designs in Chapter 4 through 7, the torsional bracing from the flange diagonals and girts/purlins is modeled by torsional springs located at the centroids of the girts/purlins, as explained in Section 3.4. The combined flexibility from the axial deformation of the flange diagonal braces and the flexure of the purlins is considered in determining the torsional bracing stiffnesses. Since the flange diagonals are assumed to be attached directly to the bottom flange, no additional flexibility due to cross-section web distortion is considered. In addition, it is assumed that there is no local deformation or slip at the connection points on either end of the flange diagonal braces. It is assumed that the girts and purlins are "rigidly pinned" to the outside flange of the columns and roof girder, i.e., there is no translation of the outside flanges relative to the bracing system. However, the girts and purlins do not offer any direct torsional restraint at the outside flange of the member. The interior columns are modeled as truss elements. A single full-depth bearing stiffener is placed in the roof girder web at the centerline of each column. The torsional brace close to the column, combined with the rafter flexural and

torsional stiffnesses, provides the predominant restraint of the out-of-plane displacements at the top of the column.

8.5 Comparison of the AISC and Simplified Bracing Requirements to Provided Values

The procedure used in Section 2.7 is adopted to evaluate the brace stiffness and strength requirements for the modular frame. At the negative moment locations on the roof girders and throughout the column lengths, the flange diagonal brace locations are considered to be only torsionally braced. Relative bracing from the roof and wall diaphragms is considered in the design to establish the girt and purlin locations as brace points for axial load and for positive bending moments on the rafters.

The required torsional brace strength and stiffness, as estimated by the application of the AISC-based equations and the simplified equations of Section 2.6 and 2.8 are summarized in Table 8.2. The brace strength and stiffness requirement is evaluated for the torsional brace on the roof girders closest to the knee and close to the top of the first interior column. One should note that $C_{tT} = 1.2$ is assumed in calculating the torsional bracing stiffness requirement at the interior column. It is important to note that if the roof girder twists at the brace points over the interior columns, leading to a lateral movement at the top of the column, the column axial force follows along the inclined deflected line of the column. This is a more critical situation than the load height effect of a transverse load that remains in the original plane of the web. However, some tipping restraint generally exists from the restoring moment caused by the eccentric bearing of the rotated girder flange on the top of the column as well as the attachment between the bottom flange of the roof girder and the top of the column.

The upper-bound estimate of the stiffness provided by a typical girt or purlin, $8EI/s$ (see Section 2.7), is again used for this example. This value is obtained by taking into account the stiffness provided by the girt/purlin when the adjacent frames do not buckle, i.e. $4EI/s$ on either side of the critical frame. Given the Z816 girts and purlins specified for this frame and the spacing of the frames s = 25 ft, one obtains,

$\beta_{provided}$ = 6,380 in-kips/rad

or in terms of an equivalent lateral bracing stiffness at a10 (the critical brace location)

$\beta_{br,provided} = \beta_{provided}/h_o^2 = 6380/25.6^2 = 9.74$ kips/inch

This value is used as the provided stiffness for the subsequent virtual test simulation.

Table 8.2 Summary of required torsional brace strengths and stiffnesses at the knee and at the top of the first interior column, expressed in terms of equivalent lateral brace stiffness, to develop the specified ASD loading.

Criterion or condition		Stiffness β_{br} kips/inch	Strength P_{br} kips, % [(a)]
Required torsional brace strength and stiffness to brace the rafter at a1 (close to the knee) for the loading from the ASD load combination	AISC	0.68	0.08, 0.5%
	Simplified	5.60	0.42, 2%
Required torsional brace strength and stiffness to brace the rafter at a10 (close to the first interior column) for the loading from the ASD load combination	AISC	5.0	0.60, 1.1%
	Simplified	17.0	1.28, 2%

(a) Percent values are of $P_{br}/((P_r h_o/2 + M_r/C_b)/h_o)$

8.6 Critical Geometric Imperfections for Virtual Simulation Analysis

When the modular frame is considered as flexibly braced, the critical out-of-alignment and out-of-straightness imperfections are generated using the influence line approach detailed in Section 3.3.2. The applied geometric imperfections are aimed at

maximizing the brace demands at the brace close to the knee (a1) and at the brace close to first interior column (a10). The influence line for this frame is similar to that for the 90 ft. clear span frame (see Fig. 3.6(b)), and hence the imperfections applied to the rafter of this frame are similar. In addition to the imperfections applied close to the knee, imperfections are also applied at the first interior column, where the maximum moment occurs in the roof girders.

Figure 8.2 shows the imperfections applied to the modular frame. An out-of-alignment of $L_b/500$ is applied to the unbraced lengths adjacent to the critical brace locations (where the brace force is to be maximized). In addition, an out-of-straightness of $L_b/1000$ is applied within these unbraced lengths.

The top of the first interior column is displaced out-of-plane by 0.098 inches at location b0, resulting in an out-of-plumbness of 1/2230 along its length. The out-of-plane displacement at b0 is limited by the out-of-plane displacement at a10, which is in turn limited by the out-of-alignment of 1/500 in the rafter unbraced lengths adjacent to point a10 and the assumption of a straight top tension flange in the roof girders. The 0.12 inch out-of-plane displacement at a10 results in an overall twist of 0.12/25.6 = 1/213 of the girder cross-section at this location.

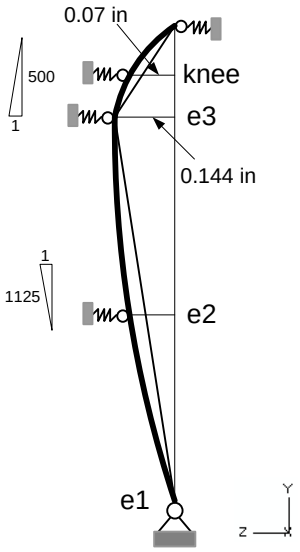

(a) column compression flange imperfections

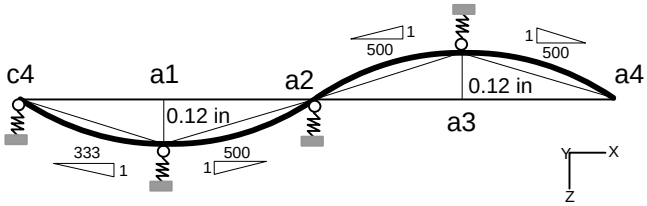

(b) rafter compression flange imperfections close to the knee

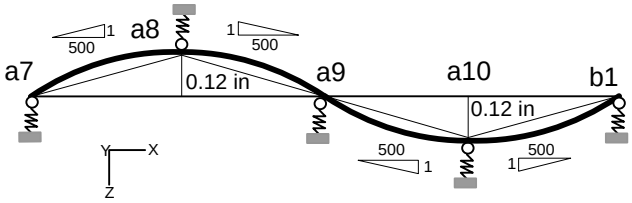

(c) rafter compression flange imperfections close to the first interior column

Fig.8.2. Flange Out-of-alignment imperfection applied to the modular frame

If an out-of-plumbness of *h*/500 is to be applied at the top of the interior column, the entire rafter would have to be shifted to meet the tolerance of L_b/500 in the rafter at the brace points. It was decided not to introduce such an imperfection in this study.

The geometric imperfection applied in the virtual test simulation is a linear combination of buckling modes and out-of-alignment and out-of-straightness imperfections, similar to that discussed in Section 6.7.

When the frame is considered as rigidly braced, a single brace out-of-alignment is applied at a1 and at a10.

Similar to the 90 ft clear span frame of Chapter 6, the modular frame is modeled initially out-of-plumb to the right (see Fig. 8.1) in the plane of the frame by 0.002*h*, where *h* is the height above the base.

8.7 Virtual Simulation Results

The bracing demands at the knee region and the first interior column (closest to the knee) are discussed for rigid and flexible bracing cases in the following subsections. The behavior for rigid bracing is discussed first.

8.7.1 Rigid Bracing

Figure 8.3 shows the load-deflection response of the modular building frame for the rigid bracing condition. It can be seen that the frame fails in a side-sway mode. The fraction of the reference load applied is shown on the vertical axis and the horizontal displacement at the eaves level is shown on the horizontal axis. The frame reaches an ultimate capacity 26% larger than the ASD ultimate strength level.

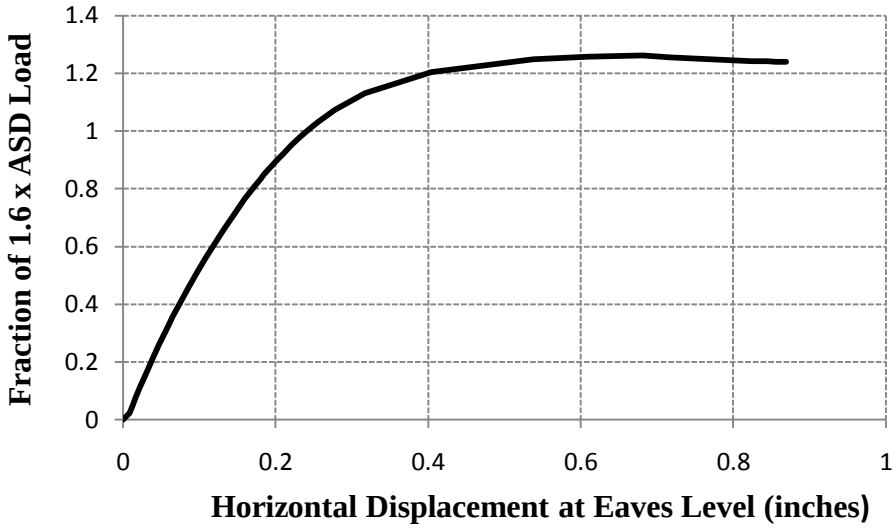

Fig. 8.3. Load versus in-plane deflection of the modular frame, rigid bracing condition.

Figure 8.4 shows the brace force demand at the knee and Figure 8.5 shows the brace force demand at the brace closest to the first interior column. The vertical axis of the plots shows the applied load fraction and the horizontal axis shows the brace force as a percentage of the internal moment at the roof girder connection to the knee, $M_{knee}^{\#}$ in Fig. 8.4 and the internal moment at the first interior column, $M_{max}^{\#}$ in Fig. 8.5. $M_{knee}^{\#}$ and $M_{max}^{\#}$ are the roof girder moment at the knee and at the first interior column at the peak load for the rigid bracing condition, respectively.

The maximum moment at the knee for the given loading is 95 ft-kips at the peak load capacity of the frame. From Fig. 8.4, the brace force at the knee is 2.8% of this value. If the AISC (2010) Eq. (A-6-9) is used, the brace force demand is estimated as 2.7% of the roof girder moment at the knee. $M_{max}^{\#}$ = 295 ft-kips is the moment at the first interior column at the peak load for the rigid bracing condition.

At the limit load of the structure, the force demand in the brace at a10 is 1.5% of $M_{max}^{\#}$. The brace moment is slightly less than the 2% estimate by the simplified equations

at this condition. Using the AISC (2010) Eq. (A-6-9), the brace force demand is estimated as 1.1% of the maximum internal moment at a10.

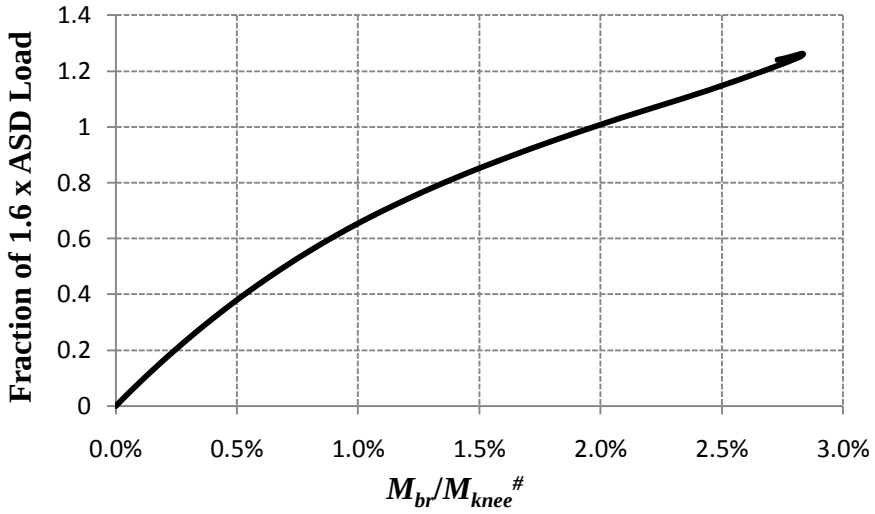

Fig. 8.4. Brace force demand at a1 (close to the knee), modular frame, rigid bracing condition, $M_{knee}^{\#}$ = moment at the knee at peak load.

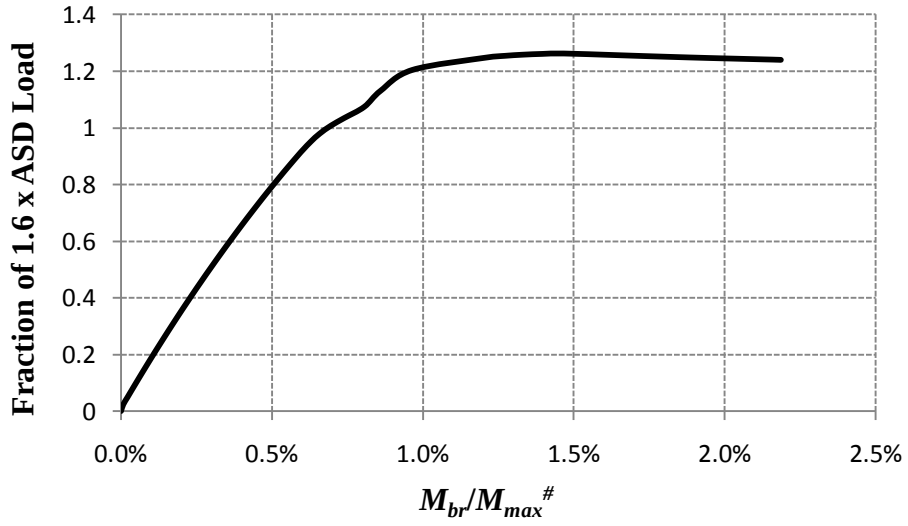

Fig. 8.5. Brace force demand at a10 (brace closest to the first interior column), modular frame, rigid bracing condition, $M_{max}^{\#}$ = moment at the first interior column at the peak load.

8.7.2 Flexible Bracing Condition

Figure 8.6 shows the brace force demand close to the knee for the flexible bracing case. The frame reaches 16% larger capacity than the ASD design load level (or 92% of

the rigidly-braced capacity). $M_{knee}^{\#\#}$ is the moment at the inside of the knee at the peak load for the flexible bracing condition. The brace force demand at the brace closest to the knee for this case is 0.37% of the roof girder internal moment at the knee.

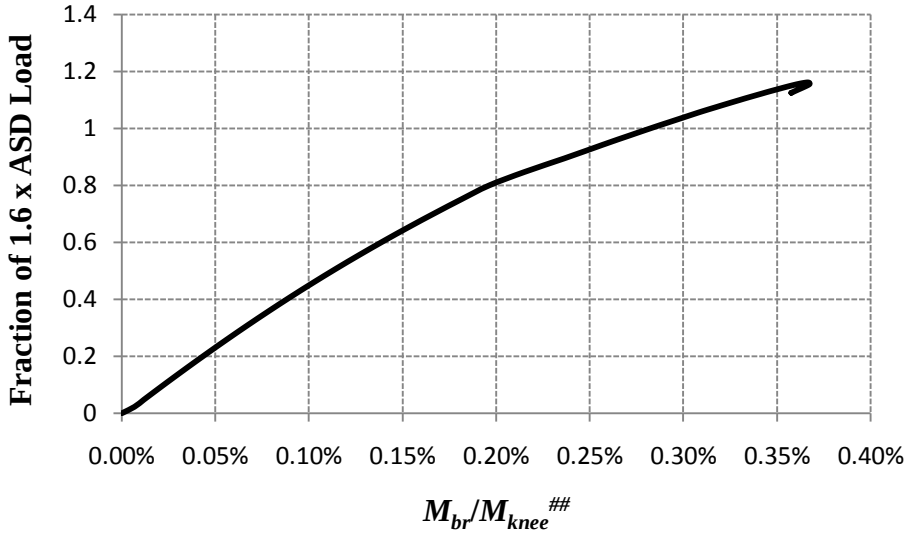

Fig. 8.6. Brace force demand close to the knee, modular frame, flexible bracing condition, $M_{knee}^{\#\#}$ = moment at the knee at peak load.

Figure 8.7 shows the brace force demand over the first interior column from this same analysis. In this case, the moment at b0 at the limit load of the structure, denoted by $M_{max}^{\#\#}$, is 256 kip-ft. At the structure maximum strength condition, the moment in the torsional brace closest to the first interior column is found to be 2.3% of the member internal moment at that location.

Table 8.3 summarizes the torsional brace strength demands at a1 and a10 at 90, 95 and 100 % of the system limit load. One can observe that all the bracing strength demands are very small until the system capacity is nearly reached.

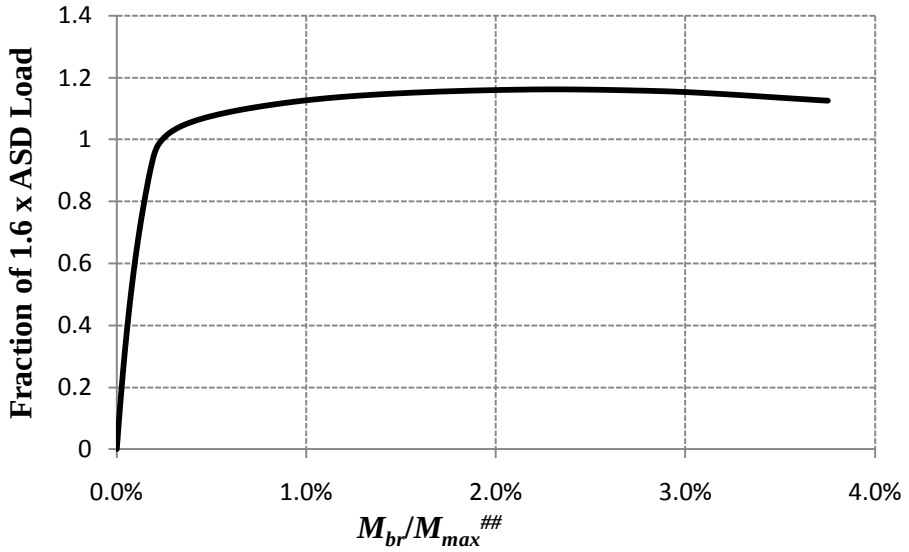

Fig. 8.7. Brace force demand at a10 , modular frame, flexible bracing condition, $M_{max}^{\#\#}$ = moment at the top of the first interior column at peak load.

Table 8.3 Summary of strength demand at the torsional braces from virtual test simulation, modular frame.

Criterion or Condition	Strength Demand at 90% of Limit Load	Strength Demand at 95% of Limit Load	Strength Demand at Limit Load
Torsional brace strength requirement at a1 (close to the knee) using provided torsional brace stiffness required to brace the frame for the loading from ASD load combination, 6380 in-kips/rad	P_{br} = 0.13 kips, 0.3%	P_{br} = 0.14 kips, 0.33%	P_{br} = 0.16 kips, 0.4%
Torsional brace strength requirement at a10 (close to the top of first interior column) using provided torsional brace stiffness required to brace the frame for the loading from ASD load combination, 6380 in-kips/rad	P_{br} = 0.4 kips, 0.3%	P_{br} = 0.8 kips, 0.7%	P_{br} = 2.7 kips, 2.3%

8.7.3 Effect of Varying the Torsional Brace Stiffness

Figure 8.8 shows the knuckle curve for the torsional brace stiffness at a10 in the modular frame. The vertical axis shows the fraction of load capacity for the rigidly

braced frame, $M_{max}/M_{max}^{\#}$, where M_{max} is the internal moment at the top of the first interior column (location a10) and $M_{max}^{\#}$ is the corresponding moment at the peak load for the rigid bracing condition. This ratio is shown because the maximum moment in the frame occurs at the interior column. Also, location a10 is the most critical in terms of the design of the braces.

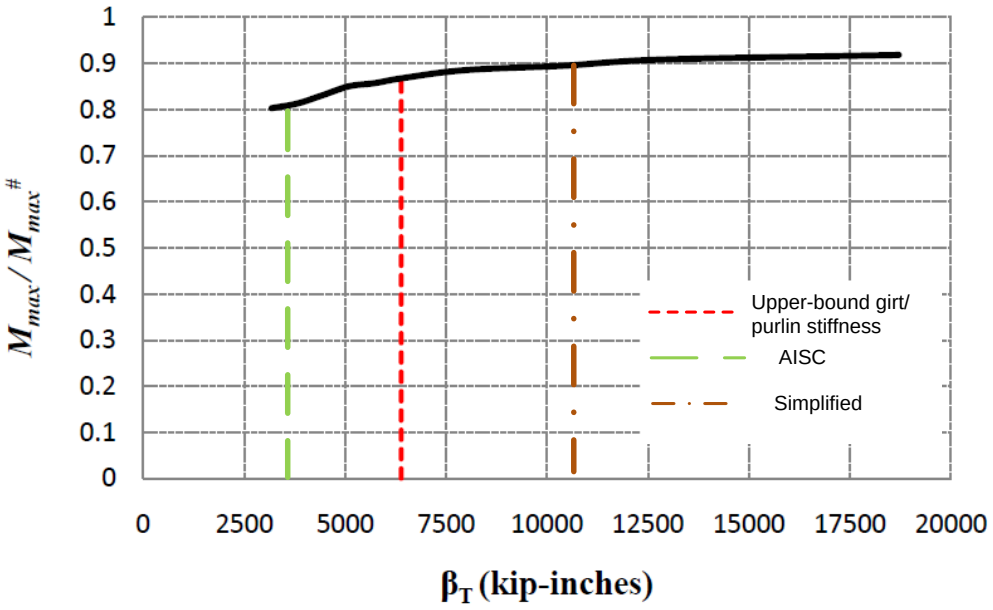

Fig. 8.8 Frame strength behavior knuckle curve for the brace at a10, modular frame, $M_{max}^{\#}$ = moment at the top of the first interior column at peak load for the rigid bracing condition.

The slope of the curve is very flat in Fig. 8.8; hence, for higher torsional brace stiffness values, the strength of the frame is insensitive to changes in brace stiffness. For brace stiffnesses smaller than the stiffness provided by a typical girt/purlin, the slope is steeper but the reduction in strength is still relatively small. However, if the stiffness provided by the girt/purlin (6380 in-kips/rad. or 9.74 kips/inch) is used, the frame develops only 92% of the ASD ultimate strength (see Fig. 8.6). The AISC estimate of the required brace stiffness for this case is 3300 in-kips/rad (β_{br} = 5.0 kips/inch) and the

simplified equations estimate the required stiffness as 11,200 in-kips/rad (β_{br} = 17.0 kips/inch).

Figure 8.9 shows a plot of the brace strength requirement close to the first interior column, normalized by the moment at the top of the column for the rigid bracing condition ($M_{max}^{\#}$),versus the torsional brace stiffness. For this frame, the brace strength requirement increases rapidly until a maximum is reached close to the torsional stiffness provided by a typical girt/purlin (6380 in-kips/rad). For stiffness values higher than this, the brace strength requirement decreases until a stiffness approximately equal to the simplified estimate of the torsional brace stiffness requirement is achieved (β_T = 11,200 in-kips/rad). After this point, the strength demand becomes nearly constant (as a percentage of $M_{max}^{\#}$) at 1.3%. For the simplified stiffness estimate, the limit load of the structure is about 90% of the rigidly braced strength (see Fig. 8.8).

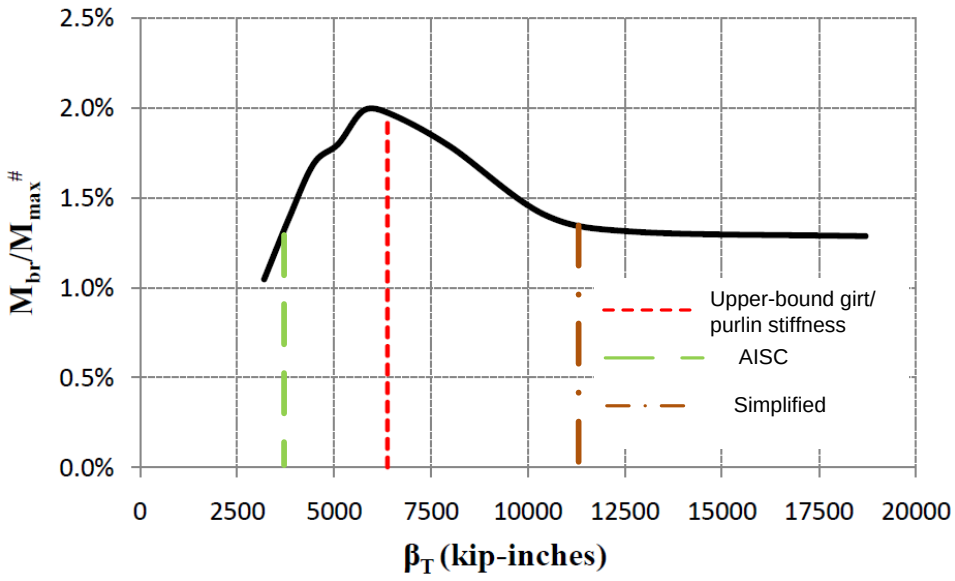

Fig. 8.9 Brace force demand curve for the brace at a10, modular frame, $M_{max}^{\#}$ = moment at the top of the first interior column at peak load for rigid bracing condition.

8.7.4 Rigid Bracing Case with Frame Sidesway Buckling Prevented

In the previous section, the demands on the critical braces are limited partly by the fact that the frame fails in a sidesway mode. If the frame is restrained against sidesway by some means (incidental or by design), the frame fails by buckling of the roof girder over the first interior column, where the largest internal moment occurs, as shown in Figure 8.10.

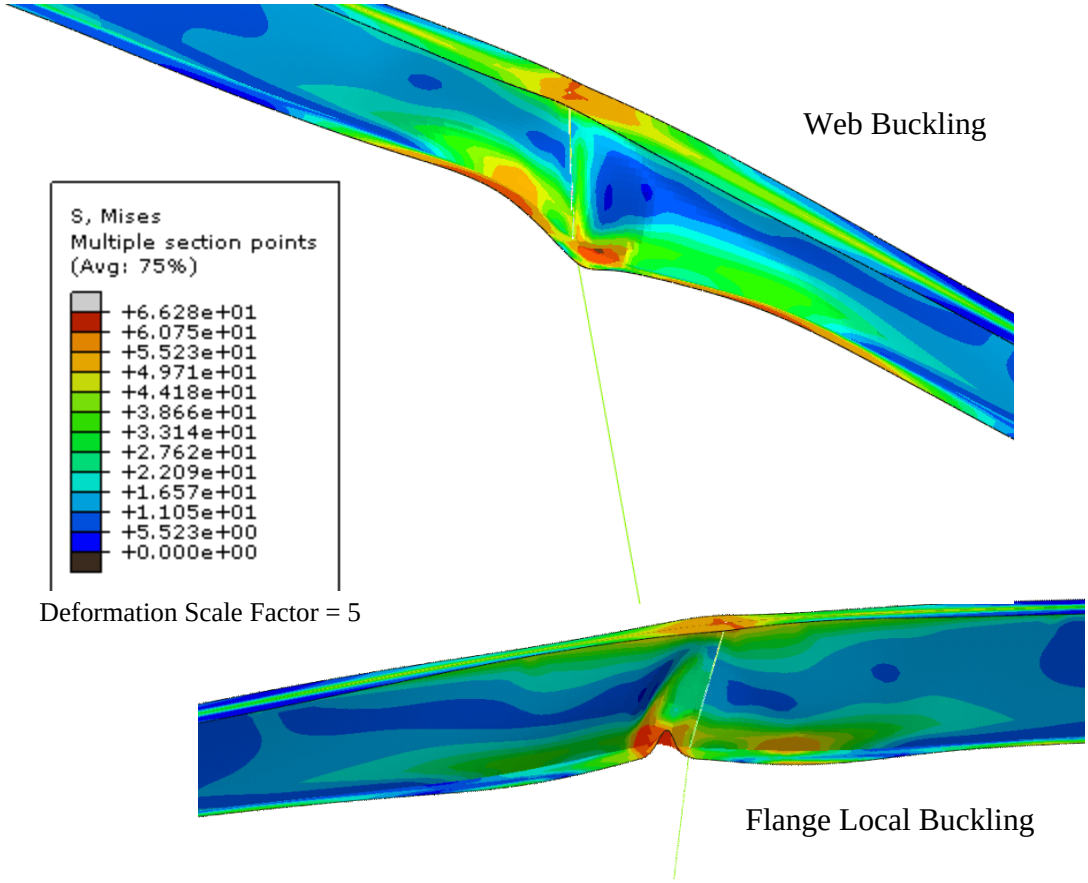

Fig. 8.10. Buckling of the frame over the first interior column at the end of the analysis, modular frame for the rigid bracing condition, no sway case.

Figure 8.11 shows the brace force demand at the knee for this case. The moment at the knee is 101 ft-kips at the load capacity of the structure in this case.

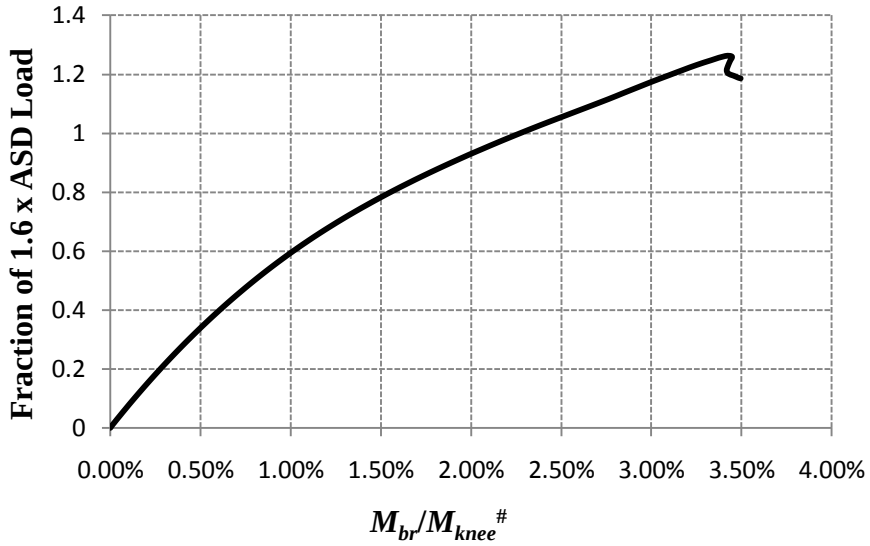

Fig. 8.11. Brace force demand close to the knee, modular frame, no sway case, $M_{knee}^{\#}$ = moment at the knee at peak load for the rigid bracing condition.

The brace force demand at the knee for this case is 3.4% of the roof girder internal moment at the knee for this condition. Figure 8.12 shows the brace force demand over the first interior column. The moment at this section for the no sway case is 276 kip-ft.

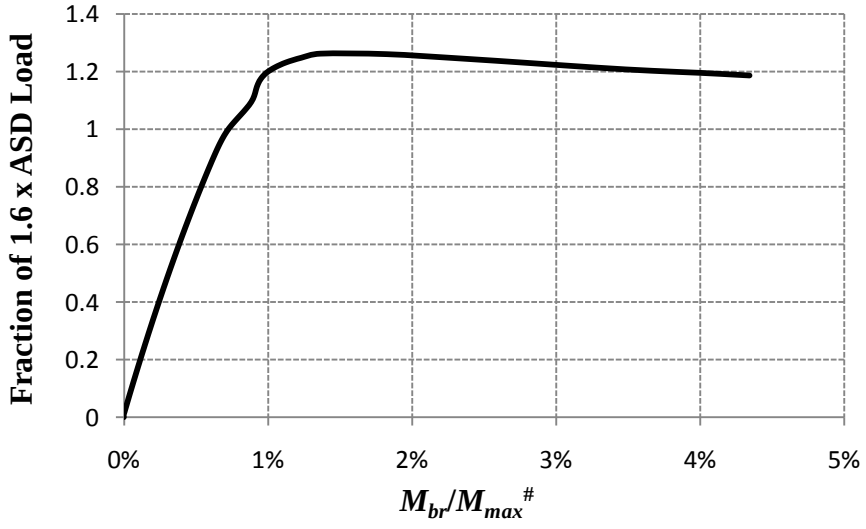

Fig. 8.12. Brace force demand closest to the first interior column, modular frame, no sway case, $M_{max}^{\#}$ = moment at the top of the first interior column at peak load for the rigid bracing condition.

The brace force demand closest to the first interior column is 1.4% of the internal moment for this condition at that location at the limit load. This value is smaller than for the no sway case. This may be attributed to the fact that the web buckle is restrained by the web stiffener over the first interior column. Since the brace lies on the other side of the stiffener, the web buckle does not contribute towards the brace force demand.

8.8 Summary

The following observations can be summarized from this example:

- The upper-bound estimate of the torsional stiffness provided by the representative minimum girt and purlin sizes is able to develop 92% of the ASD ultimate strength load level in this problem. The AISC estimate for the torsional brace stiffness is much lower than the assumed provided stiffness, but is able to develop only 80% of the rigidly-braced strength of the frame. The estimated simplified requirement is larger than the provided stiffness and develops 90% of the rigidly-braced frame strength.
- The rigidly-braced frame fails in sidesway. However, even if the sidesway is restrained, the strength of the frame does not increase significantly since the frame fails due to local buckling in the roof girder.
- The frame fails due to local buckling of the web and the flange at the first interior column where the moment is the highest.
- The strength of the frame is insensitive to the change in torsional brace stiffness at higher brace stiffness values but becomes slightly more sensitive to the brace stiffness at lower values.

- The brace strength requirement is maximum close to the estimated upper-bound stiffness provided by the minimum size girts/purlins, and decreases as the brace stiffness is increased from this value. The brace strength requirement decreases from a maximum of 2% close to upper-bound purlin stiffness of $8EI/s$ to 1.3% for the simplified estimate and higher stiffness values.

CHAPTER 9

CONCLUSIONS

9.1 Summary

This research aims to evaluate the strength and stiffness demands on the flange bracing for a range of realistic metal building members and frames. Various attributes of metal building systems are investigated that have not been addressed in prior research. Solutions from FEA virtual simulation are used to arrive at refined estimates of the bracing system demands in typical metal building frame members and systems.

The current studies build on prior research findings by focusing on the assessment of several specific examples representative of realistic bracing configurations in metal building structures. Specific attributes of these examples include:

1. Nonprismatic member geometry,
2. Members subjected to combined bending and axial compression,
3. Variable internal axial force and moment along the member lengths,
4. Unequal spacing of braces,
5. Unequal brace stiffnesses,
6. Member end conditions in which effective rigid restraint of the lateral displacements and twist rotations may not exist,
7. Complex interactions between the columns, roof girders and secondary bracing systems at knee regions,

8. Member continuity and end lateral bending and/or warping restraint effects, particularly in cases involving larger numbers of intermediate braces and in cases involving wider flanges or shorter unbraced lengths,
9. Rapid dissipation of brace stiffness and strength demands as one moves away from critically loaded unbraced lengths, particularly in members having a larger number of intermediate braces,
10. Beneficial interactions between various types of bracing.

The virtual test simulations conducted in this research satisfy the AISC (2010) Appendix 1 requirements for inelastic analysis: they include appropriate nominal initial residual stresses and initial geometric imperfections permitting a stand-alone evaluation of the strength, independent of Specification resistance equations. However, the specific simulations provided in this work are focused on evaluating the expected strengths; hence no stiffness or strength reduction factors are incorporated into the analyses. Procedures to determine critical geometric imperfections are developed and discussed in detail.

Key findings from this research are as follows:

- The brace strength and stiffness requirements are largest at the knee of the frames. This is because: (1) typically the moment at that location is highest, and (2) force transfer mechanisms between the roof girder and the column at the knee. The current bracing design provisions consider the member ends to be rigidly braced, but for frames, the restraint of the rafter and column end twisting and/or out-of-plane flange displacement is not truly rigid. Rather, this response at the knee involves complex interactions between the rafter, the column, the panel zone, and the specific configuration of the girts, purlins, flange diagonals, eave strut, and

wall and roof diaphragms in the vicinity of the knee. The resistance to out-of-plane displacement of the inside corner of the knee in this region is an important factor in determining the critical brace force demands in the system.

- This research shows, for the frames considered, that the maximum torsional brace strength requirement at the knee to develop the limit load of the structure, including cases where column buckling is observed, is on the order of 3% of the internal moment at that location. This limit appears to be relatively insensitive to the stiffness of the brace at the knee. For the various members considered in this work, the maximum torsional brace strength requirement at the structure limit load is approximately 4%. However, the system strength is approximately 95% or more of the limit load when the maximum torsional brace strength demand reaches 2 % in all the cases studied. The corresponding strength demand is approximately 1 % for the more limited number of relative bracing cases considered.
- The above *brace force* requirements, obtained from the virtual test simulations at the limit load of the study cases, are larger than the estimates obtained from the refined AISC Commentary bracing equations explained in detail in Section 2.6. Based on the studies in this research and studies by Tran (2009) and others, the refined AISC equations work relatively well for estimating required *brace stiffness* in cases where the boundary conditions match with the ones considered during the development of the equations.
- If member flange widths are increased, the brace force demand at the structure limit load, expressed as a percentage of the internal moment (or the equivalent

internal flange force) at the critical cross-section, decreases significantly. This may be attributed to the increase in the flexural rigidity of the member, EI_{eff}, and the local buckling behavior of the non-compact flanges tending to act as a fuse of sorts with respect to the actions that induce forces into the flange bracing.

- If the stiffness contribution due to roof and wall diaphragms is considered in the design, the system strength improves slightly and the brace strength and stiffness demands decrease slightly. However, the influence of the roof and wall diaphragms appears to be relatively minor in the frames considered. In these frames, the brace points are defined on the outside flanges as the points where the diaphragm is connected to the girts or purlins. The diaphragm stiffnesses are necessary to define these locations as brace points; however, the virtual simulations show that the overall framing system strength is not sensitive to the contributions from the roof and wall diaphragms for the frames considered in this work.
- The strength and stiffness demands away from the critical regions are significantly smaller than the demands at or close to the critical regions. Bracing strength demands for the cases considered are not sensitive to reductions in brace stiffness away from the critical locations. This is likely due to the emphasis on developing the knuckle value resistances in this work, and as such, effectively providing near full bracing for the frames. These findings are consistent with findings by Wang and Helwig (2005) that the critical imperfections in fully-braced beams tend to be local to the brace under consideration.

- In the cases considered in this research, where the rafter frames into the column at the panel zone at approximately 90° and the column has bracing located along its length, the column provides substantial resistance to the twist and the lateral movement of the rafter and the knee. In the 120 ft clear span frame example, where the column is unbraced along its length, this restraint is negative since the column buckles, and as such, the brace force is increased at the knee. However, this increase in the brace strength demand is relatively small.
- Bracing stiffness requirements based on achieving 90% of the rigid bracing strength appear to work well for all the cases considered, except the 120 ft clear span frame where the system doesn't even reach 90% of the rigidly braced strength for the range of stiffness considered in this research. The bracing stiffness where the system reaches 90 % of its rigidly-braced strength is a reasonable estimate of the knuckle value stiffness.
- Interestingly, the bracing strength demand, corresponding to the system limit load, tends to be largest at the knuckle value of the brace stiffness. For smaller stiffness values, the brace forces tend to decrease because the strength of the overall framing system is significantly reduced. For larger stiffness values, the brace forces tend to decrease because the stiffer bracing reduces the amount of the brace point movement while the structure limit load is not significantly affected.
- The strength and stiffness demands on the braces can be sensitive to the bracing layout for the cases considered. If the layout close to the critical regions is changed, the bracing demands may change significantly.

- The AISC torsional bracing equations typically work better than the corresponding nodal bracing equations in quantifying the bracing demands on flange braces in metal building frames. This is because the torsional bracing equations are more effective at accounting for the resistance to brace point movement provided by the member being braced.
- Simplified bracing stiffness rules based on recognizing typical maximum brace strength requirements such as those mentioned above by targeted maximum brace deformation limits under these forces are interesting in concept, but they would generally need to also account for the contribution from the member(s) to the resistance of the brace point movements in order to achieve accurate general predictions.

9.2 Recommendations for Design Practice

A number of specific recommendations can be offered for flange bracing design in metal building frames based on the results of this research:

- The enhanced requirements from the Commentary to Appendix 6 provide improved predictions of the stiffness demands on the braces for design as compared to the equations given in the Appendix 6 Specification provisions.
- A number of minor changes can be made to the presentation or format of the Appendix 6 equations to help simplify and clarify the proper application of the equations. The resulting recommendations are detailed in Section 2.6 of this report.
- It appears that the AISC torsional bracing stiffness requirement can be written in a form in which an LTB effective length factor K can be utilized with the

different unbraced lengths to account for continuity effects in members with unequal brace spacing as well as for member end rotational and warping restraint. Further work is needed to provide specific recommendations for the calculation of the *K* factors, accounting for the complex interactions between the various components of the knee region of typical metal building frames. However, it is clear that rather coarse estimates of $K < 1$ based on an interpretation of the end conditions, such as implied by Table C-C2.2, should be adequate in some situations.

- The critical torsional brace strength requirements needed to develop the system peak load can be on the order of 4 % of the corresponding internal moment in some cases. However, design of the critical braces for a 2 % strength requirement generally is sufficient to develop more than 95 % of the system limit load resistance. As such, when overall ductility of the framing system is not a key factor, such as when the frames are not designed for substantial inelastic deformation under seismic loading, it is recommended that torsional braces be designed for 2 % of the corresponding maximum internal moment in the unbraced length(s) adjacent to the brace. Limited parallel studies by Bishop et al. (2010) indicate that 2 % is a good target in these cases also for nodal lateral bracing. In addition, it is found that the comparable limits for relative (shear panel) bracing are 1 %. These limits are somewhat larger than current limits recommended in the AISC Appendix 6. The smaller Appendix 6 values are largely due to the lack of consideration of inelasticity near the structure limit load levels.

- The value 8*EI/s* is a reasonable upper bound estimate for the stiffness provided by prismatic girts or purlins (non-overlapped or nominal overlap) with flange diagonal bracing. This upper-bound estimate assumes (1) only the critical frame buckles and the adjacent frames do not, hence providing a close to rigid restraint at the far ends of the girt/purlin, (2) there is no slip in the connections between the girts/purlins and the frame members, (3) the flange diagonals frame in close to the web-flange junction such that web cross-section distortional flexibility does not affect the stiffness provided, (4) the purlins do not buckle, (5) all the bracing components remain elastic up to a point close to the limit load of the system, and (6) the frame considered is an interior frame. When any of these conditions are not satisfied, the provided stiffness is generally smaller. It is suggested that 6*EI/s* is a more easily justified coarse estimate for these stiffnesses considering the fact that the adjacent frames also may be loaded to a level near their critical condition.

9.3 Recommendations for Further Research

This research provides a reasonably comprehensive assessment of stability bracing requirements for several targeted metal building member and frame examples. Nevertheless, further studies are needed to better understand the many complex factors that influence the flange bracing response in metal building frame systems. Several worthwhile areas for future work are as follows:

- **Provided stiffness versus stiffness demands at critical regions**

This research studies the effect of brace stiffness on the strength behavior of a selected set of members and frames. It is found that providing enough stiffness in the critical regions and less stiffness at other locations does not alter the frame capacity.

It is difficult to provide a general guidance on how to calculate the stiffness provided by the girt/purlin or best estimate the stiffness required to brace the frames. This research uses an upper-bound estimate of the torsional brace stiffness based on assumptions mentioned in Section 9.2. Hence, this estimate is rather coarse and is not recommended for final design. More guidance is needed on whether the adjacent frames buckle or not and if the actual stiffness provided is close to the upper-bound estimate. However, some overall guidance is needed to achieve more uniform safety.

Various methods of estimating the required brace strength and stiffness are discussed in Ch. 2. The key to pursuing improvements in the approaches is to identify cases where they would have the most difficulty with satisfying the underlying stiffness requirement. The attributes that make these approaches work for some cases and not for others need to be recognized so that these estimates can be refined to give better estimates and be applicable to most cases. One generally needs to be mindful that, in all cases, it is undesirable to design a bracing system where the failure of one brace might lead to a progressive failure of other braces, e.g., an unzipping of the bracing system.

Improved mechanistic models are needed for estimating the critical brace force demands, both for members as well as for more complex configurations such as the knee regions in metal building frames. Decisions generally need to be reached about appropriate margins of safety relative to the knuckle stiffness values for critical bracing.

- **Strength and stiffness demands at non-critical locations**

It is observed that for the gravity loading considered, the maximum moment occurs at a particular location of the frame and a number of other locations are less heavily stressed. Hence, the bracing demands are significantly smaller at the lightly stressed regions at the limit state and thus, smaller braces can be provided. This needs to be checked for various frames for different loading conditions and different bracing layouts. Generally, it is desirable for the brace demand calculations to be based on the moment and axial force envelopes determined from the various required loadings on a given structure. It should be noted that economies realized when considering a specific loading case and the corresponding internal loadings may be reduced when it is considered that the various braces need to be designed for the envelope loadings. In addition, the corresponding economies in the bracing design may not be as large for tapered members compared to prismatic members.

More research is needed to provide recommendations of how to identify the points that should be braced for critical level brace forces and what points do not require as much strength and stiffness requirements. Further research of this option will help strike a balance between physical behavior, design economy and design simplicity.

- **Influence of local buckling on the system behavior**

For the frames, the local-buckling based imperfection applied to the system plays an important role in determining the system strength and bracing demands. More research is needed to fully understand the influence of local buckling on brace strength and stiffness demands at and away from the critical regions. As noted above, it is observed that local flange buckling generally tends to reduce the lateral or torsional bracing demands at the

structure limit load. However, it is well known from laboratory and field experiences that, when local member buckling starts to occur, the bracing force demands can rapidly increase. Consideration of this response may be more related to overall ductility design.

- **Tipping effect at interior column supports in modular frames**

For modular frames, further research is needed to determine the influence of the tipping at the interior column supports on brace strength and stiffness. That is, when the brace point at the top of an interior column moves out of plane, an out-of-plumbness is induced in the column in the out-of-plane direction. This out-of-plumbness causes a larger destabilizing effect on the roof girder than applied loads which remain directed in the original plane of the web during any girder twisting. That is, it generates an additional tipping effect. In addition to the high moment in this region, this tipping effect at the column supports may lead to large out-of-plane displacement at the top of the column, reducing the strength of the frame significantly.

- **Effect of inelastic stiffness reduction on torsional bracing requirements**

Although the AISC equations used to estimate the bracing requirements are based on elastic buckling, they seem to work well for the cases considered in this study where the system develops significant plasticity close to the critical region. More research is needed to determine the effect of inelastic stiffness reduction on the torsional bracing in metal building systems in order to better estimate the bracing requirements.

- **Combined effects of bending plus axial force on the main frame members**

The axial force in the roof girders and/or exterior columns in metal building frames is typically small compared to the bending moment, and the effects of the axial force are expected to be smaller than a number of other effects that are typically ignored. In

addition, torsional bracing is not effective to brace against flexural buckling of columns. Future research should address when the influence of bending plus axial force needs to be considered in the design of bracing, and when axial loading might be neglected. That is, it may be beneficial to consider cases with large bending and small axial force separately from cases with small bending and large axial force. Both of these conditions are generally important, but situations dominated by flexure are typically of greater importance for metal building frames.

- **Detailed evaluation of the influence of slip on bracing requirements**

As noted previously in Sections 2.2.4 and 2.5.2, it is expected that connection slip deformations potentially can be accounted for by an assumed increase in the initial imperfection displacements Δ_o. However, the potential implications of this approach and the possible limits to its validity have not been carefully studied to the knowledge of the author. Various cases should be considered to gage the influence of slip on the responses.

- **Consideration of coupling between primary load effects on girts/purlins and stability bracing effects**

The studies in this research have focused on the flange stability bracing strength and stiffness demands. In general, the primary load effects on the girts/purlins and the flange diagonals tied to them need to be considered in addition to the stability bracing force effects. As noted in Chapter 2, some second-order amplification of these primary force effects is expected. It would be useful to study the conservatism of applying the basic amplifier

$$1 / (1 - \beta_i / \beta)$$

to these primary load effects.

- **Bracing design to ensure ductile frame response**

The present research has focused on the bracing strength and stiffness requirements necessary to develop the static limit load resistance of members and frames. It is well understood that the bracing requirements generally tend to be larger to ensure the ductile response of structures, particularly under cyclic loading. These requirements are related to the post-peak bracing responses shown in the current studies. Research is needed to better understand the bracing stiffness and strength requirements necessary to ensure adequate ductility under cyclic loading.

REFERENCES

AISC (2010*). Specification for Structural Steel Building*, ANSI/AISC 360-10, American Institute of Steel Construction, Chicago, IL.

AISC (2010). *Code of Standard Practice for Steel Buildings and Bridges*, AISC 303-05, American Institute of Steel Construction, Chicago, IL.

AISC (2005). *Specification for Structural Steel Building*, ANSI/AISC 360-05, American Institute of Steel Construction, Chicago, IL.

AISC (2002). "Example Problems Illustrating the Use of the New Bracing Provisions – Section C3, Spec and Commentary," Ad hoc Committee on Stability Bracing, November (revised from original version of August 1998).

AWS (2000). *Structural Welding Code-Steel*, AWS – D1.1, American Welding Society, Miami, FL.

Bishop, C.D., Sharma, A., Kim, Y.D. and White, D.W. (2010). "Flange Bracing Requirements for Stability of Metal Building Systems," Structural Engineering Mechanics and Materials Report No. 53, School of Civil and Environmental Engineering, Georgia Institute of Technology, Atlanta, GA.

Breen, J.E., (2008). *Address at the Structures Congress*, ASCE/SEI Structures Congress

CSD (2009). "Calculations for Design of a Steel-Framed Industrial Building with Overhead Cranes: Session V," Session C8a, *North American Steel Construction Conference (NASCC)*, Phoenix, AZ, April. http://www.aisc.org/content.aspx?id=18290

Galambos, T.V (ed). (1998). *Guide to Stability Design Criteria for Metal Structures 5th Ed*., John Wiley and Sons, New York.

Griffis, L., and White, D.W. (2011). *Stability Design of Steel Buildings*, AISC Design Guide (to appear).

Helwig, T.A. and Yura, J.A. (1999). "Torsional Bracing of Columns," *Journal of Structural Engineering*, American Society of Civil Engineers, 125(5), 547-555.

Horne, M.R. and Grayson, W.R. (1983). *Parametric Finite Element Study of Transverse Stiffeners for Webs in Shear, Instability and Plastic Collapse of Steel Structures*, Proceedings of the Michael R. Horne Conference, L.J. Morris (ed.), Granada Publishing, London, 329-341.

Kaehler, R., White, D.W. and Kim, Y.D. (2011). *Design of Frames Using Web-Tapered Members*, AISC/MBMA Design Guide 25 (to appear).

Kim, Y. D. (2010). "Behavior and Design of Metal Building Frames Using General Prismatic and Web-Tapered Steel I-Section Members ," Doctoral Dissertation, Georgia Institute of Technology, Atlanta, GA, 562 pp.

Lutz, A.L., and Fisher, J. (1985). "A Unified Approach for Stability Bracing Requirements," *AISC Engineering Journal*, 22(4), 163-167.

MBMA (2006). Metal Building Systems Manual, Metal Building Manufacturers Association, Cleveland, Ohio.

Milner, H.R. and Rao, S.N. (1978). "Strength and Stiffness of Moment Resisting Beam-Purlin Connections," *Civil Engineering Transactions*, Institute of Engineers, Australia, CE 20(1), 37-42.

Nethercot, D. A. and Lawson, R.M., (1992). "Lateral Stability of Steel Beams and Columns – Common cases of restraint", *Steel Construction Institute, SCI-P-093*.

Ozgur, C., Kim, Y.D. and White, D.W. (2010). "Application of a useful procedure for calculating lateral torsional buckling effective length factors to linearly tapered I-beams," Structural Engineering Report No. 2010-56, School of Civil and Environmental Engineering, Georgia Institute of Technology, Atlanta, GA.

Plaut, R.H., and Yang, J.W. (1995). "Behavior of Three-Span Braced Columns with Equal or Unequal Spans." *Journal of Structural Engineering*, ASCE, 121(6): 986-994.

Plaut, R.H. (1993). "Requirements for Lateral Bracing of Columns with Two Spans," *ASCE Journal of Structural Division*, 119(10), 2913-2931.

Plaut, R.H., and Yang, J.G. (1993). "Lateral Bracing Forces in Columns with Two Unequal Spans." *Journal of Structural Engineering*, ASCE, 119(10), 2896-2912.

Prawel, S.P., Morrell, M.L. and Lee, G.C. (1974). "Bending and Buckling Strength of Tapered Structural Members," *Welding Research Supplement*, Vol. 53, February, 75-84.

Simulia (2009). ABAQUS, Software and Analysis Users Manual, Version 6.9

Stanway, G. S., Chapman, J. C., and Dowling, P. J. (1992a). "A simply supported imperfect column with a transverse elastic restraint at any position. Part 1: behaviour." *Proc. lnstn. Civ. Engrs., Strucs. and Bldgs.*, 94(2), 205-216.

Stanway, G. S., Chapman, J. C., and Dowling, P. J. (1992b). "A simply supported imperfect column with a transverse elastic restraint at any position. Part 2: design models." *Proc. lnstn. Civ. Engrs., Strucs. and Bldgs.*, 94(2), 217-218.

Taylor, A. C. and Ojalvo, M. (1966). "Torsional Restraint of Lateral Buckling," *Journal of the Structural Division*, ASCE, ST2, 115-129.

Timoshenko, S. and Gere, J., (1963), *Theory of Elastic Stability*, New York: McGraw-Hill.

Trahair, N. S. and Nethercot, D. A. (1982). "Bracing Requirements in Thin-Walled Structures," *Developments in Thin-Walled Structures,* 2, 93-129.

Tran, D. Q. (2009). "Towards Improved Flange Bracing Requirements for Metal Building Frame Systems" Master's thesis, Georgia Institute of Technology, Atlanta, GA.

Wang, L., and Helwig, T. A (2005). "Critical Imperfections for Beam Bracing Systems," *ASCE Journal of Structural Division*, 131(6), 933-940.

Wang, L. and Helwig, T.A. (2005). "Critical Imperfections for Beam Bracing Systems," *Journal of Structural Engineering*, ASCE, 131(6), 933-940.

Winter G. (1958). "Lateral Bracing of Columns and Beams", *Trans. ASCE*, Part 1, 125,809-925.

White, D.W., and Kim, Y.D. (2006). "A Prototype Application of the AISC (2005) Stability Analysis and Design Provisions to Metal Building Structural Systems," Report prepared for *Metal Building Manufacturers Association*, January.

White, D.W., Surovek, A.E., and Kim, S.C. (2007). "Direct Analysis and Design Using Amplified First-Order Analysis, Part 1 Combined Braced and Gravity Framing Systems," *Engineering Journal*, AISC, 44(4), 305-322.

Yura, J.A. (2001). "Fundamentals of Beam Bracing," *Engineering Journal*, AISC, 38(1), 11-26.

Yura, J. A. (1996). ''Winter's bracing approach revisited.'' *Engineering Structures* 8(10), 821–825.

Yura, J. A. (1995). "Bracing for Stability-State-of-the-Art", *Proceedings*, Structures Congress XIII, ASCE, Boston, MA, 1793-1797.

Yura, J.A. (1993). "Fundamentals of Beam Bracing," Is Your Structure Suitably Braced? 1993 Conference, Milwaukee, Wisconsin, *Structural Stability Research Council*, Bethlehem, PA, 1-40.

Yura, J. A. and Helwig, T. A. (2009). "Bracing For Stability," Short course sponsored by the Structural Stability Research Council, *North American Steel Construction Conference*, Phoenix, AZ, April.

Yura, J. A. and Phillips, B. (1992). "Bracing Requirements for Elastic Steel Beams," *Report No. 1239-1*, Center for Transportation Research, University of Texas at Austin, May, 73.

Yura, J. A., Phillips, B., Raju, S., and Webb, S. (1992). "Bracing of Steel Beams in Bridges," *Report No. 1239-4F*, Center for Transportation Research, University of Texas at Austin, October, 80.

Ziemian, R.D. (ed.) (2010). *Guide to Stability Design Criteria for Metal Structures*, Structural Stability Research Council, 6th ed., 1078 pp.